A RECOURSE-BASED SOLUTION APPROACH TO THE DESIGN OF FUEL CELL AEROPROPULSION SYSTEMS

A Thesis
Presented to
The Academic Faculty

by

Taeyun Paul Choi

In Partial Fulfillment
of the Requirements for the Degree
Doctor of Philosophy in the
School of Aerospace Engineering

Georgia Institute of Technology
April 2008

A RECOURSE-BASED SOLUTION APPROACH TO THE DESIGN OF FUEL CELL AEROPROPULSION SYSTEMS

Approved by:

Professor Dimitri N. Mavris,
Committee Chair
School of Aerospace Engineering
Georgia Institute of Technology

Dr. Philippe Masson
Center for Advanced Power Systems
FAMU-FSU College of Engineering

Dr. Danielle S. Soban
School of Aerospace Engineering
Georgia Institute of Technology

Dr. Brian German
School of Aerospace Engineering
Georgia Institute of Technology

Dr. Comas L. Haynes
Georgia Tech Center for Innovative
Fuel Cell and Battery Technologies
Georgia Tech Research Institute

Date Approved: 31 March 2008

To my family.

ACKNOWLEDGEMENTS

This rather lengthy dissertation is a testament to the patience of those who believed in me through the good and the bad of my graduate education. I am thus indebted to the following individuals, without whom the completion of this work would have never been possible, and for whom the space allotted herein is too limited to convey the full extent of my gratitude.

First and foremost, I would like to thank my advisor, Dr. Mavris, for always challenging me to better myself as not only a researcher, but also as a person. You took a chance in taking in a non U.S. citizen under your wing, who at the time had nothing but an enthusiasm for learning to offer, and for that I shall always be grateful - so thank you Doc. My very special thanks goes to my boss, Dr. Soban, for being the voice of inspiration throughout my graduate career. You believed in me even when I had lost perspective and faith in the future of this project. I am also deeply appreciative of the rest of my committee members for providing their invaluable expertise at every step of the way. Dr. Haynes has always kept me honest when it came to the development of the simulation models related to fuel cell systems. I thank Dr. Masson of CAPS for being available whenever I needed a consult on power systems design, despite being more than a few area codes away. Dr. German's knowledge of numerical optimization methods in general and aeropropulsion systems in particular was of big help in finalizing the stochastic programming portion of this research.

It is hard to imagine coming this far without my comrades in arms. My fellow graduate students gave me the much needed boost in motivation to persevere on a daily basis. I have especially enjoyed working with newly minted Dr. Taewoo

Nam, who occasionally stepped up to the role of a mentor by leveraging upon his extensive experience in the Korean aerospace industry. A tip of my hat also goes to the kind souls who have helped me complete the seemingly endless list of modeling tasks, graciously accepted my request for proof-reading, or both: Blake Moffitt, Tom Bradely, newly-initiated Dr. Eric Upton, Dongwook Lim, Bhuan Agrawal, Kyungjin Moon, Stephane Dufresne, Kyong Hun Lee, George Orouch, Young-Ki Lee, Davis Balaba, and Juhyun Kim. Thanks to all of you, I was able to accomplish twice as much in half the time it would have taken me alone.

George Matthew Adams was indeed correct in stating that "[there] is no such thing as a 'self-made' man. We are made up of thousands of others. Everyone who has ever done a kind deed for us, or spoken one word of encouragement to us, has entered into the make-up of our character and of our thoughts, as well as our success." To all my family members and loved ones back home, I want you to remember that it was your unconditional love and support that 'made' me who I am today.

From the bottom of my heart, I thank you all.

Atlanta, Georgia, Spring 2008

Contents

DEDICATION iii

ACKNOWLEDGEMENTS iv

LIST OF TABLES ix

LIST OF FIGURES x

LIST OF SYMBOLS OR ABBREVIATIONS xiv

ABSTRACT xviii

I INTRODUCTION 1

1.1 Thesis Organization 2

1.2 Motivation 3

1.2.1 Fuel Cell Basics 6

1.2.2 Algorithmic Investigation 13

1.2.3 Remedial Aspect of Engineering Design 14

II GAS TURBINE AEROPROPULSION SYSTEMS 20

2.1 Design Road Map 21

2.2 Cycle Analysis 21

2.2.1 On-Design Analysis 23

2.2.2 Off-Design Analysis 26

2.2.3 Causal and Non Causal Approaches to Modeling 30

2.3 Estimation of Installed Engine Performance and Weight 32

2.4 Engine Scalability 33

2.5 Chapter Conclusions 36

III OPTIMIZATION UNDER UNCERTAINTY 40

3.1 Probabilistic Approaches to Aerospace Systems Design 41

3.1.1 Robust Design Simulation 42

3.1.2 Joint Probability Decision Making Technique 43

3.1.3 Probabilistic Engine Design 45
3.1.4 Deterministic Solution Sampling Method 46
3.1.5 Probabilistic Aircraft Sizing Method 47
3.1.6 Summary 50
3.2 Stochastic Programming 52
3.2.1 Stages and Recourse Programs 52
3.2.2 Two-Stage Stochastic Programs with Fixed Recourse 54
3.2.3 Formulation of Recourse Function 55
3.2.4 Worth of Stochastic Programs 58
3.3 Chapter Conclusions 61
IV FORMULATION 63
4.1 Hypotheses and Research Task 63
4.2 Bounding the Problem 67
4.2.1 Architectural Space Definition 68
4.2.2 Review of Downselected Architectures 93
4.3 Creation of Simulation Environment 96
4.4 Development of Methodological Capability 98
4.4.1 Preparatory Steps 99
4.4.2 Formulation of Stages and Recourse 107
4.4.3 Surrogate Modeling of Program Functions 112
4.4.4 Two-Stage Stochastic Optimization 115
V IMPLEMENTATION 121
5.1 Preparatory Steps 122
5.1.1 Mission and Airframe Definition 123
5.1.2 Selection of Architecture Alternative 126
5.1.3 Scalability Investigation 130
5.1.4 Development of Synthesis Algorithm 132
5.2 Formulation of Stages and Recourse 142

5.2.1 First-Stage Value Function 142
5.2.2 Second-Stage Recourse 145
5.3 Surrogate Modeling of Program Functions 146
5.3.1 Modeling of First-Stage Value Function 147
5.3.2 Modeling of TPM Vectors 149
5.3.3 Modeling of Second-Stage Value Function 155
5.4 Two-Stage Stochastic Optimization 158
5.4.1 Assignment of Input Probability Distributions 160
5.4.2 Visualization of Design Domain Space 160
5.4.3 Value of Stochastic Solution 179
5.5 Lessons Learned 186
VI CONCLUSIONS 192
6.1 Academic Contributions 192
6.2 Follow-up Research Paths 195
6.2.1 Incorporation of Refined Simulation Models 196
6.2.2 Exploration of Alternate Recourse Formulations 197
6.2.3 Extension to Multi-Stage Approaches 199
6.3 Recommendations for Future Work 202
6.4 Closing Remarks 205
Appendix A AERONAUTICAL APPLICATIONS OF FUEL CELLS . . . 208
Appendix B PROPULSION-LEVEL SIMULATION ENVIRONMENT . . 234
Appendix C NEURAL NETWORK MODELING 244
Appendix D OPTIMIZER SETTINGS 245
Bibliography 250
VITA 283

List of Tables

1 Classification of Fuel Cell Technologies 7
2 Select Engine Parameter Categories and Groups 35
3 Comparison of Three Uncertainty Realization Scenarios 59
4 EVPI for Different Stochastic Solutions 60
5 VSS for Different Stochastic Solutions 61
6 Matrix of Alternatives for Fuel Cell Aeropropulsion System 69
7 Downselected Fuel Cell Aeropropulsion System Alternatives 94
8 Discretization of LAGER Mission 128
9 PEMFC Powered UAV Sizing Results 129
10 Point-Performance Requirements for SOFC-based Alternatives 130
11 Cycle Parameters: PEMFC Aeropropulsion System 131
12 First-Stage Design Variables 143
13 List of Random Parameters 143
14 Constituents of TPM Vector 145
15 DoE Ranges of First-Stage Design Variables and Random Parameters 149
16 First-Stage Value Function: Summary of Fit 153
17 TPM Vectors: Summary of Fit 153
18 Matrix of TPM Target Values 161
19 Second-Stage Value Functions: Summary of Fit 162
20 Two-Stage Optimization Solutions of **A1** 179
21 Two-Stage Optimization Solutions of **A3** 180
22 Two-Stage Optimization Results of **A2** 185
23 Two-Stage Optimization Solutions of **A2** 185
24 Database of Conventional Electric Machines 239
25 List of Select References for PEMFC Stack Sizing Model 240
26 Methods Applicable to Design of BOP Sub-systems 241

List of Figures

1 Envisioned Aviation Applications of Fuel Cell Technology 5
2 How Fuel Cells Operate 8
3 Past and Projected Improvement in Fuel Cell System Specific Power . 12
4 Deterministic Monitoring and Management of TPM 18
5 Design Process of Gas Turbine Aeropropulsion System 22
6 Parametric Cycle Analysis Results: Variation in Flight Conditions . . 25
7 Specific Performance of Ideal, Mixed-Flow Turbofan Engines 26
8 Design Point Diagrams of Turbofan Engines 27
9 Representative Off-Design Analysis Results 29
10 Approaches to Aerovehicle Sizing 37
11 RDS Methodology Flowchart 44
12 JPDM Technique Flowchart 45
13 Motivation for Probabilistic Engine Design 46
14 DSS Method for Engine Architecture Selection 47
15 Impact of Uncertainty on Aircraft Sizing 48
16 Overview of PASM 49
17 Single-Stage Nondeterministic Design Paradigm 50
18 Role of Recourse Penalty in Stochastic Solutions 58
19 DSM of Propulsion-Level Simulation Environment 97
20 Example Illustration of MPP: PEMFC Voltage Model 98
21 Procedural Map of Recourse-based Design Method 99
22 Generalized Approaches to Aerovehicle Sizing 102
23 Scalable Aeropropulsion System: Fixed Cycle 104
24 Generalized Actual Value-based Aerovehicle Sizing Process 106
25 Process Flow Map of Proposed Two-Stage Formulation 109
26 Second-Stage Value Function Algorithm 112
27 Implementation Plan of Recourse-based Design Method 122

28 Design Requirements of Notional Maritime UAV 123
29 Notional Naval UAV Configuration 124
30 Drag Polar Coefficients of Naval UAV 125
31 Candidate Fuel Cell Aeropropulsion System Architectures 127
32 Weight Breakdowns of UAV Sizing Results 129
33 UAV Take-off Gross Weight vs. TOS 131
34 Scalability Investigation of **A1**. Top: π_1. Middle: π_2. Bottom: π_3. . . 133
35 Scalability Investigation of **A2**. Top: π_1. Middle: π_2. Bottom: π_3. . . 134
36 Scalability Investigation of **A3**. Top: π_1. Middle: π_2. Bottom: π_3. . . 135
37 Generalized Specific Parameter-based Aerovehicle Sizing Process . . . 136
38 Load Profile for Sizing Auxiliary Energy Storage Device 138
39 Ragone Plot of Various Auxiliary Energy Storage Technologies 139
40 Parametric Cycle Analysis: UAV with **A3** 141
41 Neural Network-based Surrogate Modeling Process 147
42 Actual by Predicted and Residual Plots & 3D Scatter Plots: **A1** . . . 150
43 Actual by Predicted and Residual Plots & 3D Scatter Plots: **A2** . . . 151
44 Actual by Predicted and Residual Plots & 3D Scatter Plots: **A3** . . . 152
45 Actual by Predicted and Residual Plots of $\mathbf{T}(\mathbf{x}, \tilde{\xi}(\omega), \xi(\omega))$: **A1** . . . 154
46 Actual by Predicted and Residual Plots of $\mathbf{T}(\mathbf{x}, \tilde{\xi}(\omega), \xi(\omega))$: **A2** . . . 154
47 Actual by Predicted and Residual Plots of $\mathbf{T}(\mathbf{x}, \tilde{\xi}(\omega), \xi(\omega))$: **A3** . . . 155
48 Actual by Predicted and Residual Plots of $\mathbf{T}(\mathbf{y}, \xi(\omega), \xi(\omega))$: **A1** . . . 156
49 Actual by Predicted and Residual Plots of $\mathbf{T}(\mathbf{y}, \xi(\omega), \xi(\omega))$: **A2** . . . 156
50 Actual by Predicted and Residual Plots of $\mathbf{T}(\mathbf{y}, \xi(\omega), \xi(\omega))$: **A3** . . . 157
51 Substitution of Surrogates in Evaluating $Q(\mathbf{x}, \xi(\omega))$ 158
52 Automated Environment for Modeling $Q(\mathbf{x}, \xi(\omega))$ 159
53 Actual by Predicted and Residual Plots of $Q(\mathbf{x}, \xi(\omega))_{NN}$: **A1** 163
54 Actual by Predicted and Residual Plots of $Q(\mathbf{x}, \xi(\omega))_{NN}$: **A2** 164
55 Actual by Predicted and Residual Plots of $Q(\mathbf{x}, \xi(\omega))_{NN}$: **A3** 165
56 Sensitivity Analysis Results of Value Functions: $\mathbf{h_4}$ 167

57 Automated Environment for Visualization and Optimization 168
58 Contour and Surface Plots of First-Stage Space 169
59 Contour and Surface Plots of Second-Stage Space: $\mathbf{h_4}$ 171
60 Contour Plots of Solution Space: **A3** 173
61 Surface Plots of Solution Space: **A3** 174
62 Contour Plots of Solution Space: **A1** 175
63 Surface Plots of Solution Space: **A1** 176
64 Contour Plots of Solution Space: **A2** 177
65 Surface Plots of Solution Space: **A2** 178
66 Contour Plots of Unimodal Solution Spaces: **A1** & **A3** 181
67 Surface Plots of Unimodal Solution Spaces: **A1** & **A3** 182
68 Contour Plots of Solution Space: **A2** 183
69 Surface Plots of Solution Space: **A2** 184
70 Contour Plots of Unimodal Solution Space: **A2** 187
71 Surface Plots of Unimodal Solution Space: **A2** 188
72 Examples of Multi-modal Function Space 200
73 Ragone Plot of Various Power Plants 203
74 Notional Result of Mission Space Exploration 204
75 AeroVironment's Helios Prototype 210
76 Daily Energy Balance Diagrams 211
77 Internal Fuselage Arrangement of Emissionless Transport 212
78 GRC's Baseline PEMFC Aeropropulsion System Architecture 216
79 Quiet Green Transport 218
80 GRC's Baseline SOFC/GT Hybrid Power Plant Architecture 220
81 NRL's Fuel Cell Powered MAV 223
82 AeroVironment's Fuel Cell Powered Aircraft 224
83 Boeing's Planned Fuel Cell Demonstrator Airplane 226
84 Fuel Cell Powered Aerovehicles in New Era of Aviation 229
85 Georgia Tech Fuel Cell Demonstrator Aircraft 232

86 Fuel Cell Powered UAV at California State University, Los Angeles . 233
87 On- and Off-Design Analysis Structure 235
88 Example Performance Map of a Conventional Electric Motor 237
89 Advanced Optimizer Settings 246
90 Optimization Flow Map of Two-Stage Formulation 247
91 Two-Stage Optimization Results 248
92 Optimal First-Stage Design Decisions 249

LIST OF SYMBOLS OR ABBREVIATIONS

CO Carbon monoxide.

CO_2 Carbon dioxide.

KOH Potassium hydroxide.

AC Alternating Current.

ADVISOR ADvanced VehIcle SimulatOR.

AEDsys Aircraft Engine Design system analysis.

AFC Alkaline Fuel Cell.

AIAS Architecture-Independent Aircraft Sizing.

APU Auxiliary Power Unit.

BFGS Broydon-Fletcher-Goldfarb-Shanno.

BLDC BrushLess Direct Current.

BOP Balance Of Plant.

CAD Computer-Aided Design.

CAE Computer-Aided Engineering.

CCP Chance-Constrained Programming.

CDF Cumulative Distribution Function.

CEA-CREST Center for Environmental Analysis-Center for Research Excellence in Science and Technology.

CFD Computational Fluid Dynamics.

CHP Combined Heat and Power.

CPOX Catalytic Partial OXidation.

DC Direct-Current.

DEP Deterministic Equivalent Program.

DIR Direct Internal Reformation.

DMFC Direct Methanol Fuel Cell.

DoE	Department of Energy or Design of Experiments.
DSM	Design Structure Matrix.
DSS	Deterministic Solution Sampling.
EEV	Expected result of using the EV Solution.
ERAST	Environmental Research Aircraft and Sensor Technology.
EV	Expected Value.
EVPI	Expected Value of Perfect Information.
FAR	Federal Aviation Regulation.
FCV	Fuel Cell Vehicle.
FEA	Finite Element Analysis.
FLOPS	FLight OPtimization System.
GA	General Aviation or Genetic Algorithm.
GRC	Glenn Research Center.
GT	Gas Turbine.
HAPP	High Altitude Powered Platform.
HHV	Higher Heating Value.
HSCT	High-Speed Civil Transport.
HTS	High Temperature Superconductor.
ICE	Internal Combustion Engine.
IGBT	Insulated Gate Bipolar Transistor.
IIR	Indirect Internal Reformation.
IPT	Integrated Product Team.
IRMA	Interactive Reconfigurable Matrix of Alternatives.
JPDM	Joint Probabilistic Decision Making.
LAGER	Low Altitude Greatly Extended Range.
LaRC	Langley Research Center.
LDFL	LanDing Field Length.

LHV Lower Heating Value.

MAV Micro Aerial Vehicle.

MCFC Molten Carbonate Fuel Cell.

MCS Monte Carlo Simulation.

MFDCLab Multidisciplinary Flight Dynamics and Control Laboratory.

MOSFET Metal Oxide Semiconductor Field Effect Transistor.

MPP Maximum Power Point.

MRE Model Representation Error.

NASA National Aeronautics and Space Administration.

NAVAIR NAVal AIR systems command.

NEPP NASA Engine Performance Program.

NFCRC National Fuel Cell Research Center.

NN Neural Network.

NPSS Numerical Propulsion Systems Simulation.

NRL Naval Research Laboratory.

OEC Overall Evaluation Criterion.

OTS Off The Shelf.

PAFC Phosphoric-Acid Fuel Cell.

PASM Probabilistic Aircraft Sizing Method.

PEMFC Proton Exchange Membrane Fuel Cell.

PMAD Power Management And Distribution.

POX Partial OXidation.

PV PhotoVoltaic.

R&D Research and Development.

RDS Robust Design Simulation.

RFC Regenerative Fuel Cell.

RFP Request For Proposal.

RSM Response Surface Methodology.

SLS Sea Level Static.

SOFC Solid Oxide Fuel Cell.

SR Switched Reluctance.

TOFL Take-Off Field Length.

TOS Time On Station.

TPM Technical Performance Measure.

TRL Technology Readiness Level.

TSF Thrust Scaling Factor.

TSFC Thrust Specific Fuel Consumption.

UAPT URETI on Aeropropulsion Technology.

UAV Unmanned Aerial Vehicle.

URETI University Research, Engineering, and Technology Institute.

URFC Unitized Regenerative Fuel Cell.

VSS Value of Stochastic Solution.

WATE Weight Analysis of Turbine Engines.

ABSTRACT

The past few decades have witnessed a growing interest in the engineering communities to approach the handling of imperfect information from a quantitatively justifiable angle. In the aerospace engineering domain, the movement to develop creative avenues to nondeterministically solving engineering problems has emerged in the field of aerospace systems design. Inspired by statistical data modeling and numerical analysis techniques that used to be relatively foreign to the designers of aerospace systems, a variety of strategies leveraging upon the probabilistic treatment of uncertainty has been, and continue to be, reported. Although each method differs in the sequence in which probabilistic analysis and numerical optimization are performed, a common motif in all of them is the lack of any built-in provisions to compensate for infeasibilities that occur during optimization. Constraint violations are either strictly prohibited or striven to be held to an acceptable probability threshold, implying that most hitherto developed probabilistic design methods promote an avoid-failure approach to developing aerospace systems under uncertainty.

It is the premise of this dissertation that such a dichotomous structure of addressing imperfections is hardly a realistic model of how product development unfolds in practice. From a time-phased view of engineering design, it is often observed that previously unknown parameters become known with the passing of each design milestone, and their effects on the system are realized. Should these impacts happen to be detrimental to critical system-level metrics, then a compensatory action is taken to *remedy* any unwanted deviations from the target or required bounds, rather than starting the process completely anew. Anecdotal accounts of numerous real-world design projects confirm that such remedial actions are commonly practiced means

to ensure the successful fielding of aerospace systems. Therefore, formalizing the *remedial* aspect of engineering design into a new methodological capability would be the next logical step towards making uncertainty handling more pragmatic for this generation of engineers.

In order to formulate a nondeterministic solution approach that capitalizes on the practice of compensatory design, this research introduces the notion of *recourse*. Within the context of engineering an aerospace system, recourse is defined as a set of corrective actions that can be implemented in stages later than the current design phase to keep critical system-level figures of merit within the desired target ranges, albeit at some penalty. The terminology is inspired by the concept of the same name in the field of statistical decision analysis, where it refers to an action taken by a decision maker to mitigate the unfavorable consequences caused by uncertainty realizations. Recourse programs also introduce the concept of *stages* to optimization formulations, and allow each stage to encompass as many sequences or events as determined necessary to solve the problem at hand. Together, these two major premises of classical stochastic programming provide a natural way to embody not only the remedial, but also the temporal and nondeterministic aspects of aerospace systems design.

A two-part strategy, which partitions the design activities into stages, is proposed to model the bi-phasal nature of recourse. The first stage is defined as the time period in which an *a priori* design is identified before the exact values of the uncertain parameters are known. In contrast, the second stage is a period occurring some time after the first stage, when an *a posteriori* correction can be made to the first-stage design, should the realization of uncertainties impart infeasibilities. Penalizing costs are attached to the second-stage corrections to reflect the reality that getting it done right the first time is almost always less costly than fixing it after the fact. Consequently, the goal of the second stage becomes identifying an optimal solution

with respect to the second-stage penalty, given the first-stage design as well as a particular realization of the random parameters. This two-stage model is intended as an analogue of the traditional practice of monitoring and managing key Technical Performance Measures (TPMs) in aerospace systems development settings. Whenever an alarmingly significant discrepancy between the demonstrated and target TPM values is noted, it is generally the case that the most cost-effective recourse option is selected, given the available resources at the time as well as scheduling and budget constraints.

One obvious weakness of the two-stage strategy as presented above is its limited applicability as a forecasting tool. Not only cannot the second stage be invoked without a first-stage starting point, but also the second-stage solution differs from one specific outcome of uncertainties to another. On the contrary, what would be more valuable given the time-phased nature of engineering design is the capability to perform an anticipatory identification of an optimum that is also *expected* to incur the least costly recourse option in the future. It is argued that such a solution is in fact a more balanced alternative than robust, probabilistically maximized, or chance-constrained solutions, because it represents trading the design optimality in the present with the potential costs of future recourse. Therefore, it is further proposed that the original two-stage model be embedded inside a larger design loop, so that the realization of numerous recourse scenarios can be simulated for a given first-stage design. The repetitive procedure at the second stage is necessary for computing the expected cost of recourse, which is equivalent to its mathematical expectation as per the strong law of large numbers. The feedback loop then communicates this information to the aggregate-level optimizer, whose objective is to minimize the sum total of the first-stage metric and the expected cost of future corrective actions. The resulting stochastic solution is a design that is well-hedged against the uncertain consequences of later design phases, while at the same time being less conservative than

a solution designed to more traditional deterministic standards.

As a proof-of-concept demonstration, the recourse-based solution approach is presented as applied to a contemporary aerospace engineering problem of interest - the integration of fuel cell technology into uninhabited aerial systems. The creation of a simulation environment capable of designing three system alternatives based on Proton Exchange Membrane Fuel Cell (PEMFC) technology and another three systems leveraging upon Solid Oxide Fuel Cell (SOFC) technology is presented as the means to notionally emulate the development process of this revolutionary aeropropulsion method. Notable findings from the deterministic trade studies and algorithmic investigation include the incompatibility of the SOFC based architectures with the conceived maritime border patrol mission as well as the thermodynamic scalability of the PEMFC based alternatives. It is the latter finding which justifies the usage of the more practical specific-parameter based approach in synthesizing the design results at the propulsion level into the overall aircraft sizing framework. The ensuing presentation on the stochastic portion of the implementation outlines how the selective applications of certain Design of Experiments, constrained optimization, Surrogate Modeling, and Monte Carlo sampling techniques enable the visualization of the objective function space. The particular formulations of the design stages, recourse, and uncertainties proposed in this research are shown to result in solutions that are well compromised between unfounded optimism and unwarranted conservatism. In all stochastic optimization cases, the Value of Stochastic Solution (VSS) proves to be an intuitively appealing measure of accounting for recourse-causing uncertainties in an aerospace systems design environment.

Chapter I

INTRODUCTION

In light of the continued increases in computational capabilities, combined with the growing availability of user-friendly process integration and design optimization software, nondeterministic solution approaches to aerospace systems design problems are fast becoming practical for this generation of engineers. Such systems-oriented strategies come in many different guises, but virtually all of them can be characterized as methods to address the presence of imperfect information in the engineering design process. Consequently, improved elicitation of decision-critical information is possible, leading to a solution that is balanced in terms of performance, cost, quality, and various *-illities* (*e.g.*, reliability, survivability, etc). Gone are the days of traditional, deterministic approaches to product development, for which the drive towards maximum performance has been the dominating objective.

A broader scrutiny of engineering design reveals that it is inherently a multi-step process. Taking the aerospace domain as an example, all design-related activities fall under one of the major phases, which is executed in the order of conceptual design, preliminary design, detail design, manufacturing, production, and operations & support. In contrast, most hitherto developed nondeterministic methods are single-stage strategies that focus on the early phases of product development. The rationale behind front-loading the development cycle with advanced design techniques has been argued to provide improved decision-support. More insightful information about the effects of various sources of incomplete knowledge can be made available sooner rather than later, such that the rest of product development is led in the direction that maximizes the chances of attaining desirable outcomes.

Nevertheless, a single-stage approach to accounting for imperfections is not a realistic model of how the engineering process unfolds in practice. It is often the case that previously unknown parameters become known with the passing of each design milestone, and their effects on the system are observed. Should such realized impacts happen to be detrimental to critical figures of merit, then a compensating action is taken to *fix* such shortcomings, rather than starting completely anew. There would naturally be some cost associated with making the corrections after the fact. If the designer had possessed perfect information from the beginning, such extra efforts would have been entirely unnecessary. Indeed, this notion of *no free lunch*, which is one of the tried-and-tested axioms of aerospace systems design, applies here prominently.

The shaping of this dissertation research was influenced by the idea that a formal approach capitalizing on the concept of design compensations would result in a more pragmatic aerospace systems design method. The desired outcome from such real-world situations is the *here-and-now* identification of a solution that is not only optimal in terms of a relevant performance metric, but is also the one that will, on average, cost the least for any future corrective actions.

1.1 Thesis Organization

The research documented herein culminates in the formulation of a nondeterministic solution approach, which leverages on the notion of *recourse*. The term is inspired by its usage in the field of stochastic programming, which means an action taken by the decision-maker to compensate for infeasibilities caused by the realization of random parameters. In the context of engineering an aerospace system, the term *recourse* is henceforth defined as follows:

> Recourse: A set of corrective actions that can be implemented in stages later than the current design phase to keep critical system-level figures of

merit within the desired target ranges, albeit at some penalty.

The case for a recourse-based solution approach is built by presenting a proof-of-concept application to a modern aerospace engineering problem. Ultimately, several generalizations are extracted from the results to showcase the potential of expanding the application of the method to beyond the early phases of product development.

The organization of this document largely follows the progression of the scientific method, with terminology borrowed from Borer [1]. Beginning with a motivating aerospace problem of interest, several key observations are presented in the introductory chapter. The term **Observation** takes on a specific meaning in this body of work, and it is defined as "a summarized statement of insight into a particular phenomenon gained from literature, anecdotal evidence, or experience." Following one or more such observations, a formal query is raised under the title of a **Research Question**. Delineating the question serves to establish a clear context for pursuing a particular path of literary and scientific investigation, which leads to either more observations and, thus, further research questions, or conclusions that form the basis of a hypothesis. A **Hypothesis** is henceforth understood to be a "proposed solution to one or more research questions that can be tested with a variety of experiments." Lastly, the reader is directed to a multi-faceted **Research Task**. Each sub-task is designed to test the validity of a corresponding hypothesis. These formalized statements are strategically placed throughout this document in order to present the major foundational topics in a logical sequence. Wherever appropriate, key concepts and ideas are repeated to remind the reader about the objective and scope of this dissertation.

1.2 Motivation

The genesis of this thesis work can be traced back to the author's participation in the University Research, Engineering, and Technology Institute (URETI) cooperative agreement. One of the core visions of the URETI for Aeropropulsion & Power

Technology (UAPT) at its inception was "to develop revolutionary technologies and design methods in a systems-oriented environment." [2] Because the terms *revolutionary technology* are often used open-endedly in general aerospace literature, the following definitions suggested by McClure [3] are adopted herein to avoid any further ambiguity.

> Evolutionary Technology: a technological development that will incrementally advance the state of the art by improving upon one element of a system.
>
> Revolutionary Technology: a technological development or theoretical concept that initiates a fundamental change in the way that the existing system operates or makes such change possible.

From the earliest phases of the UAPT effort, fuel cells were considered as the foundational revolutionary technology around which method-oriented research thrusts were to be conducted. Fuel cell aeropropulsion technology qualifies as revolutionary technology according to the definitions given above, if the boundaries of what constitutes the system are limited to an aircraft's power plant. The manner in which a fuel cell power plant operates (direct generation of electricity from chemical fuel without combustion), as detailed in §1.2.1, does reflect a fundamental departure from the operating principles of existing aircraft engines (generation of mechanical power through combustion of chemical fuel).

Apart from being selected to support UAPT goals, there are a number of other compelling reasons to advance the general understanding of fuel cells in the aerospace domain. As the technological maturity, reliability, and cost-effectiveness of fuel cells continue to advance as shown in Figure 1, the case for considering the aeronautical applications of this particular energy-conversion technology grows stronger. Such

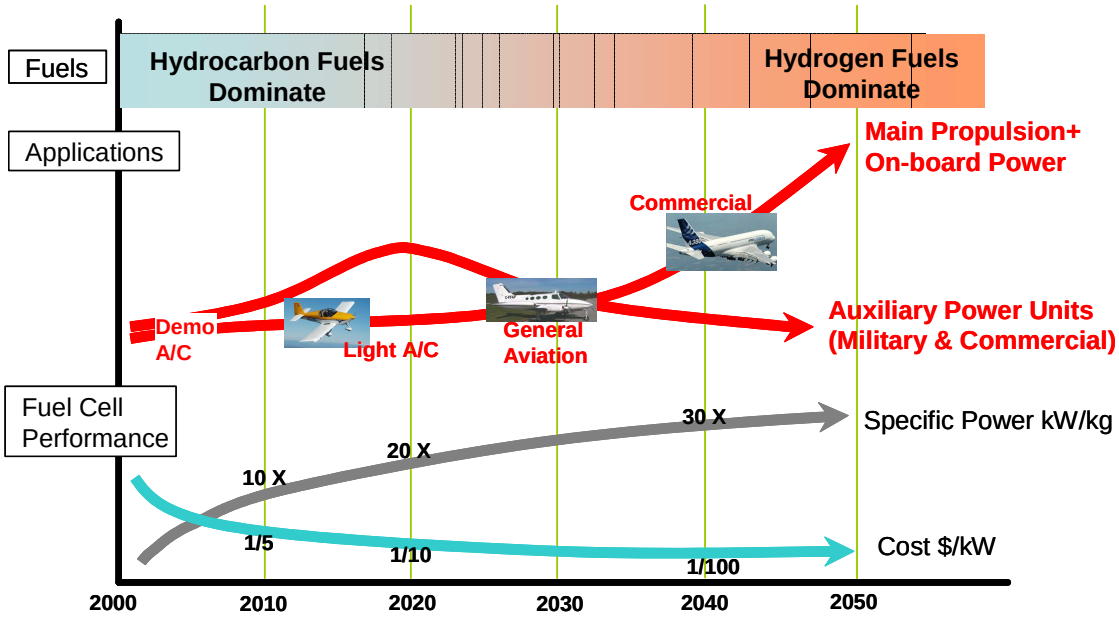

Figure 1: Envisioned Aviation Applications of Fuel Cell Technology [4]

applications are likely to contribute toward reducing the environmental impact of aviation, which has been an increasing concern as of late. The inherently higher thermal efficiency of fuel cell systems, when compared to existing gas turbine (GT) engines, also implies that the technology could enable new types of missions and aerovehicle systems, which could have major implications for both civilian and military aviation.

It was not long before a realization was made that there were largely two outstanding issues to be addressed within the confines of systems-oriented research. First, there appeared to be a need to conduct an algorithmic investigation into the manner in which fuel cell aeropropulsion systems should be parametrically modeled and simulated for the purpose of design. Secondly, the larger need for a nondeterministic strategy, which takes the remedial aspect of engineering design into consideration, became noticeable. Both of these needs ultimately inspired the conception of a recourse-based solution approach, whose appropriateness as an engineering formalism was to be demonstrated through the design of notional fuel cell aeropropulsion systems.

1.2.1 Fuel Cell Basics

In the forthcoming hydrogen economy, fuel cells are envisioned to be a key enabling technology that allows the conversion of hydrogen to electricity with limited adverse environmental consequences. A fuel cell is formally defined as a variant of galvanic cells, which directly convert the chemical Gibbs free energy into electricity via an electrochemical reaction[1]. This electrochemical reaction is dependent on the two-part process of reduction and oxidation, collectively known as a redox reaction. The typical base reactants are hydrogen (reductant/fuel) and oxygen (oxidant), and the only product from the electrochemical reaction is pure water. Fuel cells are different from other forms of galvanic cells, such as batteries, in their manner of reactant storage and consumption; base reactants are supplied as reactant streams from an external source instead of being stored in situ, and only the reactants are consumed as part of the electrochemical half-cell kinetics. Basic fuel cell components include flow fields for the reactant streams, current collectors, at least one electrolyte and two electrodes to support the redox half-cell reactions, and bipolar plates or interconnects for integrating individual cells into a fuel cell stack.

An electrode of a galvanic cell is referred to either as an anode or a cathode, depending on the nature of the half-cell reaction that takes place on its triple phase boundaries. The most general definition is that the anode is the electrode at which oxidation (the liberation of electrons) occurs, and the cathode is where reduction, which is the exact opposite process, happens. The same definitions are applicable to fuel cells. In non-regenerative fuel cells, the anode is the negative (lower potential) electrode from which electrons headed towards a load emerge and the cathode is the positive (larger potential) electrode that receives the electrons passed through the load.

[1]The primary source of information on fuel cells used throughout this dissertation is Larminie and Dicks [5], unless otherwise noted.

Table 1: Classification of Fuel Cell Technologies

Fuel Cell Type	Operating Temp. (ºC)	Premier Applications
Alkaline	90 - 100	Space Military 
Proton Exchange Membrane	30 - 100	Transportation 
Direct Methanol	20 - 90	Portable 
Phosphoric Acid	150 - 220	Stationary 
Molten Carbonate	600 - 700	Stationary 
Solid Oxide	500 - 1100	Stationary Transportation 

Fuel cells are conveniently classified according to their electrolyte type. Some of the more prevalent types of fuel cells are listed in Table 1, along with their range of operating conditions and application potential. It appears that fuel cells can be distinctly classified by temperature, just as well as by electrolyte, and this is not by coincidence. The physicochemical characteristics of the electrolyte dictates the range of possible operating temperatures of a fuel cell, and the temperature range, in turn, impacts the thermomechanical requirements of the various cell components. Additionally, a cell's operating temperature is related to the type and form of fuel it can oxidize, which ultimately leads to system-level considerations, such as fuel storage and reformation. Low-temperature fuel cells typically require pure hydrogen due to the presence of the anode catalyst that cannot tolerate carbon monoxide (CO) or carbon dioxide (CO_2) and will either need a large reservoir of pure hydrogen or costly and complex devices capable of producing high-quality hydrogen. On the contrary, high-temperature fuel cells are more tolerant to such impurities and are even capable

of using some as part of the redox process. They also possess the additional benefit of being able to recycle waste heat in, a process known as combined heat and power (CHP) or cogeneration. Nevertheless, high-temperature operation has its own lists of disadvantages, namely slow start-up time, significant thermal shielding requirements, and low durability .

Regardless of its type, the electrolyte in a fuel cell electrically bridges the anode and the cathode by conducting ions from one electrode to the other, while keeping the fuel and oxidant streams separated. Depending on the kind of ions that permeate through the electrolyte, a fuel cell can either be cationic or anionic. Cationic fuel cells are typically low-temperature cells, whose electrolytes conduct cations (hydrogen protons) from the anode to the cathode. Anionic fuel cells are usually high-temperature cells, whose electrolytes conduct anions (oxygen ions) from the cathode to the anode. Figure 2 shows the operation of cationic and anionic fuel cells. Note how the location of product (water) formation changes, but the direction of the electron flow remains the same. Such a direct energy conversion process without any thermodynamic cycles

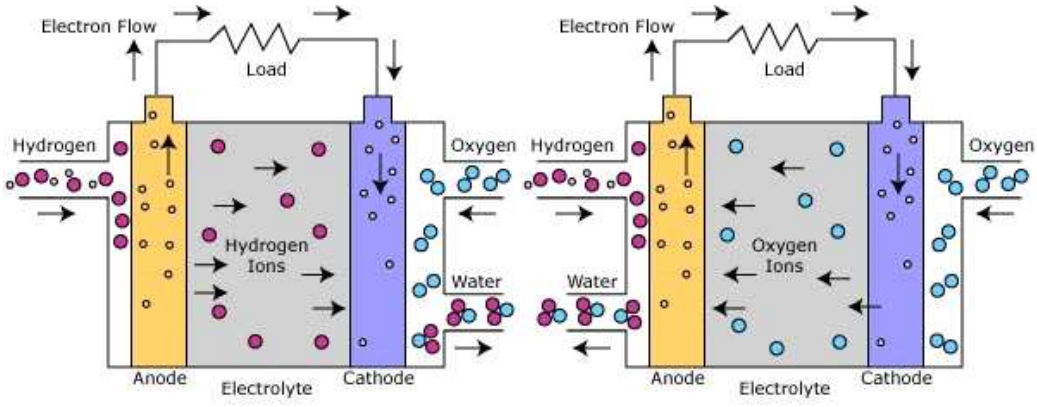

(a) Cationic (Low Temperature) Fuel Cell (b) Anionic (High Temperature) Fuel Cell

Figure 2: How Fuel Cells Operate [6]

associated with combustion or rotating parts results in an environmentally neutral, silent, and efficient method of harnessing electrical power. State of the art efficiency figures of fuel cells are reported at electrical efficiencies on the order of 50% at rated

power and 60% at quarter-power for large low-temperature fuel cell systems [7]; 23% to 36% electrical efficiencies for smaller cells [8]; and overall thermal efficiencies that approach 85% when high-temperature fuel cell systems are used for CHP applications [9].

Alkaline fuel cells (AFCs) have become famous for their usage in the U.S. Space Program, first in the Apollo-series missions to the moon [10] and later in the Space Shuttle Program [11]. The name is derived from an aqueous alkaline solution, usually potassium hydroxide (KOH), that serves as the electrolyte. Potassium hydroxide happens to be one of the cheapest standard chemicals available in the market, and coupled with the fact that the cathode of an AFC can be made of non-precious metals, AFCs will most likely continue to remain the least expensive kind of fuel cells to manufacture. However, KOH can easily be poisoned by even trace amounts of CO_2 in the atmosphere, a key disadvantage that has been attributed to the technology's limited success in commercialization [12]. Although the technology's crucial role in modern fuel cell history is well acknowledged, the relative importance of AFCs has been declining in recent years, and especially so with the commercial success of proton exchange membrane fuel cells (PEMFCs).

Proton exchange membrane, or polymer electrolyte membrane, fuel cells are currently considered to be the leading technology for future vehicular applications [13]. The latest survey of fuel cell prototype or demonstration automobiles (including buses) known to date in the U.S. reveals that more than 90% of these vehicles have employed PEMFCs as their power plants [14, 15]. Such a widespread acceptance of PEMFCs in the automotive industry is often credited to the following attributes, which make the technology especially suitable for passenger vehicles: compactness, *i.e.*, high specific power (power-to-weight ratio) and volumetric density (power-to-volume ratio); fast start-up time; high durability; and low temperature operation. At present, PEMFCs are arguably the most technologically mature among all fuel cells,

but this has not always been the case. Ballard Power Systems is principally responsible for resurrecting the technology in the 1980's. Prior to 1984, PEMFCs had lost out in favor of AFCs to the Apollo missions, despite the fact that it was the first operational fuel cell technology to be on board a manned spacecraft - the Gemini 3 [16]. Substantial investment in the technology over the past decade has allowed many improvements to be made in enhancing the performance and cost characteristics of PEMFCs; however, the same challenges responsible for the downfall of the technology in the late 1960s still persist. Water management, which has a direct influence on cell performance, is non-trivial; the usage of platinum is still a cost-driver, and hydrogen of the utmost purity is required to prevent CO-poisoning of the membrane. Direct methanol fuel cells (DMFCs) are essentially PEMFCs that are fed with liquid methanol [17], but their power densities are still an order of magnitude smaller than hydrogen-fueled PEMFCs [18]. Consequently, DMFCs are envisioned to be more suitable for low-power, high-energy applications, such as replacements for batteries in portable electronics [19].

Having been developed almost exclusively for stationary applications, such as distributed power generation, phosphoric-acid fuel cells (PAFCs) are best described as medium-temperature cells. The operating temperature is higher than that of a PEMFC, but it is not high enough to do without noble-metal catalysts. As the name implies, liquid phosphoric acid, contained in a Teflon-bonded silicon carbide matrix, is the electrolyte. The basic operating principles are similar to that of a PEMFC, that is, PAFCs are cationic, but unlike PEMFCs, PAFCs have meaningful cogeneration capability and are more tolerant to CO than PEMFCs, allowing moderately efficient CHP systems with external fuel reformers to be built. Such characteristics make PAFCs suitable as stand-alone or backup power generation devices at distributed, premium-power installations such as banks, hospitals, and research facilities. Because PAFC technology was the first fuel cell technology to be commercialized, its reliability

and power quality have been demonstrated over the years in real operations [20]. There is at least one occasion in which the technology was used to power a bus [21, 22].

The last two types of fuel cells listed in Table 1 utilize high-temperature fuel cell technology. Molten carbonate fuel cells (MCFCs) are appropriately named due to the molten mixture of alkali metal carbonates that are retained in a chemically inert, ceramic matrix of lithium aluminum oxide. Operating temperatures exceeding the range of PAFCs allow MCFCs to employ less expensive non-precious metals as electrocatalysts at the electrodes, and also make it possible to internally reform the supplied fuel stream within the stack, further reducing cost [23]. MCFCs are unique in the sense that CO_2, in addition to oxygen, is required at the cathode to carry out the redox reactions. This, coupled with the fact that CO can be used as fuel instead of hydrogen, makes MCFCs particularly suitable for centralized, natural gas and coal-based power plants and marine applications, where giant "Hot Module" type assemblies and slow-startup time (around 14 to 16 hours) are deemed less important than the advantages provided by cogeneration and fuel flexibility [24]. The status of the technology seems to be closely following that of PAFC, with a number of developers in the U.S., Europe, and Asia actively pursuing commercialization [25].

Operating in temperature regions beyond those of MCFCs, the electrolyte of solid oxide fuel cells (SOFCs), which is made out of oxide ion-conducting ceramic material, nonetheless remains in its solid-state [26]. The resulting mechanical simplicity allows the shaping of SOFCs into different geometric configurations, such as tubes, planes, and monoliths. Similar to MCFCs, SOFCs are capable of oxidizing CO instead of hydrogen. Nevertheless, the difference between the two technologies is that SOFCs, unlike MCFCs, do not require CO_2 at the cathode, and the higher operating temperatures of SOFCs allow internal reforming to be carried out at the anode without additional catalysts [27]. Another distinct opportunity of SOFC technology is that

bottoming cycles, either with a steam turbine or a GT, are now feasible, in addition to simpler CHP implementations [28]. The demonstration of the practicality of such SOFC/GT hybrid systems is a relatively new occurrence, making this an area of active research in the SOFC community [29]. Lastly, recent advances in lower, intermediate-temperature SOFCs [30], as well as planar SOFC stack designs, have made the applications of SOFC systems to be realized on a much smaller scale than previously thought practical; for instance, as an auxiliary power source on ground vehicles [31, 32, 33, 34].

The rate at which fuel cell technology has advanced during its relatively short history in the automotive sector has been remarkable. Figure 3 shows that a seven-fold increase in the specific power of PEMFC systems was achieved in just five years, a trend which can be corroborated from other publicly available sources [35]. Such

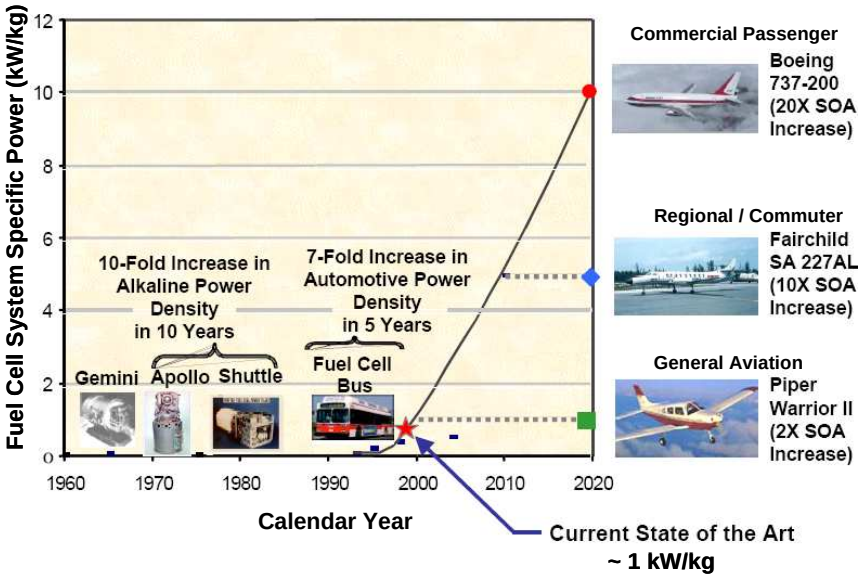

Figure 3: Past and Projected Improvement in Fuel Cell System Specific Power [36]

a high rate of demonstrated growth forms an encouraging basis for considering the aeronautical applications of the technology, as it implies that certain types of fuel cells may be realizable for aviation within the transitory time frame to the hydrogen economy. Figure 3 is essentially a graphical representation of this perception

since it shows the extrapolation of past improvement rates of PEMFC systems to 2020. Although Figure 1 shows a different extrapolation, and thus a different projection for when it may be possible for fuel cells to penetrate various segments of the aircraft transportation sector, the crux of the message is the same: continued "advances in fuel cell technology ... power densities, promoted by automotive and other transportation sectors, will eventually displace combustion-based propulsion in the aviation industry." [37]

1.2.2 Algorithmic Investigation

The capability to quantify the geometric scale, as well as the propulsive scale of an aerovehicle, known as *aircraft sizing*, is universally considered to be the cornerstone of modern aerovehicle design work. It is usually the first step in the chain of analysis activities, without which a new vehicle design is never done. Aircraft sizing is intrinsically a cross-disciplinary task, requiring the synthesis and concurrent execution of, at minimum, aerodynamic, structural, and propulsion analysis capabilities. For conceptual aerovehicle design work, it is often sufficient to idealize the information provided by aerodynamics and structures as drag polars and simplified weight estimation relationships for a given airframe configuration. The traditional algorithmic approach to incorporating the disciplinary knowledge of aeropropulsion system designers is through the utilization of engine *decks*, which capture the thermodynamic performance of a notional engine, and its weight scaling law.

Such propulsion-level analysis capability is currently the missing link in the creation of an algorithmic process for conceptually designing a fuel cell powered aerovehicle. This is in stark contrast to the state-of-the-art engine design capability, which has now become common knowledge in the airbreathing jet propulsion circles. Decades of numerous commercial and military engine development programs have culminated in a grand repository of publicly available knowledge. For example, collegiate-level

textbooks precisely outline the conceptual engine design process; typical ranges for design parameter and figure of merit values; and rules-of-thumb type approaches for a wide family of engine architectures. Many years of trial and error have also established a general consensus on the type of aviation missions a given engine architecture is best suited for.

Unfortunately, none of the capabilities enumerated above are yet sufficiently mature in the fledgling field of fuel cell aeropropulsion. This predicament is formally recognized as the following generalized observation:

> **Observation 1:** Limited disciplinary knowledge with regards to a revolutionary type of aeropropulsion system impedes the cavalier application of traditional aircraft sizing and synthesis algorithms.

In short, there exists a vacuum of well-established and traceable modeling and simulation algorithm for creating a new fuel cell aeropropulsion system architecture that is optimized according to certain needs, requirements, or missions; quantitatively estimating the performance and size of the chosen architectural elements (*i.e.*, subsystem components) based on first-order physical principles; and implementing the quantitative analysis and sizing of the aeropropulsion system. Until the above elements become readily available, no prior assumptions regarding the best practice to integrate the results of the design activities at the propulsion level into the overall aircraft sizing process can be made about an unprecedented aeropropulsion system.

1.2.3 Remedial Aspect of Engineering Design

There is little contention that the end-goal of any engineering design activity is to identify the *best* solution, or a group of solutions, according to one or more target criteria. Nikolaidis explains that the primary job of the designer is to discover a single "outcome" with the highest "payoff" amongst "alternative courses of action" [38]. One addendum to this is that the final solution should also be the one that

satisfies all design constraints, which, if violated, impart detrimental consequences to key system-level figures of merit (*e.g.*, weight, performance, and -illities such as feasibility, viability, reliability, etc).

From a temporal perspective, engineering design is a multi-phase process that gradually develops a product into perfection. The maturity of an aerospace system is often quoted to evolve along the six-tiered sequence of conceptual design, preliminary design, detailed design, manufacturing, production, and operations & support [39]. Raymer outlines a similar four-staged procedure of conceptual design, preliminary design, detail design, and fabrication [40] as the simplified design paradigm for developing aerospace vehicles. A more refined breakdown is given by Dieter [41] who re-defines Asimow's classic eight-phase engineering design process [42] into a four-phase conceptual design, three-phase embodiment design, and a single-phase detail design.

Such idealized process models of design are sufficient to enlighten the reader on the major activities that are performed per each milestone. Nevertheless, the textbook examples listed above neglect to highlight one aspect of design that is just as, if not more, critical to the success of a real engineering system, which shall be henceforth referred to as the *remedial* aspect of engineering design. The terminology serves to accentuate the fact that key system-level metrics are continuously monitored throughout the design phases, and if necessary, a set of *corrective actions* is authorized to maintain them within the desired or required bounds. For instance, the National Aeronautics and Space Administration (NASA) Systems Engineering Handbook recommends that such Technical Performance Measures (TPMs) should be those "that must fall within well-defined (quantitative) limits for reasons of system effectiveness or mission feasibility." [43] End-of-mission dry mass, injected mass, power demand, and a few other metrics are cited as appropriate high-level TPMs for the design of

planetary spacecraft. Should its injected mass be found to exceed the launch vehicle's payload specification mass, then it is explained that the project manager has a variety of recourse options depending on the severity of the violation, the point in time within the design phase, and available resources (*e.g.*, removal of an instrument, modification of mission objectives, and request for a larger launch vehicle).

An anecdotal account of Pratt & Whitney's engine development program provides a real-world example of recourse being practiced to keep a TPM in check. The following is an extended quote from Kandebo [44], which reports on the company's experience with two engine architectures, one for the conventional takeoff and landing (CTOL) configuration and the other for the short takeoff/vertical landing (Stovl) version of the F-35 Lightning II.

> Currently, the Stovl F135 is 72 lb. below the specification weight and 230 lb. above target weight. By definition, "target weight" is that which is 6% below the engine's not-to-exceed-weight; "specification weight" is that which is 3% below the not-to-exceed weight, Gostic said. All performance calculations are made using the not-to-exceed weight.
>
> "Right now we have a plan to get the Stovl engine to the target weight, and have identified a number of things to actually get the engine below the target," Gostic said.
>
> The story is similar for the CTOL version. "We are about 10 lb. above the target weight [for the F135 CTOL version] and 171 lb. below the specification weight," he said. As with the Stovl engine, Pratt is working on a number of areas that could bring CTOL engine weight below the target.

Although the article is elusive on the details of planned corrective actions, it nonetheless indicates that recourse is an important contributing element in the successful

fielding of an engineered system. This line of reasoning is formally acknowledged as:

> **Observation 2**: Recourse is both a recommended and commonly practiced means of ensuring the success of an aerospace system from a time-phased view of engineering design.

Here, success is viewed from the system's life-cycle perspective. It is thus interpreted to be measured in terms of how well the delivered system is capable of meeting or even exceeding all performance requirements and expectations.

Prior to a debate on the best option for recourse to be initiated, the job of monitoring key TPMs falls on the systems engineer. He or she is responsible for tracking the demonstrated value of a TPM against a pre-determined "planned profile" or "margin requirement" as shown in Figure 4. Whenever an alarmingly significant discrepancy between the planned and actual values is realized, it warrants a serious discussion on which corrective action should be taken, given the available resources at the time, as well as other managerial considerations, such as scheduling and budget constraints.

In light of the inevitability of recourse in an engineering design process, a *wait-and-see* philosophy like the one described above will not likely result in the most cost-effective corrective action. What would be more valuable from a project management standpoint is the ability to identify an optimal design that is also expected to incur the least amount of penalizing cost to correct future design phases. However, it is evident from Figure 4 that the trajectories of the demonstrated TPM values are difficult to predict with certainty. There could be a number of reasons for the variability in the TPM value, but one prominent cause is the presence of uncertainty, which can originate from a variety of sources. Kirby identifies the following as the sources from which imperfect information can arise in the design of an aerospace system: customer requirements, analysis tool fidelity, manufacturing tolerances, immature technologies, and uncontrollable, external factors, such as the cost of aviation fuel

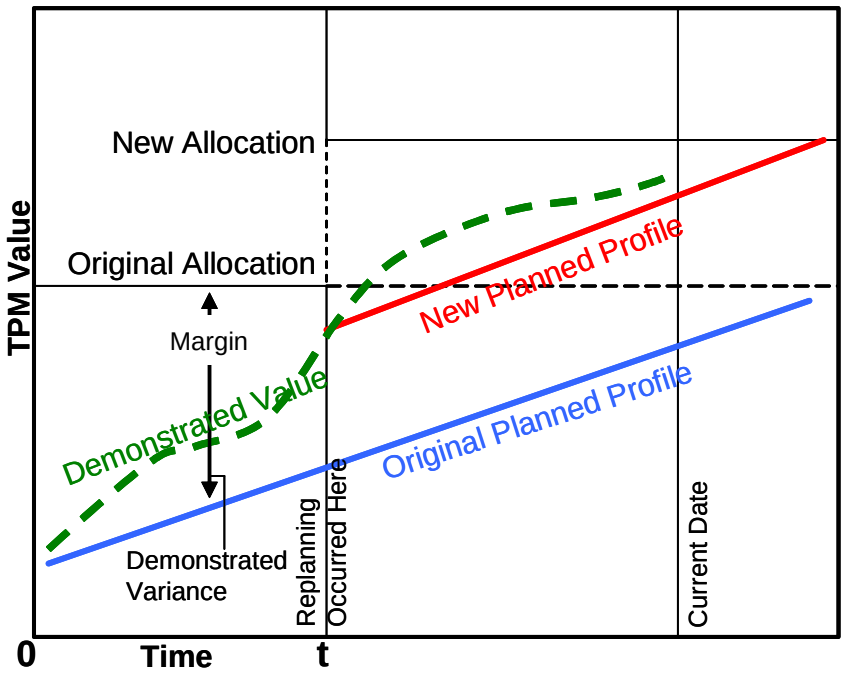

(a) Planned Profile Method

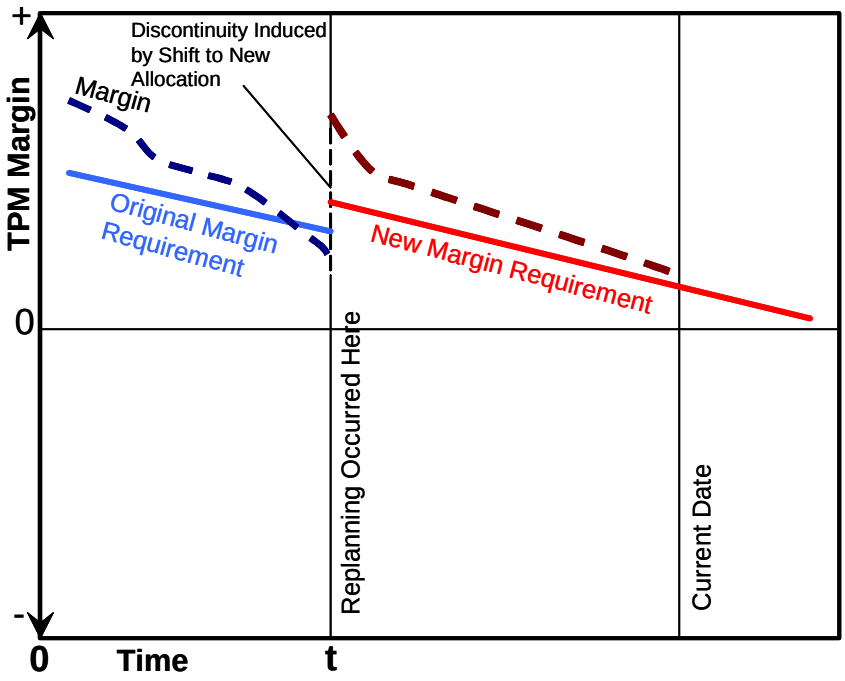

(b) Margin Management Method

Figure 4: Deterministic Monitoring and Management of TPM [43]

[45]. Regardless of its source, the presence of uncertainty is more of a burden than a boon to design engineers, as it complicates the evaluation of a point-solution in a deterministic manner. This dilemma is formally recorded as the final observation of this chapter:

> **Observation** 3: The anticipatory identification of a design optimum, which is also expected to be the least costly solution in terms of potential recourse, is complicated by the influence of various sources of uncertainty that persist throughout the system's development life cycle.

Both of the above-mentioned observations precipitated the literature review on optimization under uncertainty, which is the subject of Chapter 3.

Chapter II

GAS TURBINE AEROPROPULSION SYSTEMS

It is no secret that new technologies enable the engineering of unprecedented systems. The history of aviation is abound with such examples: *e.g.*, cantilevered-wing, modern jet engines, etc. According to Maier and Rechtin [46], the secret behind the success of such revolutionary systems has been a strong function of "someone's vision of where [the new technology] can be applied to advantage." This implies that the process of designing a particular technology-driven system is just as important as the underlying technology itself.

As far as the fuel cell aeropropulsion system is concerned, however, the idiosyncrasies regarding its conceptual design process is yet to be elucidated. The first observation introduced in §1.2.2 serves to underline the specific lack of a modeling and simulation algorithm that enables the assessment of the system's performance and gravimetric qualities from an aircraft sizing and synthesis perspective. Because it is often the case that multiple design alternatives must be quantitatively compared to one another during conceptual aerovehicle design work, it is preferable to have an algorithm that is balanced, in terms of accuracy and speed. This insight led to the declaration of the first research question:

> **Question 1**: Without sacrificing analysis accuracy, what algorithmic approach would result in a computationally efficient synthesis of a fuel cell aeropropulsion system design environment into an aircraft sizing framework? (Observation 1)

In an attempt to establish both a theoretical and a procedural benchmark for comparing alternative enabling technologies of aeropropulsion, a literature review of traditional GT engines was done with an emphasis on their design aspect. What follows is an introduction to the conceptual design process of GT aeropropulsion systems as recommended by the leading authors in the field.

2.1 Design Road Map

Mattingly defines an aeropropulsion system as "a unit submerged in a fluid medium about and through which the fluid flows" that consists of an engine, "an energy-transfer mechanism which increases the kinetic energy of the fluid passing through the system," and a housing unit, such as a nacelle or a duct, about the engine [47]. Systems whose engines rely on the principle of GT propulsion have become the principal means of aeropropulsion since the emergence of the turbojet engine in the late 1930s. Figure 5 shows the road map process of designing a new GT aeropropulsion system. The highlighted elements within the figure are of particular relevance to this dissertation since they are the two steps that constitute the core of conceptual engine design activities[1].

2.2 Cycle Analysis

Both "thermodynamic design point studies" and "off-design performance" of Figure 5 are two different manifestations of cycle analysis. Cycle analysis is the study of "thermodynamic changes of the working fluid (air and products of combustion in most cases) as it flows through the engine." [47] It is a form of quasi-one-dimensional gas dynamics pioneered by Frank E. Marble of the California Institute of Technology for designing aircraft GT propulsion systems and later refined and perfected by Oates [49], Kerrebrock [50], and Mattingly [47]. As a process, cycle analysis is initially

[1]Mattingly et al refer to this phase as the "preliminary propulsion design sequence." [48].

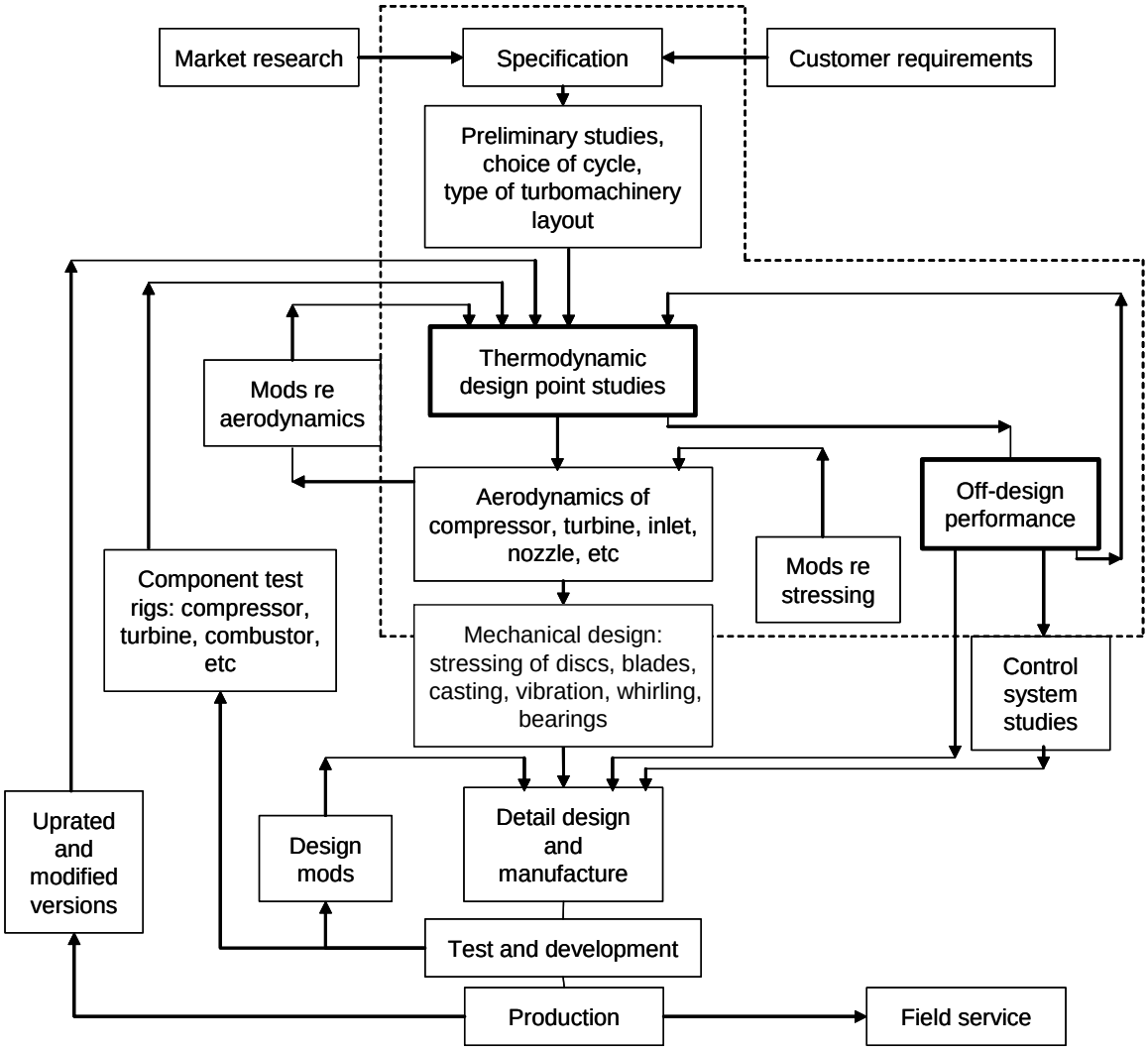

Figure 5: Design Process of Gas Turbine Aeropropulsion System [48]

implemented in two stages: thermodynamic design point studies or on-design analysis followed by off-design (performance) analysis. Subsequent iterations may become necessary between the two analyses until a satisfactory engine design is found.

Since the thermodynamic principles behind cycle analysis are based on the steady-state thermo and fluid dynamic aspects of the engine only, it cannot account for any aspects of the propulsion system related to the engine's housing or transients. The performance losses associated with installing an engine into a nacelle, for example, must be estimated via a procedure that is related to, but nonetheless separate from,

cycle analysis. Likewise, the analysis of transient engine performance is usually reserved for design phases beyond which cycle analysis is useful. Therefore, it is customary in literature to refer to the results of cycle analysis as *uninstalled*, steady-state aircraft engine performance[2].

2.2.1 On-Design Analysis

The first step of mathematically creating an aero engine is implementing on-design analysis. As the name implies, on-design analysis allows the performance evaluation of an engine at the operating condition it is designed to: *i.e., the design point*. Regardless of possible aero engine architectures (turbojet, turbofan, turboprop or turboshaft), the elements of a design point belong to one of the following categories: flight conditions, design limitations, component performance, and design choices [48]. Parameters representing forward flight Mach number, ambient pressure, and temperature allow the engine designer to choose an operating flight condition from a list of envisioned mission segments, such as sea level static (SLS), take-off, top-of-climb, cruise, loiter, etc. The performance of each GT engine component is modeled through the change in property ratios (*e.g.*, pressure and temperature), mass flow rates, and efficiency across the component. Parameters in the design limitations group are used to imposing upper limits on certain component efficiencies and temperatures in order to keep the engine's design within realistic bounds. The last category, design choices, contains high-level parameters that dictate the engine's cycle, such as fan pressure ratio, compressor pressure ratio, bypass ratio, stator outlet temperatures, etc. Hence, these input variables are also known as *cycle parameters* [51].

The primary figures of merit for measuring uninstalled engine performance are: specific thrust ($F/\dot{m}_0$); thrust specific fuel consumption (S); thermal, propulsive,

[2]Uninstalled engine performance *does* reflect losses due to the power extraction from low and high compressors, as well as the bleed air used for driving the mechanical, pneumatic, hydraulic, and auxiliary power systems.

and overall efficiencies (η_{TH}, η_P, η_O). Specific thrust is a fundamental performance metric to evaluate since, to a first-order, it is highly correlated with engine weight, frontal area, and volume. Generally it is advantageous to minimize thrust specific fuel consumption (TSFC), S, to save on both fuel weight and cost. A thorough engineer would provide the reference heating value, or enthalpy of formation, of the fuel used to evaluate S. Both η_{TH} and η_P are indicative of how efficiently the chosen cycle is able to first convert fuel energy to kinetic energy and later to transfer it to useful propulsive power. Overall efficiency is obtained by simply multiplying the other two efficiency figures.

The difficulty in proposing a proper on-design condition is that, theoretically, any operating condition can be chosen as the design point. This is less of an issue in the design of terrestial GT engines, for which it is customary to choose an operating point where the majority of primary function will take place. Such a practice is almost never done for a weight-conscious aero engine, whose design point is often matched to the flight condition requiring the most amount of thrust or power for a relatively shorter duration, such as during SLS or take-off. To complicate matters further, the design points of the various aero engine components, such as fans, compressors, combustors, turbines, mixers, afterburners, heat exchangers, etc., must be considered concurrently to minimize the deviation of each component's design point from that of the engine.

Fortunately, there exists a procedure for arriving at a suitable aero engine design point. Termed *parametric cycle analysis* by Mattingly et al, it is designed to facilitate the systematic repetition of on-design analysis, allowing the designer to observe a wide range of performance trends. Charts such as those shown in Figure 6 can aid in evaluating the ranges of flight conditions, for which a given engine type would be applicable. Conversely, the most promising engine type for a given mission requirement may be identified using the same charts. A carpet plot, similar to the one shown in Figure 7 for a notional turbofan engine type, is an especially useful tool for defining

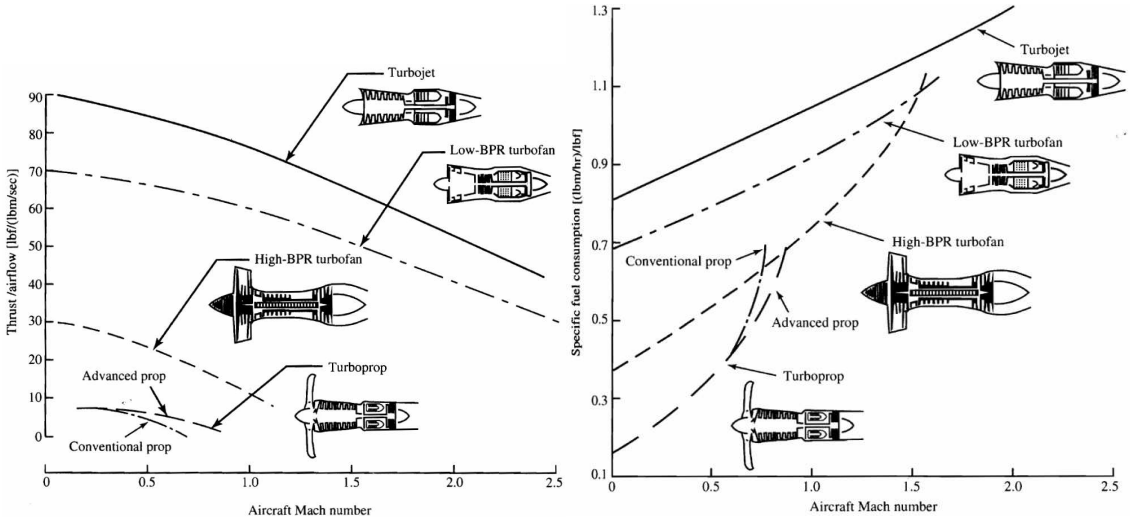

(a) Specific Thrust Trends (b) TSFC Trends

Figure 6: Parametric Cycle Analysis Results: Variation in Flight Conditions [47]

the ranges of key cycle parameters according to the upper (and if necessary, lower) limits on $F/\dot{m}_0$ and S. The symbols π_c and α represent compressor pressure ratio and bypass ratio, respectively. The bounds can be narrowed further by employing a parameter-by-parameter sensitivity analysis, which would measure how strong or weak overall performance is related to a particular cycle parameter. The results of such sensitivity studies are known as *design point exchange rates* [51]. Within those bracketed ranges, various cycle parameter settings and combinations can be explored to observe the resulting engine performance in the form of *design point diagrams*, whose representative examples are illustrated in Figure 8. It can be observed that the assumption of an ideal engine[3] becomes erroneous for a high bypass ratio cycle, and an optimum fan pressure ratio and bypass ratio exist with respect to TSFC. Such design point studies lay the groundwork for identifying the optimal design point before proceeding to the next step in engine cycle analysis.

[3]An ideal engine cycle analysis assumes the following: isentropic compression and expansion; constant-pressure combustion; negligible fuel flow rate; perfect gas with constant specific heats; exhaust stream is expanded to ambient pressure [47].

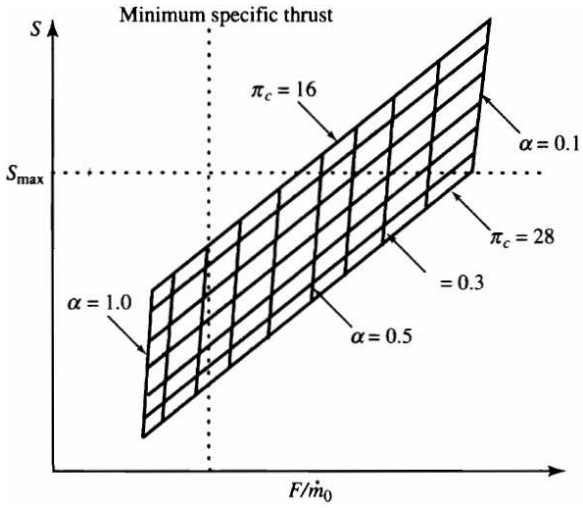

Figure 7: Specific Performance of Ideal, Mixed-Flow Turbofan Engines [47]

2.2.2 Off-Design Analysis

The parametric cycle analysis results shown in §2.2.1 give the illusion that a single engine's performance is mapped out over its operational envelope. This, however, cannot be further from the truth. Because the performance metrics are presented in terms of normalized ($F/\dot{m}_0$, S) and non-dimensional (η_{TH}, η_P, η_O) figures, each point on Figures 6 through 8 actually represents a unique engine, whose cycle, geometry (volumetric size), and architecture are determined as per its design point. The next logical step of the engine design process would then be to assess the performance capability of a specific engine, chosen at the end of parametric cycle analysis, in its entirety. Such an activity would require evaluating the fixed engine's performance at operating conditions other than the design points at the so-called off-design points. It is this portion of cycle analysis, appropriately termed *off-design analysis*, that is the topic of this section.

Off-design analysis, by its nature, cannot be carried out unless the three previously-mentioned engine characteristics - cycle, geometry, and architecture - are known. Of the three, the engine cycle is unequivocally defined in terms of the cycle parameter choices and values during parametric cycle analysis. The information regarding

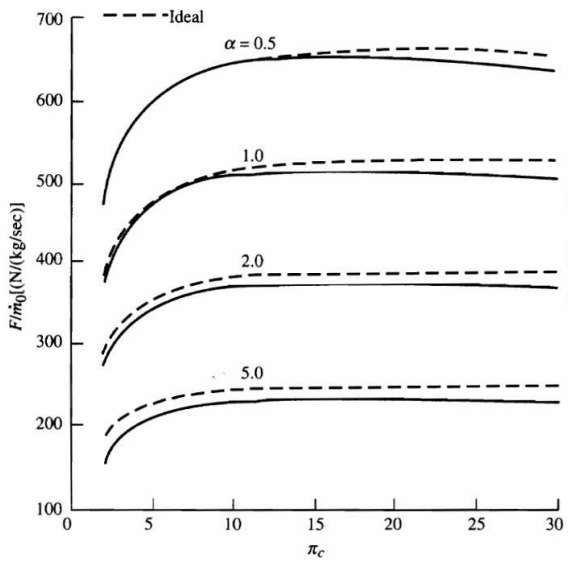

(a) Specific Thrust vs. Compressor Pressure Ratio

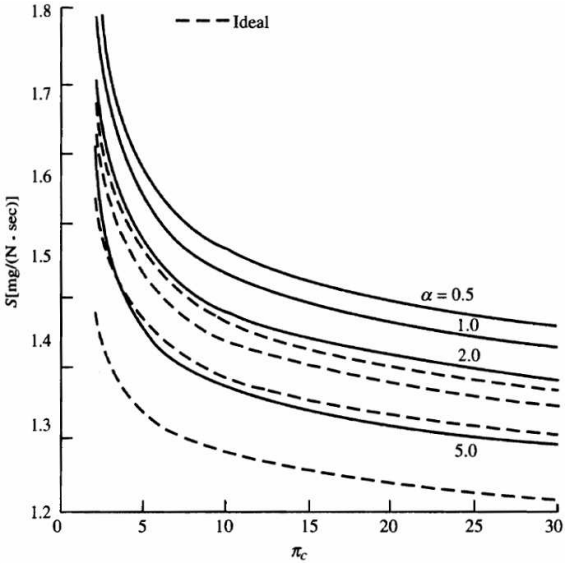

(b) TSFC vs. Compressor Pressure Ratio

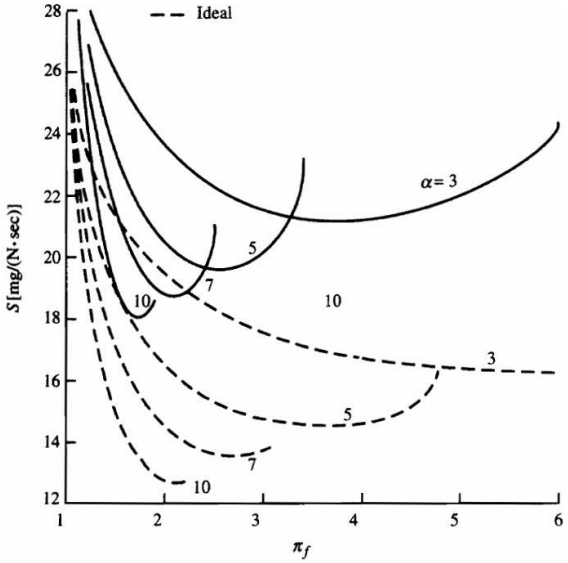

(c) TSFC vs. Fan Pressure Ratio

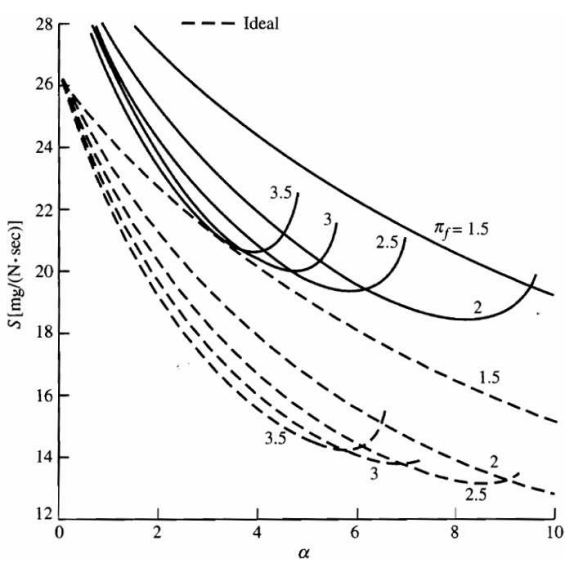

(d) TSFC vs. Bypass Ratio

Figure 8: Design Point Diagrams of Turbofan Engines [47]

the two remaining characteristics, however, must be leveraged upon component-level design (analysis and sizing) and engine layout work. Both activities are known to typically take place in an iterative fashion with on-design analysis prior to the start of off-design analysis [51]. Once all of the above pieces of information are available, the cycle designer is able to estimate the captured airflow rate, $\dot{m_0}$, which signifies the volumetric scale of the designed engine. The knowledge of $\dot{m_0}$ is crucial, as it now allows engine performance to be expressed in terms of nominal figures of merit, which are more intuitively meaningful than their normalized (specific) counterparts.

The primary independent variables of off-design analysis are flight conditions and throttle (thrust or power control) settings. A mental picture that may help envision how off-design analysis works is that of a pilot flying the aircraft through different forward flight speed and altitude combinations, throttling the engine in the process, to achieve the desired maneuver or flight path. In such a context, the name *engine performance analysis,* advocated by Mattingly et al, appears to be more descriptive than the conventional moniker, off-design analysis. Regardless, it is imperative that cycle designers map out the thrust and fuel consumption trends of the designed engine at critical flight conditions to ensure successful compatibility with a required mission. Several examples off-design analysis results that display an engine's thrust-lapse and fuel consumption behavior are shown in Figure 9.

For a first-cut answer, one may assume constant component performance states during an off-design analysis run, although it is not the most accurate means of modeling. The standard industry practice for engine performance analysis is to utilize a performance map for each component to evaluate the change in component pressure ratios, efficiencies, temperatures, etc., with the changing engine-level demands. Each map, in turn, is the result of performing both design point and off-design analyses at the component level, and is, strictly speaking, uniquely associated with a component of specific architecture and size.

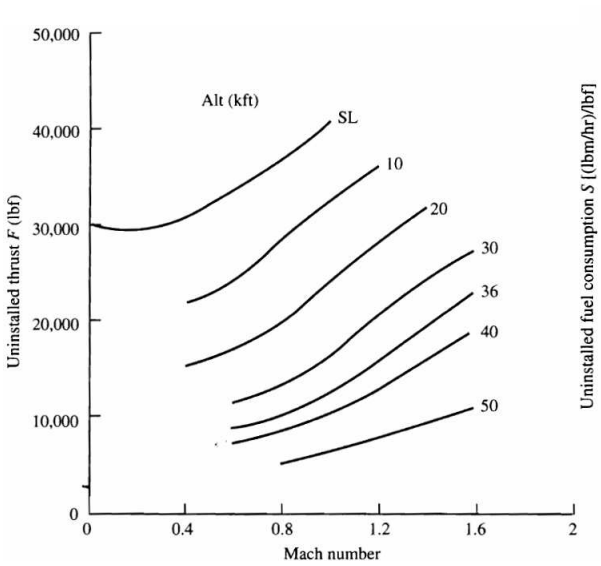

(a) Thrust Lapse: Afterburner On

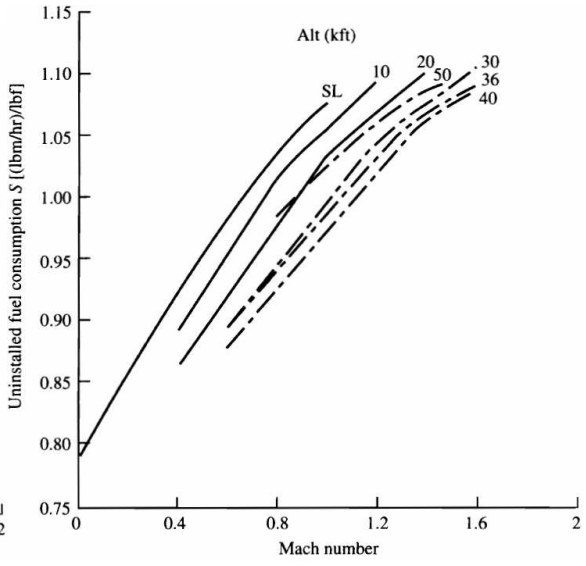

(b) TSFC Behavior: Afterburner Off

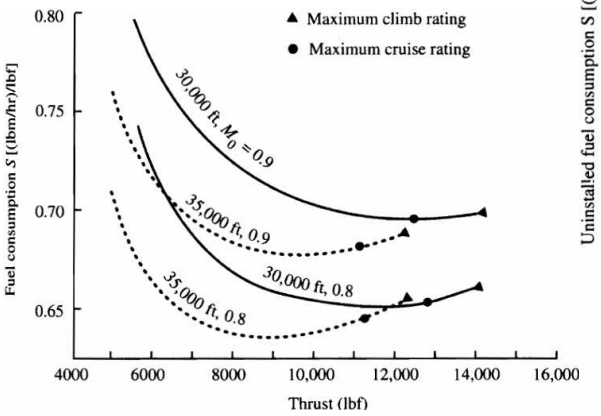

(c) Partial-throttle Performance of JT9D-70 (solid) and JT9D-70A (dashed)

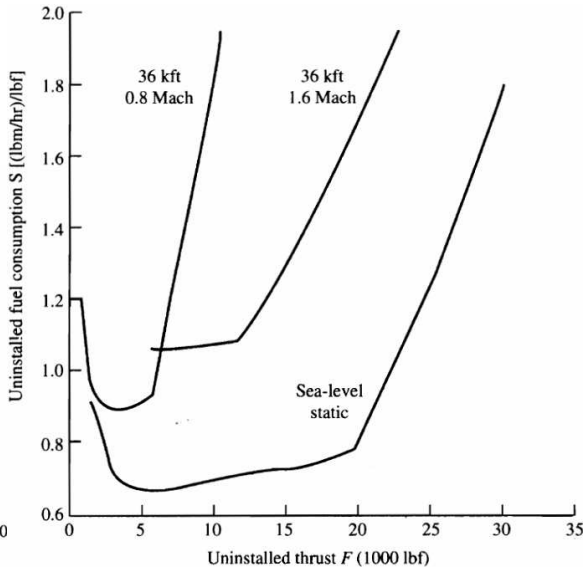

(d) TSFC vs. Partial-throttle

Figure 9: Representative Off-Design Analysis Results [47]

Should the findings up to this point yield unsatisfactory results, the designer has the freedom to return to parametric cycle analysis and determine a new design point. With time and resources permitting, the exchange may have to be repeated as many times as necessary, as indicated by the iteration loop between the two instances of cycle analysis shown in Figure 5.

2.2.3 Causal and Non Causal Approaches to Modeling

A slight digression is in order here to introduce an aspect of modeling that pertains specifically to creating parametric models. Largely, there exist two different approaches to organizing the "work flow [52]" of a model's functional relationships: backward-looking and forward-looking, which were first coined by the Southwest Research Institute in developing the Program for new generation vehicles Systems Analysis Toolbox (PSAT) [53]. The emergence and industry-wide acceptance of similar codes that allow the simulation of "drive cycles [54]" for Hybrid Electric Vehicles and Fuel Cell Vehicles (FCVs) have been largely responsible for the dissemination and confusion over the exact meaning of the two approaches in ground vehicle design communities. For example, Ricardo Consulting Engineers Ltd. refers to the backward- and forward-looking approaches as "quasi-stationary" and "dynamic transient" approaches in describing the company's Hybrid-Zero Emission Mobility (HY-ZEM) model [55]. The popular Advanced Vehicle Simulator (ADVISOR) program, which is a product of the U.S. National Renewable Energy Laboratory, labels itself as a "backward-facing simulation [56]" model.

The distinction between the two modeling approaches revolves around how the causality of a system's architecture is chosen to be represented. Appropriately, the names backward- and forward-looking are meant to alert a model builder's attention to the possible strategies he or she can leverage upon when creating an analysis flow path. The term backward-looking is used to signify that the sequence of analyses is

in reverse order of the modeled architecture's causality, whereas the name forward-looking implies the opposite. *Causality* refers to the physical, causal interrelationships between the sub-systems when the system is in operation. This point is made more clearly when an aeropropulsion system's causality is examined as follows.

In actuality, the pilot starts and inputs a throttle command to the engine, whose sub-system components such as fuel injectors, combustor, turbines, compressors, and fans then respond in a fixed sequence to produce thrust. The causality, thus begins with the pilot or a throttle command, and ends with a performance metric (thrust) that is available with the given command. The backward-looking approach to model this phenomenon would be to start from thrust, and reverse-trace through the various energy conversion paths between the engine sub-systems until the analysis arrives at the correct throttle command that, when issued, would result in the same amount of thrust. The forward-looking modeling approach here, on the other hand, would be to treat the pilot's throttle command as the first link of the analysis. All subsequent calculation steps would then be endeavored to follow the same manner (and order) of interactions among the idealized engines' sub-systems to estimate how much thrust would be available from the throttle command. In the hopes of accentuating this association with causality, Hauer [57] has proposed that the two approaches be alternatively named "non causal" and "causal" modeling approaches.

Depending on a model's conceived purpose, one modeling philosophy of representing architectural causality may be more appropriate than the other. For example, the non causal strategy lends itself to developing a system sizing model. Such a model must necessarily have a reverse causality structure, as the goal of modeling here is to approximate the gravimetric, volumetric, and geometric scale of a system as a function of certain performance targets. The causality-following work flow of a forward-looking model, on the other hand, naturally allows itself to be an analysis model for performance evaluations or control law development. In addition, "rapid

prototyping [58]," referring to the direct transfer from data into hardware, such as developed control algorithms and hardware-in-the-loop simulations, are only possible with causal models.

2.3 Estimation of Installed Engine Performance and Weight

The analysis of installed engine performance is a subject that has grown into a field of its own. More than 30 years of trial and error in the industry has served to accentuate the importance of proper airframe/engine integration, thus allowing it to become an area of heavy investment. The stakes involved are high for both airframe and engine developers to minimize the impact imparted by engine installation losses, such as reduced aircraft/engine performance and operability and increased total development cost and time.

One way to account for the installation penalty is to treat it as an additional drag force the engine must overcome. The simplest means of estimating this drag term at the conceptual design stage is to assume its magnitude and scale down the uninstalled thrust, accordingly. The Aircraft Engine Design System Analysis (AEDsys) program, which is a companion software to Mattingly et al [48], has an option to achieve this by applying a Thrust Scaling Factor (TSF). TSF is applied to the uninstalled thrust, calculated via the off-design analysis routine, to match it with the required installed thrust at a given flight condition [59].

A more accurate way of estimating the installed engine performance is to directly quantify the drag, or loss in thrust, at the source. For example, methods for estimating installation losses at the inlets, diffusers, and nozzles can be found in several collegiate textbooks on aeropropulsion systems [60, 61, 49]. Mattingly et al [48] present the steps for quantifying the subsonic inlet drag, supersonic (internal and external) inlet drag, and exhaust nozzle drag, which are also contained in the accompanying

AEDsys software. More sophisticated analysis methods that also allow the estimation of nacelle drag can be implemented using INSTAL [62] and the NASA Engine Performance Program (NEPP) [63].

The estimation of installed engine performance ends with the sizing of inlet and nozzle exit areas, which are the final missing pieces to estimating engine weight. Gerend and Roundhill first attempted to find a statistical correlation between cycle parameters and engine size (weight and dimensions) [64]. Onat and Klees developed a more accurate method of sizing an aero engine, which the Weight Analysis of Turbine Engines (WATE) code is based on [65]. WATE receives the cycle analysis results of NEPP as inputs to build up the weight and geometry of the designed engine from the component level. A preliminary mechanical design approach, one which is a conglomeration of empirical relationships and material characterization, is utilized to size a component that satisfies the structural, as well as physical requirements/constraints, such as maximum temperature, strain, stress, etc., in all off-design conditions.

2.4 Engine Scalability

Prior to the creation of a conceptual aircraft design environment, the topic of engine scalability becomes worth exploring. An engine of a fixed architecture is henceforth defined to be *thermodynamically scalable* if the given engine's thrust-lapse and fuel consumption behavior are found to only depend on its cycle over a reasonable design range. Discovering the extent to which the employed analysis environment results in a scalable engine, is an important pre-conceptual design activity because engine scalability heavily influences the synthesis approach to integrating the engine design process into the larger aerovehicle sizing and synthesis framework.

As it turns out, all aero engines that are in use today intrinsically possess linear scalability. This is due to the fact that all GT engine performance calculations, to a first order, adhere to the relationships dictated by what is known as *parameter*

groups. Parameter group relationships are concise representations of the "fundamental fluid dynamic process within an engine component [51]," which are derived using the famous Buckingham PI theorem. Table 2 reproduces some of the more important higher-level parameter group categories from Chart 4.1 of Ref.[51]. The beauty of the parameter group approach is that fixing one parameter group uniquely defines all other groups within the same category. In turn, fixing the engine architecture, geometry, and cycle would uniquely define all parameter groups across all four categories, allowing the parameter group relationships to become the means of evaluating the performance of the engine at new fluidic (dimensionless), cycle (quasidimensionless), off-design (referred), or geometric (scaling) conditions. The use of referred parameter groups is actually a fundamental building block of an off-design analysis method known as *matching* [51].

It is straightforward to realize why modern aero engines are photographically scalable by symbolically exploring the relationships dictated by the scaling parameter groups. Linearly scaling up an existing engine by a factor of two - *ceteris paribus* - results in the mass flow increasing by a factor of four; uninstalled (gross) thrust and output power increasing by a factor of four; and constant TSFC, compressor efficiency and turbine efficiency. Constant TSFC and efficiencies are indicative of the exact same fuel consumption behaviors; whereas, the equal factor increase in captured air flow and gross thrust would result in the same proportional lapse rates for uninstalled thrust. When more detailed, "real engine" effects are captured by the analysis process, however, a designed engine may not be necessarily scalable. Such second-order scaling effects will become increasingly pronounced as the dimensions for engine component clearances, radii, thickness, surface finish, etc. reach practical and/or mechanical limits, and the variation in engine performance will no longer adhere to what the scaling parameter group relationships predict theoretically.

From a systems integrator's perspective, an engine design environment producing

Table 2: Select Engine Parameter Categories and Groups [51]

Performance parameter	Dimensionless group	Quasidimensionless group	Referred parameter	Scaling parameter
Mass flow (W)	$\frac{W * \sqrt{(T1 * R)}}{DI^2 * P1 * \sqrt{(\gamma)}}$	$\frac{W * \sqrt{(T1)}}{P1}$	$\frac{W * \sqrt{(\theta)}}{\delta}$	$\frac{W * (\theta)}{DI^2 * \delta}$
Fuel flow (WF)	$\frac{WF * FHV * \sqrt{(R)} * ETA31}{CP * DI^2 * P1 * \sqrt{(T1 * \gamma)}}$	$\frac{WF * FHV * ETA31}{P1 * \sqrt{(T1)}}$	$\frac{WF * FHV * ETA31}{\delta * \sqrt{(\theta)}}$	$\frac{WF * FV * ETA31}{DI^2 * \delta * \sqrt{(\theta)}}$
Shaft power (PW)	$\frac{PW}{\gamma * DI^2 * P1 * \sqrt{(\gamma * R * T1)}}$	$\frac{PW}{P1 * \sqrt{(T1)}}$	$\frac{PW}{\delta * \sqrt{(\theta)}}$	$\frac{PW}{DI^2 * \delta * \sqrt{(\theta)}}$
Shaft power SFC (SFC)	$\frac{SFC * FHV * \gamma * R * ETA31}{CP}$	SFC * FHV * ETA31	SFC * FHV * ETA31	SFC * FHV * ETA31
Gross thrust (FG)	$\frac{FG}{\gamma * DI^2 * P1}$	$\frac{FG}{P1}$	$\frac{FG}{\delta}$	$\frac{FG}{DI^2 * \delta}$
Thrust SFC (SFC)	$\frac{SFC * FHV * \sqrt{(\gamma * R)} * ETA31}{CP * \sqrt{(T1)}}$	$\frac{SFC * FHV * ETA31}{\sqrt{(T1)}}$	$\frac{SFC * FHV * ETA31}{\sqrt{(\theta)}}$	$\frac{SFC * FHV * ETA31}{\sqrt{(\theta)}}$
Specific thrust (SFG)	$\frac{SFG}{\sqrt{(\gamma * R * T1)}}$	$\frac{SFG}{\sqrt{(T1)}}$	$\frac{SFG}{\sqrt{(\theta)}}$	$\frac{SFG}{\sqrt{(\theta)}}$
Compressor efficiency (ETA2)	ETA2	ETA2	ETA2	ETA2
Turbine efficiency (ETA4)	ETA4	ETA4	ETA4	ETA4

a scalable engine is more desirable than the one that does not. Figure 10 shows two possible approaches to sizing an aerovehicle. Regardless of the chosen approach, the required inputs from the engine designer are a means of estimating the engine weight based on (reference-point) installed thrust (T_{SL}) and fuel consumption rates at flight conditions specified by the mission analysis. When engine scalability holds, both capabilities can be made available through work done off-line and independently from those at the vehicle level, and in forms that are easily integrable. A scalable engine signifies that only a one-time investment in engine performance analysis is sufficient, as long as the cycle remains intact. Such thrust-lapse and fuel consumption characteristics are most commonly provided in a standardized, tabular format, referred to as an engine *deck* [67]. The relationship between the geometric/photographic scale of the engine and its weight can be concisely captured as a simple polynomial equation. Codes such as WATE can be employed off-line to generate such an engine weight scaling law over a reasonable range of installed thrust.

On the contrary, the absence of engine scalability necessitates a tight coupling between the constraint analysis, mission analysis, vehicle weight estimation, and engine design. Cycle analysis and engine weight estimation cannot exist as separate entities from the aircraft sizing process, as they must be consulted every time each of the vehicle-level analysis requires an input from the engine design level. Even in the simplest case of a fixed-cycle engine, it can be observed that the specific parameter-based aircraft sizing approach cannot be used without a scalable engine. Only the actual value-based approach is applicable with a non-scalable engine, since a new engine deck and a new engine weight must be evaluated every time T_{SL} and aircraft take-off gross weight (W_{TO}) are iterated upon.

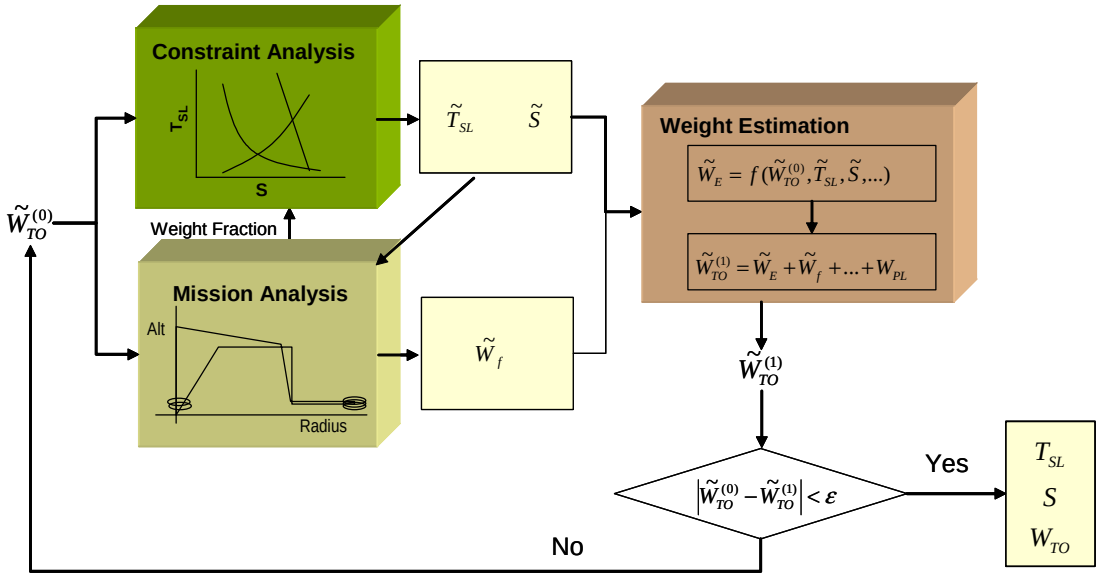

(a) Actual Value-based Approach

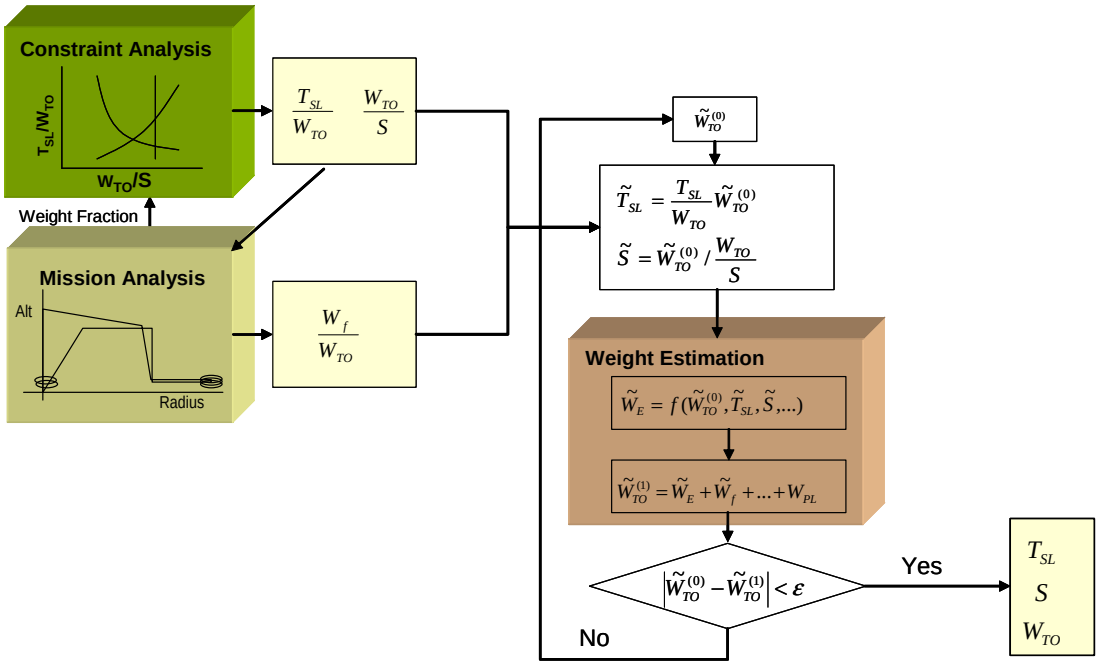

(b) Specific Parameter-based Approach

Figure 10: Approaches to Aerovehicle Sizing [66]

2.5 Chapter Conclusions

The literature survey into the best design practices for modern GT aeropropulsion systems reveals that there exists a process which is not only algorithmically elegant, but also computationally efficient. The fact that investigative procedures, such as parametric cycle analysis and engine performance analysis are commonly practiced in the jet propulsion design community, demonstrates the importance of exploring the disciplinary-level design space. It is also no accident that the principal outputs of legacy engine design codes are engine decks and weight scaling law. Both are products of past engine designers' understanding of system scalability, as defined in §2.4, and exploitation of empirical know-how that such table-lookup routines result in acceptable analysis accuracy when applied to aircraft sizing. Based on hitherto presented material, a number of generalizations can be drawn as follows.

Above all, whatever computing environment is ultimately chosen for implementing fuel cell aeropropulsion design, the algorithmic sequence of on-design analysis, sizing, and off-design analysis appears to be a useful modeling structure to emulate. It results in an integrated work flow that encompasses both the non causal and causal modeling approaches, although the nature of this distinction is not explicitly explained by Mattingly et al [48]. The on-design analysis is a backwards approach since it starts from a point-performance requirement and ends with a parametrically designed engine. Subsequently, the gravimetric scale and volumetric size of the aeropropulsion system can be determined. The off-design analysis, either as a stand-alone process of engine-deck generation or as an integrated routine with mission analysis, is very much a forward-looking process in its direction of work flow. When these three algorithms are seamlessly integrated into one, what results is a highly modular, flexible, and parametric design tool.

Should such a simulation environment be available, then the *cycle* characteristics of a given fuel cell aeropropulsion system could also be examined. These kinds of

disciplinary trade and sensitivity studies are imperative to discover which system-level inputs significantly affect which thermodynamic, gravimetric, and volumetric figures of merit, analogous to how the cycle parameters are known to dictate those characteristics of traditional aero engines. Eventually, the accumulated insights into interdependencies between the dominant design parameters would allow the elicitation of any patterns regarding the cycles and system performance (*e.g.*, thrust lapse, power lapse, fuel consumption, etc.) or mission requirements (high altitude loiter, low speed cruise, take-off field length constraint, etc.).

The concept of engine cycle is intimately related to the issue of system scalability. If a chosen cycle for a given engine architecture is found to result in a scalable fuel cell aeropropulsion system, then a synthesis algorithm similar to that of the specific parameter-based approach would be applicable. Such a finding would be preferable for practical reasons, as detailed in §2.4. Therefore, investigating the scalability of an unprecedented aeropropulsion system within the fidelity of the established disciplinary simulation environment would be a challenging, yet rewarding task.

Chapter III

OPTIMIZATION UNDER UNCERTAINTY

In reality, the occurrence of an ideal design scenario in which the engineering problem at hand is completely void of imperfect information is exceptionally rare. Gallie asserts that an "absolutely detailed forecast of any particular concrete example" is unattainable, since "whatever information is available, and however many rules for applying data are provided, there is always some degree of irreducible uncertainty in a situation." [68] Although notional, the trajectories of the demonstrated TPM values depicted in Figure 4 imply that the influence of various uncertainties make it difficult to predict when and how much recourse will be required along an engineering system's development cycle.

The traditional practice of accounting for uncertainties, which still persists to this day, is to convert what is inherently a nondeterministic problem into a deterministically solvable condition [69]. This is largely done in two ways. First, various simplifying assumptions, based on precedents, empirical knowledge, intuition or even educated guesses, can be utilized to "remove" any perceived uncertainties from design analysis. The inherent weakness of such a practice is that the quality of the results is only as good as that of the assumptions. Secondly, design margins are applied to ensure some degree of safety against the possibility of later constraint violations due to currently imperfect information. This kind of better-safe-than-sorry attitude, however, tends to produce overly conservative designs that could have been further optimized. Both are, thus, less-than-rigorous practices that facilitate engineers to ignore, rather than understand, the full impact of uncertainties in the engineering design process.

Fortunately, the past three decades have seen an explosive interest in the scientific and engineering communities to approach the handling of uncertainty from a more quantitative and mathematically rigorous angle. Much progress in attempts to better understand how to resolve uncertainty-ridden challenges have been reported from many disciplinary directions, including economics, systems engineering, management science, computer science, artificial intelligence, etc., and relatively new fields, such as risk assessment [70]. In the aerospace engineering domain, the initiative to develop creative approaches to solving nondeterministic engineering problems, has been led by the field of aerospace systems design. Inspired by statistical data modeling and numerical analysis techniques that did not use to constitute the core of an aerospace engineering curriculum, a number of *advanced design methods*, with a particular emphasis on the probabilistic treatment of uncertainty, have been proposed.

This important realization led to the conception of the second research question to be answered over the course of this dissertation:

> **Question 2**: Are there elements of existing advanced aerospace systems design methods that can serve as foundational formalisms for identifying an optimal recourse decision regarding fuel cell aeropropulsion system design? (Observations 2 and 3)

The survey of literature was consequently expanded to include recently emergent advanced methods, whose origins were motivated by the desire to perform design optimization in the presence of different uncertainties. As it turns out, all hitherto proposed methods happen to be single-stage strategies, whereas recourse is fundamentally a two-stage process.

3.1 Probabilistic Approaches to Aerospace Systems Design

One noticeable trend in the field of aerospace systems design has been a gradual shift in focus away from the prototypical, deterministic solution approaches and towards

those that enable nondeterministic analysis and optimization activities. Over the past decade, the Aerospace Systems Design Laboratory (ASDL) at the Georgia Institute of Technology has been at the forefront of this movement by supporting research into the application of advanced design methods to a wide array of aerospace systems [71]. The emergence of probabilistic approaches to quantifying various sources of uncertainty has been made popular since the seminal publication of Robust Design Simulation (RDS) and the Joint Probabilistic Decision Making (JPDM) technique. Both methods were one of the first formal attempts at demonstrating the benefits of probabilistically treating uncertainties for high-risk, high-stakes engineering problems, such as the design of a high-speed civil transport (HSCT). Although more recent studies, such as the work of Chae [72], have attempted to capture the "non-probabilistic manifestation" [73] of uncertainty via fuzzy sets or possibility theory [74], the probability theory still remains the dominant uncertainty handling formalism in most systems-oriented design settings. What follows is a chronological summary of several distinguished probabilistic approaches to aerospace vehicle and propulsion design problems.

3.1.1 Robust Design Simulation

Perceiving it to be an urgent issue to address, Mavris et al proposed RDS as an answer to the then perceived negligence of uncertainty in the aerospace vehicle design community [75]. As its name implies, RDS is applicable to situations for which obtaining a robust solution is more valuable than a design that is deterministically optimized for a point-performance requirement. The concept of robustness adapted here is akin to that of Taguchi's robust parameter design approach [76], whose objective is to identify the solution that displays the least amount of sensitivity to "noise variables;" *i.e.*, modeled sources of uncertainty.

The salient features of the method, which are shown in Figure 11, include the application of a specific surrogate modeling technique ("Response Surface Equation");

probabilistic modeling ("Noise Variables") and simulation ("Monte-Carlo Analysis") of known sources of uncertainty; and a single overall evaluation criterion (OEC) in the form of a cumulative probability. Unlike Taguchi's Orthogonal Arrays, RDS allows the nondeterministic treatment of uncertainties through Monte Carlo Simulation (MCS). The gambling-inspired moniker refers to a numerical sampling method which randomly selects a value for each noise variable in accordance with the shape and range of a prescribed probability distribution. By optimizing the design towards maximum probability of achieving a certain threshold level, RDS uncovers a vehicle design solution that is, in effect, robust to the variability imparted by the represented sources of uncertainty.

3.1.2 Joint Probability Decision Making Technique

Bandte, one of the brains behind RDS, later extended the single-criterion approach to probabilistic analysis that he had helped pioneer. Consequently, the JPDM technique was formulated in an attempt to perform multi-criteria optimization under a nondeterministic engineering design paradigm [77]. Figure 12 illustrates the intricacies of JPDM, which can either be utilized as a management-level product selection tool or a system-level optimization method.

JPDM is procedurally similar to RDS in that the inputs are partitioned to deterministic control variables and nondeterministic noise parameters. Both surrogate modeling ("RSE") and MCS form the backbone of attaining a probabilistic response, and the goal of optimization is to maximize the system's probability of success. The ingenuity of JPDM lies in the seventh step, in which a joint probability of simultaneously meeting multiple evaluation criteria, as opposed to a univariate probability of satisfying a single criterion, can be evaluated from five statistical methods. Like its predecessor, the merit of applying probability theory to quantify economic uncertainties in an aerospace systems design environment was demonstrated on the

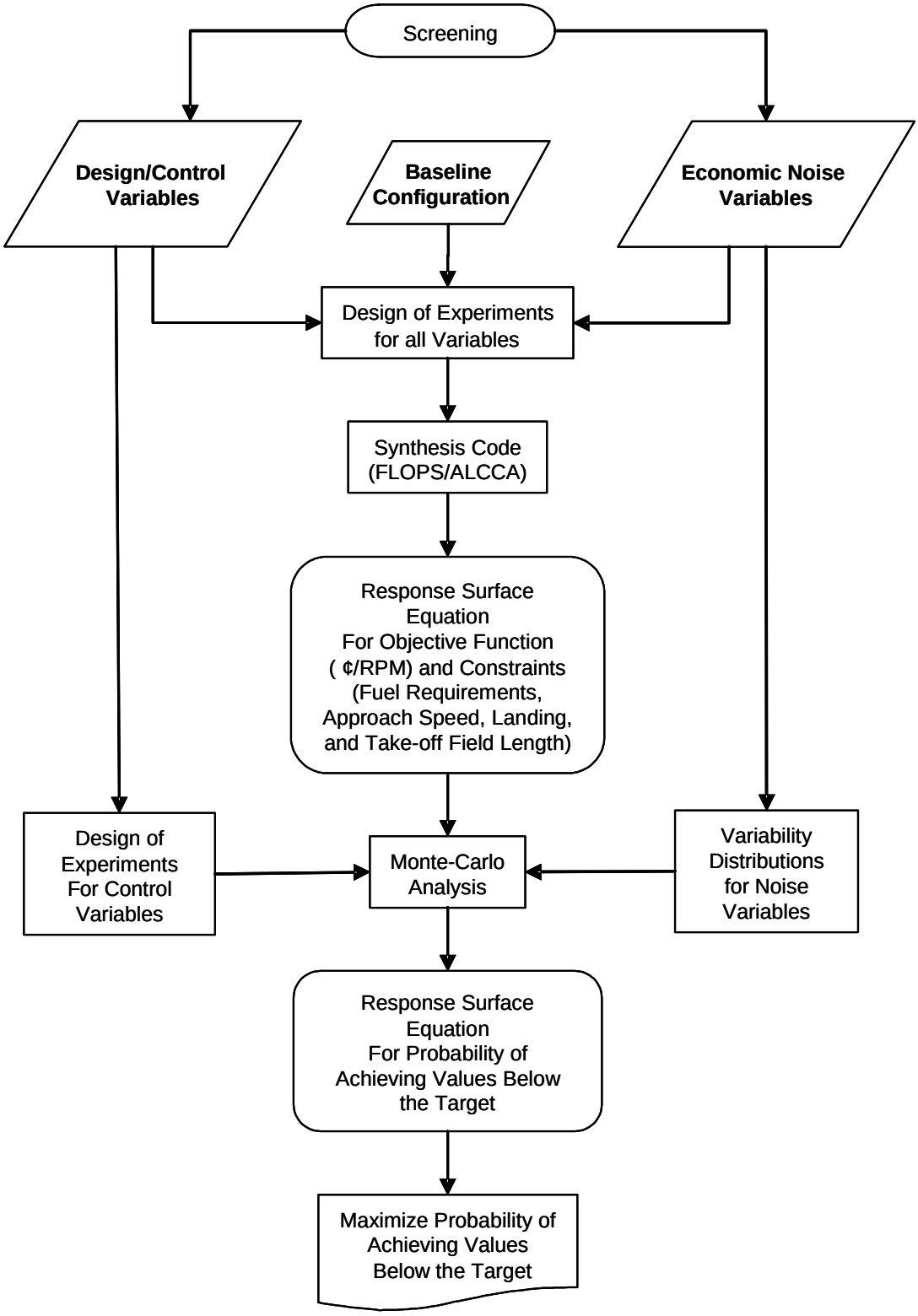

Figure 11: RDS Methodology Flowchart [75]

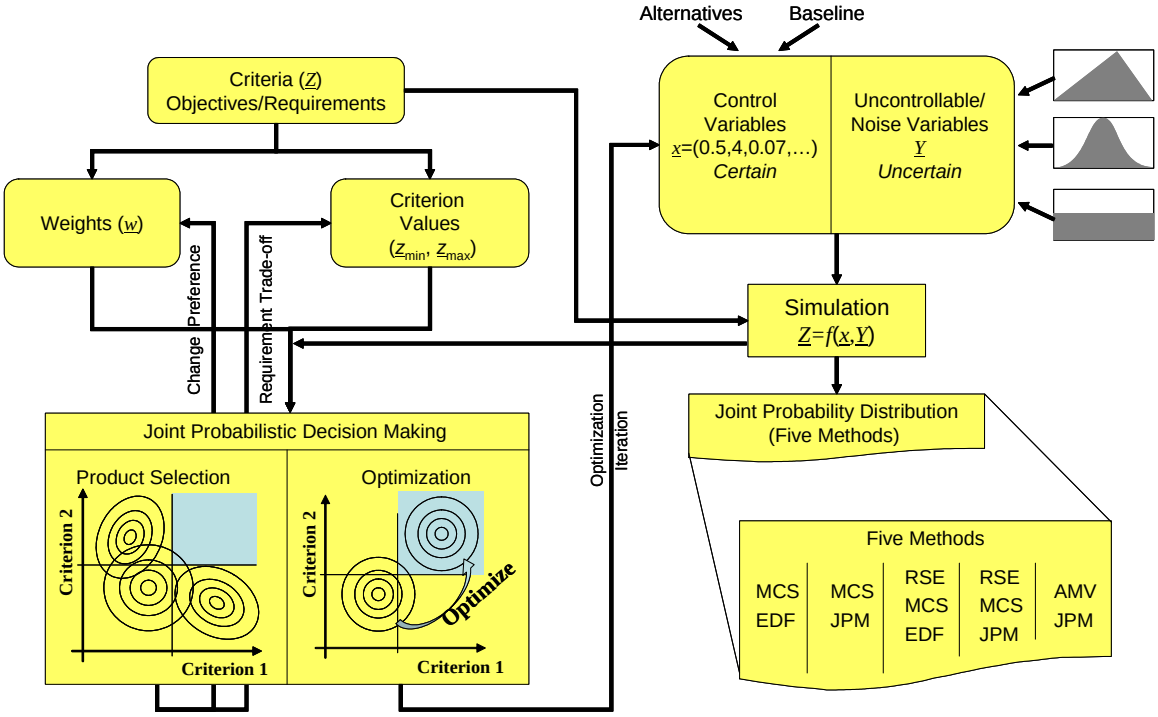

Figure 12: JPDM Technique Flowchart [77]

optimization of a notional HSCT concept.

3.1.3 Probabilistic Engine Design

Roth [78] discusses the possible sources of uncertainties that can affect the design of a new aircraft engine with the aid of Figure 13. Thrust and engine core weight are given as examples of uncertainties that are external to the design activities; *e.g.*, cycle analysis, sizing, etc. To an engine manufacturer, both metrics become uncertain design requirements, as indicated by the notional probability distributions on the outside of the abscissa and ordinate, which complicate pinpointing the engine design point in a deterministic manner. The dashed isolines of probability density around the design point are indicative of this dilemma.

In contrast, the uncertainties that are internal to the engine design process are illustrated to manifest themselves as solid probability density contours within the core design space. Projecting whether or not the physics-driven growth trend of a given

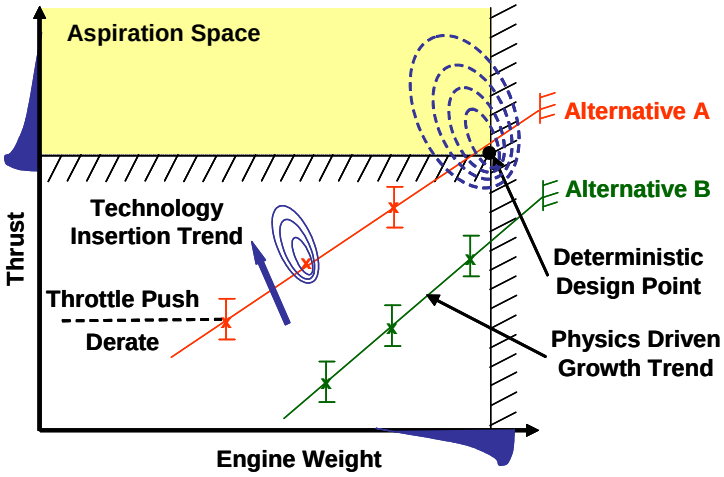

Figure 13: Motivation for Probabilistic Engine Design [78]

engine architecture will be able to reach the aspiration space is difficult due to the influence of technological, mission requirements, cycle, aircraft design, environmental, regulatory, and manufacturing uncertainties. This observation leads Roth to conclude that "the probability of a given engine meeting the ultimate requirements is described by the intersection of two joint probability distributions: the requirements uncertainty distribution and the engine design uncertainty distribution."

3.1.4 Deterministic Solution Sampling Method

In response to the absence of a systematic method by which to account for an internal source of engine design uncertainty, Nam et al [79] introduced a probabilistic optimization method that was (algorithmically) inspired by, but not (philosophically) based on, RDS and JPDM technique. The authors' Deterministic Solution Sampling (DSS) method enables the identification of the most probable engine architecture for satisfying uncertain future regulatory constraints regarding nitrogen oxides, CO_2, and noise emissions. Some of the same salient features of RDS and JPDM technique, such as surrogate models ("RSE"), MCS, OEC, and probability of success, are also the important building blocks of the DSS method, as shown in Figure 14.

It is nonetheless important to realize that the ultimate goal of DSS is to attain

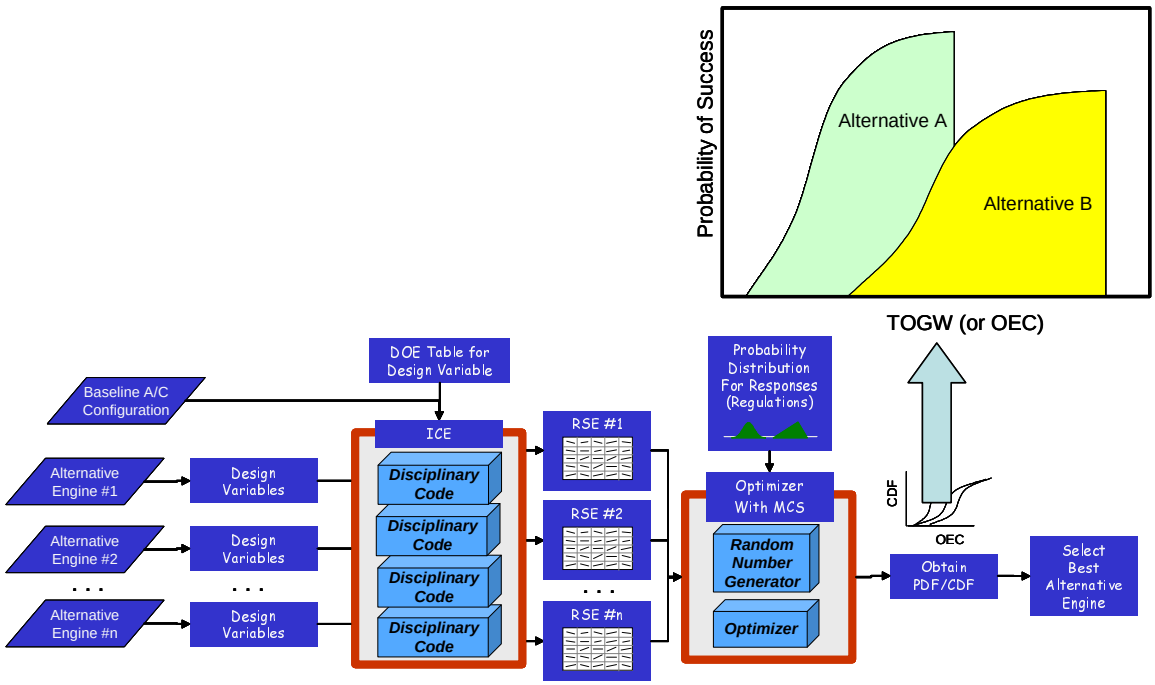

Figure 14: DSS Method for Engine Architecture Selection [79]

a probabilistic cumulative distribution function (CDF) from optimization results, rather than optimizing for maximum probability of success. Here, MCS is literally used to sample regulatory constraint values from pre-defined probability distributions, after which a deterministic optimization is carried out on a metric of interest, such as weight, or an OEC. The focus is thus weighed more towards decision support than decision making, as the DSS method is most useful in showing with how much probability the optimum can be expected to fall between a certain band of OEC values. For the same reason, the method, per se, does not produce a single design solution (*i.e.*, decision).

3.1.5 Probabilistic Aircraft Sizing Method

The algorithm for sizing an aerovehicle concept is analogous to a single-objective, constrained optimization problem, in which the balance between the required and available amounts of geometric, gravimetric, and propulsive scales are endeavored to be matched. This becomes apparent as one scrutinizes Figure 10. The optimization

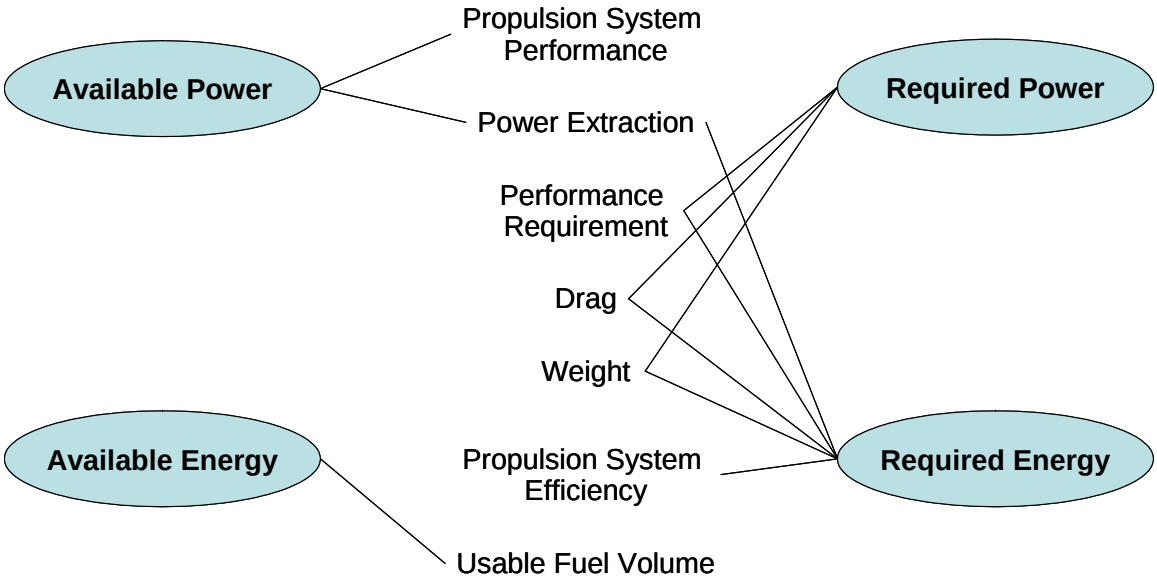

Figure 15: Impact of Uncertainty on Aircraft Sizing [66]

routine is represented as the iterative loop to calculate W_{TO} that also implicitly accounts for the fuel balance, as per the constraints shown in the constraint analysis diagram.

How the presence of uncertainty impacts this optimization process is illustrated in Figure 15. Under the influence of imperfect information, both the "Available" and "Required" quantities cannot be expressed deterministically, resulting in the following nondeterministic expression for aircraft sizing:

$$\begin{aligned} \min_{\mathrm{x}} \quad & \tilde{f} \\ \text{s.t.} \quad & \tilde{P}_{available} \geq \tilde{P}_{required} \\ & \tilde{E}_{available} \geq \tilde{E}_{required} \end{aligned} \tag{1}$$

The $\tilde{\cdot}$ symbol above a variable is used to distinguish a nondeterministic parameter from a deterministic one, as per the convention used in Nam [80].

If probability theory is again adapted to quantify these nondeterministic parameters, then, in essence, Eq.(1) indicates that aircraft sizing under uncertainty is an

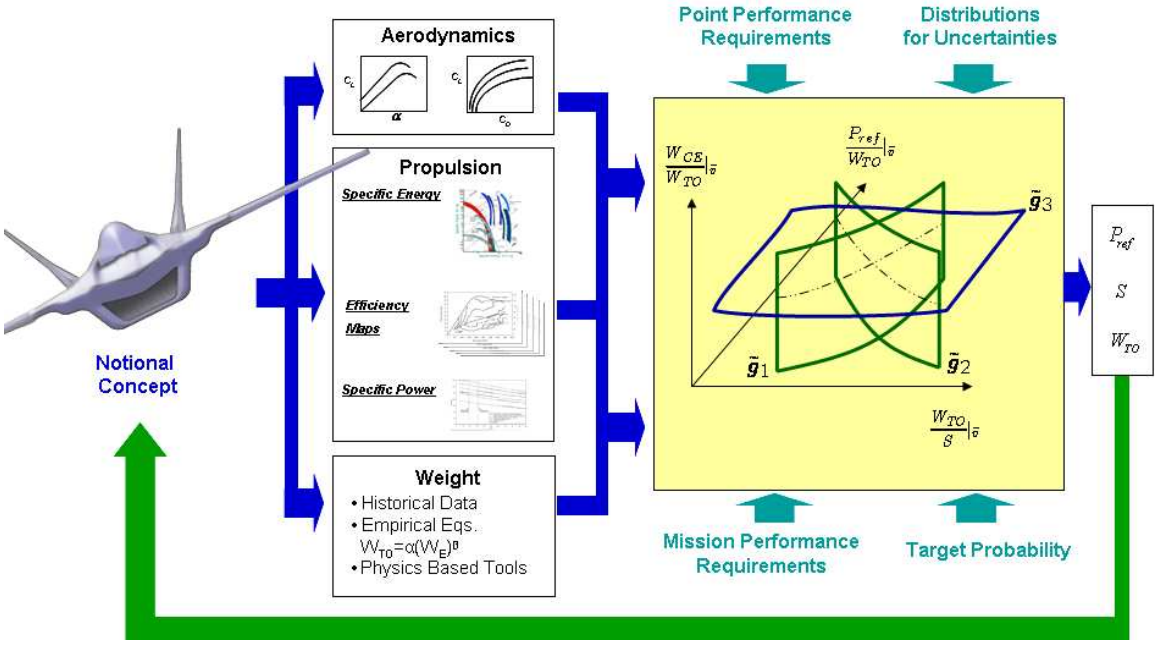

Figure 16: Overview of PASM [66]

optimization problem with a probabilistic objective function and probabilistic constraints. Prior to the work of Nam [66], this kind of probabilistically constrained optimization challenge had not been addressed in the field of aircraft vehicle design. A closer inspection of RDS reveals that, although the method is claimed to allow "probabilistic, constrained optimization," [75] it is in fact still a *deterministic*, constrained optimization, *whose objective function is the probability of target achievement*. Moreover, the constraints employed in RDS are assumed to be deterministic, which is also the case for the JPDM technique.

Motivated by the above-mentioned deficiencies in state-of-the-art probabilistic design methods, Nam developed the Probabilistic Aircraft Sizing Method (PASM) shown in Figure 16. PASM is best described as a nondeterministic aircraft sizing formalism inspired by Chance-Constrained Programming (CCP). The goal of CCP is to find a solution which would, on average, satisfy all constraints with target probabilities $\alpha \in [0, 1]$. This concept of a chance-constrained optimization dates back to the seminal 1959 work of Charnes et al [81], which Haneveld and Van Der Vlerk [82]

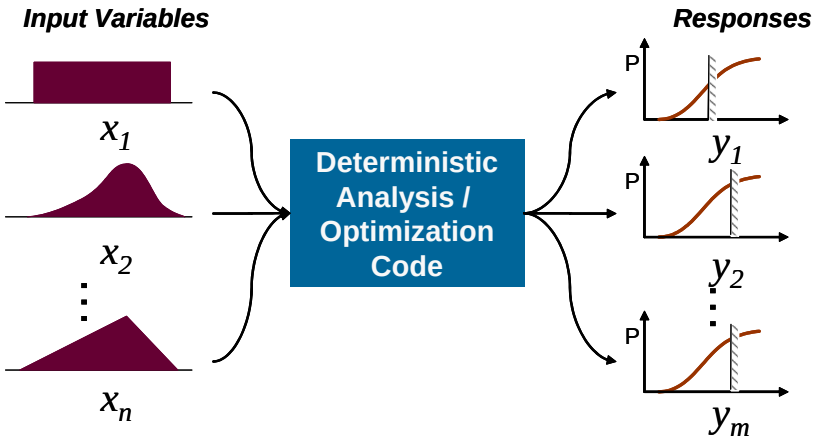

Figure 17: Single-Stage Nondeterministic Design Paradigm

remark as a method based on the "qualitative risk concept." Here, risk is understood to be the associated cost, monetary or otherwise, due to violating the uncertain constraints. Nam embraces this underlying philosophy of CCP by explaining that the objective of PASM is to mitigate "the risk associated with uncertainty to the level deemed acceptable by a decision maker."

3.1.6 Summary

The emergence of nondeterministic solution strategies indicates that the need to account for uncertainty in a modern aerospace systems design environment is both real and imperative. The same need becomes also relevant when one accepts the certainty of recourse in engineering design, as argued in §1.2.3. In retrospect this was the reason behind reviewing the literature on probabilistic design methods, all of which contain elements of uncertainty analysis and optimization.

Fundamentally, all reviewed advanced methods operate under the nondeterministic analysis paradigm shown in Figure 17, which is an adaptation from Ref.[66]. Uncertainties, which are mapped to appropriate input variables for the problem at hand, are first quantitatively modeled as probability distributions. Due to the inputs being probabilistic, the output, or response variables of a design activity are also estimated in a probabilistic manner. RDS, JPDM, and DSS methods more or less

follow the above paradigm in constructing empirical cumulative probability distributions of vital system-level metrics, based on MCS results. Being a CCP-inspired strategy, PASM invokes a similar procedure to estimate the probabilities of constraint violations for a given design.

From the perspective of optimization under uncertainty, the paradigm shown in Figure 17 leads to a single-stage approach to the design of an engineering system. The four methods differ in the order in which uncertainty analysis and optimization are performed, but they can all be characterized as solution schemes with a single optimization loop. There are no built-in provisions to compensate for constraint violations, which occur during optimization. Rather, infeasibilities are strictly prohibited and are attempted to be avoided at all costs. For instance, an optimum in an RDS or a JPDM setting is a solution that has the maximum probability of achieving a target while satisfying all deterministic constraints. The DSS method produces a cumulative probability distribution of optimal solutions, all of which are not allowed to be infeasible designs. PASM is also formulated to avoid constraint violations, although the optimum in this case is a design that is also the least likely to be infeasible once all the effects of modeled uncertainties are taken into consideration.

Such a single-stage nature of existing strategies is indicative of a need to formally integrate the remedial aspect of engineering design into the underlying philosophies of contemporary nondeterministic solution methods. This realization forms the basis of the last observation, which is as follows:

> **Observation 4**: The single-stage nature of established probabilistic solution strategies are indicative of the need to formalize a new design method that is capable of handling recourse, which is intrinsically a two-stage phenomenon.

The reader is reminded that the two-stage notion of recourse can be found in §1.2.3.

3.2 Stochastic Programming

Broaching the topic of optimization in the presence of uncertainty revealed an opportunity to develop a new probabilistic solution approach around the remedial aspect of aerospace systems design. It is reiterated that recourse is fundamentally about correcting an *a priori* design in an *a posteriori* manner. That is, should the design that was considered to be the most probable solution in the previous stage turn out to display too large a deviation from expected TPM values at some point in the development phase, then a concerted effort is made to fix the problem in the most cost-effective way.

From an algorithmic standpoint of developing a new methodological capability, this implies that not only uncertainty analysis, but also a routine for recourse should be embedded inside a larger optimization loop. Because such an arrangement of design resources represents a noteworthy departure from existing, single-stage probabilistic formalisms, most of which possess a decoupled structure regarding probabilistic analysis and numerical optimization (the exception to this is PASM), the aforementioned insight is formalized as the final research question of this document.

> **Question 3**: How can a recourse-based solution approach be formulated in such a way as to be relevant to the design of modern aerospace systems in general, and be applicable to the design of fuel cell aeropropulsion in particular? (Observation 4)

The scope of literature search is thus expanded once again to encompass a more in-depth discussion of optimization under uncertainty. In particular, a class of nondeterministic optimization techniques, known as stochastic programming, is introduced.

3.2.1 Stages and Recourse Programs

Stochastic programming is the name given to the modeling approach involving optimization problems with uncertainty. The usage of the term "stochastic" is meant

to highlight the nondeterministic nature of involved parameters, data, or both. It is assumed that the modeler has prior knowledge regarding the probability distributions of known sources of uncertainty, or some means of estimating them. The dual use of "programming" is evident in its synonymous meaning with "optimization" and with reference to "the fact that various parts of the [optimization] problem can be modeled as linear or nonlinear mathematical programs." [83] This mathematically rigorous framework for optimization under uncertainty should not be confused with certain exploratory optimization algorithms, such as Simulated Annealing [84] and Genetic Algorithm [85]. Although such techniques are sometimes called stochastic optimization methods, the reference to "stochastic" here is to the random manner in which a global optimum is endeavored to be found in a multi-modal design space and has nothing to do with the presence of uncertainty in program parameters.

One branch of classical stochastic programming models, which formally introduces the concept of *stages* in an optimization setting, is the recourse program. All recourse programs are characterized by their distinction between the first-stage and second-stage decisions. The first stage is defined as the time period in which a number of *a priori* decisions are arrived at before the exact values of the uncertain parameters are known, whereas the second stage corresponds to the period when a number of *a posteriori* solutions are found after the realization of said uncertainty. Therefore, any one instance of a recourse program follows the order of: (a) the identification of first-stage decision(s), (b) the determination of uncertainty, which is followed by (c) the arrival at second-stage solution(s) after taking into account the effects of uncertain parameter(s) observed in (b). Exactly what kind of action is envisioned to be implementable in the second stage further distinguishes one stochastic recourse programming model from another.

3.2.2 Two-Stage Stochastic Programs with Fixed Recourse

In case that the goal of the second stage is to correct any infeasibilities arising in the first-stage decision due to uncertainty realization, the general recourse program described in the previous section can be formulated as a two-stage stochastic program with fixed recourse. Dantzig [86] and Beale [87] are credited for the inauguration of Eq.(2) below, which is regarded as the classical model of recourse programming. Examples of extending the basic ideas of two-stage stochastic linear programs to multistage linear, nonlinear, and integer programs are found in various introductory textbooks, one of which is Ref.[83].

$$\begin{aligned} \min_{\mathrm{x}} \quad & z = \mathbf{c}^T\mathbf{x} + \mathbb{E}_\xi \left[\min \mathbf{q}(\omega)^T\mathbf{y}(\omega)\right] \\ \text{s.t.} \quad & \mathbf{A}\mathbf{x} = \mathbf{b} \\ & \mathbf{T}(\omega)\mathbf{x} + \mathbf{W}\mathbf{y}(\omega) = \mathbf{h}(\omega) \\ & \mathbf{x} \geq 0 \\ & \mathbf{y}(\omega) \geq 0 \end{aligned} \tag{2}$$

Eq.(2) must be described in terms of the vectors and matrices related to the first stage, as well as those of the second stage. Assuming that $\mathbf{c}$ is a known first-stage vector in $\Re^{n_1}$ (*i.e.*, its size is $n_1 \times 1$), $\mathbf{b}$ is a known first-stage vector $\Re^{m_1}$, and $\mathbf{A}$ is a known first-stage matrix of size $m_1 \times n_1$; a single instance of the $n_1 \times 1$ design variable vector $\mathbf{x}$ represents a decision in the first stage. If uncertainty is represented by Ω, which is the set of all outcomes of a random experiment, then a realized outcome ω determines the second-stage vectors $\mathbf{q}(\omega) \in \Re^{n_2}$ and $\mathbf{h}(\omega) \in \Re^{m_2}$, as well as the matrix $\mathbf{T}(\omega)$ of size $m_2 \times n_2$, all of which are functions of ω. The random parameter vector $\xi^T(\omega) = (\mathbf{q}(\omega)^T, \mathbf{h}(\omega)^T, \mathbf{T_1}.(\omega), \ldots, \mathbf{T_{m_2}}.(\omega))$, where $\mathbf{T_i}.(\omega)$ is the ith row of $\mathbf{T}(\omega)$, is the collection of all stochastic elements of the second-stage problem. With the realization of $\xi^T(\omega)$, a corresponding second-stage solution is recorded in vector $\mathbf{y}(\omega)$.

The $m_2 \times n_2$ matrix $\mathbf{W}$ is termed the *recourse matrix*, which is assumed to be fixed. That is, the same rule or scenario is implemented in the second stage for all realizations of ω that necessitate a corrective action to the first-stage decision. The notation for the second-stage solution vector does not imply that $\mathbf{y}(\omega)$ is functionally dependent on ω, which is the case for the aforementioned second-stage vectors and matrices. Rather, it conveys the fact that different realizations of uncertainty will most definitely lead to different $\mathbf{y}(\omega)$, as dictated by the second-stage objective of minimizing $\mathbf{q}(\omega)^T\mathbf{y}(\omega)$.

As indicated by the overall objective function z, the goal of stochastic recourse programming is to find a first-stage decision that is optimum with respect to not only the deterministic objective $\mathbf{c}^T\mathbf{x}$, but also the expected value of second-stage corrections. This expected value is quantified as the mathematical expectation of optimal recourse actions taken over all possible future ω realizations. In essence, it represents a solution that is, on average (*i.e.*, expected to be), the least likely option to fix in the yet uncertain future.

3.2.3 Formulation of Recourse Function

The presentation of the two-stage stochastic recourse program, as Eq.(2), is referred to as the "extensive form." It clearly shows the association of a single, second-stage solution vector to a possible realization of $\xi^T(\omega)$. A more condensed version of this programming formulation is known as either the "implicit representation" or the "deterministic equivalent program (DEP)," which is shown below.

$$\begin{aligned} \min_{\mathbf{x}} \quad & z = \mathbf{c}^T\mathbf{x} + Q(\mathbf{x}) \\ \text{s.t.} \quad & \mathbf{A}\mathbf{x} = \mathbf{b} \\ & \mathbf{x} \geq 0 \end{aligned} \tag{3}$$

$$\text{where} \quad Q(\mathbf{x}) = \mathbb{E}_\xi \left[Q(\mathbf{x}, \xi(\omega)) \right] \tag{4}$$

$$\text{and} \quad Q(\mathbf{x}, \xi(\omega)) = \min_{y} \left\{ \mathbf{q}(\omega)^T \mathbf{y} | \mathbf{W}(\omega)\mathbf{y} = \mathbf{h}(\omega) - \mathbf{T}(\omega)\mathbf{x}, \mathbf{y} \geq 0 \right\} \tag{5}$$

With the introduction of the second-stage value function $Q(\mathbf{x}, \xi(\omega))$, the DEP form emphasizes the fact that the second-stage solution $\mathbf{y}(\omega)$ is the result of its own constrained optimization problem. Eq.(5) should be understood as the value of the second-stage for given realizations of ω and $\mathbf{x}$. Then, Eq.(4) represents the expected value of a corrective action at the second stage for taking $\mathbf{x}$ in the first stage. This is why $Q(\mathbf{x})$ is often called the *recourse function* in literature.

Globally, the explicit relationship between $\mathbf{y}(\omega)$ and uncertainty is de-emphasized in the implicit representation form. The implicit relationship between the first-stage decision and second-stage correction is accentuated via the recourse function instead. When this before-and-after effect is captured using a penalizing approach, what results is a recourse formulation known as "simple recourse" that does not make a distinction between $\mathbf{x}$ and $\mathbf{y}(\omega)$. The DEP form of Eq.(3) can be further simplified into a simple recourse model by re-casting the recourse function as follows:

$$Q(\mathbf{x}) = \mathbb{E}_{\xi} \left[\sum_{i \in I} \left(q_i^+ \eta_i(\mathbf{x}, \omega)^+ + q_i^- \eta_i(\mathbf{x}, \omega)^- \right) \right] \tag{6}$$

where q_i^+ and q_i^- represent unit penalty costs due to, respectively, surpluses $\eta_i(\mathbf{x}, \omega)^+ = \max\{0, \eta_i(\mathbf{x}, \omega)\}$ and shortages $\eta_i(\mathbf{x}, \omega)^- = \max\{0, {}_i(\mathbf{x}, \omega)\}$. The terminology indicates the direction of resulting deviation from the i^{th} random constraint, $\eta_i(\mathbf{x}, \omega) = \mathbf{T_i}(\omega)\mathbf{x} - \mathbf{h_i}(\omega)$, due to a given realization of ω and first-stage decision $\mathbf{x}$. It is assumed that there are a total of m different linear constraints; *i.e.*, $i \in I = \{1, \ldots, m\}$.

The underlying idea of simple recourse models is that the corrective action in the second stage is to compensate for infeasibilities should they occur after the realization of uncertainty. A penalizing cost is associated to such compensations to model the reality that correcting for a bad first-stage decision is costlier than not needing to recourse at all. The recourse penalty should also be made sufficiently large with respect

to the first-stage objective. Otherwise, a trivial solution resulting in an optimal value for $\mathbf{c}^T\mathbf{x}$ will always be obtained regardless of the number of second-stage (random) constraints or uncertain parameters.

How the recourse penalty affects the overall decision is demonstrated using the following linear programming problem with nondeterministic constraints.

$$\begin{aligned} \min_{\mathrm{x}} \quad & f = x_1 + x_2 \\ \text{s.t.} \quad & g_1 = \xi_1 x_1 + x_2 \geq 7 \\ & g_2 = \xi_2 x_1 + x_2 \geq 4 \\ & x_1 \geq 0 \\ & x_2 \geq 0 \\ \text{where} \quad & \xi_1 \sim U(1,\, 4) \\ & \xi_2 \sim U(\tfrac{1}{3},\, 1) \end{aligned} \tag{7}$$

Here, $U(a, b)$ represents a uniform probability distribution bounded by the real-valued integers a and b. This bounds the possible outcome of ω to fall between 1 and 4 for ξ_1, and 1/3 and 1 for ξ_2. The stochastic recourse version of the same problem can be written as follows:

$$\begin{aligned} \min_{\mathrm{x}} \quad z \quad &= \quad x_1 + x_2 + \mathbb{E}[Q_1(x_1\,, x_2,\, \xi_1)] + \mathbb{E}[Q_2(x_1\,, x_2,\, \xi_2)] \\ Q_1(x_1\,, x_2,\, \xi_1) \quad &= \quad \begin{cases} c_p(7 - \xi_1 x_1 - x_2) & \text{if} \quad (7 - \xi_1 x_1 - x_2) > 0 \\ \text{otherwise} \qquad 0 \end{cases} \\ Q_2(x_1\,, x_2,\, \xi_2) \quad &= \quad \begin{cases} c_p(4 - \xi_2 x_1 - x_2) & \text{if} \quad (4 - \xi_2 x_1 - x_2) > 0 \\ \text{otherwise} \qquad 0 \end{cases} \\ \text{where} \quad \xi_1 \sim U(1,\, 4) \quad &\text{and} \quad \xi_2 \sim U(\frac{1}{3},\, 1) \end{aligned} \tag{8}$$

Each recourse function can be numerically computed as the mean value of the corresponding second-stage value function after a large number of random experiments.

The resulting two-stage optimization quickly becomes a computationally intensive process. A case in point, each optimum shown in Figure 18 had to be found by running 10,000 cases of descriptive Monte Carlo sampling [88] *every time* the Modified Method of Feasible Directions optimization algorithm [89] evaluated the objective and constraint functions. The optimization results clearly indicate that if the cost of

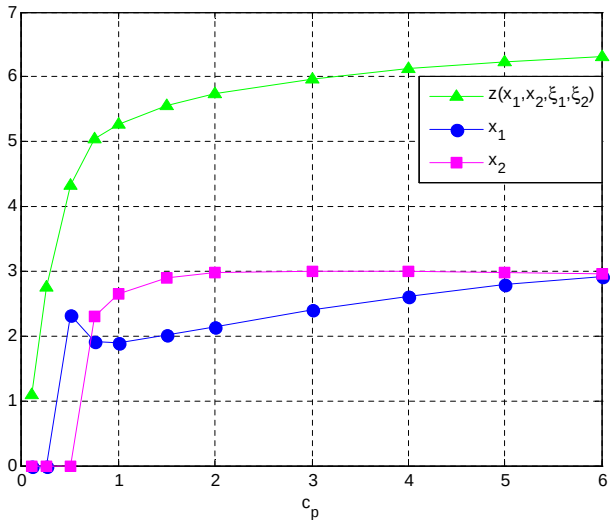

Figure 18: Role of Recourse Penalty in Stochastic Solutions

recourse is cheap (*i.e.*, the value of c_p is small), then there is no clear and present need to find a stochastic solution that is well-hedged against possible unfavorable outcomes. Under such circumstances, one would just have to go with a solution that is the cheapest now and perform corrective actions as they become needed.

3.2.4 Worth of Stochastic Programs

As discussed in the beginning of this Chapter, one way to cope with nondeterministics in design is to *assume* how the sources of uncertainty will be realized. For example, conceptual and preliminary engineering analyses are often done by assuming pessimistic realization of imperfect information. Developing a system to the so-called worst-case scenario is equivalent to applying design margins as a hedge against future

variations in TPM values, as shown in Figure 4. Although mathematically not rigorous, the application of design margins is, nonetheless, a tempting option for design engineers and project managers alike. There is no denying that it is a very convenient way to explain away the presence of uncertainty from an implementation standpoint.

Anticipating the future realizations of uncertain events in such a deterministic, scenario-based manner is said to result in "wait-and-see" solutions, first coined by Madansky [90]. The moniker is a direct reference to the act of *waiting and then seeing*, albeit virtually, the final values of the random parameters, before proceeding with the optimization. Table 3 lists the optimum solutions of Eq.(7) depending on pessimistic (worst), optimistic (best), and unbiased (average) estimations of ξ_1 and ξ_2 from their respective probability distributions[1].

Table 3: Comparison of Three Uncertainty Realization Scenarios

	Worst	**Average**	**Best**
ξ_1	1	5/2	4
ξ_2	1/3	2/3	1
x_1^*	1.95354	1.63639	1.36369
x_2^*	5.04646	2.90902	2.63631
f^*	7.00000	4.54541	4.00000
g_1^*	7.00000	7.00000	8.09107
g_2^*	5.69758	4.00000	4.00000

The worth of a solution that is identified via a stochastic recourse program, as compared against the wait-and-see solutions, can be measured by two quantities: the Expected Value of Perfect Information (EVPI) and Value of the Stochastic Solution (VSS). The discussion that follows refers to the linear programming models of Eqs.(7) and (8) in explaining what each measure signifies, and how the information can be used to justify the additional efforts of implementing stochastic programming.

[1]The superscript star symbol above the variables and functions indicate that those points were evaluated at the optimum.

3.2.4.1 Expected Value of Perfect Information

EVPI is a measurement of worth, having the ability to forecast the future. Every time one fixes or assumes the value for a random parameter, it is equivalent to knowing in advance (virtually waiting and seeing) what that realization would turn out to be. Mathematically, EVPI is defined as the difference between the stochastic solution and the expectation of a discrete number of wait-and-see solutions. The latter, in the case of Eq.(7), becomes the average of the three optimum solutions listed in Table 3. Table 4 lists the EVPI with respect to different stochastic solutions at various levels of recourse penalty. The results are indicative of the rather obvious outcome: the capability to forecast knowledge with certainty is worth more when the implementation of the second-stage corrections is costly.

Table 4: EVPI for Different Stochastic Solutions

	$c_p = 1$	$c_p = 2$	$c_p = 3$	$c_p = 4$	$c_p = 5$	$c_p = 6$
$\mathrm{E}[f^*_{\mathrm{Wait-and-See}}]$	5.18180	5.18180	5.18180	5.18180	5.18180	5.18180
f^*	5.27763	5.73715	5.97318	6.12688	6.23711	6.32033
EVPI	0.09583	0.55534	0.79138	0.94507	1.05530	1.13853

3.2.4.2 Value of Stochastic Solution

If EVPI is perceived as how much a decision maker is willing to pay for perfect forecasting, then VSS is a measurement of the cost of entirely ignoring uncertainty. The act of replacing ξ_1 and ξ_2 by their mean values is treated as an example of neglecting the presence of uncertainty. In order to compute VSS, the optimization problem is first solved deterministically with ξ_1 and ξ_2 fixed at the mean values of their probability distributions to obtain an Expected Value (EV) solution. The optimum of the unbiased scenario listed in Table 3 qualifies as an EV solution for the example problem at hand. With the first-stage decision fixed at $x_1 = 1.63639$ and $x_2 = 2.90903$, a finite number of uncertainty scenarios are evaluated in the second stage. The average of the resulting objective function values is known as the

Expected result of using the EV solution (EEV). Finally, VSS is computed as the difference between the EEV and the stochastic solution. Table 5 lists a number of VSS corresponding to different c_p values. As expected, the more balanced (higher c_p values) a stochastic solution is, the greater the value is of accounting for uncertainty.

Table 5: VSS for Different Stochastic Solutions

	$c_p = 1$	$c_p = 2$	$c_p = 3$	$c_p = 4$	$c_p = 5$	$c_p = 6$
EEV	5.29298	6.04054	6.78810	7.53566	8.28321	9.03077
f^*	5.27763	5.55670	5.73715	5.97318	6.12688	6.23711
VSS	0.01534	0.30339	0.81492	1.40878	2.04611	2.71044

3.3 Chapter Conclusions

In an effort to assemble the foundational elements for a recourse-based design method, the scope of the literature survey was extended from modern systems analysis strategies to the field of optimization under uncertainty. The need to formally address the phenomenon of recourse was perceived from the single-staged and decoupled manner in which existing probabilistic design formalisms implement uncertainty analysis and design optimization. This, in turn, led to the discovery of stochastic programming, with which a number of parallels can be drawn with the remedial aspect of systems development.

Above all, the concept of stages appears to be a natural way to model the time-phased process of engineering design. It is especially convenient that each stage can be defined to include any number of sequences or events. For example, the first stage may encompass all development phases up to detailed design, during which optimal solutions are sought by making deterministic assumptions about the unknowns. Once such previously uncertain information becomes resolved in manufacturing through testing and demonstration activities, then the succeeding phases can be considered the second stage, in which the evolution of TPM values is intensely scrutinized.

Secondly, in stochastic programming terms, recourse means a corrective action

that is taken to mitigate the unfavorable consequences, if any, of realized uncertainty. Such notion of *a posteriori* compensation is intrinsically compatible with the author's definition of recourse, as given in §1.1, and thus, seems relevant to consider as the basis for addressing the presence of uncertainty in an engineering design process.

Thirdly, the past successes of the simple recourse model [83] indicates the applicability of the penalizing approach in solving various real-world phenomena. The same formulation should also be pertinent to the design of an engineering system since getting it right the first time is almost always less costly than fixing it after the fact.

Chapter IV

FORMULATION

In this pivotal chapter, a matching **Hypothesis** to each of the three questions is introduced. Each hypothesis embodies a carefully postulated response, based on the relevant thematic evidence and knowledge that were acquired throughout the literature review process, to the specific challenges identified by the research questions. Subsequently, the formulation of a recourse-based solution approach, and its application to the design of notional fuel cell aeropropulsion systems, are presented as the **Research Task**. Each sub-task should be understood as an experiment devised to test the validity of the claims put forth by one or more hypotheses. As alluded to in §3.3, this two-stage, nondeterministic design formalism was inspired by the fundamental ideology behind stochastic programming.

4.1 Hypotheses and Research Task

Any attempt at defining a formal method that captures the remedial aspect of product development should, first and foremost, include a plan for assessing the additional cost of design corrections. Although two-stage stochastic programming models seem to provide a suitable framework for building a recourse-based solution approach to nondeterministic engineering problems, Birge and Louveaux warn that the interpretation of stages and recourse is "not only problem dependent but also context dependent." [83] Further complicating matters is the fact that the first-stage objective and the expected cost of recourse must be in the same *currency*, *i.e.*, units. With the exception of the simplest systems, the path of penalty propagation from engineering corrections to TPMs may not be so transparent, warranting prudence on the design engineer's part in properly modeling the second-stage value function.

Coupled with this issue is the need to perform random experiments *concurrently with* optimization. Even the simplest stochastic program, which is the two-stage model with simple recourse, possesses a bi-leveled structure: uncertainty analysis is embedded in the global optimization loop. The cost of recourse is represented by an expected penalty cost model, which is endeavored to be minimized, along with a single first-stage objective. Nevertheless, such interpretation of mathematical expectation of a random variable is only appropriate under the strong law of large numbers, necessitating what could be considered a prohibitive amount of random sampling runs to evaluate $Q(\mathbf{x}, \xi(\omega))$. It is, therefore, not unreasonable to envisage the combined applicability of MCS with an appropriate surrogate modeling technique.

A necessary prerequisite to all this is the capability to quantitatively predict the TPM of a given fuel cell aeropropulsion system. One way of ensuring such a capability for an unprecedented engineering system is modeling and simulation. The two approaches to building computational models offer guidance as to the appropriate structure of each model, depending on the type of relationship to be represented. As discussed in §2.2.3, the physical principles are best modeled via the causal, or forward-looking, approach, whereas the backward-looking, or non causal, approach is more appropriate for capturing scaling relationships. It is especially fitting here that computational models should be created, as they are prescriptive ("by predicting and/or duplicating [91]") and lend themselves easily to be computerized. The latter trait is a necessary condition for simulation [92].

The above generalizations formed the basis for postulating the following three hypotheses. The order in which the research questions are addressed are as follows:

> **Hypothesis 1**: Investigating the scalability of a desired fuel cell aeropropulsion system, within the fidelity bounds of the created simulation environment, is an essential prerequisite for the suggestion of a synthesis

algorithm that balances computational overhead against analysis accuracy. (Question 1)

Hypothesis 2: It is possible to model the remedial action at the second stage, necessitated by the rapidly evolving nature of fuel cell technology, via the combined application of appropriate Design of Experiments, constrained optimization, and Surrogate Modeling techniques. The expected cost of recourse can then be numerically computed via a Monte Carlo sampling of the meta-modeled value function. (Question 2)

Hypothesis 3: If the recourse function computed as per Hypothesis 2 is found to result in a largely uni-modal solution space of a given fuel cell aeropropulsion system, then it is plausible that an optimal solution to a formulation based on the premises of two-stage stochastic programming can be found using path-building optimization techniques. (Question 3)

The validity of each hypothesis was decided to be tested by a number of *virtual* experiments. A holistic approach was taken, whereby each experiment was to be conducted over the course of method development and implementation, as detailed below:

Research Task: Formulate and implement a recourse-based solution approach to the design of fuel cell aeropropulsion systems, which includes the following sub-tasks as part of its major steps:

Sub-task 1: Create a simulation environment that allows the rapid performance modeling and sizing of a fuel cell aeropropulsion system, given its architecture. For a fixed cycle, investigate if the system's physical scale, over a reasonable range, has any bearing on its thermodynamic efficiencies and power-lapse characteristics. Suggest a synthesis algorithm

that is compatible with either the actual value-based approach or specific parameter-based approach to aircraft sizing, depending on system scalability. (Hypothesis 1)

Sub-task 2: Design a two-stage recourse programming model around the simulation environment created in sub-task 1. Define the stages and the remedial action which constitutes recourse. Identify all value, cost, merit, and constraint functions, with a particular emphasis on modeling the second-stage value function. Wherever necessary, utilize an appropriate Design of Experiments technique as a preparatory step towards meta-modeling each function. Create surrogate models of all program functions over a reasonable range of design variables and random parameters, and validate their goodness of fit and predictive capabilities. (Hypothesis 2 and 3)

Sub-task 3: Visualize the N-dimensional space of the recourse function with the aid of the second-stage value function meta-modeled in sub-task 2 and Monte Carlo sampling. Should it appear to be mostly unimodal, then recast the extensive form of the two-stage program in the implicit representation. Solve the resulting program with a gradient-based optimization algorithm. Compare the optimal solutions attained from multiple starting points as a check for possible non-convexities which may be present in the unexplored dimensions. (Hypothesis 2 and 3)

The purpose here is to gather sufficient quantitative evidence that can provide insight into the reasonableness of the embodied claims. Should all aspects of the hypotheses check out, then by extension, it is equivalent to having demonstrated the proposed strategy's effectiveness in simulating the remedial aspect of system development, which, to the best of this author's knowledge, has remained elusive in the

aerospace domain. At minimum, certain elements of the developed techniques should be applicable to similar engineering challenges.

4.2 Bounding the Problem

It is beyond the scope of this research to encompass the pre-conceptual stages of engineering design. These early phases are the time for synthesizing the disorganized fusion of "insights, vision, intuitions, judgment calls, ... dreams, hopes, needs, and technical possibilities [46]" into a tangible concept. In order to rise up to this creative challenge, a group of collaborators often form what is known as an Integrated Product Team (IPT). The IPT eventually identifies a small number of manageable system architectures which will be further analyzed in later design phases. Maier and Rechtin [46] suggest the following differentiation between an architecture and a system.

> System: a collection of things or elements which, working together, produce a result not achievable by the things alone.
>
> Architecture: the structure - in terms of components, connections, and constraints - of a product, process, or element.

The above definitions clarify that a system is the sum of its parts, and every system possesses an underlying architecture. In defining architecture, further clarification is obtainable if more descriptive terms, such as *interrelationships* or *interconnections* are used in place of "structure" to express the same idea. Thus, to paraphrase the above definition, an architecture can be interpreted as *the representation of the interrelationships between entities that are interconnected to compose a system.*

Arriving at these handfuls of architectural permutations is a non-trivial activity that requires a significant amount of organizational resources in terms of manpower, time, etc. Countless hours of deliberations among the IPT members are often necessary to differentiate the final few from all other possible system architectures. It is

certainly a daunting task for one person to do justice to, even with the aid of recently emergent qualitative techniques that aspire to enable the popular group decision-support methods to be more single-user friendly.

4.2.1 Architectural Space Definition

The sheer magnitude of the architecting problem can be demonstrated via the Matrix of Alternatives, first proposed in the late 1940's by Fritz Zwicky [93], who also published a book on Morphological Analysis in 1969 [94]. When applied to define a system's architectural space, the rows represent the system's functional decomposition results, and the possible alternatives are populated column-wise. Table 6 is one such Matrix of Alternatives conceivable for the problem of interest, showing 4,199,040 numbers of architectural paths to realizing a fuel cell aeropropulsion system. This figure was calculated by limiting the choices to only one alternative per row. In actuality, certain functions, such as Turbomachinery, BOP, and PMAD, may require more than one element to constitute a working system. If such is the case, then the possible number of architectural permutations reach on the order of thousands of trillions, resulting in an overwhelmingly vast combinatorial space.

It is thus clear that even with a simulation code that is capable of evaluating all of the permutations in existence, a feat that is next to impossible in an academic environment, running a one-second simulation on each and every architecture would take many millennia. Of course, some of the available choices are physically or technologically incompatible permutations (*e.g.*, liquid H_2 and CPOX). This issue is one of the most well-recognized disadvantages of Morphological Analysis: the more complex a system is, the greater the dimensionality of its attributes becomes, resulting in an extremely difficult decision-making problem for a solitary designer.

Table 6: Matrix of Alternatives for Fuel Cell Aeropropulsion System

Functions	**Alternatives**					
Energy Conversion	AFC	PEMFC	DMFC	PAFC	MCFC	SOFC
Propulsion	DC Motor	AC Induction Motor	BLDC Motor	SR Motor	Cryogenic Motor	HTS Motor
Energy Source	Gaseous H_2	Liquid H_2	Methanol	Petroleum-derived Liquid Fuels	Coal Gases	Natural Gases
Primary Energy Storage	Conventional Fuel Tank	High-pressure Tank	Cryogenic H_2 Storage Tank	Metal Hydrides	Glass Microspheres	Carbon Nanofibers
Auxiliary Energy Storage	Lead Acid Battery	Nickel-based Battery	Sodium-based Battery	Lithium Battery	Metal Air Battery	Ultracapacitor
Turbomachinery	Roots Compressor	Lysholm Compressor	Centrifugal Compressor	Axial Flow Compressor	Radial Turbine	Axial Flow Turbine
Fuel Processing	Steam Reformation	Autothermal Reformation	CPOX	Indirect Internal Reformation	Direct Internal Reformation	
BOP	Humidifier	Intercooler	Combustor	Heat Exchanger	Pump	Controllers
PMAD	Thyristor	MOSFET	IGBT			

Recently in the aerospace systems design literature, several developments endeavoring to address this shortfall of Morphological Analysis, while preserving its usefulness as a creative design tool, have been reported. The most notable of them all is the Interactive Reconfigurable Matrix of Alternatives (IRMA) proposed by Engler et al [95]. IRMA automates the majority of human-in-the-loop tasks, such as filtering out alternatives according to some user-defined criteria, *e.g.*, compatibility, technological maturity, life-cycle costs, etc. This feature greatly enhances the usage of the Matrix of Alternatives as a single-user tool by minimizing the number of times an IPT must convene to deliberate. In addition, it incorporates a qualitative tool for ranking the alternatives in each row, or across multiple rows, for differentiating contentious permutation selections. The current spreadsheet version of IRMA is, nonetheless, not as easily reconfigurable as it is led to believe, thus requiring a complete recoding of the tool for a brand new pre-conceptual design problem. A case in point, Soban and Upton embraced the core ideals of IRMA, but eventually developed a separate spreadsheet-based tool titled, Qualitative Interactive Evaluation Tool, for identifying candidate fuel cell aeropropulsion system architectures for a naval Uninhabited Aerial Vehicle (UAV) [96].

Other authors have suggested exploring the concept space defined by the Matrix of Alternatives in a quantitative manner. Specifically, the application of advanced exploratory optimization techniques, such as Genetic Algorithm or Ant Colony Optimization have been advocated by Buonanno [97] and Villeneuve [98], respectively. Although appearing novel on paper, the tools that result from such methods have limited practical value other than the original design problems for which they were created.

Therefore, instead of attempting a cursory pass at single-handedly examining the combinatorial space of fuel cell aeropropulsion system architectures, the problem was bounded by assuming the architectural choices for beginning conceptual design had

already been narrowed down. Justifications for these particular choices follow in the remainder of this section. In order to prevent the selected architectural paths to be results of biased opinions, a wide variety of published sources that contemplate the advantages, *as well as* the disadvantages of fuel cell system architectures, were referenced[1].

4.2.1.1 Energy Conversion Alternatives

Amongst the six technological options listed in the matrix, the two that are widely considered to be the most applicable for transportation systems in the fuel cell industry are PEMFC and SOFC technologies. As covered in §1.2.1, all prototype FCVs known to date are designed around the PEMFC technology, with the buses at Georgetown University, running on PAFCs, being the only exceptions to the norm. No instances of SOFCs being utilized as the primary power plant on a ground vehicle have yet to be reported. The technology is, however, beginning to prove itself as a serious contender to the dominance of PEMFCs by expanding its premier market base to that of automotive Auxiliary Power Units (APUs).

Thus far, PEMFC technology has been the favorite choice of aviation visionaries. Earlier analytical work at NASA Langley Research Center (LaRC), which became the predecessor to the technology demonstrator efforts later at NASA Dryden, focused on a regenerative concept based on PEMFCs [100, 101]. The reason for adapting such an architectural choice appears to have been influenced by the demonstrated effectiveness of the Regenerative Fuel Cell (RFC) system on board the Space Shuttle Orbiter, which was the most prominent example of fuel cells in the aerospace sector at the time. Close to 20 years later, the revived interest on fuel cells led the researchers at NASA Glenn Research Center (GRC) to focus on modeling an electric aeropropulsion system based on PEMFC technology for both General Aviation (GA) [102] and commuter-type

[1] Unless noted otherwise, either Larminie and Dicks [5] or Larminie and Lowry [99] was extensively referenced in preparing the sections that follow.

transport aircraft [103].

The latest publications originating from NASA on the area of fuel cell aeropropulsion, however, reflect the agency's shift in focus from PEMFCs to SOFCs. A few of the researchers, who had authored the papers on PEMFC modeling work, moved on to create physics-based analysis [104] and sizing [105] models that are of much higher fidelity than the empirical models used for the previous PEMFC studies. These models were created in support of a series of seminal studies on the aeronautical applications of SOFC, including an SOFC/GT hybrid APU [106, 107] and an SOFC powered High-Altitude Long-Endurance (HALE) UAV [108][2]. This increased interest towards SOFC technology is further shown in a joint study between Boeing and GRC, as reported in Atreya et al, which declared the superiority of SOFCs over PEMFCs or Internal Combustion Engines (ICEs) for future HALE UAV applications [111].

Unfortunately, it is still difficult to reach an unequivocal consensus on which fuel cell technology is the better alternative based on the findings of literature review alone. All instances of successfully demonstrated fuel cell powered flight to date have capitalized upon the maturity and commercial availability of PEMFC technology, as summarized in Appendix A. In addition, the advocates of SOFCs neglect to mention many of the hurdles that must be overcome to render this particular technology feasible for transportation applications, such as low weight specific power; less robustness to frequent start and stop cycles, which is critical for vehicular operations; more burdensome ancillary equipment needed to manage the complex fluidic and thermodynamic interactions between the sub-system components; the need for *hot boxes*, namely extra layers of insulation to protect the environment around the high temperature components; material concerns such as proneness to fatigue, thermal expansion,

[2]The collaborative work between MSE and LaRC, reported by Alexander et al [109, 110] a few years prior to the aforementioned studies, also favor SOFCs for the design of an emissionless transport aircraft, although the models used for their analyses were of less fidelity. It is interesting to note that the work of Alexander et al is never acknowledged in any of the studies.

etc. All of the above concerns contributed to the indecision about which of the two alternatives should be exclusively studied in this thesis work. It was eventually decided that both PEMFC and SOFC technologies, on their own merit, deserved to be considered in parallel.

4.2.1.2 Propulsion Alternatives

The second row of the matrix lists six technological options that can fulfill the function of motor-driven propulsion. From left to right, the alternatives are placed in the order of technological sophistication. The available choices represent a diverse mix of off-the-shelf hardware, as well as more experimental and newly conceived designs.

The Direct-Current (DC) motor is the forerunner of all modern electric motor technology, having been conceived by William Sturgeon in 1832 [112]. It implements the simplest method of exploiting the phenomenon of electromagnetic force. The Biot-Savart Law of electromagnetism states that a current carrying wire generates a circular magnetic field around the wire [113]. If such a wire is immersed in a stationary magnetic field, then a force acting on the wire is developed. The direction of the resultant Lorentz force is perpendicular to both the wire and the surrounding magnetic field, thus allowing the generation of torque. A brushed DC motor consists of at least a pair of permanent magnets to generate the stationary magnetic field, a minimum of one wire coil through which the DC flows, and a commutator that ensures the direction of the resultant torquing action is maintained with each revolution. The classical arrangement of the above components is such that: (a) the wire coil is the rotating part, or the rotor, of the machine; (b) the permanent magnets form the stationary part, or the stator, of the motor; and (c) the brushes and the commutator combined become the armature, or the points across which an input voltage is supplied.

Such a mechanically commutating design, however, is the Achilles' Heel of classical

brushed DC motors and causes a number of undesirable characteristics which limit the applicability of this particular motor technology to small portable or domestic appliances. For one, the constant rubbing between the brushes and the commutator leads to many wear and tear problems that make the DC motor to be the least reliable of the listed six. What is worse is that the frictional heat generated by the commutating action occurs inside the motor core, from which it is difficult to be removed. The trapped heat adversely impacts the electrical efficiency of the motor as the resistance of DC carrying the wires increases with increasing temperature. Sparks caused by friction and the maximum current density per unit area of brush materials also bound the upper limit of the motor's maximum rotational speed and output power, respectively. In contrast, the motor types introduced next are all electronically commutating designs.

The operation of an Alternating Current (AC) induction motor is based on the principle of rotating magnetic field, which was first discovered and exploited by Nikola Tesla in 1882 [114]. It is a very mature technology, commonly found over a large spectrum of power scales, ranging from consumer electronics to industrial applications rated at hundreds of kW. Conducting materials, usually copper coils, are wrapped around the stator of an induction motor, which is supplied with a polyphase electrical supply to induce a *rotating* magnetic field emanating inwards. Note that this is in contrast to the *stationary* magnetic field of DC motors. Another difference to recognize is that the armature is placed on the stator, as opposed to on the rotor. Once set in motion, the rotating magnetic field induces an electric current on the rotor coils - or field windings - in accordance with the principles of electromagnetism. This induced current in turn produces an opposing magnetic field which forces the rotor to chase after the rotating magnetic field, thus generating torque. As one can visualize, there is no physical contact between the rotor and the stator, which prevents the build-up of heat inside the motor from both mechanical and electrical losses. In

any case, the majority of electrical losses occur in the stator windings that draw AC power, but this exterior part of the machine can be much more readily cooled than the inside of a DC motor for more efficient operations.

One is initially led to believe that a brushless DC (BLDC) motor is the classical DC motor without the brushes. In actuality, it is really an AC synchronous motor. AC because the throughput current magnetizing the stator variates to create the rotating magnetic field, and synchronous because the rotor turns in synchronism with the supply frequency or its sub-multiple. The technology is, nonetheless, termed BLDC in honor of the fact that a DC power supply is required, and the motor's torque/speed characteristics resemble that of a brushed DC motor. There is, however, little physical resemblance between a BLDC motor and a DC motor. The BLDC motor consists of a permanent magnet in its rotor and coils in its stator, whereas the typical internal layout of the brushed DC motor is the exact opposite of what was just described.

The main difference between the AC induction and BLDC motors is the manner in which commutation is implemented. Similar to the AC induction motor, the armature of the BLDC is located in its stator. Instead of being connected to a polyphase electrical supply, however, the BLDC motor draws DC from a DC power source, such as batteries or fuel cell systems. It is the motor's sophisticated electronic controller that manages the pulsing and distribution of the DC throughout the stator windings, such that a rotating magnetic field can be generated without polyphasing currents. Because the rotor is a permanent magnet, the near-instantaneous interaction between the two magnetic fields results in a motor whose speed can be controlled in synchronism with the rotating outer field. This is why BLDC motors are sometimes referred to as permanent magnet synchronous motors in the literature.

The circuitry of controllers attached to off-the-shelf BLDC motors is not dissimilar to that of an inverter, which is covered in §4.2.1.9. Due to modern sensor and microprocessor technologies, very precise adjustments of motor speed and torque can

be done without sacrificing efficiency. The permanent magnet rotor design of BLDC motors also results in one less source of electrical losses compared to the conventional induction motors. This is why even the low-end BLDC motors that are air cooled display peak efficiencies, which are a couple of percentages higher than air-cooled induction motors. More advanced water or oil-cooled BLDC motors are reported to bring an order-of-magnitude improvement in specific power over two-pole induction motors.

The switched reluctance (SR) motor represents yet another solution to the challenge of efficient brushless commutation. Simpler in principle than either the induction or BLDC motor technologies, an SR motor exploits the *reluctance* of the magnetic field to stay out of alignment. The stator is again where the DC-powered armature is located and through which a rotating magnetic field is created. The rotor, however, is nothing more than a piece of magnetically soft iron because it only needs to be able to disturb the induced magnetic field lines. Once disturbed, the field will attempt to revert back to its symmetrical state, inducing the torque that turns the rotor in the process. If the magnetization and demagnetization of the stator windings surrounding the rotor can be precisely managed by an electronic controller, then a smooth production of torque is possible. Both the peak efficiency and specific power of SR motors fall somewhere in between the performance and gravimetric envelopes of induction and BLDC motors.

Motor efficiency is a function of several sources of losses that occur at different parts of the motor. Amongst these, the electrical losses occurring at the coils are known as copper losses in honor of the fact that copper wires have been, and still are, the dominant choice for field windings on an electric motor, regardless of its type. Copper losses can be reduced with better cooling of the windings since there is an inverse relationship with temperature and the electrical resistivity of conductors. Cooling technology thus becomes a key enabler for attaining highly efficient and power

dense electric machines.

Although scant, reports of experimental work on electric motors cooled by cryogenic liquids are found in the literature. In 1991, Long Electromagnetics, Inc. manufactured a 1 MW (1341 hp) prototype electric machine for the U.S. Air Force [110]. One of the Long motor's unique design features was high-purity aluminum wires, instead of the conventional copper windings. Both the stator and rotor were cooled with liquid hydrogen, which enabled the aluminum wires to possess a current density of 80,000 A/in^2, resulting in a very compact and efficient machine. At just 200 lbs, the efficiency of the measured efficiency of the motor was a phenomenal 99.48%. In a 2003 paper, Wickenheiser et al also mention a research thrust at NASA, whose goal is to demonstrate a 10 hp motor cooled with liquid nitrogen [103].

Another class of electric motors that operate at cryogenic temperatures are superconducting motors. The most commonly found superconducting motor design is an AC synchronous motor, consisting of a conventional stator (wound from copper), but whose field winding in the rotor is made out of a superconducting material. The High Temperature Superconductor (HTS) motor listed on the matrix refers to a specific AC synchronous motor design with a rotor wound from Bi-2223 tapes [115]. If the temperature of the superconducting winding can be maintained between 20 and 50 K, then the motor can exhibit a number of advantages over conventional, iron-cored synchronous motors, including theoretical efficiency that approaches 99%, due to the negligible DC losses in the rotor winding; very compact and lightweight design, due to the extremely high current density of the HTS wire; more responsive dynamic behavior, due to the removal of iron from both the rotor and stator, not to mention the resultant savings in weight. The downside of applying superconducting motor technology to transportation applications is the rather stringent need for cooling. Cryogenic cooling of the rotor, which is a non-trivial issue, is not optional, but required. Air-cooling the armature, in this case the stator, winding has also been

identified as one of the challenging areas that require further investigation by the leading researchers of HTS motor technology [116].

Ultimately, the decision regarding whether a given motor technology would be chosen as one of the final propulsion alternatives was based on a multitude of factors, including electrical performance, gravimetric characteristics, current industry trends, and ease or difficulty of access to publicly available data. It was clear from the beginning that the brushed DC motor would not be capable enough to be applicable for aeropropulsion. Although spectacular claims on both the performance and size of cryogenically cooled, but not superconducting motors were found, the lack of more rigorous information in the open literature could not justify considering the technology henceforth. The SR motor was acknowledged to be the closest rival to the BLDC motor, but it has yet to prove itself as a serious contender to the commercial dominance of BLDC technology. BLDC motors are currently favored by the leading developers of hybrid-electric ground vehicles, such as UQM, Honda, and Toyota. The three remaining motor types - AC induction, BLDC, and HTS motors - seemed to represent a balanced portfolio of the tried-and-tested, up-and-coming, and highly advanced technologies. Therefore, all three are treated as available architectural elements in the remainder of this document.

4.2.1.3 Energy Source Alternatives

All fuel cell types, with the exception of DMFC, must be supplied with hydrogen - in one form or another - to carry out the redox process. Elemental hydrogen, however, is exceptionally rare on Earth, and therefore it must be processed from other natural resources, such as fossil fuels or water. In the strictest sense of the terms, only coal and natural gases should be referred to as energy sources. Both represent the primary reservoirs, or the *sources* of all usable energy on our planet. Hydrogen, methanol, and petroleum-derived liquid fuels are actually energy carriers, since these substances

must be artificially produced from the planet's natural energy sources. In the context of this document, however, any matter that can fuel the fuel cells qualifies as an alternative for fulfilling the function of energy source; *i.e.*, the source of energy on board the aircraft.

Amongst the listed alternatives, coal and natural gases are not considered further because the scope of this research encompasses up to the aerovehicle system level. In reality, the hydrogen that gets distributed throughout its production, storage, and delivery infrastructure would be mass-produced from fossil fuels, such as coal and natural gases through the process of fuel reformation. A more environmentally sound and sustainable method of hydrogen production is the process of water electrolysis, the power for which can come from a variety of renewable sources such as solar, wind, and geothermal energy, etc.

One of the well-known drawbacks of PEMFC technology is that the cells require an extremely pure grade of hydrogen. Any trace amounts of CO and other impurities, such as sulfur, will permanently poison the membrane. If fuel reformers that are compact, efficient, and responsive enough to be carried on board a moving vehicle are available, then methanol, as well as heavy hydrocarbons like gasoline, can become potential energy sources for PEMFCs. Much active research on advancing the state of the art of reformer technology has been reported in the automotive sector in the late 1990s to early 2000s. Automakers such as DaimlerChrysler and Opel were early adopters of methanol reformers, while other organizations like Nuvera, Johnson Matthley, and General Motors pursued gasoline-reforming technology. A number of methanol or gasoline-fueled PEMFC driven passenger cars have been demonstrated as a result of this concerted effort. Nevertheless, in August of 2004, the U.S. Department of Energy (DoE) chose to cease the funding for all on-board fuel processing research and development (R&D) from the Hydrogen, Fuel Cells &

Infrastructures Technologies Program [117], practically nullifying all other fuel options besides gaseous and liquid hydrogen, as far as the transportation applications of PEMFCs go. A case in point, every automaker's current flagship FCV is either a liquid or a gaseous hydrogen-fueled PEMFC driven vehicle.

Conversely, SOFC technology is an alternative that is intrinsically compatible with reformates. In addition to hydrogen, CO can be oxidized by the SOFC, whose solid-state electrolyte also happens to be very tolerant of CO_2. This implies that the reactant stream entering the anode can be a *dirty* mixture of hydrogen, CO, CO_2, steam, nitrogen, etc, which are in fact the dominant constituents of reformates processed from petroleum-derived liquid fuels. A number of on-board fuel processing options are available for producing this kind of hydrogen and CO rich gas, including internal reformation. A more in-depth comparison of the technological options for on-board fuel processing appears in §4.2.1.7. Designating liquid hydrocarbons as the exclusive energy source of SOFCs brings an additional benefit of allowing one to sidestep the need for hydrogen storage, which is the subject of the following section.

4.2.1.4 Primary Energy Storage Alternatives

Besides the conventional fuel tank, which becomes the only available energy storage option for an aeropropulsion system architecture with SOFCs, all listed alternatives are different methods of storing hydrogen. The main obstacle in adapting hydrogen as an aviation fuel is its low energy density. Hydrogen possesses almost three times as much energy as petroleum-derived liquid fuels on a gravimetric basis. But for the same volume, its energy content becomes less than half of conventional aviation fuels, making hydrogen a double-edged sword. The ideal hydrogen storage device would, thus, allow the containment of as much hydrogen as possible on a per volume basis, while being structurally light enough to be carried on board a flying vehicle.

The high-pressure tank embodies the simplest and most mature method of hydrogen storage. Gaseous hydrogen is pressurized up to thousands of psi in order to maximize both the gravimetric and volumetric storage efficiency; *i.e.*, the fraction of stored hydrogen mass in relation to total tank mass and volume. The tank can be manufactured from a wide variety of materials, such as aluminum, steel, titanium alloy, or carbon composites. Hydrogen storage tanks rated at 5,000 and 10,000 psi have already been certified according to a number of safety standards, such as ISO 11439 (Europe) and NGV2 (U.S.), and are commercially available to be integrated into FCVs, albeit in low production numbers [117]. Nevertheless, compressed hydrogen tanks are relatively low-capacity alternatives from a storage-efficiency point of view. State-of-the-art mass and volume fractions of hydrogen stored in 5,000-psi tanks are 5.7% and 1.5%, respectively. Doubling the storage pressure to 10,000-psi improves the volumetric capacity to 2.5%, but at the cost of gravimetric storage efficiency, which is reduced to 2.4%. The figures are metrics measured at the system-level (tank, hydrogen, and all support equipment), and not just with respect to the tank itself.

The cryogenic hydrogen storage tank is an insulated, strongly reinforced vacuum or Dewar flask. It represents the most efficient method of storing hydrogen, in terms of volumetric capacity. By cryogenically cooling hydrogen to its liquid state at around 22 K, it is possible to significantly increase the density of hydrogen, which is 0.084 kg/m^3 at STP, to 71 kg/m^3. Therefore, state-of-the-art liquid hydrogen tanks are reported to have a volumetric storage capacity of 3.6%, which is more than double the efficiency of 5,000-psi tanks, and a gravimetric capacity greater than that of 10,000-psi tanks [117]. Even with proper insulation, however, the liquid hydrogen cannot remain permanently stored. The hydrogen inside the tank will begin to boil off; that is, slowly evaporate, thus raising the internal pressure of the containment vessel. This is perceived as one of the major technical challenges for adapting liquid hydrogen storage for vehicular

applications, as the build-up of hydrogen gas must be periodically vented and the storage sub-system must always be oversized to compensate for the boil-off.

Hydrides are compounds that are formed by bonding with the negative ion of hydrogen. In the context of energy storage, metal hydrides refer to a class of metals or metallic alloys that enable the absorption and release of hydrogen gas. Such reactions are entirely chemical in nature, and do not require any additional support systems other than the connecting valves to a fuel cell system. A spent hydride cartridge can be refilled with hydrogen in a manner similar to that of a high-pressure storage cylinder. Despite their inherent simplicity, metal hydrides are gravimetrically inefficient storage methods - less than 1% hydrogen by mass. Metal hydrides are, however, quite efficient in terms volumetric capacity, approaching the levels attainable with cryogenic tanks.

Hydrogen can also be stored in spheres of glass engineered with a diameter on the order of micrometers. The tiny spheres have the property of becoming permeable to hydrogen when heated and impermeable when cooled, thusly allowing themselves to be amenable as hydrogen storage devices. Although glass microspheres release hydrogen endothermically similar to metal hydrides, the level of heat that must be supplied for a practical flow rate of hydrogen excludes them from being compatible with a low-temperature system like PEMFCs. For instance, in order to expedite the purge rate that is on the order of thousands of hours at room temperature, the spheres are required to be heated up to 300 °C for a still miserly period of 15 minutes [118].

Carbon nanofibres are perhaps the most exotic methods of hydrogen storage one can be considered. As the name implies, these are fibrous carbon materials that are synthesized in a nanoscale environment. One micrometer is equal to 1,000 nanometers, and a human hair, by comparison, is on the order of hundreds of nanometers. By making carbon filaments at the nanometer scale, the structure can be made to have greater surface area and porosity that allow practical amounts of hydrogen absorption - and thus storage - near ambient conditions. The initial craze on carbon

nanofibres as the next-generation hydrogen storage device began after the seminal work of Chambers et al, who reported measuring gravimetric storage capacity of 67% in graphitic nanofibres around 50 to 1000 nm in length and 5 to 100 nm in diameter [119]. Since then, researchers in this field experimented with single-walled nanotube and multi-walled nanotube designs. It is unfortunate that widely varying reports of experimental results, some of which were declared unreproducible, have caused much debate on the efficacy of carbon nanofibres as a reliable medium for hydrogen storage [120].

In summary, none of the identified hydrogen storage methods are without drawbacks. Each presents its own set of technical challenges that must be addressed before the technology becomes viable for aeropropulsion applications. Carbon nanofibres and glass microspheres could be excluded without much contention on the basis that these are yet highly speculative technologies, allowing the high-pressure tank, cryogenic tank, and metal hydrides to emerge as the main contenders. Amongst these three alternatives, the liquid hydrogen option is the most well-balanced storage technology, in terms of gravimetric storage efficiency, volumetric capacity, and technical maturity. Storing hydrogen in cryogenic liquid form provides the additional synergistic benefit of having an on-board cryogenic bath available to be used for cooling the HTS motor [115]. This, in turn, allows the elimination of a cryocooler, which is heavy and voluminous, as an architectural element of a PEMFC-based aeropropulsion system. The reported success of AeroVironment's Global Observer program [121] is an especially encouraging development that paves the way for ultimately resolving the concern over sufficient insulation and boil-off compensation at high altitudes.

4.2.1.5 Auxiliary Energy Storage Alternatives

A survey of various powertrain architectures proposed for FCVs reveals that an auxiliary energy source is a physically small, yet functionally important architectural

element of the system. Fuel cells in general, and the direct hydrogen types, such as PEMFCs in particular, are inherently good load followers [122]. That is, the fuel cell system is capable of keeping up with variable power demands without long transients between steady states. But conceivably for transportation applications, there would be instances when an abrupt change in the load demand exceeds the response time of the fuel cell system, potentially leading to catastrophic consequences. Incorporating an auxiliary energy source, which can serve as an *energy buffer* between the fuel cells and near-instantaneous load fluctuations, into the system would not only increase system reliability, but also provide a supplementary power source capable of augmenting propulsion in short bursts, *e.g.*, acceleration during turbulence due to wind gusts, etc. In a fuel cell aeropropulsion system, an auxiliary energy source is likely to play all of the above roles, in addition to serving as the energy source for meeting the engine thrust or power transient requirements as per the Federal Aviation Regulations (FARs).

In this regard, the ideal auxiliary energy source for a fuel cell power plant would be a device with a fast load-response time, high specific power, but not necessarily high specific energy. Battery technology, thus, easily lends itself as the top candidate for this particular function. All five battery types listed in the matrix are commercially available technological alternatives. Ultracapacitor technology is also a potential alternative, due to its inherent simplicity, compactness, well-balanced specific power (W/kg) and specific energy (W-hr/kg) characteristics. Both types of technologies fall under the general category of electrochemical cells.

Similar to how fuel cells are categorized by their electrolytes, so can batteries be distinguished by their electrolyte materials. All listed galvanic cells, besides the metal air batteries, are secondary electrochemical cells that can be charged, as well as discharged. Charging is defined as supplying current to the battery or ultracapacitor, rather than the normal operation of drawing out, or discharging current.

The task of choosing one of these electrochemical cells in favor of another is complicated by the concept of charge or Amphour capacity. Batteries, and also ultracapacitors, are rated in terms of Amphour, which is a measure of the amount of deliverable electric charge. Unfortunately, the capacity of a galvanic cell depends on the manner of usage, with a slower discharge time resulting in a larger capacity. For example, a nominally 42 Amphour battery rated for a 10-hour discharge would have a capacity of approximately 46 Amphours, if discharged slowly over a 20-hour period, and 36 Amphours if more rapidly drained in 2 hours. Because the capacity is a variable quantity, as outlined above, it is difficult to accept the results of comparing the galvanic cells based on gravimetric and volumetric characteristics, such as specific power, specific energy, and energy density, without knowing the associated Amphour ratings. The downselection problem becomes more challenging if the intended application is for unevenly-spaced pulses of power bursts, similar to those envisioned to occur during an aerovehicle mission. As the energy content of each voltaic cell no longer becomes a metric for distinction in such a scenario, the final decision cannot be reached without carefully considering other attributes, such as nominal cell voltage, Amphour efficiency, self-discharge, number of life cycles, recharge time, dependency on temperature, cooling needs, etc. It was, therefore, decided that the choice regarding auxiliary energy storage should be postponed until the simulation environment was finalized.

4.2.1.6 Turbomachinery Alternatives

In the strictest sense of the term, turbomachinery generally refers to rotary machines that transfer energy between a rotor and a fluid. Here it is loosely applied to describe the function of moving and delivering fluids within a system. More specifically, the function of turbomachinery is, henceforth, used to mean the continual delivery, compression, or expansion of *air* via rotating machinery.

Air delivery is a critical function in all but the smallest of fuel cell systems, and one without which fuel cells cannot generate power. For both PEMFCs and SOFCs, air must be continually supplied to a cell's cathode to sustain the electrochemical reaction. This supply rate should also be controllable, so that the fuel cells are able to respond to variable loads. Additionally, the fuel cell stack would often need to be pressurized for optimal electrochemical performance. Stack pressurization would, nonetheless, be a necessity in aerovehicular applications since the ambient air pressure during flight is always lower than the atmospheric or above-atmospheric pressure ranges at which most fuel cell systems are rated.

Compressor technology, thus, represents an excellent means for achieving both air delivery and pressurization, with the same hardware, in a fuel cell aeropropulsion system. Compressors are essentially fluid moving devices that achieve the function of turbomachinery by transferring the kinetic energy of the rotor to fluid or gas. Such a turning mechanism also serves to raise the total pressure (and also temperature) of rotating fluid relative to its original state.

All four compressor alternatives listed in the matrix are technologically mature options, currently found in many engineering applications. Despite this fact, only one alternative appears to be capable of delivering the range of flow rates and back pressures that would be required by a fuel cell aeropropulsion system at reasonable efficiencies - the centrifugal or radial compressor. All other compressor types either lack the ranges of pressure boost at typical flight altitudes (roots), flow rates (Lysholm), or efficiency (axial flow). As if to support this point, the majority of reported air management simulations on automotive-scale PEMFC systems model the centrifugal compressor (*e.g.*, see the works of Kulp [123], Cunningham [124], Pukrushpan [125], and Fletcher et al [126]). AlliedSignal Aerospace Equipment Systems, which has now been absorbed by Honeywell Engines & Systems, has also done extensive work in this area since 1999 to develop a FCV-ready and motor-driven turbocompressor system.

The project has now evolved into its fourth phase, with the proposed centrifugal compressor/electric motor/expander configuration projected to meet the 2005 DoE performance, weight, volume, and cost targets [127]. The centrifugal compressor is also featured in all of the seminal NASA studies on an aerospace SOFC/GT hybrid system, previously mentioned in §4.2.1.1.

On the other end of the turbomachinery spectrum, lie the turbines. Turbines work oppositely from compressors in that a fluid stream that had already been set in motion transfers the kinetic energy to the rotor. The rotor shaft can then be used to either do mechanical work or generate electricity, if connected to a generator. This has made turbines an integral part of systems that leverage upon the highly energetic waste heat via CHP or bottoming cycles. Most practical turbines come either as radial or axial designs. Radial turbines are basically inverse centrifugal compressors. In the GT world, this type of turbine technology is considered to be applicable to small-scale power domains - "small" meaning less than 500 kW. For larger systems, the axial turbine is the standard workhorse of large GT engines, generators, or steam power generators that are rated beyond MW load. Consequently, the ranges of aeropropulsion loads that are investigated by this dissertation eliminates the axial turbine as a feasible alternative.

Lastly, a judgment call was made not to include an expander (turbine) as part of a PEMFC-based aeropropulsion system's architecture. The resultant increase in weight and analysis complexity was deemed unworthy of the extra effort for designing a power plant, whose exhaust air stream would not even reach a temperature of 100 °C and a pressure of 3 bar. The radial turbine was, however, chosen to always be part of an SOFC-based system, whose high-temperature and pressure air-exhaust justify the inclusion of such a bottoming cycle.

4.2.1.7 Fuel Processing Alternatives

Petroleum-derived liquid fuels can be made into gaseous reformates, or fuel gas, containing rich amounts of hydrogen, in addition to CO_2, CO, and other trace amounts of hydrocarbons through a process known as fuel reformation. Several different reformer technologies are available, each utilizing a unique method of processing raw hydrocarbon fuel.

The most fundamental of them all is steam reformation, which is also the most common and technologically mature methods currently in practice. Steam reformers are widely used to produce bulk quantities of industrial-grade hydrogen from methane. The oxygenolysis reactions, which enable reformation, occur when fuel and water are mixed on top of a nickel catalyst bed at temperatures beyond 500 °C. Increasing the operating temperature of the reformer and decreasing its pressure, produce favorable conditions for reformates richer in hydrogen. However, the main disadvantage of steam reforming technology is the fact that both steam and heat must be continuously supplied to sustain the endothermic reformation reaction. Water outweighs hydrogen by a factor of 9 on the molecular level, and the basic steam reformation of methane requires one mole of water for a mole of methane to produce one mole of CO and three moles of hydrogen. An aerovehicle carrying a reservoir of water just to reform fuel into hydrogen would, thus, be a very ineffective design from a cost-benefit perspective for the kind of prolonged range and endurance regimes this dissertation is interested in examining. Therefore, steam reformation technology is not included as one of the final alternatives for on-board fuel processing.

Autothermal reformation is another fuel processing method that requires water, although not as much as steam reformation. The process is a combination of the endothermic steam reformation and an exothermic partial oxidation (POX) reaction. During a POX reaction, hydrocarbon fuel reacts with oxygen, and heat is released in the process - enough to facilitate the steam reforming portion of the autothermal

sequence. The resultant synergistic advantage is that a much simplified reformer design, one which *automatically* balances its heat loads, is possible. Nonetheless, this does not alter the fact that a source of water is still needed on board, which is unacceptable for weight-conscientious aerovehicular applications.

Catalytic partial oxidation (CPOX) is the POX reaction in the presence of a catalyst, usually platinum-metal or nickel. The catalyst beds enable the POX process to happen at temperatures less then 1200 °C, which puts less strain on heat management for transportation applications. Compared to steam reformation or autothermal reformers, CPOX is considered to be the least efficient reformation method. About half the fuel is immediately lost in providing the necessary energy to carry out the exothermic POX reaction. Still, the intrinsically simple (no extra thermal management equipment other than insulation) and compact (absence of supplementary water reservoir) designs of CPOX reformers make them an attractive option for aviation applications. The recent progress reported from SOFCo is especially encouraging news for the aviation sector, as the company has made significant progress in developing highly compact CPOX reformers that can process Diesel [128].

Lastly, two possible variations of internal fuel reformation are discussed. The electrochemical half-cell reactions within a fuel cell are, as previously mentioned, exothermic. The ramification here is that certain high-temperature fuel cell systems operate at high enough temperature ranges to release sufficiently energetic heat that can, in turn, sustain the endothermic forms of fuel reformation. Internal reforming technology, thus, offers an elegant approach to simplifying the system architecture, while concurrently cooling the fuel cell stacks. The overall result is an integrated fuel processing/fuel cell system, which can be made even more compact than a system with a separate CPOX reformer.

Indirect internal reformation (IIR) is more descriptive by its alternative moniker: integrated reforming. Plate reformers, coated with catalysts, can be distributed in

close proximity to the anode of the SOFC, which runs hot enough to provide the necessary thermal energy for steam reformation. Alternatively, reforming catalysts can be directly embedded within the fuel gas distribution path of each SOFC. Regardless, the technology is not entirely self-sufficient in generating steam, and therefore, IIR is not considered further.

As the name implies, direct internal reformation (DIR) is, in fact, steam reformation that occurs directly on the anode surface. High-temperature fuel cells are anionic cells, whose product water in steam form exit through the anode side. SOFCs currently operate in the hottest temperature regimes amongst all fuel cell types, and the nickel content of the SOFC anode surface provides an ideal site for DIR to take place. Already examples of DIR on SOFCs have been reported, first by Siemens Westinghouse and most recently by Franklin Fuel Cells [129]. The company claims it has developed an industry-first, patented Copper-Ceria anode technology that is highly coking-resistant and sulfur-tolerant, thus, enabling the DIR of virtually any petroleum-derived liquid fuel.

4.2.1.8 Balance of Plant Alternatives

In the fuel cell literature, the term balance of plant (BOP) is a reference to all other components of a fuel cell power plant, besides the fuel cells. The components that fulfill the functions of primary and auxiliary energy storage, turbomachinery, and fuel processing reviewed in the previous sections are sometimes included in the BOP, depending on how the architectural boundaries of a fuel cell system are defined. For the sake of clarity, this dissertation makes a distinction between such functions and the functions performed by the much smaller*, extra* components, whose ancillary, yet functionally critical roles, often go unnoticed.

Different fuel cell types impose different thermomechanical needs on the subsystem level, impacting the final architectural composition of the entire system. For

example, various amounts of fluids and gases (except air, which is accounted under turbomachinery) must be circulated throughout the system to serve several different purposes. In the case of PEMFCs, the air stream entering the cathode would most likely have to be cooled down to match the modest operating temperatures of the stack, after being compressed to elevated levels of pressure and temperature. Such an air stream, even after cooling, would still be too dry to be directly supplied to the fuel cell stack without a humidification step in between. An SOFC stack would impose an opposite requirement for the cathode air stream to be pre-heated to match its significantly higher operating temperature. Moreover, it is quite possible that multiple heat exchangers of different sizes and forms may be needed to allow the various electric, electromechanical, and electrochemical components - including the fuel cells - to operate near their peak efficiency ranges. Hydrogen or liquid fuel must also be made available for the stack or the reformer to access from its storage device. On the other side, unutilized fuel gas, as well as water that is produced as the by-product of the electrochemical half-cell reactions, must be purged from the system. All of the above functions necessitate the inclusion of pumps and controllers (*i.e.*, pressure regulators, control valves, etc.) in the BOP sub-system.

As such, none of the BOP alternatives listed in the matrix are meant to be capable of single-handedly achieving all of the required ancillary functions. The choices are, rather a collective representation of the technological options that can be appropriately mixed and matched to support the architectural choices made at the other functional junctures.

4.2.1.9 Power Management and Distribution Alternatives

The last row of the Matrix of Alternatives represents the power electronics options, which, in combination with one another, can fulfill the function of Power Management and Distribution (PMAD). As hitherto discussed, the architectural composition of a

fuel cell system include a variety of loads, most of which require a specific form of current, voltage, or both to operate. Electric motors used for both propulsion and compressor drives also need electronic means of motor start-up, speed control, torque command, etc. Similar to those of the BOP, the auxiliary, yet functionally significant roles of power regulation and conversion devices, should not be ignored.

Each of the three architectural alternatives is a core component in creating electric circuits that can either step up or step down DC voltage. All three are electronic switches capable of connecting or disconnecting a current path from the power source, such as fuel cells, to the load at set frequencies. When used in conjunction with inductors and diodes, any one of these switches can form a step-down regulating circuit, also known as the buck regulator. The addition of a capacitor enables the creation of a step-up or a boost regulator. The particular choice of an electric switch is of less importance to the system designer than knowing the range of losses one can expect from passing power through a DC-DC converter. However, the continual advancement in insulated gate bipolar transistors (IGBTs) are quickly making the thyristors to become obsolete in the kW regimes of PMAD. Since metal oxide semiconductor field effect transistors (MOSFETs) are commonly used in low-voltage, low-power (below 1 kW) applications, only the type of DC-DC converters based on IGBT technology are, henceforth, considered.

Certain electrical components may require the supply of alternating currents to carry out their sub-system functions. In order for both the AC induction and HTS motors to be compatible with a fuel cell power plant, an inverter, which is the terminology used to describe the process of converting DC voltage to that of AC, must also be part of the PMAD architecture. Architecturally similar to boost or buck regulators, inverters are also circuits of the same kinds of electronic switches and free-wheeling diodes.

The primary purpose of an inverter is to approximate the sinusoidal form of AC

from a DC voltage source. Depending on the type of AC load to be matched by the fuel cells, either a single-phase or three-phase inverter can be applicable. It turns out that the three-phase inverter is the suitable alternative due to the results of the propulsion motor choices. Both the AC induction and synchronous (also HTS) motors, in power ranges applicable for aircraft propulsion, are likely to be three-phase machines; that is, having three sets of armature windings. Since no other loads than these motors are likely to require alternating currents within a fuel cell aeropropulsion system (inverters obviously do not apply to a system with a BLDC propulsion motor), all references to an inverter shall henceforth imply it is a three-phase inverter.

4.2.2 Review of Downselected Architectures

In summary, the row-wise choices of the alternatives listed in Table 6 resulted in two classes of fuel cell aeropropulsion system architectures: the three that are based on PEMFC technology and another three that are based on SOFCs. The detailed architectural composition of each system is enumerated in Table 7. Since it is beyond the interest of this research to include any risk factors associated with considering highly advanced technological components, the downselected architectures do not explicitly reflect any penalties, such as higher monetary cost, for pushing the technological boundaries.

Within the same class, the sub-system choices were organized according to three hypothetical growth scenarios of enabling technologies. Commercially available products, as well as those components satisfying the 2005 U.S. DoE technical targets, were assigned to the system with an off-the-shelf (OTS) architecture. The intermediate-level architecture was made to consist of technological alternatives that are projected to reach the 2010 DoE technical target values. The most technologically advanced architecture was conceived with sub-system alternatives forecasted to demonstrate the long-term DoE technical targets by 2015. As presented in §4.3, the intention behind

Table 7: Downselected Fuel Cell Aeropropulsion System Alternatives

Functions	**Alternative 1**	**Alternative 2**	**Alternative 3**	**Alternative 4**	**Alternative 5**	**Alternative 6**
Technology Growth Scenario	Off-the-shelf	Intermediate	Advanced	Off-the-shelf	Intermediate	Advanced
Energy Conversion	PEMFC	PEMFC	PEMFC	SOFC	SOFC	SOFC
Propulsion	AC Motor	BLDC Motor	HTS Motor	AC Motor	BLDC Motor	HTS Motor
Energy Source	Liquid H_2	Liquid H_2	Liquid H_2	Jet A	Jet A	Jet A
Primary Energy Storage	Cryogenic H_2 Storage Tank	Cryogenic H_2 Storage Tank	Cryogenic H_2 Storage Tank	Conventional Fuel Tank	Conventional Fuel Tank	Conventional Fuel Tank
Auxiliary Energy Storage	To be determined (TBD)	TBD	TBD	TBD	TBD	TBD
Turbomachinery	Centrifugal Compressor	Centrifugal Compressor	Centrifugal Compressor	Centrifugal Compressor Radial Turbine	Centrifugal Compressor Radial Turbine	Centrifugal Compressor Radial Turbine
Fuel Processing	N/A	N/A	N/A	CPOX	CPOX	DIR
BOP	Humidifier Intercooler Heat Exchanger	Humidifier Intercooler Heat Exchanger	Humidifier Intercooler Heat Exchanger	Fuel Pump Combustor Air Heater	Fuel Pump Combustor Air Heater	Fuel Pump Combustor Air Heater
PMAD	DC-DC Converter 3-Phase Inverter	DC-DC Converter	DC-DC Converter 3-Phase Inverter	DC-DC Converter 3-Phase Inverter	DC-DC Converter	DC-DC Converter 3-Phase Inverter

the above schema was to model the performance, gravimetric metrics, or volumetric characteristics of each component to improve in the direction of more aggressive technology growth assumptions. Therefore, in the case where the available alternatives for a given function could not be easily identified with any DoE technical targets, such architectural options were placed in order of increasing technological sophistication. Several sub-systems, whose contribution to system-level metrics was expected to be minor, were modeled only at the OTS level for simplicity (*e.g.*, radial turbines, fuel pumps, and air heaters).

Another significance of bounding the scope of research to the six downselected candidate alternatives is that it allows one to observe the important trade between fuel efficiency and system weight. All PEMFC-based systems listed in Table 7 consist of much lighter sub-system components and less complex BOP than those powered by SOFCs. For example, the advanced PEMFC system does not need a dedicated cryocooler for the cylindrical HTS motor, since the on-board liquid hydrogen also doubles as the source of cryogenic coolant. The SOFC-based system, on the other hand, requires a cryocooler to be part of its architecture for the superconducting motor to function. Nevertheless, SOFCs are unquestionably capable of converting energy more efficiently than PEMFCs, which lead to less required fuel weight for the same sizing conditions. The most interesting aspect of this trade would be to discover the weight differential (fuel and tank combined) between on-board cryogenic hydrogen storage versus carrying conventional Jet A fuel.

4.3 Creation of Simulation Environment

Several reasons motivated the creation of a new simulation environment as called for in **Sub-task 1**. Above all, the revolutionary status of fuel cell aeropropulsion meant that an absence of public-domain analysis tools, even at the conceptual design level, was inevitable. This is in contrast to how a plethora of aerospace engineering

design and analysis codes is freely available through various government and academic websites. What was needed was an adequate simulation platform that would enable the kind of scalability investigation described in §4.4.1.3, as well as notionally emulate the developmental process of alternatives listed in Table 7. A novel design tool, which is the product of integrating legacy and homegrown codes, was thus born out of the aforementioned necessities. The following is a brief outline of what can be achieved with this propulsion-level simulation environment, including some of its salient features.

Figure 19 portrays the modeling structure of the said environment in a Design Structure Matrix (DSM) format. Inspired by the algorithmic sequence of on-design analysis, sizing, and off-design analysis that is customary in GT engine design, it is intended as an engineering tool for sizing and modeling the performance of a fixed-architecture fuel cell aeropropulsion system. It can also be characterized as a power-based design approach, since power, rather than thrust, is the main figure of merit that influences the system-wide gravimetric and performance characteristics. Such a schema has the additional benefit of enabling the seamless modeling of DoE technical target values, which are often based on power.

On-design analysis serves as the backbone of both power-based sizing and off-design analysis. Here, the objective is to find a steady-state solution whereby the system's fuel cells produce sufficient power to meet the sum total of each sub-system's power draw *as well as* the flight and cycle conditions dictated by the design point. The user has the option to set the operating current density of the fuel cell stack based on a desired efficiency value or in reference to the area-specific Maximum Power Point (MPP). As shown in Figure 20, the default is to set the current density corresponding to the MPP, since it results in the highest specific power for a given power requirement. Another user-definable option allows the toggling between lower (LHV) and higher (HHV) reference heating values. Any constraints pertaining to current

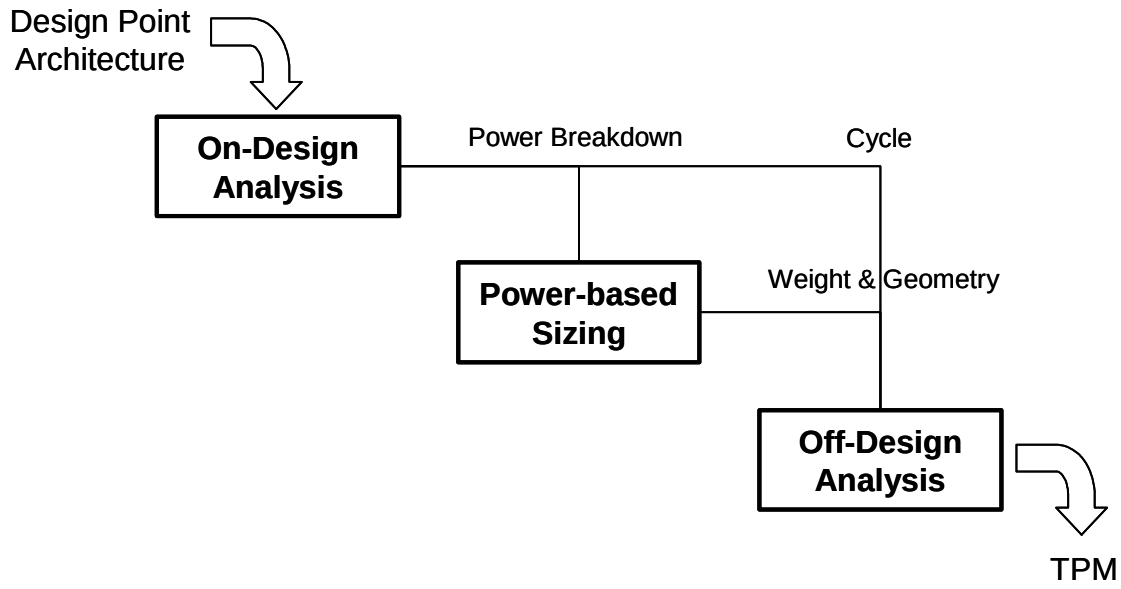

Figure 19: DSM of Propulsion-Level Simulation Environment

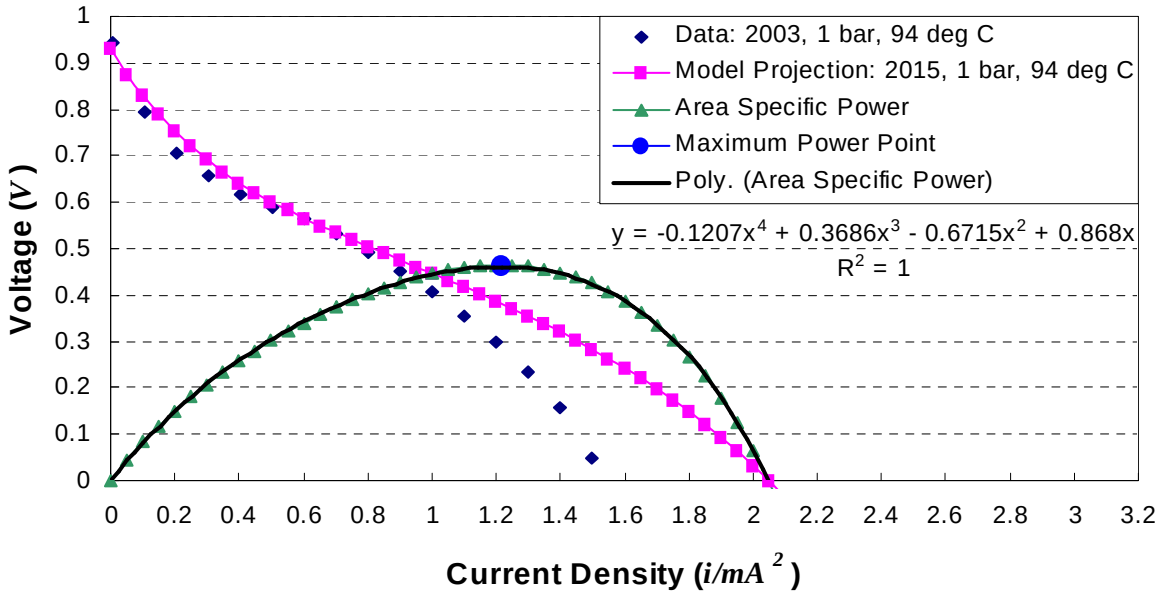

Figure 20: Example Illustration of MPP: PEMFC Voltage Model

draw, mass flow, or temperature are also honored wherever necessary. The results of on-design analysis are subsequently utilized by the sizing routine, which outputs a component-by-component weight and volume breakdown. Such gravimetric and geometric information is utilized during off-design analysis, whose list of steady-state TPM outputs include, but are not limited to: available thrust, available shaft output power, efficiency of all sub-system components, fuel consumption, etc. Physical constraints, such as upper temperature limits or pressure drops, are again closely monitored in all calculations. Depending on the system alternative, an iterative procedure may or may not be required inside each DSM element.

The assembling of all analysis and sizing models was facilitated by Phoenix Integration's Analysis Server and ModelCenter [130]. Not only do these software packages provide a graphically intuitive means of creating integrated simulation environments, but also an automation capability unparalleled in any other process synthesis programs. Tasks requiring the repetitive execution of portions or all elements of the environment - such as parametric cycle analysis, surrogate modeling, and engine deck generation - have thus been fully automated. The implementation results presented in Chapter 5 are testament to the full extent of these capabilities.

4.4 Development of Methodological Capability

With the problem scope narrowed down to a few manageable architectures, and after the establishment of an accompanying simulation environment, the heart of the formulation process could be started. Figure 21 shows the visual representation of the resulting methodological capability. The interdependencies between the steps of the formulated strategy are decomposed and presented next in the order of their proposed implementation.

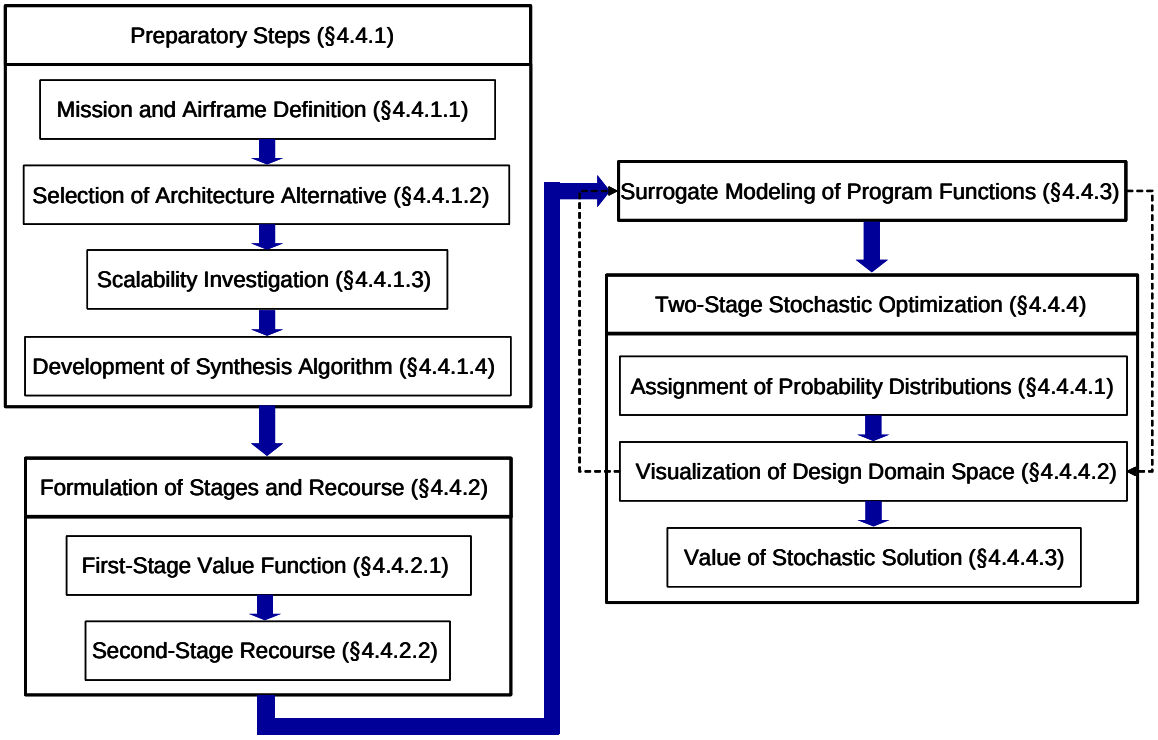

Figure 21: Procedural Map of Recourse-based Design Method

4.4.1 Preparatory Steps

The scope of this thesis includes the creation of a computerized environment for automating and implementing the proposed method. It does not, however, include providing a how-to user's manual as part of this documentation. By doing so, the intention is to emphasize the intricacies of the solution process, rather than accentuating all the salient features of a new design tool. Tool creation is, thus, considered a means to an end, and not the end itself.

Nevertheless, making a concerted effort to create a tool of sufficient fidelity and appropriate computational overhead for the proof-of-concept application *is* part of this research's *modus operandi*. As such, a number of preliminary steps are necessary in order to simulate the design process of fuel cell aeropropulsion systems with recourse.

4.4.1.1 Mission and Airframe Definition

The flight envelope to be created should represent an unprecedented mission profile, belonging to a region of the aviation mission space that has not been explored with conventional engine architectures. This mission should also be created to fully leverage upon the innate energy-efficient characteristics of fuel cells in order to simulate the kind of mission space expansion that is anticipated. For example, a flight profile with either greatly extended range or time on station (TOS) would be both ideal candidates. Such a mission may also be specifically created in response to a new need (communication, scientific research, surveillance, etc) or for a particular entity in the civilian, government, or military sector.

Airframe definition refers to designing the geometric configuration of the air-vehicle that is envisioned to perform the conceived mission. Only the external configuration, known as the outer mold lines, needs to be of concern. A variety of legacy, as well as commercial geometry modeling tools, are available for the job. Issues related to internal packaging are typically dealt with at phases beyond conceptual design, using more sophisticated Computer-Aided Design (CAD) or Engineering (CAE) tools.

The configuration designer's engineering knowledge and intuition should guide him or her in shaping the wing, fuselage, empennage, propulsor, etc. to be as compatible with the intended mission as possible. It would make little sense, for instance, to design a slender, swept-wing configuration with ducted fan propulsors for low-altitude, high-endurance surveillance-type missions. Rather, an airframe with a high aspect-ratio wing and a motor-driven propeller, resembling the geometric configuration shown in Figure 85, would be a more appropriate choice. Basic aerodynamics analysis can also offer guidance as to how aerodynamic shape optimization, if any, should be attempted. In any case, the aerodynamic characteristics of the final configuration must be evaluated and prepared in a *drag polar* format, which is one of the required elements for aircraft sizing.

4.4.1.2 Selection of Architecture Alternative

This is the step where the propulsion-level simulation environment, described in §4.3, is prepared according to the conceived aviation mission. Any one of the six architectural choices listed in Table 7 are as good a starting point as any, as long as the user is familiar enough with the fidelity limits and built-in assumptions of the integrated models.

4.4.1.3 Scalability Investigation

Designing a fuel cell powered airframe concept to perform a representative aviation mission requires the development of an appropriate algorithmic approach for synthesizing the disciplinary knowledge at the propulsion level into an aircraft sizing framework. Such design work would follow either of the two aerovehicle sizing approaches shown in Figure 22, depending on whether or not the considered fuel cell aeropropulsion system turns out to be scalable. Although not explicitly shown, the drag polar is what allows the aerodynamic performance of the airframe to be evaluated in both the constraint and mission analyses. As vehicle aerodynamics is not dependent on scale, and only on geometric configuration, the validity of the same drag polar is assumed to hold, over a reasonable range of Reynolds number and scale factors, an underlying premise of aircraft sizing.

Figure 22 is, in fact, a generalization of Figure 10, which illustrates the traditional thrust-and-fuel-balance formulations, as per Nam [66]. As indicated by the replacement of T_{SL} with P_{ref}, which represents the reference-point shaft power, both are power-and-energy-balance approaches that are better suited for designing all-electric aircraft. Both approaches are similar to their traditional counterparts, in that a given aeropropulsion system's scalability is a prerequisite for the more practical, specific parameter-based approach.

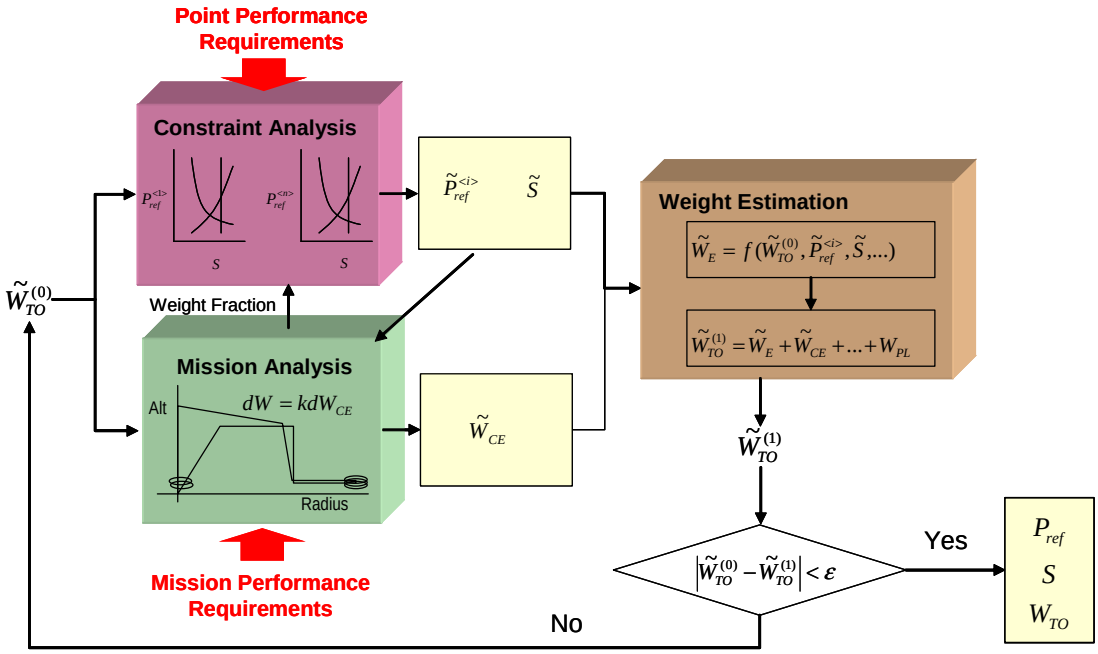

(a) Generalized Actual-Value Based Approach

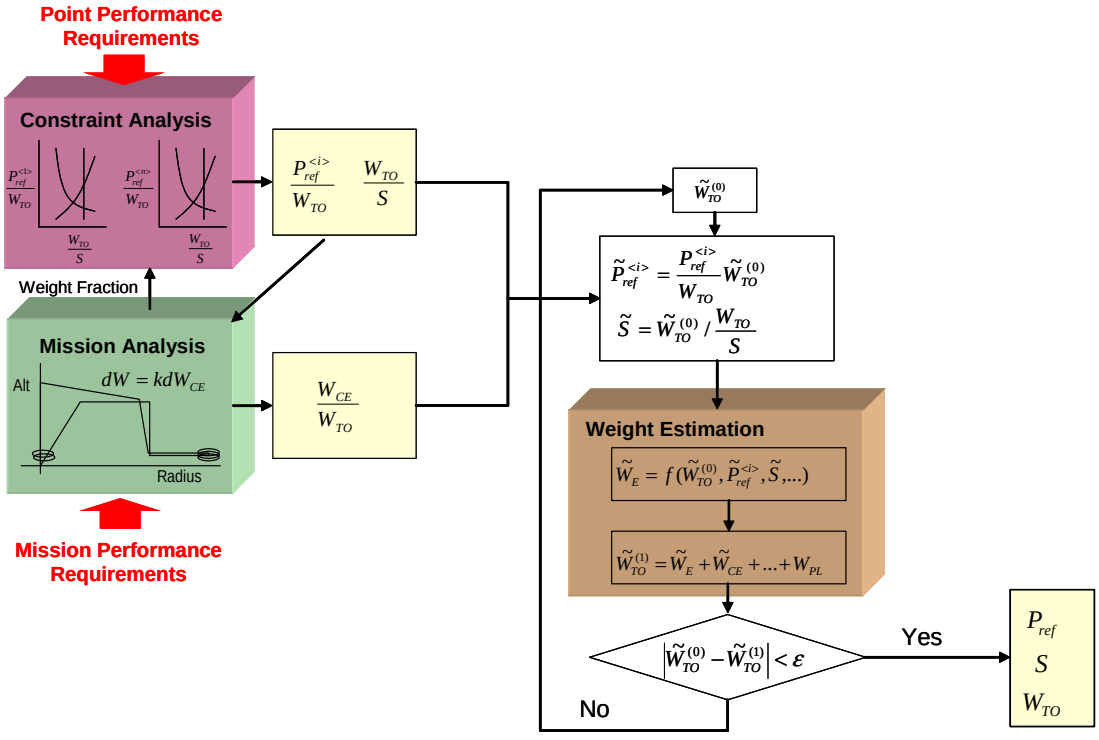

(b) Generalized Specific-Parameter Based Approach

Figure 22: Generalized Approaches to Aerovehicle Sizing

As presented in §2.4, a conventional GT aeropropulsion system is said to be scalable because its fuel consumption and thrust-lapse trends are known to be affected by the chosen engine cycle only. Figure 23 illustrates a notional example of one such scalable aeropropulsion system of a fixed architecture. It is noteworthy to mention that the trends are *not* for the same system. Rather, the shown engine designs, E_1 through E_3, are physically different from one another. As it can be seen, the design-point thrust has little bearing on the system's SFC, which remains relatively constant with respect to engine scale. Another noteworthy occurrence that should be detectable for a scalable system is the off-design performance resembling the shown thrust-lapse behavior. Regardless as to which reference condition the system is sized, the decrease or lapse in available thrust at off-design points must be found to follow roughly the same ratio for the system to be declared scalable. System scalability can be further confirmed if similar results are noted at more off-design conditions and for different cycle parameter settings.

An analogous process can be implemented to investigate the scalability of a fixed-architecture fuel cell aeropropulsion system using the developed simulation environment. Instead of thrust and thrust-lapse, however, more relevant metrics to monitor are P_{ref} and power-lapse ratio α, which is defined as the ratio of available shaft power at an off-design condition to P_{ref}. The usage of efficiency in place of SFC may appear to be more intuitive, but both metrics should display the same trend, as long as the reference heating value is used in a consistent manner. There are no absolute guidelines as to how many off-design points per each cycle should be evaluated, nor the number of recommended cycles per architecture to be investigated. In this author's opinion, it would be satisfactory to evaluate a few select off-design conditions that are most critical to the chosen mission over a small number of extreme and intermediate cycle parameter settings.

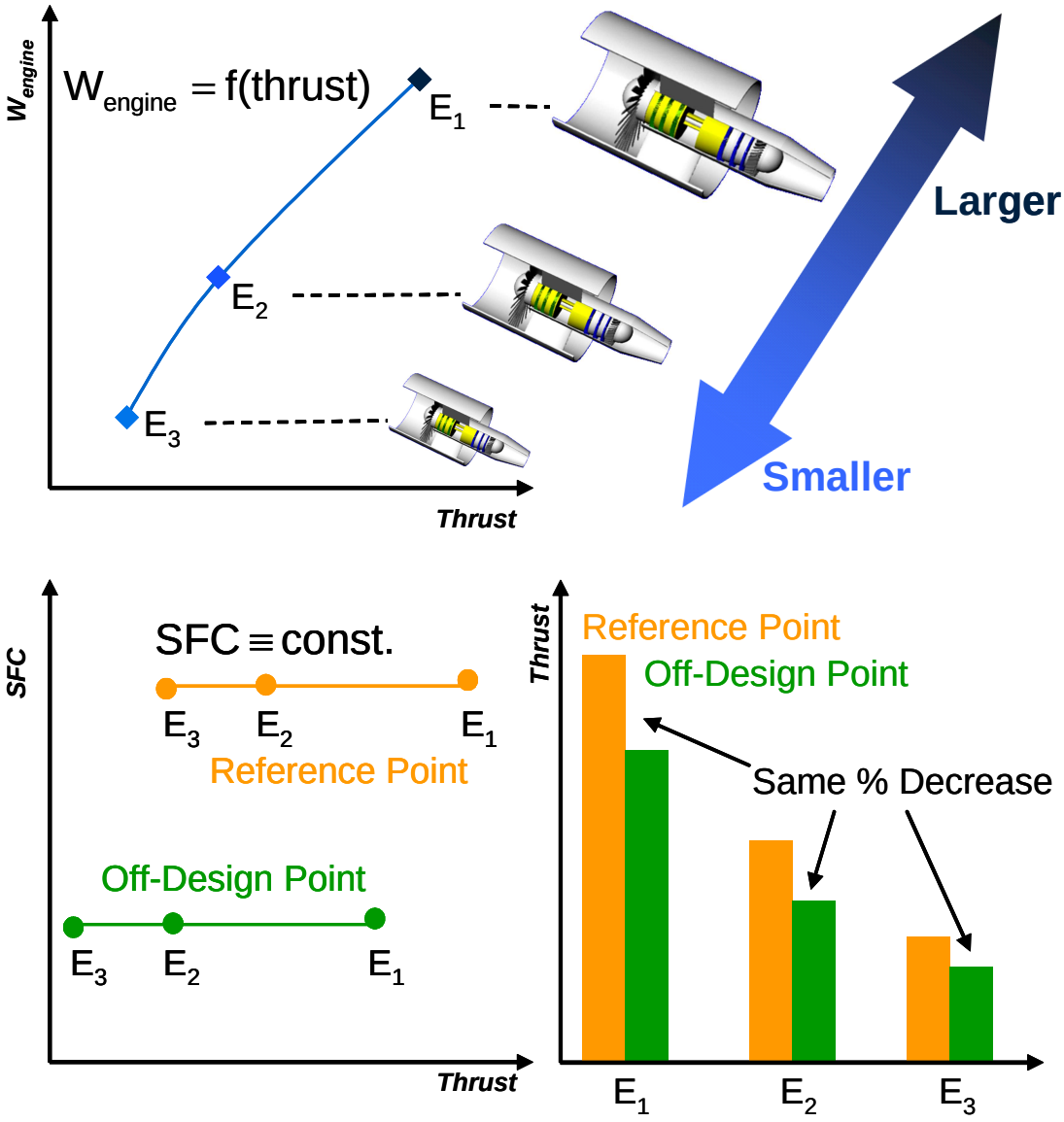

Figure 23: Scalable Aeropropulsion System: Fixed Cycle

4.4.1.4 Development of Synthesis Algorithm

If the aeropropulsion system of interest is found to be scalable in the previous step, then the specific parameter-based approach to aircraft sizing becomes implementable. Under such a circumstance, the off-design analysis capability of the simulation environment is utilized to generate an aeropropulsion deck. Finer resolutions are always preferable for analysis accuracy, if those extra number of off-design points can be afforded computationally. In addition, the aeropropulsion system needs to be sized over a range of P_{ref} settings, while holding the cycle parameters constant, so that a weight scaling law can be extracted from the scaling results, as also shown in Figure 23. The principle of scalability ensures that the same deck file is valid so long as the aeropropulsion system's cycle is not altered. Consequently, the aerovehicle sizing process can be carried out in terms of the specific parameters shown in Figure 22(b) for a single point performance requirement (*i.e.*, one combination of power-to-weight ratio, $\frac{P_{ref}}{W_{TO}}$, and wing loading, $\frac{W_{TO}}{S}$) and the given mission. The deck file is utilized during the energy balance sequence that computes $\frac{W_{CE}}{W_{TO}}$, the required weight fraction of the primary, consumable energy source (liquid H_2 in the case of a PEMFC-based system and Jet A fuel for an SOFC-based architecture), whereas the weight scaling law is synthesized into the overall vehicle weight estimation routine that photographically perturbs the scales of all components of the aerovehicle until convergence on W_{TO} is achieved.

In the case that the considered architecture results in a non-scalable system, the actual value-based approach becomes the sole option to designing the aerovehicle. The tight coupling between the propulsion-level analysis environment and that at the vehicle-level necessitates a computationally demanding sizing process shown in Figure 24.[3] Instead of being independent from the aircraft sizing process, the propulsion-level

[3]If Jet A is used as fuel, then the hydrogen tank sizing routine illustrated in the Figure is omitted.

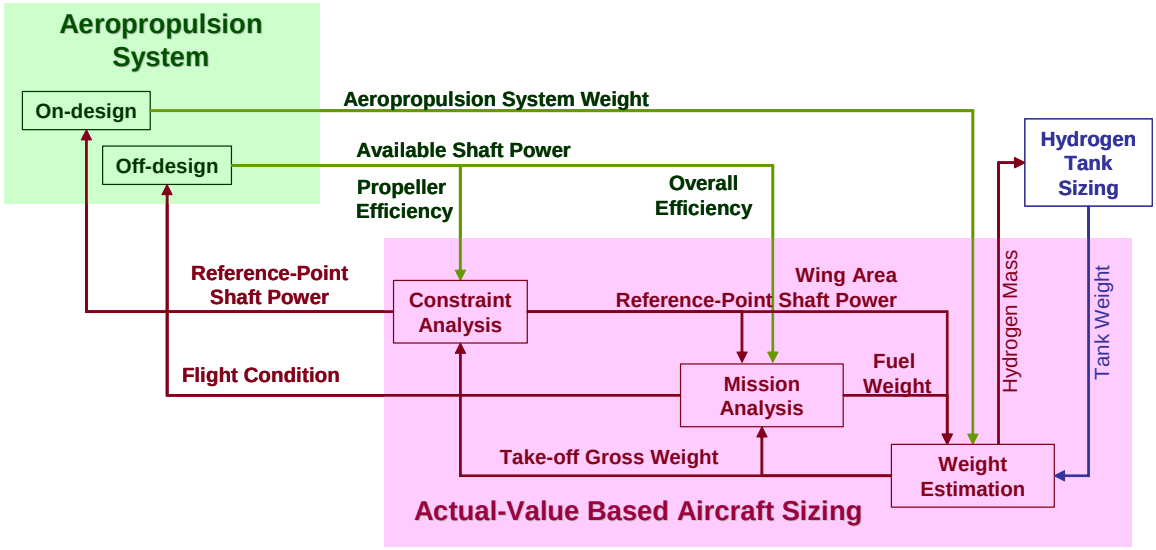

Figure 24: Generalized Actual Value-based Aerovehicle Sizing Process

analysis environment must now be concurrently invoked with the constraint analysis, mission analysis, and weight estimation routines. The overall process is also highly iterative, consisting of the inner iteration loop within weight estimation, as well as an outer loop that iterates on P_{ref}. Therefore, every time P_{ref} changes, the on-design analysis must be employed to determine the weight of the aeropropulsion system, and the off-design analysis needs to be executed to provide the energy consumption characteristics of this designed system at each discretized point of the given mission profile. The absence of scalability prevents a single deck file to replace the entire off-design routine, and thus, greatly decelerates convergence.

From a practical point of view, it is reiterated that the specific parameter-based approach is the preferred choice between the two aerovehicle sizing methods. Both the deck file and weight scaling law are totally reusable for a different airframe configuration with the same mission. Perhaps the greatest merit of the approach, however, is that it allows the propulsion-level design activities to be conducted independently from those at the aerovehicle-level. As seen in Figure 22(b), the iteration loop for computing W_{TO} can be isolated from the process to estimate fuel weight (W_{CE}),

which is implemented during mission analysis. Because mission analysis essentially becomes a table-lookup algorithm with a deck file, the convergence towards W_{TO} can be made almost instantaneously for a single point on the constraint analysis diagram. Such computational expediency enables the application of a numerical optimizer to the aerovehicle sizing process, which would be computationally prohibitive with the actual-value approach for obvious reasons. The difference in the wait-time between the two design approaches may not appear to be a concerning issue when aircraft sizing is attempted for a solitary propulsion-airframe concept at irregular intervals. It will, however, become clearly noticeable in batch jobs, in which the sizing process must be repeated for hundreds of differently designed aeropropulsion systems.

4.4.2 Formulation of Stages and Recourse

If the remedial aspect of designing an engineering system is to be modeled in recourse programming terms, then it is imperative that a clear distinction be made between the first and second stages. Due to the limitless nature of a stage to encompass any number of time-phased activities, prudence is required in deciding at which point the uncertainties are defined to be realized and their impact on the system's TPM is observed. It would make little sense, for instance, to define the first stage to consist of all phases up to detailed design and the second stage to be post-manufacturing, when the applicability of an available simulation environment is limited to conceptual design. Determining the stages will, thus, not only affect the scope of the attempted recourse-based solution approach, but also influence the constituents of first- and second-stage design vectors $\mathbf{x}$ and $\mathbf{y}$.

Figure 25 displays the algorithmic overview of the proposed two-stage programming formulation. It is best described as a nested double loop structure with a probability analysis routine embedded inside the larger optimization loop, which is used to compute the mathematical expectation of the "cost" to remedy a first-stage

design. The overall, aggregate-level goal is to reach a system-level solution in the present (here and now) with which to proceed the remainder of the design activities, and with the understanding that will likely be the least penalizing design to remedy in the later design phases. Such a desire is indicated by how the objective at the second stage is not just any recourse action, but an action incurring the least amount of recourse cost, *given* a first-stage design *and* one particular realization of uncertainty.

4.4.2.1 First-Stage Value Function

One of the fundamental assumptions of stochastic programming is that the probability distributions governing uncertainties are available, or at the very least, can be estimated to lie within a certain set of possible values. Such a notion of representing imperfect information through either Classical or Bayesian justifications is considered to be the most established of all quantitative uncertainty-handling formalisms [131]. In the context of the proof-of-concept design task, the presence of uncertainty is modeled by defining the random parameter vector $\xi(\omega) \in \Re^m$. Each element of the vector $\xi(\omega)$ is designated ω_i, where $i \in I = \{1, \ldots, m\}$, and it is assumed that the realization of ω_1 has no effect on the outcome of ω_m.

In order to formulate a solution approach that is aligned with the fundamentals of recourse programming, the so-called first stage must be formulated to cover a time period when the above-mentioned uncertainties are yet to be realized. The delineation between the first and the second stage is quite clear in Eq.(2) because the first-stage objective, $\mathbf{c}^T\mathbf{x}$, is not a function of uncertainty. Unlike this classical linear programming model, however, the random parameters are likely to affect the evaluation of key system-level metrics, no matter which capability of the simulation environment is invoked.

The above reasoning led to the declaration of the *first-stage value function* that

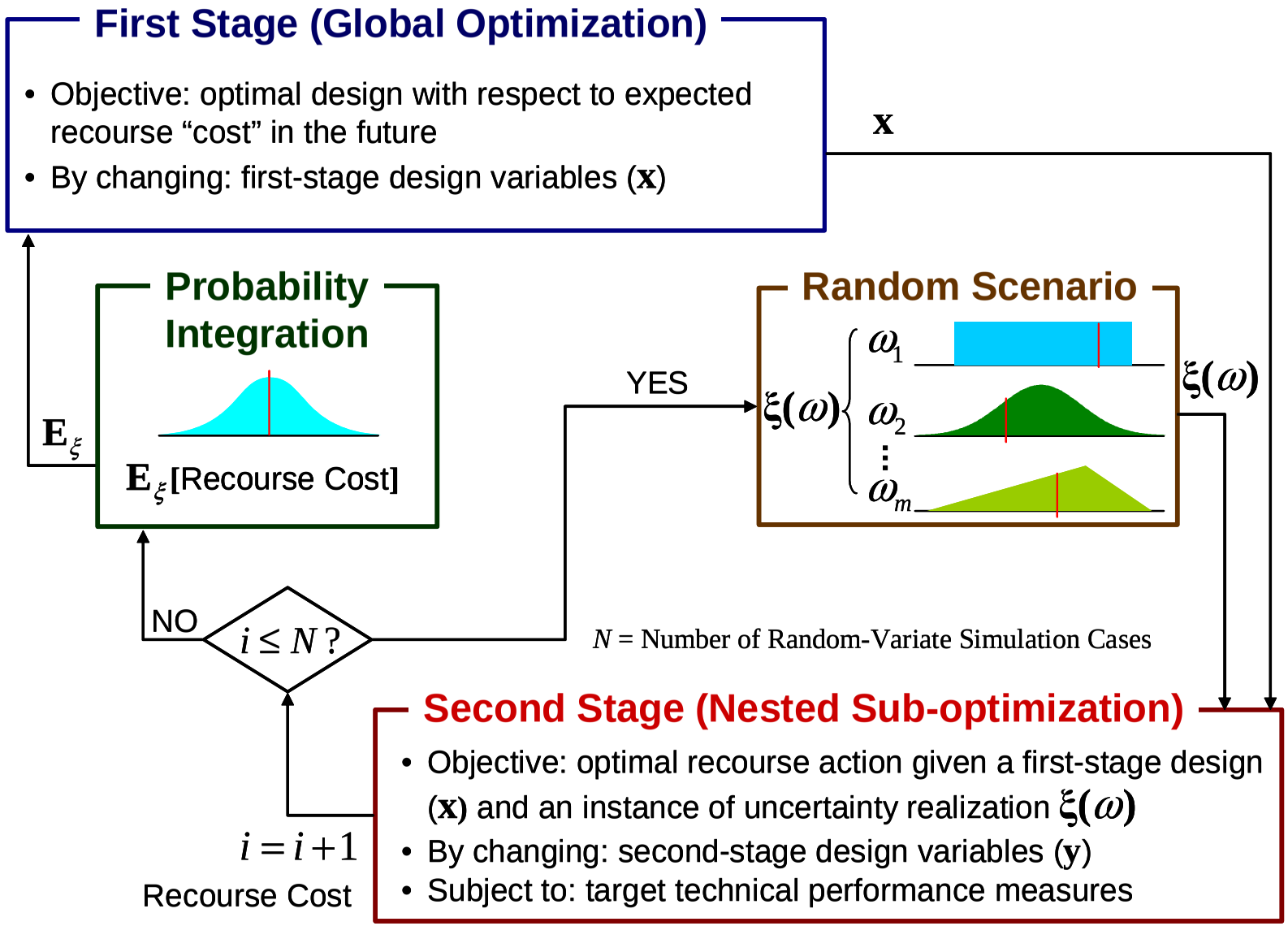

Figure 25: Process Flow Map of Proposed Two-Stage Formulation

is not only dependent on $\mathbf{x}$, but also on $\xi(\omega)$

$$f = \mathbf{M}(\mathbf{x}, \xi(\omega)) \cdot \mathbf{I}^T \tag{9}$$

where $\mathbf{I}$ is a $1 \times n$ vector of ones. Henceforth, the first stage is defined to encompass a series of design activities that are executed for a given $\mathbf{x}$ and $\tilde{\xi}(\omega)$, where $\tilde{\xi}(\omega)$ represents holding ω constant at a deterministically assumed value. The realization of $\xi(\omega)$, followed by the observation of the $1 \times n$ vector $\mathbf{M}(\mathbf{x}, \xi(\omega))$, is then considered to be the transitional phase between the first and second stages.

4.4.2.2 Second-Stage Recourse

Another underlying assumption behind a stochastic recourse program is that any detrimental effects imparted by the realization of randomness can be corrected, although at a penalizing cost. The oft-quoted Inventory Problem [132] is a perfect example of such recourse penalties. Should the realization of previously uncertain market demand happen to exceed the vendor's stocked inventory, or first-stage decision x, then the vendor can *fix* the situation in the second stage by back-ordering the required shortage at a cost of b per item. Recoursing to back-orders is considered a penalizing action with respect to the vendor's profit; since b here is numerically greater than c, which is the cost of the original order on a per-item basis. In the case that the true demand is less than x, then a holding cost of h per item is incurred.

The general implication of the above Inventory example is that, regardless of the modeled real-world phenomenon, there must exist sufficient degrees of freedom in the second stage to remedy the damages. Following the maxim of *no free lunch*, the cost of the second-stage recourse, which must be quantifiable in the same *currency* as the first-stage value function, should be made greater than arriving at the same solution in the first stage. Otherwise, there is neither the motivation nor the means of evaluating what to do in the first stage. If the cost of back-ordering were less than c or even free, for instance, then why should the vendor even bother to order in

advance of demand realization?

In light of these insights, what follows is the proposition of the second-stage value function, whose algorithm is shown in Figure 26, that can be generally applicable to engineering design scenarios:

$$
\begin{aligned}
Q(\mathbf{x}, \xi(\omega)) = \quad & \min_{\mathrm{y}} \sum_{j \in J} q_j \eta_j(\mathbf{x}, \mathbf{y}, \xi(\omega)) \\
\text{s.t.} \quad & \mathbf{g_2}(\mathbf{y}, \xi(\omega)) = \mathbf{T}(\mathbf{y}, \xi(\omega), \xi(\omega)) - \mathbf{h} \quad \geq 0 \\
\text{b.c.} \quad & \mathbf{y}^l \leq \mathbf{y} \leq \mathbf{y}^u
\end{aligned}
\tag{10}
$$

$$
\text{where } \eta_j(\mathbf{x}, \mathbf{y}, \xi(\omega)) = \tag{11}
$$

$$
\begin{cases}
M_j(\mathbf{y}, \xi(\omega)) - M_j(\mathbf{x}, \xi(\omega)) \\
\text{if} \quad \mathbf{g_1}(\mathbf{x}, \xi(\omega)) = \mathbf{T}(\mathbf{x}, \tilde{\xi}(\omega), \xi(\omega)) - \mathbf{h} < 0 \\
\text{otherwise} \qquad 0
\end{cases}
$$

The formulation is inspired by the simple recourse model of Eq.(6) in that a vector of penalty constants, rather than variables, is employed. The elements of this vector, q_j, is multiplied by η_j, which is made functionally dependent on the difference between the two instances of the first-stage value function. When this value is non-zero, it represents the cost of having to recourse a particular first-stage design $\mathbf{x}$, whose predicted TPM outcomes in the first stage, $\mathbf{T}(\mathbf{x}, \tilde{\xi}(\omega), \xi(\omega))$, turn out to be unacceptable because of a specific realization of $\xi(\omega)$. The objective of the second stage, thus, becomes finding the least costly way of correcting the now infeasible design.

The rather convoluted notation for the TPM vector is necessary to represent the fact that a TPM is measured after the realization of $\xi(\omega)$, but for a system that had been designed to $\mathbf{x}$ and $\tilde{\xi}(\omega)$. Should this realized outcome happen to fall below a prescribed target, h_k, then fixes are made to the system as to keep the vital TPMs in check. In this regard, h_k can be imagined to be a snapshot of a planned TPM trajectory at a particular t that falls within the boundaries of the second stage.

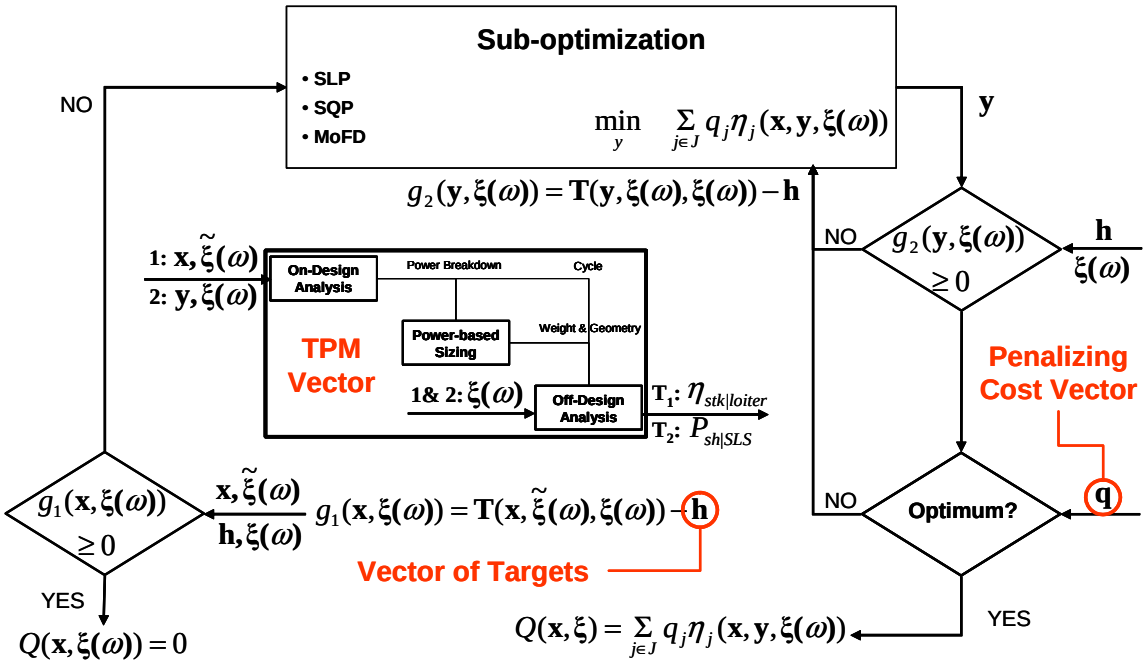

Figure 26: Second-Stage Value Function Algorithm

Exactly what kind of remedial actions can be taken would depend on a number of factors, such as the available fidelity of the simulation environment, modeled design phases, remaining degrees of freedom to physically alter a hardware component, etc. Here, such compensations are assumed to be made by way of $\mathbf{y}$, and in a manner that results in the outcome of the second-stage TPM vector, $\mathbf{T}(\mathbf{y}, \xi(\omega), \xi(\omega))$, being greater than or equal to $\mathbf{h}$. Similar to before, the peculiar expression signifies that, in the second stage, the TPM is evaluated after knowing $\xi(\omega)$ to which the system was recoursed as per $\mathbf{y}$ and $\xi(\omega)$. Lastly, the subscript $j \in J = \{1, \ldots, n\}$ indicates the dimension of $\mathbf{M}(\cdot, \xi(\omega))$, and $k \in K = \{1, \ldots, p\}$ gives the sizes of the target and constraint vectors.

4.4.3 Surrogate Modeling of Program Functions

With the first-stage and second-stage value functions defined as per Eqs.(9) and (10), it becomes possible to formulate the recourse function $Q(\mathbf{x})$ - a pivotal element of two-stage stochastic programs. Eq.(4) indicates that, no matter what penalty model is

used for the second-stage value function, its mathematical expectation is considered as the recourse function, namely $Q(\mathbf{x}) = \mathbb{E}_{\xi}[Q(\mathbf{x}, \xi(\omega))]$. Therefore, the recourse function should be formulated to yield the cost of taking a compensatory action, to which $Q(\mathbf{x})$ is expected to converge in the presence of uncertainty.

In order for such an interpretation to hold true, as per the strong law of large numbers, a sufficiently large number of random experiments must be performed to observe the impact of ω, and thus $\xi(\omega)$, on a system designed to $\mathbf{x}$. The challenge here does not stem from random aspect of simulation per se, but rather from the need to perform a large number of design analysis in conjunction with the random experiments. Numerous arithmetic techniques that enable the sampling of an observation, or a variate, ω on a random parameter from a prescribed probability distribution Ω have been perfected over the years, and their algorithms are now standard features of leading statistical data modeling and analysis software packages. For examples of such "random-variate generators," inquisitive readers are directed to Law and Kelton [133] to gain an appreciation for the breadth and depth of the issues surrounding the subject matter.

One only needs to take a cursory look at Eq.(10) to realize the ramifications of needing a large sampling of ω and, therefore $\xi(\omega)$. Even for a single realization of the random parameter vector and a fixed $\mathbf{x}$, evaluating the second-stage value function is a non-trivial task due to its formulation as a constrained optimization problem. All program functions must be evaluated whenever the optimizer makes changes to $\mathbf{y}$, with the exception of $\mathbf{T}(\mathbf{x}, \tilde{\xi}(\omega), \xi(\omega))$ which only needs a single computation to determine whether or not recourse in the second stage would be necessary. This means that, depending on which outputs of the simulation environment reported in §4.3 are desired as the TPMs, embedded iterative and/or sub-optimization routines may require tens of minutes in attaining a single measure for $Q(\mathbf{x}, \xi(\omega))$. In such a case, the elicitation of the recourse function becomes virtually impossible as tens

of thousands of random variates are likely to be required in estimating the required statistical quantities with a high enough precision.

Therefore, and as conjectured in **Hypothesis 2**, Surrogate Modeling is utilized here as a technique for bridging the need to couple a random-variate generator with the developed simulation environment, while holding the computational overhead at a reasonable level. A surrogate or meta-model is an approximation model represented by a closed-form mathematical equation, whose exact algebraic form depends on the type of statistical data modeling techniques used for its creation (*e.g.*, Response Surface Methodology (RSM) [134], Kriging [135], Neural Networks [136], etc.) In the general technical literature that deals with computational experiments, Surrogate Modeling is understood to be comprised of: (a) implementing a Design of Experiments (DoE) technique to prepare a matrix of inputs to the simulation environment; (b) creating or fitting surrogate models based on the collected simulation results, called responses or sampled evaluation points; and (c) appraising or validating the predictive capabilities of the created surrogates.

A variety of techniques for generating DoE tables, each with its unique list of advantageous and disadvantageous ramifications when utilized as a sampling engine for Surrogate Modeling, also exist [137]. Because it is difficult to predict in advance which experimental design will work best with which surrogate modeling technique, especially for a hitherto unexplored design space, it is recommended that at first, as many different DoE / Surrogate Modeling combinations are tried out as time and resources permit.

Regardless of which DoE and surrogate construction techniques are ended up being employed, it does not change the fact that a considerable amount of computational resources are required up front in evaluating the sampling points. The appraisal or validation of the fitted surrogates is also a non-trivial, human-in-the-loop task, for which a degree of subjective judgment is necessary. Such extra steps are well worth

the effort, as Surrogate Modeling offers one important practical advantage over real simulation models: computationally cheap reusability. A surrogate can be reused many times in evaluating a response at different conditions much more quickly than running the actual simulation model again, once its goodness of fit is verified via at least more than one statistical diagnostics measure. This beneficial characteristic of surrogate models can be fully exploited in eliciting the recourse function by creating the surrogates for $\mathbf{M}(\mathbf{x}, \xi(\omega))$, $\mathbf{M}(\mathbf{y}, \xi(\omega))$, $\mathbf{T}(\mathbf{x}, \tilde{\xi}(\omega), \xi(\omega))$, and $\mathbf{T}(\mathbf{y}, \xi(\omega), \xi(\omega))$. Once the validity of these surrogates are confirmed, they can be utilized in obtaining a meta-model of the second-stage value function $Q(\mathbf{x}, \xi(\omega))$, which allows the rapid evaluation of $Q(\mathbf{x})$ for any first-stage design $\mathbf{x}$ with an appropriate random-variate generator.

4.4.4 Two-Stage Stochastic Optimization

Being able to elicit the recourse function through the combined usage of a Surrogate Modeling technique and a random-variate generator enables the heart of the proposed method to be defined. It is reminded that this dissertation was initiated with the goal to develop a systems-oriented capability, which allows the identification of optimal design under uncertainty - "optimal" in the sense that it is the design that will cost the least to recourse. This objective can be met by formulating an optimization problem, whose overall merit function is minimizing the sum of the expectation of the first-stage value function and the recourse function.

$$\begin{aligned} \min_{\mathbf{x}} \quad & z = \mathbb{E}_{\xi}\left[f\right] + Q(\mathbf{x}) \\ \text{b.c.} \quad & \mathbf{x}^{l} \leq \mathbf{x} \leq \mathbf{x}^{u} \end{aligned} \tag{12}$$

If necessary, Eq.(12) can be made into a more general program by adding any inequality or equality constraint functions that are not affected by uncertainty (*i.e.*, only dependent on $\mathbf{x}$).

Over the years, many path-building, domain-spanning, and exploratory optimization algorithms that can solve Eq.(12) have been developed. Some of the more mature and popular algorithms are widely available through a host of commercial design integration, automation, and optimization software packages, as well as mathematical analysis and programming languages. Regardless of the chosen numerical optimizer, the solution process is anticipated to be computationally expensive because a closed-form expression for a mathematical expectation is not likely to be obtainable for real engineering problems. The present formulation is also built upon the usage of normalized polynomial or transcendental surrogate models, which further complicates the derivation of an analytical expression for either $\mathbb{E}_{\xi}[f]$ or $Q(\mathbf{x})$ within an optimization loop. Therefore, a random-variate generator, such as a Monte Carlo simulator, with a large number of sampling cases must, thus, be employed to numerically evaluate both components of z with acceptable precision.

4.4.4.1 Assignment of Input Probability Distributions

Amongst the quantitative formalisms for handling imperfect information, probability theory has had the longest developmental history. Its origin can be traced back to the 1660s when Classical Theory first emerged, followed by Relative Frequency Theory (statistics) in 1866, and Subjective or Bayesian Theory in circa 1950. Being the first quantitative uncertainty handling technique has allowed the mathematics of probability theory to flourish as the dominant method for uncertainty quantification and propagation in many fields of engineering and science. Nevertheless, Smithson challenges his readers to reflect on the fundamental issue of probabilistically modeling uncertainty by posing the following question: "Where are initial probabilities to come from?" [70]

In preparation for simulation studies which must account for one or more random aspects of the modeled phenomenon or system, it is recommended that sufficient

quantities of empirical data are cultivated on a random parameter of interest[133]. Standard techniques of statistical inference can then be applied to ensure that the most appropriate theoretical distribution function is fitted to the data. The remainder of the simulation is carried out by sampling from the fitted distribution, rather than using the observed data directly. Such a capability to model probability distributions of both the continuous and discrete types are readily available in popular statistical data analysis and modeling software packages.

Selecting a representative input probability distribution becomes obscured when it is not possible or very difficult to collect such data. In the absence of the empirical data needed for constructing input probability distributions, the best one can do is to follow heuristics. A heuristic, whose etymology is Greek (*heurisko*, meaning "I find"), is a statement encapsulating some aspect of past experience, wisdom, and insight that is applicable to the task at hand. An insightful heuristic can, thus, serve as a practical guideline that is otherwise unobtainable through analytical means alone.

According to Law and Kelton [133], three theoretical probability distributions have proved to be popular amongst simulation practitioners who had to subjectively assign probability distributions. The simplest of the three, in both theory and practice, is the uniform distribution. This probability density function is recommended when very little can be elicited about the random parameter other than the range $[a,\ b]$, where both a and b are in $\Re$ and $a < b$. When it is possible to estimate the mode c of the random parameter, in addition to its range, the triangular distribution becomes a natural choice, due to its intrinsic shape. Lastly, a truly parametric approach would be to assign a beta distribution, whose form can be easily altered by changing its two shape parameters α_1 and α_2. Both the uniform distribution and the limiting cases of the triangular distribution (right and left triangles: $c \rightarrow b$ and $c \rightarrow a$) are special cases of the beta distribution on the normalized scale of $a = 0$ and $b = 1$.

4.4.4.2 Visualization of Design Domain Space

The kind of unavoidable computational burden that is present in the formulated solution approach discourages the application of domain-spanning or exploratory optimization techniques, which inherently require a large number of function calls. It is, thus, preferable that path-building algorithms, and especially the more efficient gradient-based optimizers, are found to be applicable in solving Eq.(12). This requires visualizing the N-dimensional design space of z to check for unimodalness, as all gradient-based methods are prone to getting trapped near a local extremum should the domain happen to be multi-modal.

Fortunately, another benefit of having surrogate models is that the design domain space can be easily visualized through a variety of multi-dimensional surface and contour plots. With the right software package, the design engineer is able to observe how the topology of the domain space is affected by the design variables in an interactive manner. What is desired to be seen is that each 3-dimensional space displays a largely unimodal surface; that is, there is only one notable protrusion. Otherwise, there is always a likelihood for a gradient-based algorithm to mistake a local optimum for a global one, thus, prematurely terminating the optimization process.

When the visualization results indicate serious multimodalness (*i.e.*, many peaks and troughs), and the application of exploratory techniques, such as Simulated Annealing and Genetic Algorithm are still unwanted, then there are very few options, other than re-fitting the surrogates over a different domain. The recourse function, for instance, could be elicited for several different values of h_k to see if it results in a less multi-modal design space. A surrogate-based visualization environment also offers the means of carving out certain regions across multiple dimensions for the same purpose. For example, constraining the lower and upper output bounds of each surrogate could shade out the infeasible regions of the design space, thereby illuminating new feasible boundaries of the tightened domain. One could then interactively adjust the design

variable ranges one at a time to reverse-engineer their new upper and lower bounds. In the case that the explored domain space appears to be moderately multi-modal, then it may be sufficient to utilize visualization as a guide in selecting a good starting point (*i.e.*, near a global extremum) for optimization.

4.4.4.3 Value of Stochastic Solution

In summary, several enabling M&S elements need to be established before the two-stage recourse problem of Eq.(12) can be solved. These are, in the order of their presentation:

- Simulation environment that allows parametric cycle analysis, power-based sizing, and performance analysis of a fuel cell aeropropulsion system.
- Capability to apply suitable DoE and Surrogate Modeling techniques on said simulation environment.
- Availability of a gradient-based optimizer and a random-variate generator.

Once all of the above requisite conditions are met, the proposed solution approach can be implemented to demonstrate the value of accounting for the remedial aspect of engineering design. This value, in stochastic programming terms, is known as the VSS, and it can be quantified as follows.

The first order of business is to obtain the EV solution of Eq.(12). As introduced in §3.2.4.2, the EV solution is defined as solving a nondeterministic problem in a deterministic manner:

$$\begin{aligned} \min_{\mathbf{x}} \quad & z = \mathbf{M}(\mathbf{x}, \tilde{\xi}(\omega)) \cdot \mathbf{I}^T + Q(\mathbf{x}, \tilde{\xi}(\omega)) \\ \text{b.c.} \quad & \mathbf{x}^l \leq \mathbf{x} \leq \mathbf{x}^u \end{aligned} \tag{13}$$

where $\tilde{\xi}(\omega)$ represents the unbiased assumption about the modeled uncertainties. The EEV is then calculated by evaluating the mathematical expectations of f and

$Q(\mathbf{x}, \xi(\omega))$ with the probability distributions defined in §4.4.4.1, and with $\mathbf{x}$ fixed at the EV solution.

Subsequently, the stochastic solution to Eq.(12) is found by using the surrogates as outlined in §4.4.3, and a random-variate generator that samples from the same input probability density functions. The worth of accounting for the remedial aspect of engineering design is directly measurable by computing the VSS, which is simply the difference between the EEV and the stochastic solution. If the VSS turns out to be positive, then it can be interpreted as the cost of neglecting to anticipate design recourse.

Chapter V

IMPLEMENTATION

In this body of work, fuel cells mark both the beginning and the end of the research scope. The study of this particular revolutionary technology inspired the creation of a new nondeterministic design strategy in the first place, but it also became the foundational element of the method's proof-of-concept demonstration. As it turns out, the integration of fuel cell technology into aeronautical systems is a contemporary problem of interest in the aerospace domain.

The U.S. Naval Air Systems Command (NAVAIR) awarded a research contract to ASDL in 2005 to conduct a top-level assessment of a notional UAV that utilizes fuel cell technology. Personnel at NAVAIR were mostly interested in the design and engine integration issues related to utilizing fuel cells as the primary method of naval aeropropulsion or as the source of secondary power for UAV-class aircraft. This study was a holdover from a previous work ASDL had done for NAVAIR, in which the feasibility of replacing the APU on the Lockheed Martin P-3 Orion with fuel cell powered alternatives had been investigated.

Although this author was never employed in either of the NAVAIR contracts, his knowledge of and modeling experience with fuel cell systems kept him involved with the projects on an indirect basis. Early versions of the author's simulation environment reported in §4.3 were utilized in both studies, thereby influencing the recommendations made by ASDL to NAVAIR. In turn, the insights gained from interacting with those who conducted the NAVAIR-sponsored work provided a justifying context for carrying out the implementation portion of the **Research Task**, as illustrated in Figure 27.

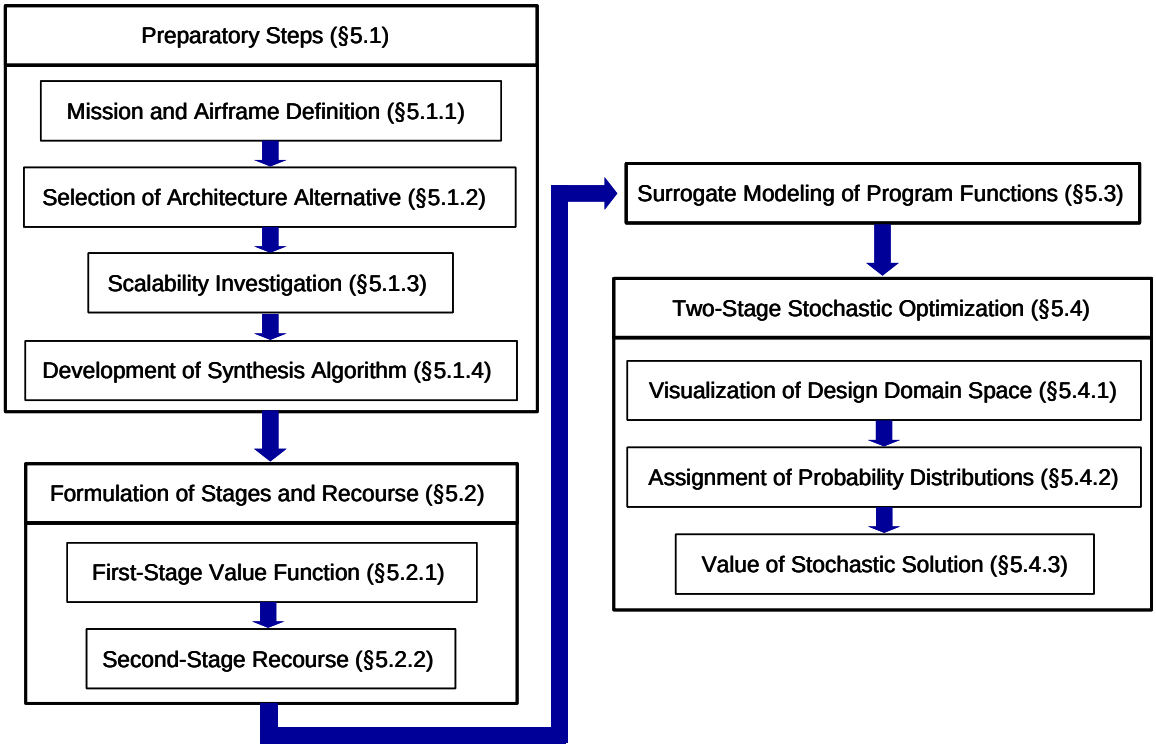

Figure 27: Implementation Plan of Recourse-based Design Method

5.1 Preparatory Steps

NAVAIR's interest in fuel cells revealed the classes of missions and aerovehicles for which the benefits of this revolutionary technology were envisioned to be maximized. The Command expressed an interest in pursuing fuel cell aeropropulsion for a wide range of naval usages including precision strike; broad area maritime surveillance; HALE; and short-range reconnaissance, surveillance, and target acquisition. These missions were intended to be fulfilled by different classes of UAVs, ranging from jet-propelled fixed-wing configurations to propeller-driven designs. Although by no means clearly defined in quantitative terms, the information was useful in arriving at a suitable mission profile, a baseline airframe configuration, and candidate propulsion system architectures for implementing the formulated solution approach.

Mission Profile

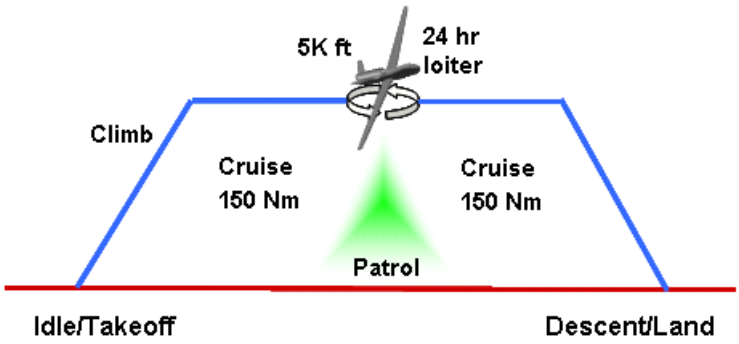

Point Performance

TOFL	1500 ft, Hot Day, over 35 ft obstacle clearance
Climb	300 ft/min at 5,000 ft of altitude
Level Flight	118 knot at 5,000 ft of altitude
Approach	23 knot
LDFL	1,500 ft over 50 ft obstacle clearance

Figure 28: Design Requirements of Notional Maritime UAV

5.1.1 Mission and Airframe Definition

The specification of a mission profile is generally perceived as the starting point of all aerovehicle design activities. The associated mission requirements, which are usually formalized as a top-level requirements document as known as the Request for Proposal (RFP), include all major performance goals and constraints that profoundly impact the aerodynamic, propulsion, and structural make-up of the aircraft.

Figure 28 displays both the mission and point-performance requirements that were envisaged to one day drive the design of a naval UAV suitable for maritime border patrol. The flight profile was inspired by a class of missions advocated by Mavris et al [138], dubbed LAGER for Low Altitude Greatly Extended Range. Missions falling under the LAGER class are deliberately limited in cruise altitude in order to minimize parasitic losses to Turbomachinery and BOP sub-systems, thus allowing the vehicle's aeropropulsion system to fully take advantage of the fuel cell system's high-energy efficiency.

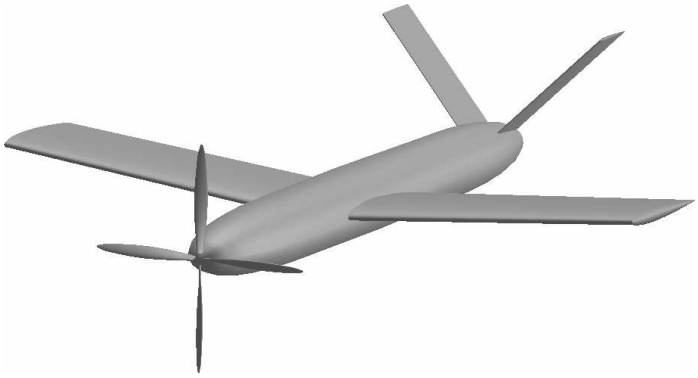

Figure 29: Notional Naval UAV Configuration

Every effort was made to construct a LAGER profile that is realistic for its intended purpose. To this end, the RFP for a Multi-Role Endurance UAV study announced by NAVAIR in 2000 [139], as well as the CONOPS data for the Pioneer system [140], were consulted to elicit the specific mission and point-performance requirements shown in Figure 28. The requirements for Take-off Field Length (TOFL) and Landing Field Length (LDFL) were added so that the unmanned aircraft could, if needed, be operated remotely from a Navy carrier.

The baseline airframe configuration accompanying the mission profile was designed with compatibility in mind, rather than aerodynamic optimization. As seen from Figure 29, the UAV is a conventional tractor configuration with a cylindrically-shaped fuselage. All major aerodynamic surfaces could be kept basic - that is, not tapered nor twisted - because the UAV is intended to spend the majority of its flight time in low subsonic regimes. However, the straight wing's aspect ratio was set at 10 to keep the aircraft's lift-to-drag ratio high during its loitering segments. An assortment of legacy geometric-modeling and aerodynamic-analysis tools were used to extract the aerodynamic characteristics of the notional UAV. The three dimensional surfaces shown in Figure 29 were first created using the Vehicle Sketch Pad [141], then analyzed in both VORLAX [142] and BDAP [143] programs to construct the drag polars depicted in Figure 30.

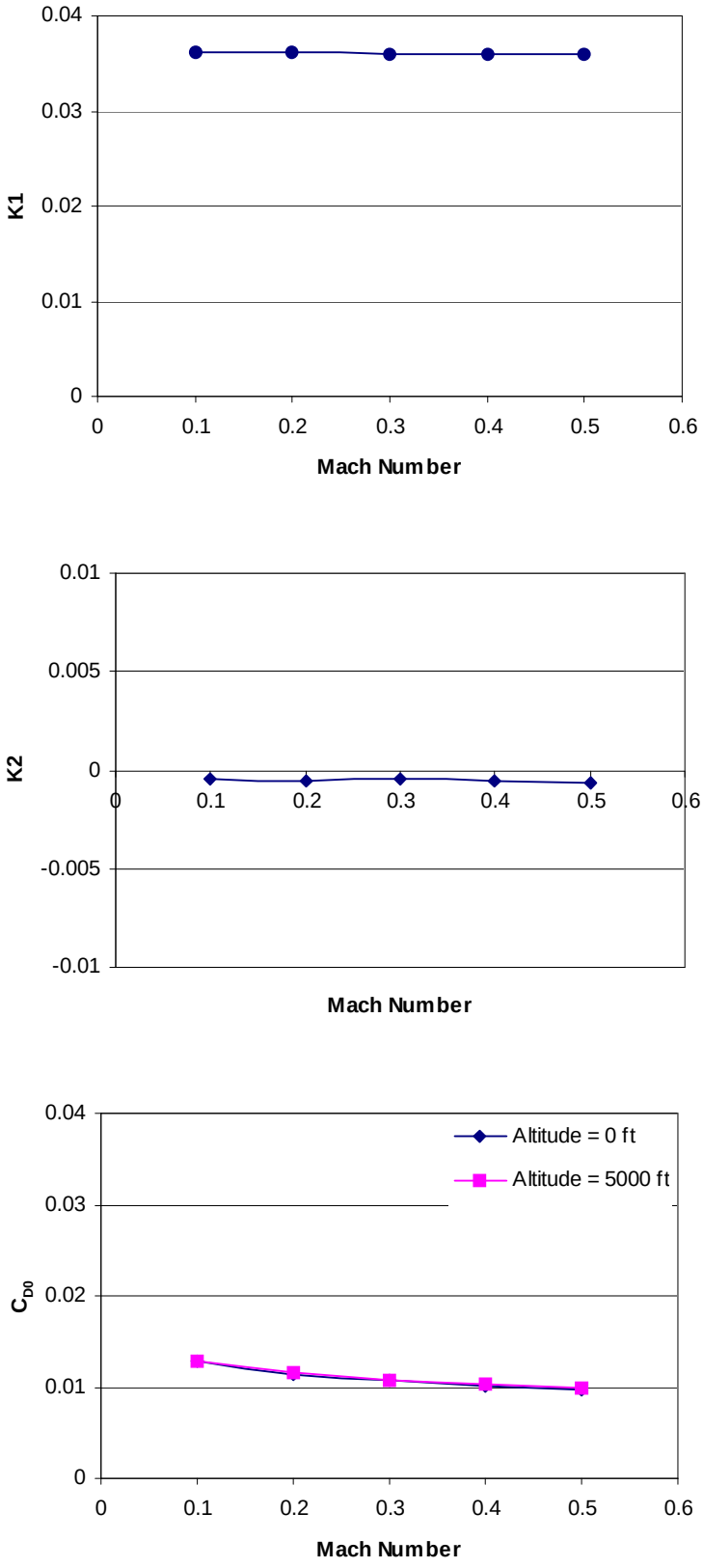

Figure 30: Drag Polar Coefficients of Naval UAV

5.1.2 Selection of Architecture Alternative

The fact that the six alternatives listed in Table 7 can be equally divided into three architectures based on PEMFCs and the other three that utilize SOFCs highlights the current lack of consensus on the fuel cell technology's applicability to aviation. Although an unequivocal answer that addresses all the concerns of the entire aeronautics community has been elusive thus far, and most likely remain elusive for the foreseeable future, the issue was decided to be explored within the scope of the LAGER problem. The focal point of the investigation was whether or not the higher fuel efficiency of an SOFC-based architecture results in enough savings in fuel weight and the weight of the Energy Storage sub-system to justify the increase in the weight of other major architectural elements.

Following the nomenclature of Table 7, the architectures of Alternatives 1 through 3 are represented by the schematic diagram shown in Figure 31(a), while those of Alternatives 4 and 5 correspond to Figure 31(b). The architectural layout of Alternative 6 would look the same as Figure 31(b) without the reformer and with a cryocooler for the HTS motor. Each Alternative was subsequently allowed to drive the sizing of a fuel cell powered UAV performing the LAGER mission shown in Figure 28 with the airframe illustrated in Figure 29. A fixed payload weight of 300 lbs was assumed to be sufficient for the kind of sensor and aviation packages the UAV would need to become functional. The generalized actual value-based sizing approach shown in Figure 24 was invoked with an "On-design" point set to the "Level flight" requirement of Figure 28 and "Off-design" analysis performed at each "Mission Analysis" point listed in Table 8. The reference-point shaft power, P_{ref}, was selected to be the shaft power needed for the "Level flight" condition, making α numerically greater than 1 in all segments leading up to cruise. An in-house developed spreadsheet that is capable of sizing the cryogenic H_2 storage tank, based on the work of Chambliss et al [144], was embedded in the "Mission Analysis" tool created by Nam [66]. The reference heating

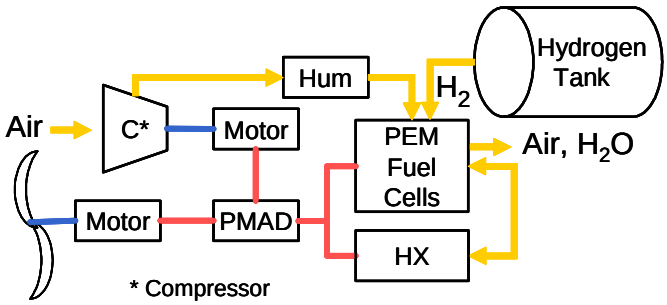

(a) PEMFC Based Architecture

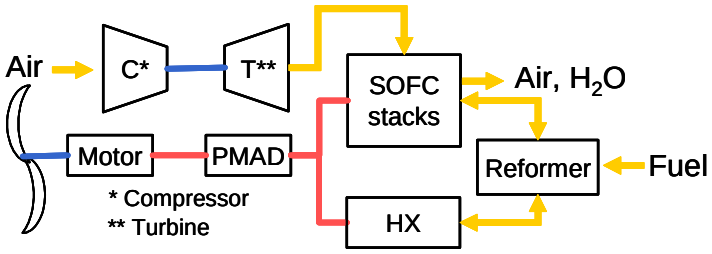

(b) SOFC Based Architecture

Figure 31: Candidate Fuel Cell Aeropropulsion System Architectures

value of hydrogen was set to its LHV.

The vehicle sizing results for the PEMFC-based aeropropulsion systems are listed in Table 9, along with the outcomes of both constraint analysis and mission analysis. It was found that the low specific power and marginal performance of Alternative 1 (**A1**) rendered a very heavy design. Alternatives 2 and 3 (**A2** and **A3**) yielded reasonable outcomes of power-to-weight ratio, wing loading, wing area, and take-off gross weight, whose detailed breakdown is shown in Figure 32. As expected, the fuel fraction came out low in both cases (5.3% and 6.0%, respectively), whereas the weight fraction of the cryogenic H_2 storage tank (9.5% and 11.2%, respectively) was found to be comparable to that of the entire aeropropulsion system (40.1% and 22.6%, respectively). These sizing results reflect how infusing advanced technologies at the aeropropulsion system level drives the vehicle-level design. As expected, advancements

Table 8: Discretization of LAGER Mission

Segment	**Flight Maneuver**	**Mach**	**Altitude (ft)**	**Duration (min)**	**Distance (mi)**
1	Warm up	0.00	0	20.000	0.000
2	Take-off Acceleration	0.04	0	0.634	0.248
3	Take-off Rotation	0.07	0	0.050	0.039
4	Constant Speed Climb	0.08	250	0.646	0.563
5	Constant Speed Climb	0.09	750	0.528	0.517
6	Constant Speed Climb	0.09	1250	0.531	0.527
7	Constant Speed Climb	0.09	1750	0.530	0.531
8	Constant Speed Climb	0.09	2250	0.537	0.546
9	Constant Speed Climb	0.10	2750	0.533	0.548
10	Constant Speed Climb	0.096	3250	0.535	0.553
11	Constant Speed Climb	0.097	3750	0.534	0.554
12	Constant Speed Climb	0.097	4250	0.535	0.557
13	Constant Speed Climb	0.097	4745	0.524	0.547
14	Constant Speed Climb	0.14	4995	0.416	0.626
15	Cruise	0.18	5000	55.698	110.000
16	Loiter	0.08	5000	360.000	0.000
17	Loiter	0.08	5000	360.000	0.000
18	Loiter	0.08	5000	360.000	0.000
19	Loiter	0.08	5000	360.000	0.000
20	Cruise	0.18	5000	55.698	110.000
21	Descent	0.15	3500	10.000	0.000
22	Loiter	0.08	2000	10.000	0.000
23	Loiter	0.08	2000	45.000	0.000

Table 9: PEMFC Powered UAV Sizing Results

	A1	A2	A3
Power-to-Weight Ratio (ft/s)	30.0	29.3	29.4
Wing Loading (lbs/ft^2)	8.5	9.0	9.1
Wing Area (ft^2)	665	495	199
Power Required at Take-off (hp)	308	238	97
Take-off Gross Weight (lbs)	5651	4460	1806

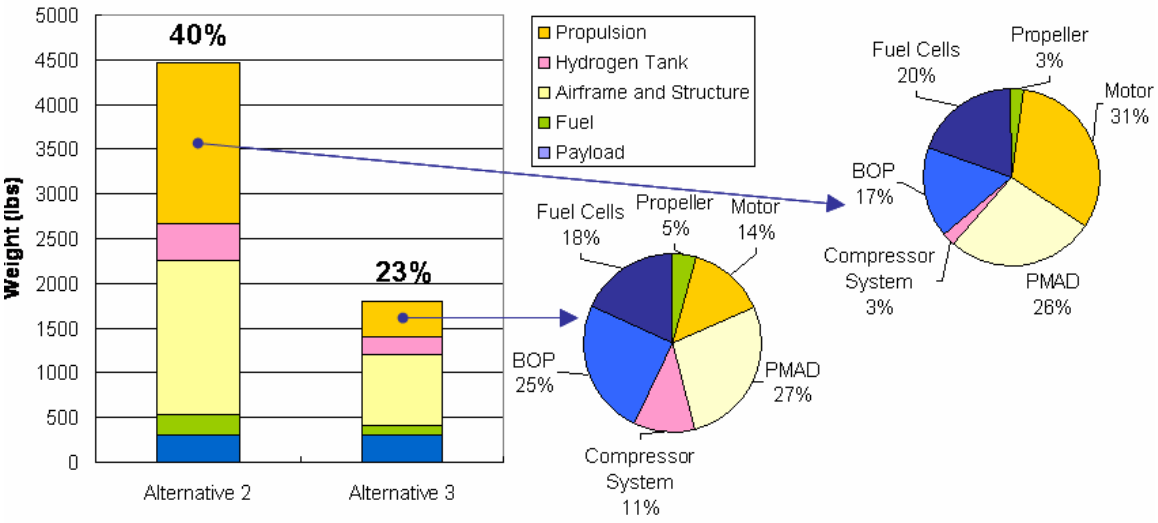

Figure 32: Weight Breakdowns of UAV Sizing Results

in gravimetric characteristics, electrochemical efficiencies, and electromechanical efficiencies translate into reduced take-off gross weight, wing area, and reference-point power. The weight breakdown of the aeropropulsion system offers further insights into which architectural elements require the most aggressive technological development. Judging from the shown pie-charts, these are, in order of urgency: PMAD, propulsion motor, BOP, PEMFC stack, and Turbomachinery ("Compressor System").

On the contrary, none of the SOFC-based systems resulted in a feasible UAV design capable of performing the LAGER mission defined as per Figure 28. That is, no convergence on P_{ref} was found as per the actual value-based sizing algorithm shown in Figure 24. This finding indicates that although SOFC technology is more efficient than a PEMFC on a per-cell basis, the specific power of an SOFC stack is roughly a third of a PEMFC stack's. Moreover, the cases of infeasibilities imply

Table 10: Point-Performance Requirements for SOFC-based Alternatives

TOFL	5000 ft, Hot Day, over 35 ft obstacle clearance
Climb	150 ft/min at 5,000 ft of altitude
Level Flight	70 knot at 5,000 ft of altitude
Approach	57 knot
LDFL	1,500 ft over 50 ft obstacle clearance

that the advantage of not requiring on-board hydrogen storage was more than offset by additional BOP equipment, such as hot boxes (Alternatives 4, 5, and 6), CPOX reformers (Alternatives 4 and 5), and cryocoolers (Alternative 6). Convergence on P_{ref} became possible with Alternatives 5 and 6 only after several point-performance constraints were significantly relaxed, as listed in Table 10.

Utilizing these relaxed point-performance requirements and the same actual value-based sizing approach, Agrawal recorded the impact of increasing the TOS requirement on W_{TO} [145]. The objective of this study was to investigate the existence of a crossover point with respect to PEMFC-based Alternatives, from which trading system weight for efficiency begins to make sense. Instead, what is apparent from the divergent trend of Figure 33 is that such a trade is neither fair nor practical for the given mission and airframe[1]. Due to the above findings, all SOFC-based aeropropulsion systems were shelved from further implementation steps.

5.1.3 Scalability Investigation

As postulated in **Hypothesis 1**, the discovery, or lack thereof, of system scalability is the key to suggesting the most practical algorithm for integrating the propulsion-level knowledge into the larger activity of aerovehicle sizing. This required investigating whether or not the analysis results confirmed or denied the scalability of PEMFC-based systems within the fidelity bounds of the developed simulation environment. In preparation, relevant parametric models were calibrated to simulate the on- and

[1] Aircraft sizing with Alternative 3 was done as per the baseline point-performance specifications.

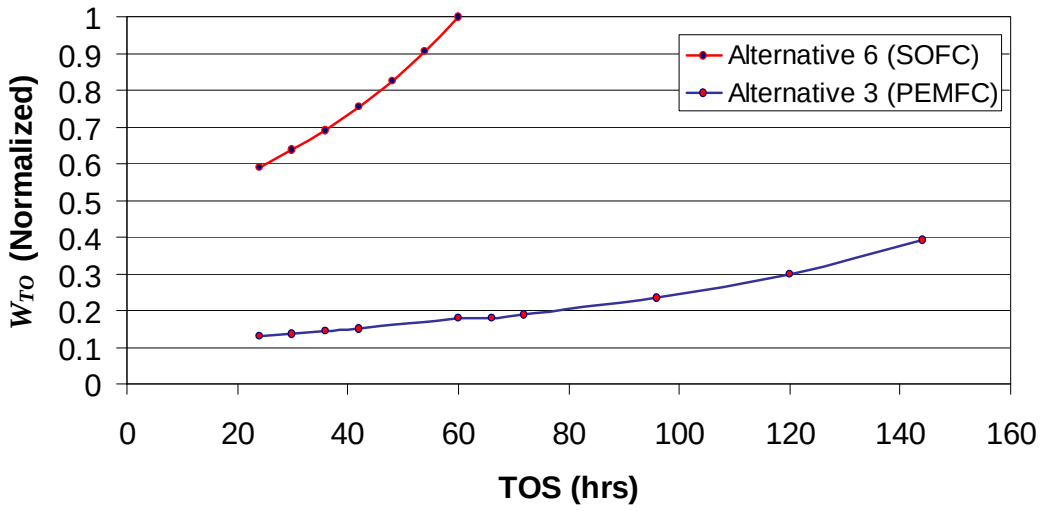

Figure 33: UAV Take-off Gross Weight vs. TOS

Table 11: Cycle Parameters: PEMFC Aeropropulsion System

Parameter	Symbol	Units	π_1 (low)	π_2(ref)	π_3(high)
Fuel Cell Stack Temperature	T_{stk}	°C	65	80	94
Fuel Cell Stack Pressure	P_{stk}	bar	1.5	2.0	3.5
Anode Water Content	a_{an}	N/A	0.8100	0.9500	0.9999
Cathode Water Content	a_{ca}	N/A	0.8100	0.9500	0.9999
Fuel Utilization Coefficient	u_f	N/A	0.8100	0.9000	0.9999

off-design performance behaviors of Alternatives 1, 2, and 3.

Keeping true to the spirit of cycle analysis, the independent variables listed in Table 11 were designated as the *cycle parameters*. This pairing was done on the basis that the listed inputs are those which significantly affect some of the most significant system-level metrics, such as fuel consumption, thrust and power-lapse ratios, current draws, etc. One setting of these parameters defines the *cycle* to which the given fuel cell aeropropulsion system is designed, as well as the cycle-parameter vector π.

For each Alternative, its scalability was investigated at the "low," "ref," and "high" cycles, as per Table 11. The investigation was a two-pronged process, requiring both the on- and off-design capabilities. First, on-design analysis was commenced for a given P_{ref} and α of 1 at SLS. Subsequently, off-design analyses were performed at the mission segments corresponding to "Cruise" and "Loiter" of Table 8. This process

was repeated for a range of P_{ref} values to observe the relationship between SFC and system scale and to explore the dependency, if any, of power-lapse to system scale.

The collected simulation results were plotted as illustrated in Figures 34 through 36, where normalized P_{ref} values are plotted on the abscissas, while the ordinates represent either the SFC - in pounds of fuel per horsepower per hour - or α. As seen, negligible deviations in SFC were measured for all three cycles, even when the scale of the system was doubled. Another trend to note are the lapses in available shaft power. The percentage drops in α from the reference point (SLS) to cruise and loiter remain nearly constant regardless of system size, as shown in all three Figures. These findings were deemed sufficient to declare all three PEMFC-based Alternatives as scalable systems within the boundaries of the implementation task.

5.1.4 Development of Synthesis Algorithm

The results of the previous step, which support the thermodynamic scalability of the PEMFC-based alternatives, justified the creation of a specific parameter-based synthesis algorithm, depicted in Figure 37. This was made possible due to the union between the simulation environment described in §4.3 and the Architecture-Independent Aircraft Sizing (AIAS) spreadsheet developed by Nam [66].

In compliance with the assumptions of AIAS, the overall efficiency, η_{oa}, is defined as the ratio of available (shaft) power to the total power generated by the fuel cell stack:

$$\eta_{oa} = \frac{P_{ava} \cdot 746}{P_e} \eta_{stk} \tag{14}$$

where the available power at a specific off-design condition, P_{ava}, and stack output power, P_e, are in units of horsepower and watts, respectively. It is obvious that this is the algorithmic approach that leverages upon the decoupling of the propulsion-level design work from that at the aerovehicle level. Consequently, the developed synthesis

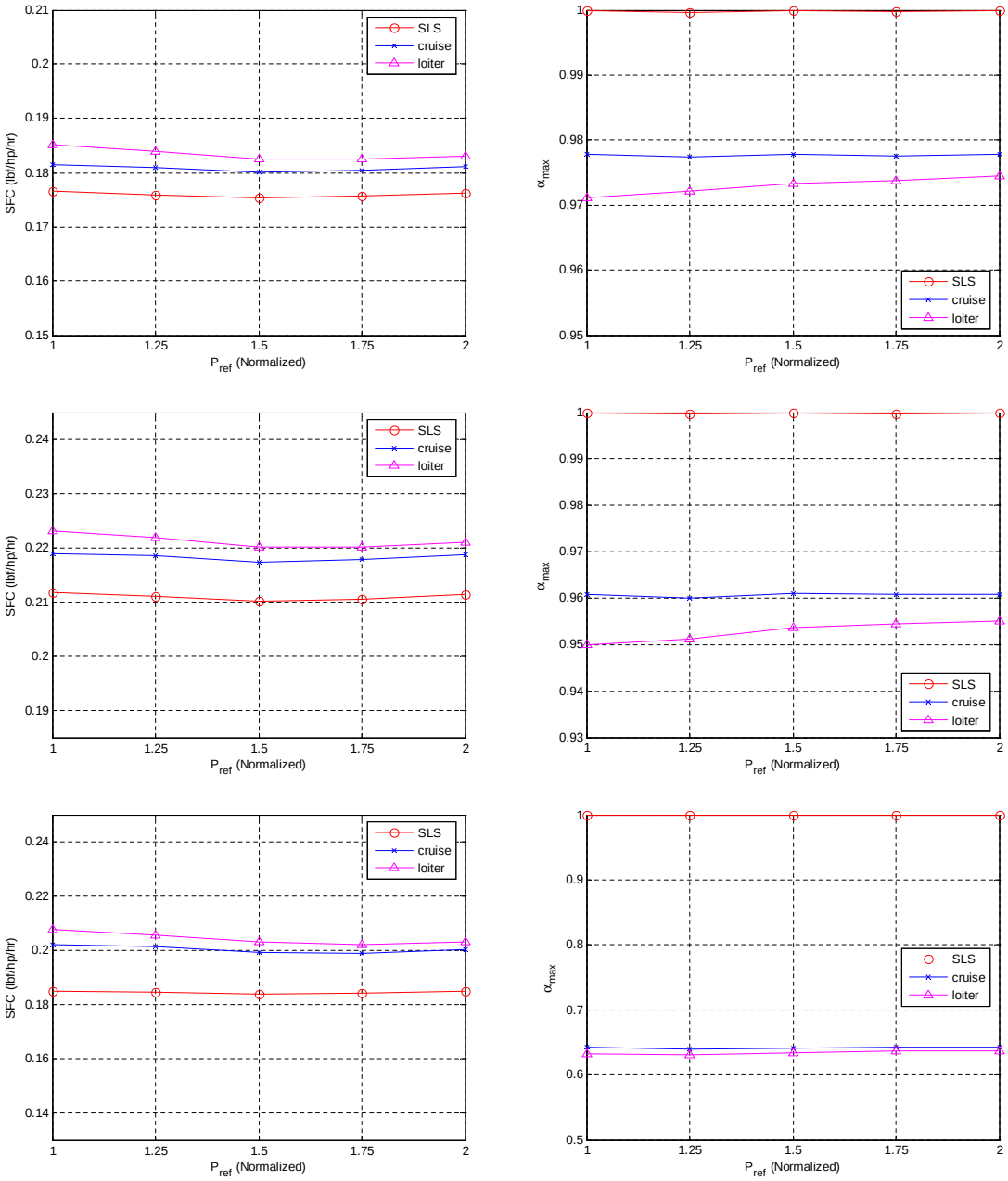

Figure 34: Scalability Investigation of **A1**. Top: π_1. Middle: π_2. Bottom: π_3.

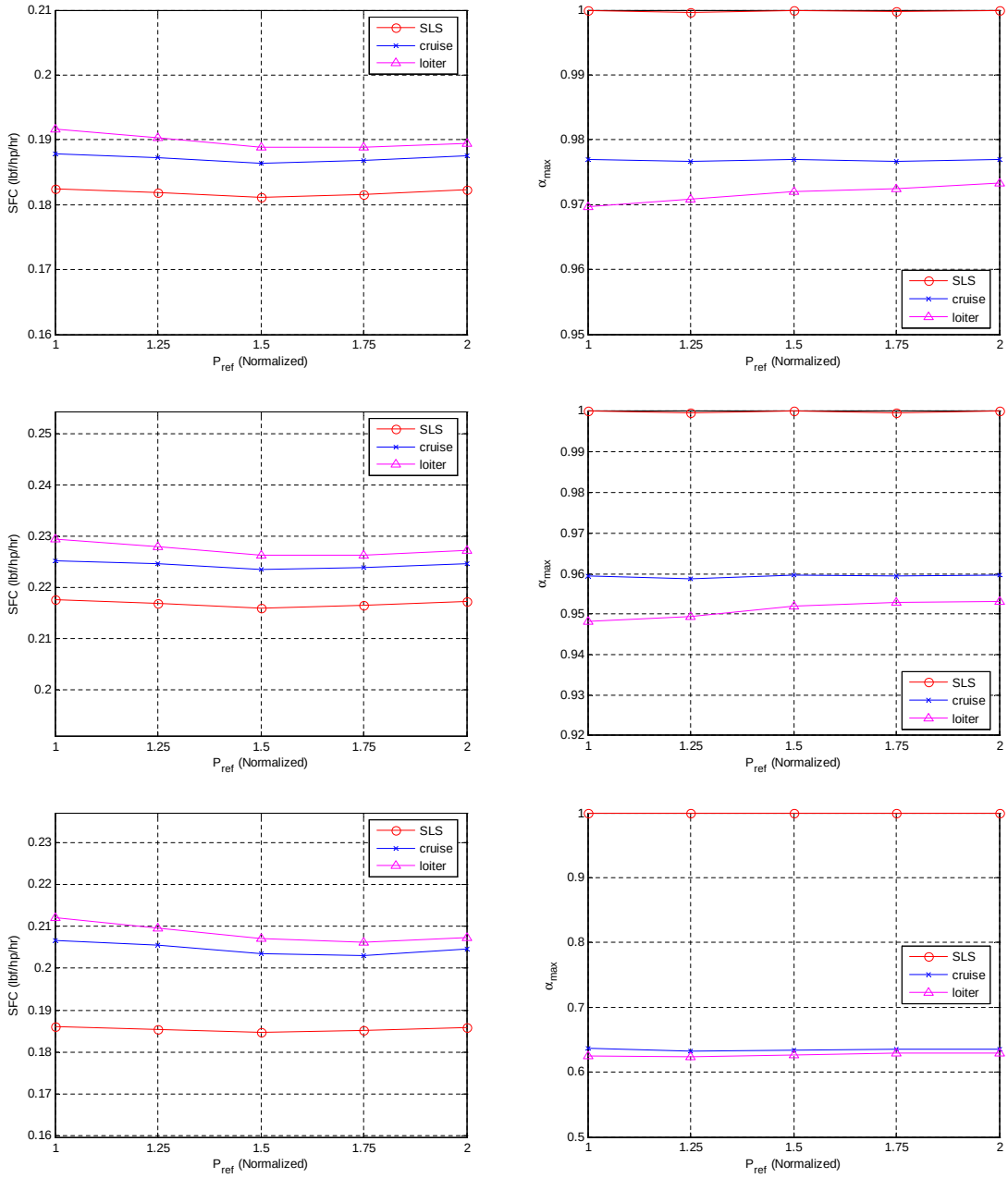

Figure 35: Scalability Investigation of **A2**. Top: π_1. Middle: π_2. Bottom: π_3.

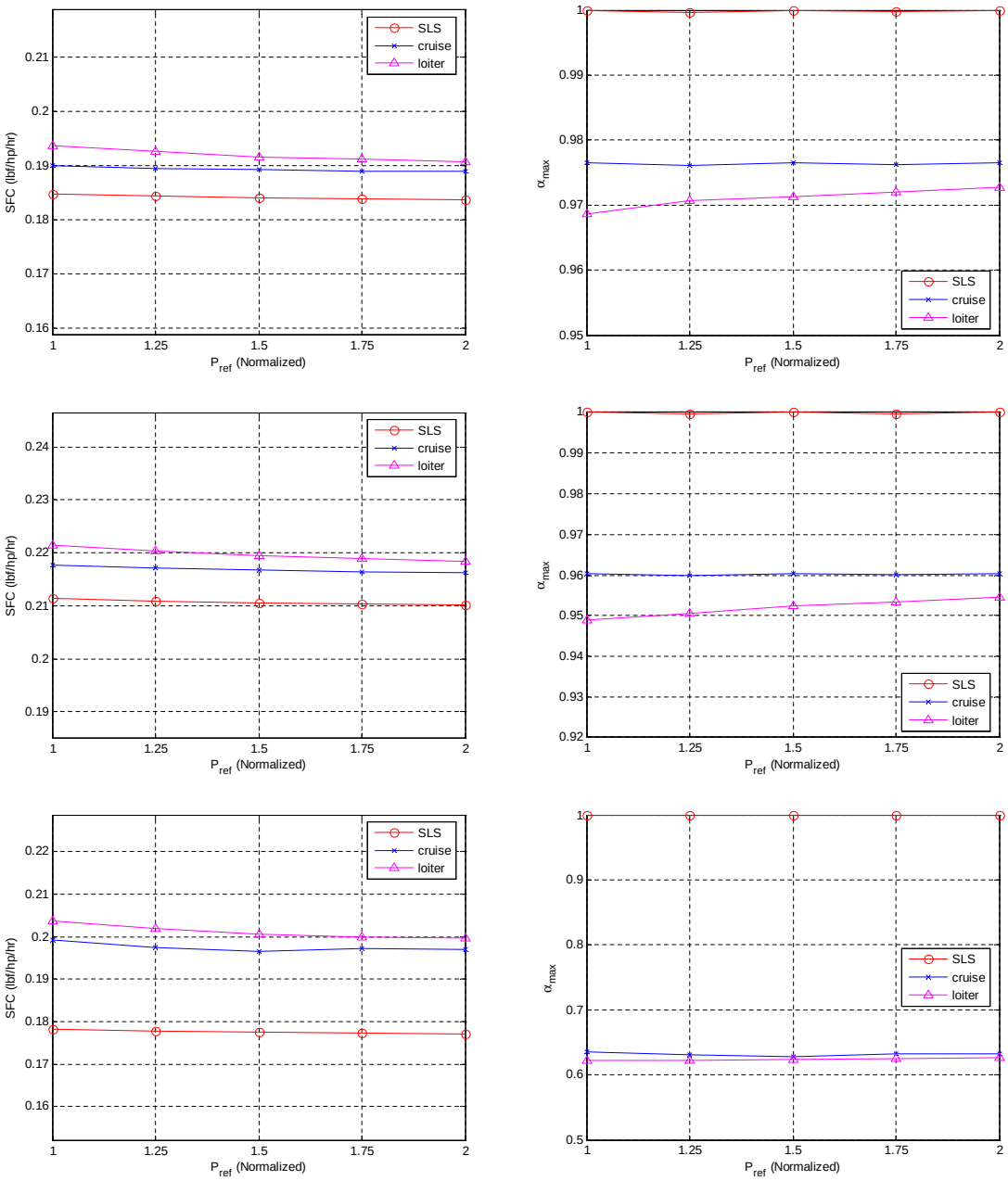

Figure 36: Scalability Investigation of **A3**. Top: π_1. Middle: π_2. Bottom: π_3.

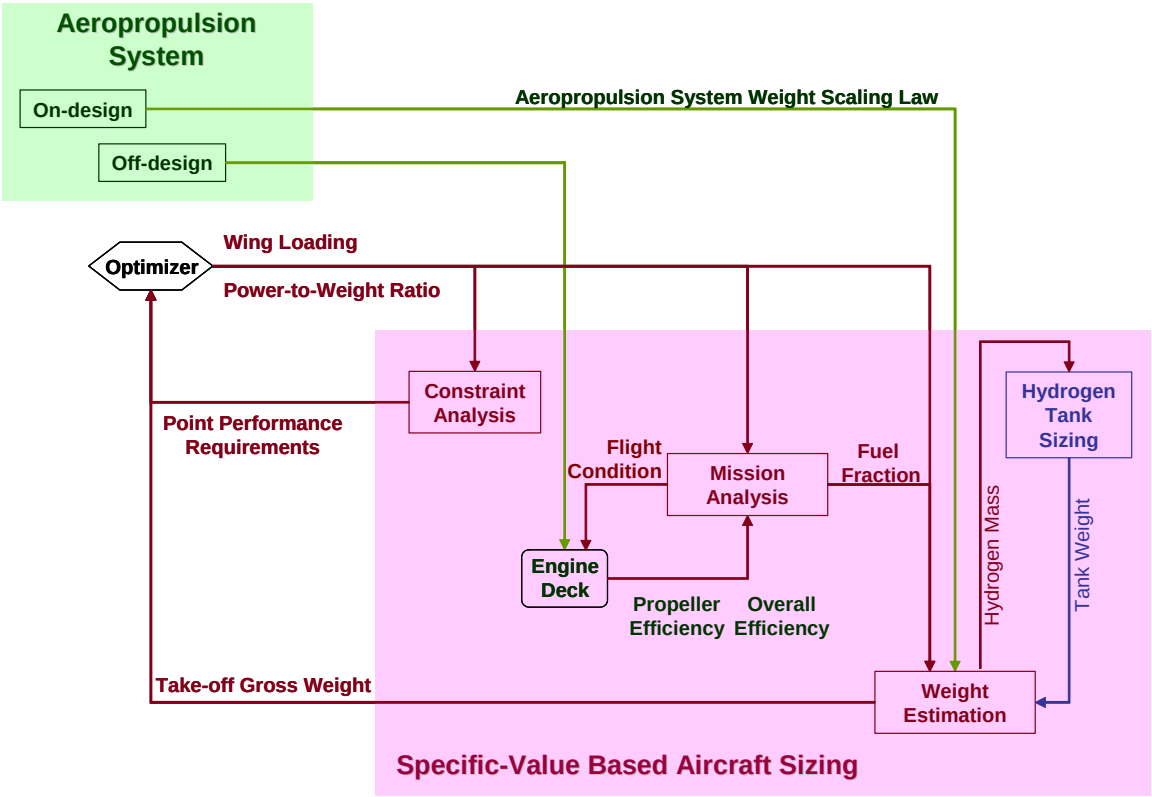

Figure 37: Generalized Specific Parameter-based Aerovehicle Sizing Process

algorithm requires significantly lower computational overhead than the actual value-based algorithm shown in Figure 24, given an engine deck and a weight scaling law for a cycle of interest. The inclusion of a numerical optimizer here would not have been practical if it were not for the resulting computational expediency.

In order to limit the loss in analysis accuracy from turning the Mission Analysis into a table-lookup routine, a third-party Matlab toolbox called `LibLip` is utilized in interpolating propeller and overall efficiencies. The toolbox provides a useful function for robustly and accurately interpolating from a multivariate *scattered* data source [146], and is, thus, well-suited for unpreprocessed data sets like engine deck files.

5.1.4.1 Choice of Auxiliary Energy Storage Technology

One noticeable omission in Figure 31(a) is a block for an auxiliary energy storage subsystem. Such a *pure* power system architecture is the ideal candidate for vehicular

propulsion from a systems integrators perspective due to many favorable characteristics, such as high total efficiency, low cost, reduced system weight, etc. While fuel cell based architectures without a battery and DC-DC converter have been postulated [147], a power system without an auxiliary energy storage device would be a difficult sell in practice due to the lack of an energy buffer, as outlined in §4.2.1.5.

With the finalization of the synthesis algorithm, a trade study could be finally conducted to discover the most suitable galvanic cell technology for the LAGER mission. The objective here was to identify the lightest battery or ultracapacitor option, which holds sufficient energy to protect the sized UAV against a "Balked Landing" scenario, as per FAR §23.77(b) [148]:

> Each normal, utility, and acrobatic category reciprocating engine-powered airplane of more than 6,000 pounds maximum weight and each normal, utility, and acrobatic category turbine engine-powered airplane must be able to maintain a steady gradient of climb of at least 2.5 percent with -
>
> (1) Not more than the power that is available on each engine eight seconds after initiation of movement of the power controls from minimum flight-idle position;
>
> (4) A climb speed equal to V_{REF}, as defined in §23.73(b).

where the reference landing speed, V_{REF}, was assumed to be equal to 1.3 times the stall speed, V_{stall}. Exploiting the well-known relationship between wing loading and stall speed thus yields:

$$V_{REF} = 1.3V_{stall} = 1.3\left(\frac{2}{\rho C_{L_{max}}}\frac{W_{TO}}{S}\right) \tag{15}$$

where the density of air, ρ, at sea-level is 0.0024 slug/ft^3 and the maximum lift coefficient, $C_{L_{max}}$, for an untapered and plain-flapped wing is 1.8 [40].

In order for the LAGER UAV to meet the above regulatory requirement in the event of a failed landing attempt, sufficient shaft power to hold the aircraft at a climb

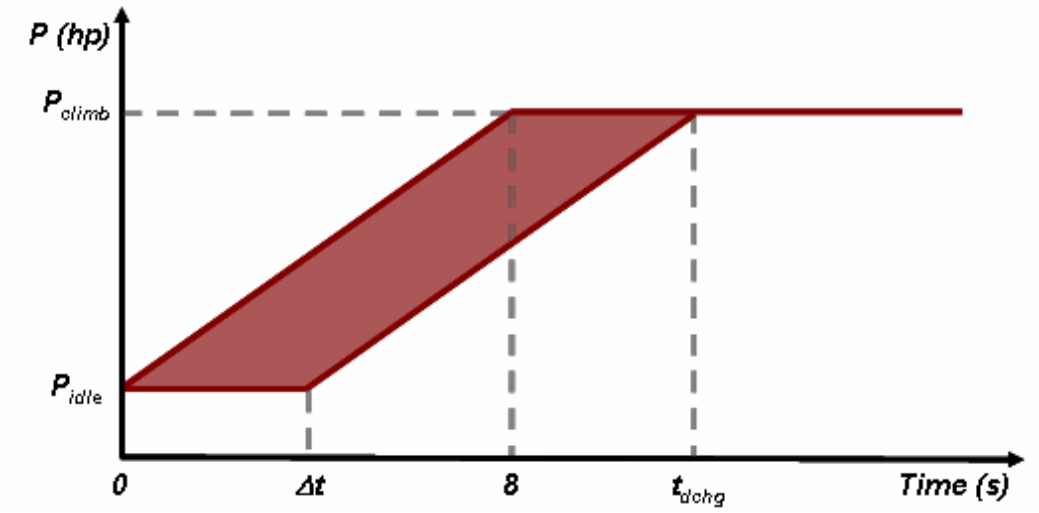

Figure 38: Load Profile for Sizing Auxiliary Energy Storage Device

gradient, dh/ds, of 0.025 must be delivered to the propulsion motor. The power required to perform this flight maneuver can be estimated via Nam's AIAS method [66]. Manipulating the equation for constant speed climb as follows yields:

$$P_{climb} = W_{TO}\frac{\beta V_{REF}}{\eta_p \alpha}\left\{K_1\left(\frac{\beta}{q}\frac{W_{TO}}{S}\right) + K_2 + \frac{C_{D_o}}{\left(\frac{\beta}{q}\frac{W_{TO}}{S}\right)} + \frac{1}{V_{REF}}\left(\frac{dh}{dt}\cdot\frac{dh}{ds}\right)\right\} \quad (16)$$

The terms ds/dt and V_{REF} cancel out, allowing the evaluation of Eq.(16) for an aircraft weighing W_{TO}. All three drag polar coefficients - K_1, K_2, and C_{D_o} - as well as the dynamic pressure, q, and propeller efficiency, η_p, are calculable for sea-level flight conditions once V_{REF} is available from Eq.(15). Lastly, the vehicle's weight fraction, β, at the time of performing the above maneuver should be available from the mission analysis portion of the AIAS method.

The above-mentioned FAR dictates that the aircraft's power plant be able to ramp up from flight-idle power, P_{idle}, to P_{climb} in 8 seconds. Assuming this to be a linear load profile, Figure 38 depicts how the auxiliary galvanic cell can assist the fuel cells, which intrinsically have some transient response time of $\triangle t$ seconds. Therefore, the shaded area of Figure 38 represents the energy requirement, E_{climb}, for the auxiliary power system, and the sum of 8 and $\triangle t$ seconds becomes the duration of the discharge

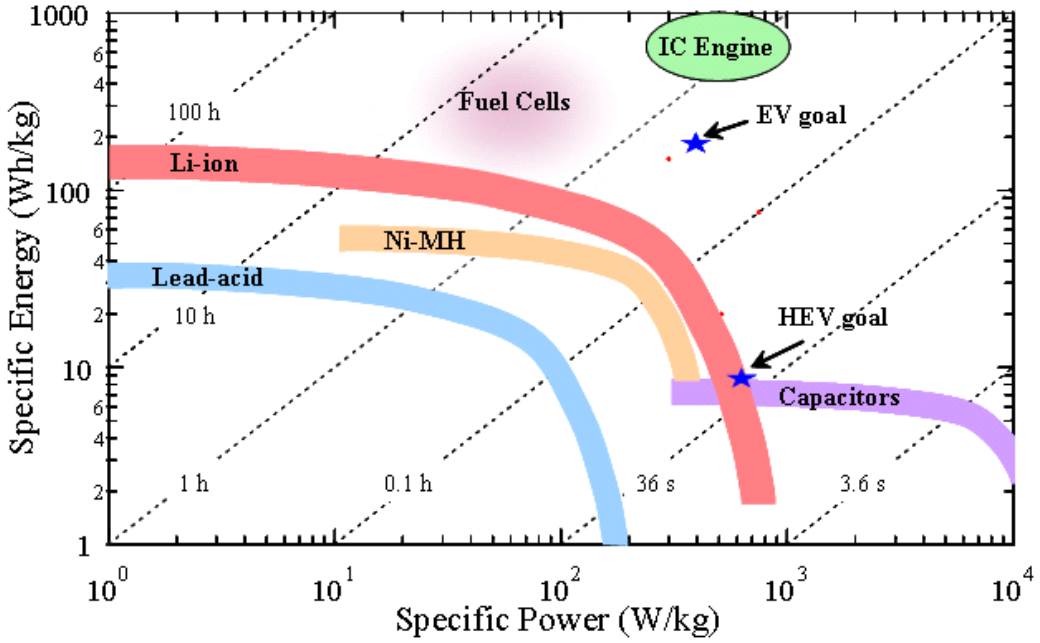

Figure 39: Ragone Plot of Various Auxiliary Energy Storage Technologies [149]

time, t_{dchg} in a single balked landing. Both information can be further used in sizing the sub-system via a Ragone Plot like the one shown in Figure 39. The plot confirms the sensitivity of a galvanic cell's capacity (energy content) to its usage - the shorter the t_{dchg}, the smaller the available specific energy. Since the state-of-the-art PEMFC systems are built to satisfy $\triangle t$ of 1 second for 10-90% operations [150], the total time-scale - even after allowing multiple balked landings for conservatism - is on the order of tens of seconds. Figure 39 clearly shows that ultracapacitor technology is the only sensible option that yields sufficiently high specific energy for such pulsing operations. As such, it was chosen as the exclusive auxiliary energy source for all three Alternatives.

5.1.4.2 Sample Parametric Cycle Analysis

Figure 40 shows the results of implementing parametric cycle analysis with the developed synthesis algorithm. The cycle parameters listed in Table 11 were perturbed one at a time while holding the others constant, in order to observe its impact on a

vehicle-level metric of interest, such as take-off gross weight. Each cycle parameter went through five, evenly-discretized settings, thus culminating in a total of 25 cycles and 25 aircraft sizing cases. Optimization was performed for each case to obtain the combination of power-to-weight ratio and wing loading that resulted in minimum W_{TO}. A scaling law, regressed from data mined from Figure 39, as well as other Ragone Plots found in Ref.[151], was utilized in sizing the ultracapacitor to be sufficient for up to three balked landing attempts. Normalized linear scales were used in both abscissas and on the ordinate of Figure 40(b), where 0 and 1 represent each end of the spectrum.

The shown trends reveal the dominance of T_{stk} and P_{stk} in affecting W_{TO} - arguably one of the most important figures of merit to an aircraft designer. It is suggested that significant savings in vehicle weight are possible just by designing the fuel cells to operate at the right temperature and pressure. In both cases, there is a hint of a setting that results in optimal aircraft weight. Such is indicative of the fact that the cost of higher fuel efficiency for a fuel cell system is often greater in terms of parasitic losses, which are unavoidable if the Turbomachinery and BOP sub-systems must be taxed harder. Additional performance and weight penalties are associated with running the fuel cells too hot, such as membrane dry-out and the need for extra insulation and cooling.

Although less pronounced, the three remaining cycle parameters were also found to contribute toward weight reduction. The membrane hydration model embedded in the propulsion-level simulation environment correctly predicted that operating an anode dry from the beginning imparts a greater adverse consequence than operating a cathode with less humidity. In PEMFCs, the occurrence of back-diffusion, or the flow of water from the cathode to the anode, tends to be more pronounced than the phenomenon of electro-osmotic drag, or the undesirable transport of water molecules from the anode to cathode via proton conduction in the same direction. The net effect

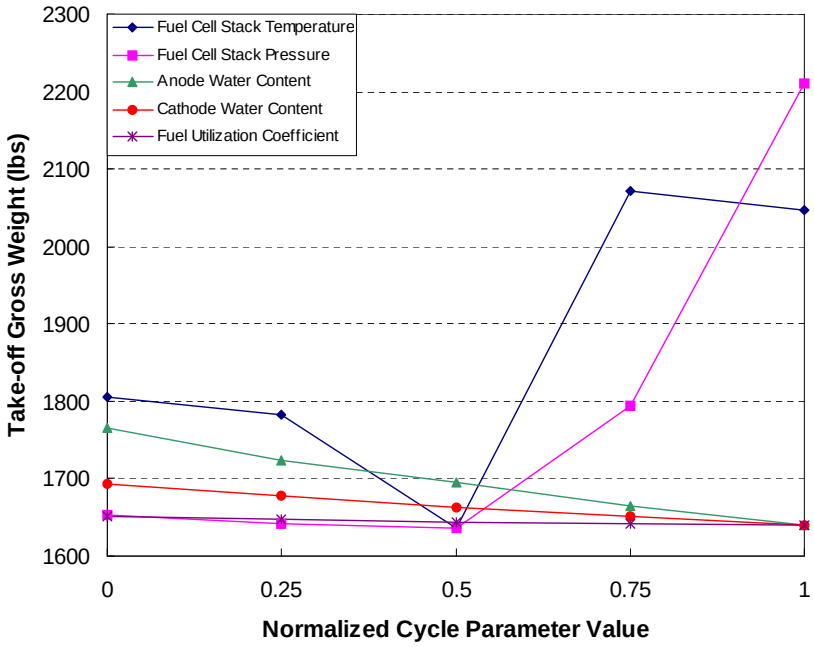

(a) Real-valued Sensitivies

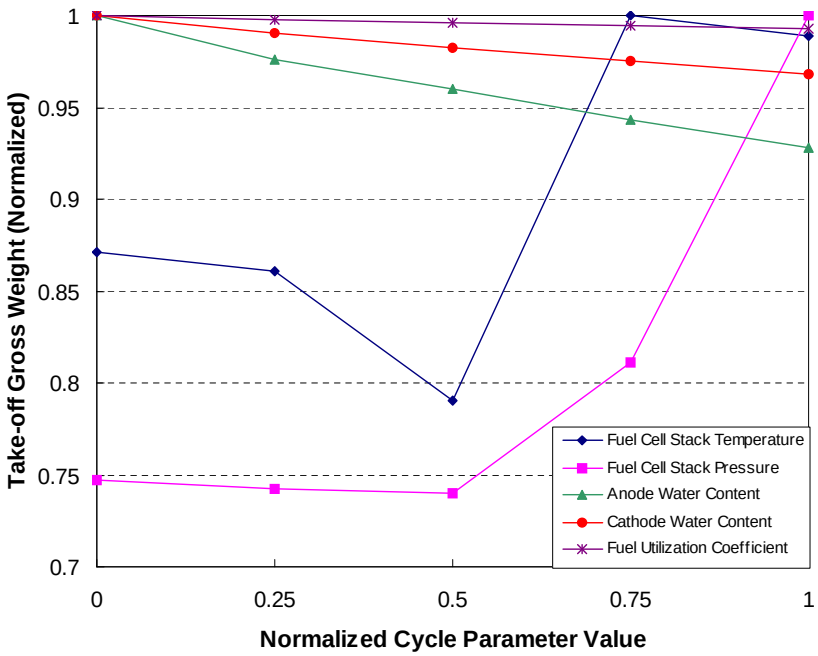

(b) Normalized Sensitivies

Figure 40: Parametric Cycle Analysis: UAV with **A3**

at moderate to high current densities is that the anode almost always becomes drier more rapidly than the cathode during operation. It would, thus, be more prudent to select a cycle that keeps the anode more hydrated than the cathode at all times.

Lastly, fuel utilization was shown to display the least amount of impact, largely because hydrogen is - gravimetrically speaking - a very energy-dense fuel. Improving u_f yields less than a percentage reduction in W_{TO} even after the reserves for an additional 55 minutes of low-speed flight, hydrogen boil-off in the tank, and the coolant needs for the HTS motor were taken into account. Overall, the study demonstrates the importance of conceiving a suitable engine cycle for the given mission, airframe, and aeropropulsion system architecture.

5.2 Formulation of Stages and Recourse

It is reiterated that the main intention of this research is to showcase a solution process, rather than delivering a case-study on a real product development example. The reader is reminded that the **Research Task** states the objective of this thesis as the demonstration of the merits of accounting for recourse in a notional product development setting. The design of a fuel cell aeropropulsion system was presented as an example engineering challenge of contemporary interest, as first discussed in §1.2.1 and subsequently justified in §5.1.1. Therefore, presented next are the outcomes of implementing **Sub-task 2** within the structural and fidelity bounds of the simulation environment, which was created as part of completing **Sub-task 1**.

5.2.1 First-Stage Value Function

A closer scrutiny of the disciplinary-level simulation environment discloses that there are fourteen major input variables. Six of these fourteen variables are P_{ref} and the five cycle parameters listed in Table 11. Two of the remaining eight inputs only affect the system gravimetrically, while the other six affect the amounts of power and current draws among the architecture components. Collectively, all fourteen

Table 12: First-Stage Design Variables

Parameter	Symbol	Association with $\mathbf{x}$	Units
Reference-Point Shaft Power	P_{ref}	x_1	hp
Fuel Cell Stack Temperature	T_{stk}	x_2	°C
Fuel Cell Stack Pressure	P_{stk}	x_3	bar
Anode Water Content	a_{an}	x_4	N/A
Cathode Water Content	a_{ca}	x_5	N/A
Fuel Utilization Coefficient	u_f	x_6	N/A

Table 13: List of Random Parameters

Parameter	Symbol	Association with $\xi(\omega)$	Units
3-Phase Inverter Efficiency	η_{mmc}	ω_1	N/A
Compressor Motor Efficiency	η_{cm}	ω_2	N/A
Compressor Motor Controller Efficiency	η_{cmc}	ω_3	N/A
Buck Regulator Efficiency	η_s	ω_4	N/A
Boost Regulator Efficiency	η_{dcdc}	ω_5	N/A
Heat Exchanger Effectiveness	ε_{hx}	ω_6	N/A
BOP Specific Power	SP_{bop}	ω_7	hp/lbs
PMAD Specific Power	SP_{pmad}	ω_8	hp/lbs

parameters dictate the design of a notional fuel cell aeropropulsion system.

Tables 12 and 13 list how the above-mentioned input variables correspond to the stage-based recourse programming model. The cycle parameters, as well as P_{ref}, are assigned as elements of the first-stage design variable vector $\mathbf{x}$ due to their dominant role in impacting all system-level behaviors. The pairing results in a 6×1 vector of first-stage design variables.

The decision to populate the random parameter vector $\xi(\omega)$ with the quantities listed in Table 13 is not too arbitrary. Each quantity is chosen to be parametrized in a nondeterministic manner because it is either affected by technological or "epistemic [152]" uncertainties. Therefore, the resulting 8×1 vector of random parameters represents the quantities that would become fixed according to the expert's or designer's "belief [153]" under the deterministic design paradigm.

Defining $\mathbf{M}(\mathbf{x}, \xi(\omega))$ is a critical step, because the modeling of second-stage recourse hinges upon which metric is the value function at the first stage. A first-stage

value function must uniquely depend on given realizations of $\mathbf{x}$ and $\xi(\omega)$ vectors (*i.e.*, its numerical value should not be affected by factors other than those listed in Tables 12 and 13). In this regard, the weight of the aeropropulsion system is the sole qualifying metric, as all others are also dependent on the "Mission Analysis" points listed in Table 8. This line of reasoning yields a vector with the following form

$$
\begin{aligned}
&M_1 = W_{prop}(P_{ref}) \\
&M_2 = W_{mm}(P_{ref}) \\
&M_3 = W_{stk}(\mathbf{x}, \omega_i) \quad \text{and} \quad i \in \begin{cases} I = \{2, \ldots, 6\} & \text{if} \quad \text{Alternative} < 3 \\ \text{otherwise} & I = \{1, \ldots, 6\} \end{cases} \\
&M_4 = W_{cp}(\mathbf{x}, \omega_i) \quad \text{and} \quad i \in \begin{cases} I = \{2, \ldots, 6\} & \text{if} \quad \text{Alternative} < 3 \\ \text{otherwise} & I = \{1, \ldots, 6\} \end{cases} \\
&M_5 = W_{bop}(\mathbf{x}, \omega_i) \quad \text{and} \quad i \in \begin{cases} I = \{2, \ldots, 7\} & \text{if} \quad \text{Alternative} < 3 \\ \text{otherwise} & I = \{1, \ldots, 7\} \end{cases} \\
&M_6 = W_{pmad}(\mathbf{x}, \omega_i) \quad \text{and} \quad i \in \begin{cases} I = \{2, \ldots, 6, 8\} & \text{if} \quad \text{Alternative} < 3 \\ \text{otherwise} & I = \{1, \ldots, 6, 8\} \end{cases}
\end{aligned}
\tag{17}
$$

where the elements, in order of their numerical ascendancy, represent the weights of: propeller, propulsion motor, fuel cell stack, compressor system, BOP and PMAD system. Each element of the vector and its functional dependency to the constituents of $\mathbf{x}$, $\xi(\omega)$, or both are detailed in Eq.(17). The conditional dependencies highlight how η_{mmc} is separately accounted for in modeling $\mathbf{A_3}$, whereas it is bookkept together with η_{mm} in simulating the other alternatives. Finally, the first-stage value function becomes

$$
f = W_{PSA}(\mathbf{x}, \xi(\omega)) = \mathbf{M}(\mathbf{x}, \xi(\omega)) \cdot \mathbf{I}^T \tag{18}
$$

where W_{PSA} stands for the weight of a certain propulsion system alternative, and the identity vector is the same as that introduced in §4.4.2.1.

Table 14: Constituents of TPM Vector

Parameter	Symbol	Association with $\mathbf{T}(\cdot, \xi, \xi)$	Units
Fuel Cell Stack Efficiency at Loiter	$\eta_{stk\|\text{loiter}}$	$T_1(\cdot, \xi, \xi)$	N/A
Available Shaft Power at Take-off	$P_{sh\|\text{SLS}}$	$T_2(\cdot, \xi, \xi)$	hp

5.2.2 Second-Stage Recourse

The selection of $W_{PSA}(\mathbf{x}, \xi(\omega))$ as the first-stage value function compelled the second-stage value function, $Q(\mathbf{x}, \xi(\omega))$, to also be in the units of lbs. Consequently, the penalty of taking recourse in the second stage has come to be quantified in terms of extra system weight - a cost that would be unnecessary if the designer had the ability to predict the *future* (*i.e.*, realization of $\xi(\omega)$). Moreover, it is assumed that the hypothetical engineering process emulated herein still holds sufficient degrees of design freedom in the second stage to justify remedial actions, should they become necessary. It is further assumed that such compensatory actions can be adequately modeled by equating the second-stage design variables to the deviation from the first-stage solution (*i.e.*, $\mathbf{y} = \mathbf{x} \pm \triangle\mathbf{x}$).

Both figures listed in Table 14 of merit not only qualify as TPMs, as per the recommendation of Ref.[43], but also correspond to the metrics that a real engine manufacturer will strive to maximize. They also embody the design philosophy that the ideal aerospace power plant is the one that is sized for take-off (maximum power), but not too over-sized, as to result in excessive fuel weight. When evaluated in conjunction with the vector of target values, $\mathbf{h}$, the TPM vector can help quantify either the first-stage constraint vector, $\mathbf{g_1}(\mathbf{x}, \xi(\omega))$, or the second-stage constraint vector, $\mathbf{g_2}(\mathbf{y}, \xi(\omega))$.

Lastly, q_j, an element of the penalty vector $\mathbf{q}$, is defined as a constant that is greater than 1 if $\eta_j(\mathbf{x}, \mathbf{y}, \xi(\omega)) > 0$ but otherwise lies between 0 and 1. Each element is intended to match up with an M_j so that their multiple could signify the additional weight incurred from recourse, as per Eq.(11). The dot product of these two vectors,

$\mathbf{q}$ and $\eta(\mathbf{x}, \mathbf{y}, \xi(\omega))$, then yields one instance of the second-stage value as indicated by Eq.(10).

5.3 Surrogate Modeling of Program Functions

The creation of surrogates is the bridging step between the formulation of a two-stage recourse program and its numerical implementation. Without these so-called meta-models, obtaining a stochastic solution, as per Eq.(12), becomes practically impossible in a single-user computing environment. The reader is reminded that the motivating factors for pursuing Surrogate Modeling are discussed in §4.4.3.

Figure 41 illustrates the process used for creating the surrogate models of all program functions. As shown, artificial neural networks became the exclusive means of capturing the often non-linear relationships between the independent, or input, variables and dependent, or output, variables. The primary reason behind the adoption of the neural network (NN) techniques was due to the growing dimensionality of the pattern recognition task. The relatively high number of input variables implied that custom-made DoE tables became necessary if the more tried-and-tested RSM were to be employed. In contrast, the generation of NN-based surrogates offered the means of utilizing simpler space-filling DoE algorithms. Preliminary comparison studies between the applications of RSM and neural networks for the same program functions also indicated that the latter method resulted in better-fitted surrogates with a lesser number of sampling runs, when the additional sampling cases required for examining the Model Representation Error (MRE) of response surface equations were included.

JMP, a statistical software package marketed by the SAS Institute Inc., was instrumental in the creation of the NN-based surrogates for $\mathbf{M}(\mathbf{x}, \xi(\omega))$, $\mathbf{T}(\mathbf{x}, \tilde{\xi}(\omega), \xi(\omega))$, $\mathbf{T}(\mathbf{y}, \xi(\omega), \xi(\omega))$, and $Q(\mathbf{x}, \xi(\omega))$. The program offers an intuitive graphical user interface that is akin to a spreadsheet-type environment, as well as a wide variety of options to analyze, visualize, and manipulate statistical information [154]. All data

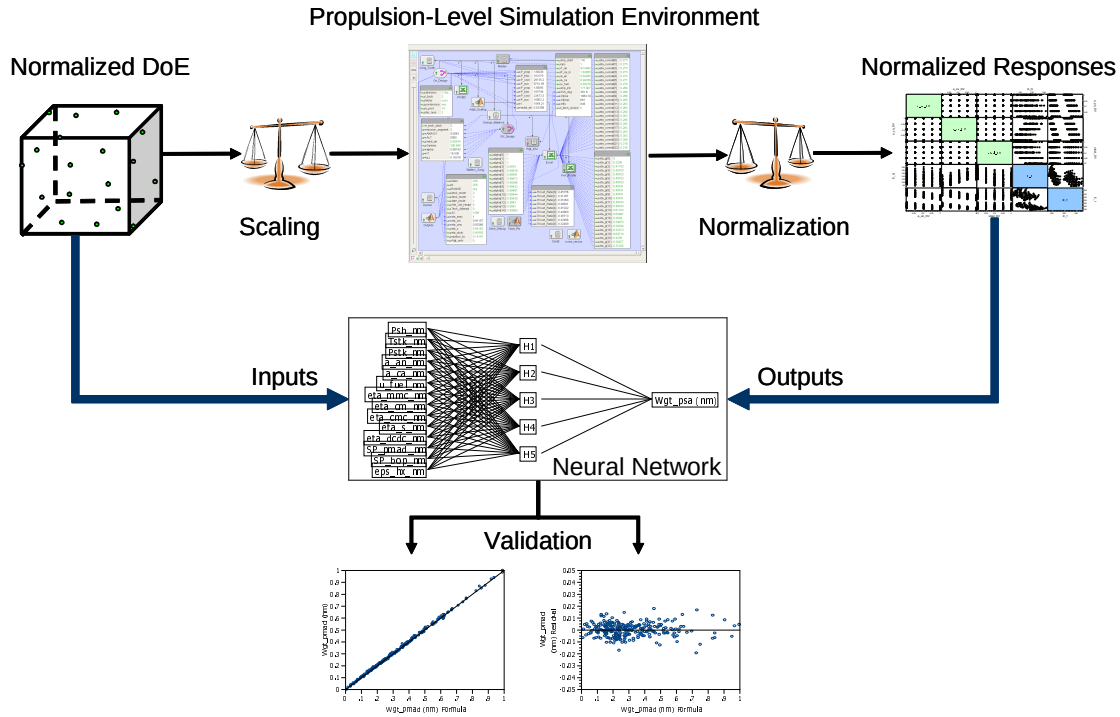

Figure 41: Neural Network-based Surrogate Modeling Process

were normalized to the ranges [0,1] in JMP to prevent the artificial neurons from confusing the true influence of a variable with the impact due to its magnitude [155]. The only exception to this was the normalized DoE table, which was generated using the `lhsdesign` function in Matlab R2006a [156].

5.3.1 Modeling of First-Stage Value Function

One of the first dilemmas a researcher faces in using space-filling designs is the determination of the sample size (*i.e.*, the number of rows in the DoE table). Whereas the matrix size is something that becomes explicitly calculated for all response surface and full factorial designs, no such mathematical relationships are available for space-filling designs. Both JMP and Matlab automatically organize the columns of the DoE matrix in accordance with the number of user-specified independent variables, but still ask for the sample size to be input.

Fortunately, a couple of rules of thumb have been published regarding the minimal sample size for regression analysis. Hair et al [157] reports that at least five observations per independent variable are necessary to ensure the generalizability of the fitted model. A more conservative ratio of 10 to 1 is reported by Halinski and Feldt [158], as well as Miller and Kunce [159], which implies that an input matrix of at least 140 by 14 in size is required to model any of the program functions. Interestingly enough, the Custom Designer feature of JMP 7 suggests 129 observations as an I-optimal DoE with 14 independent variables. For conservatism, this sample size was decided to be doubled, and the resulting 258 by 14 Latin Hypercube Design was utilized in all subsequent regression exercises.

The real-value ranges for all 14 independent variables are listed in Table 15. Each row of the DoE table was, thus, scaled accordingly before being input to the propulsion-level simulation environment. Segment 1 of the discretized LAGER mission listed in Table 8 was chosen as the reference point for all cases. Therefore, the on-design analysis and sizing portion of the environment had to be repeatedly executed, after which the resulting elements of $\mathbf{M}(\mathbf{x}, \xi(\omega))$ were collected. This 258 by 6 output matrix had to be imported into JMP, normalized to the ranges [0,1], and finally utilized in fitting the necessary neural networks.

Because JMP implements a single-layer approach to neural networking, the number of artificial neurons, or "hidden nodes" as called within JMP, determines the predictive capability of the resulting surrogate model. In an attempt to prevent the generation of an overfit surrogate, the number of hidden nodes were gradually incremented until a meta-model with both an acceptable R^2 value and residuals not exceeding $\pm 5\%$ was found. The method of K-Fold cross-validation was found to result in small MRE, or a high cross-validation R^2 ("CV RSquare" in JMP). The number of cross-validation groups, K, was another option directly under the user's control.

Table 15: DoE Ranges of First-Stage Design Variables and Random Parameters

Parameter	Symbol	Units	Minimum	Maximum
Reference-Point Shaft Power	x_1	hp	130 (**A1**) 100 (**A2**) 90 (**A3**)	390 (**A1**) 300 (**A2**) 270 (**A3**)
Fuel Cell Stack Temperature	x_2	°C	65	94
Fuel Cell Stack Pressure	x_3	bar	1.1	2.5
Anode Water Content	x_4	N/A	0.81	0.9999
Cathode Water Content	x_5	N/A	0.81	0.9999
Fuel Utilization Coefficient	x_6	N/A	0.8	0.9999
3-Phase Inverter Efficiency	ω_1	N/A	0.8	0.99
Compressor Motor Efficiency	ω_2	N/A	0.8	0.99
Compressor Motor Controller Efficiency	ω_3	N/A	0.8	0.99
Buck Regulator Efficiency	ω_4	N/A	0.75	0.99
Boost Regulator Efficiency	ω_5	N/A	0.75	0.99
Heat Exchanger Effectiveness	ω_6	N/A	20	30
BOP Specific Power	ω_7	hp/lbs	0.6	1.6
PMAD Specific Power	ω_8	hp/lbs	0.5	0.9

Table 16 and Figures 42 through 44 provide the summary of fit in tabular and graphical formats. In each case, it was possible to obtain an R^2 value of over 0.99 and a residual band of ± 0.05 with a relatively small number of hidden nodes.

The surrogate models of M_5 and M_6 were not created by fitting NNs to the outputs of BOP weight and PMAD system weight, respectively. Instead, NNs to P_e were first fitted from the same data sets used for creating the surrogates for M_3 and M_4 at all three technology levels. Such an act allows both M_5 and M_6 to be evaluated through the same surrogate of stack output power - one only has to divide it by the appropriate specific power value to obtain the needed weight figure. This interrelationship between the power, weight, and specific power are confirmed by the three-dimensional scatter plots that are also part of Figures 42 through 44 .

5.3.2 Modeling of TPM Vectors

A two-step process was necessary in creating surrogate models for the first-stage TPM vector, $\mathbf{T}(\mathbf{x}, \tilde{\xi}(\omega), \xi(\omega))$. First, the system was sized to the same 258 settings of $\mathbf{x}$

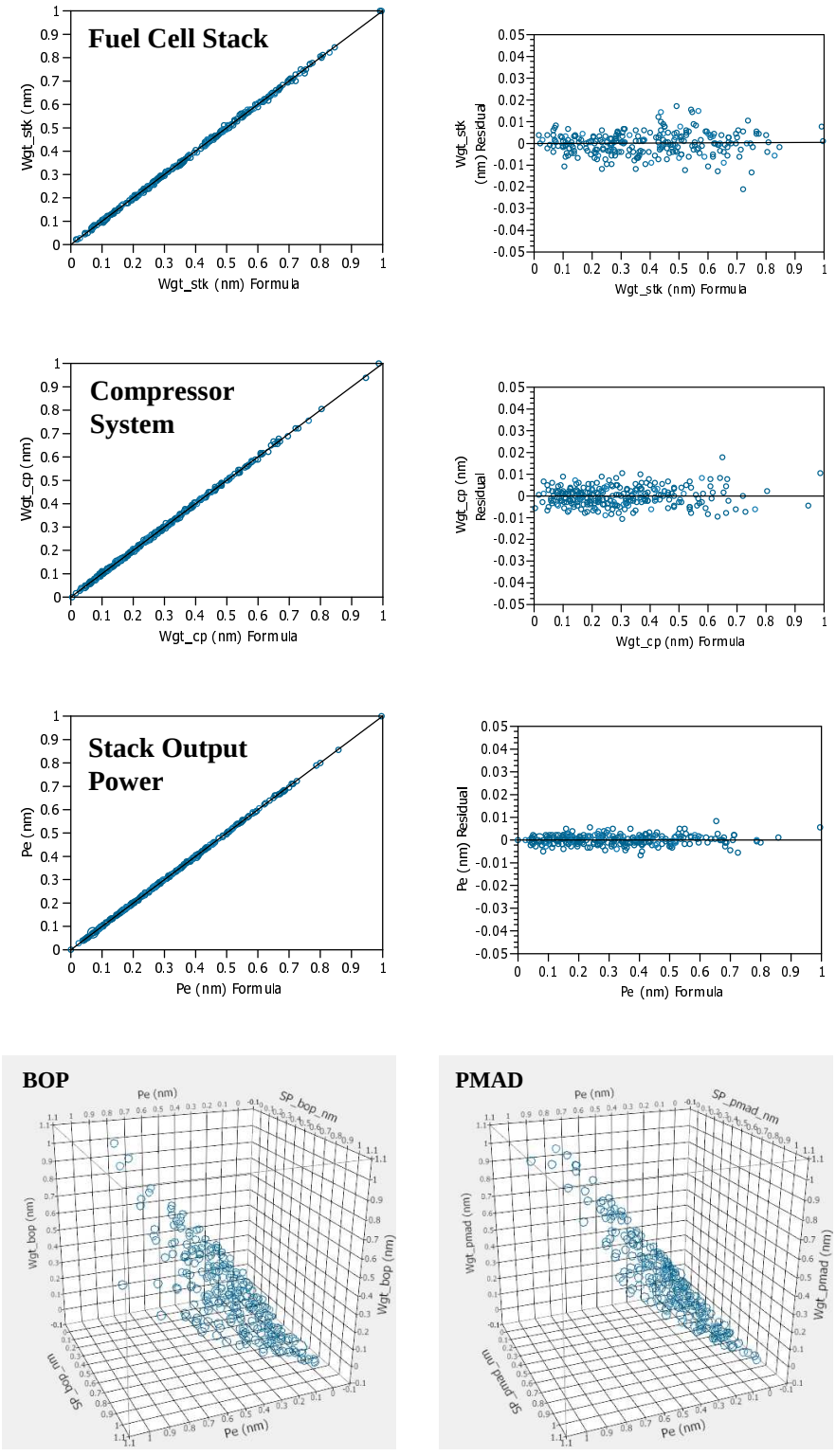

Figure 42: Actual by Predicted and Residual Plots & 3D Scatter Plots: **A1**

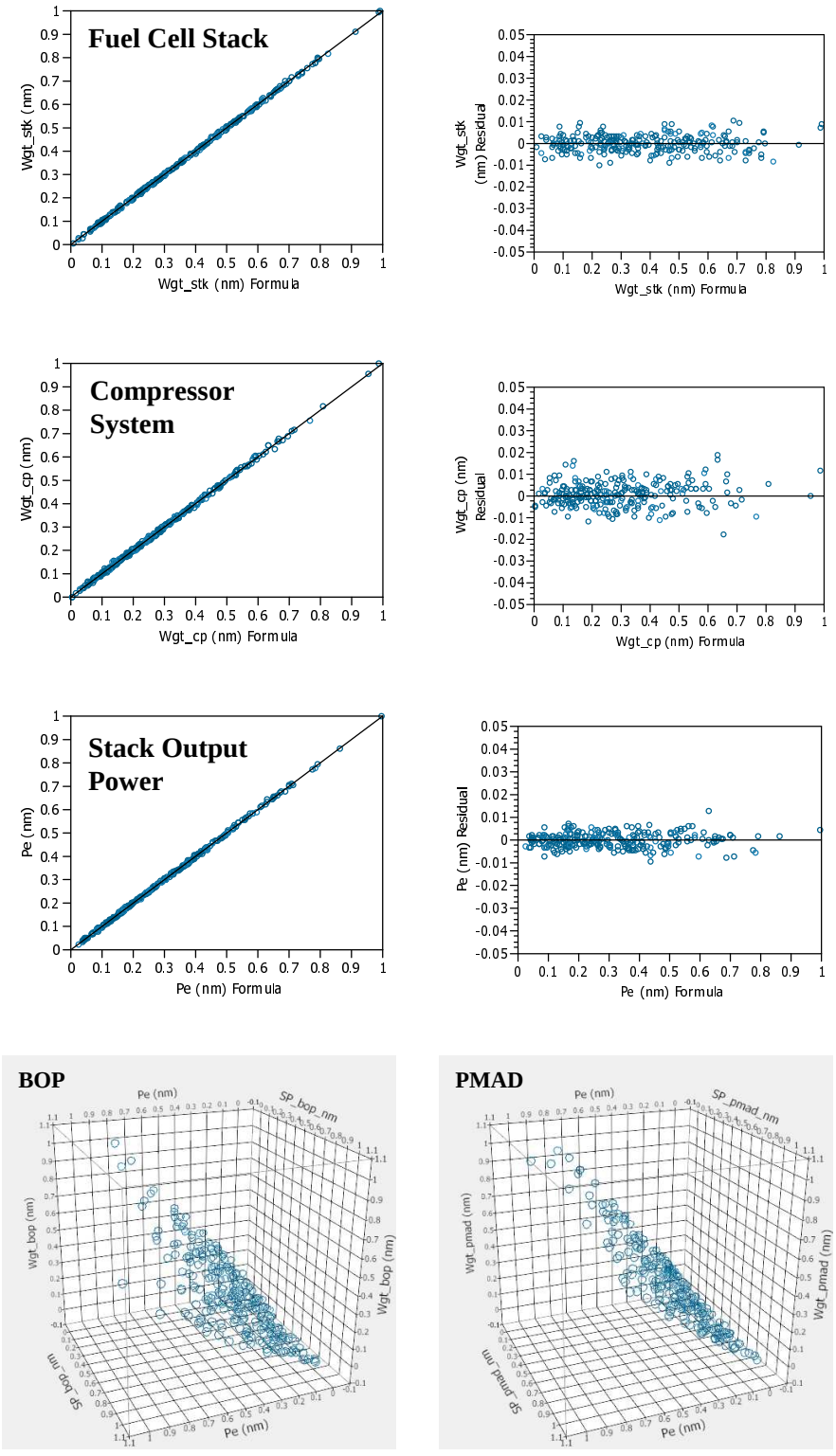

Figure 43: Actual by Predicted and Residual Plots & 3D Scatter Plots: **A2**

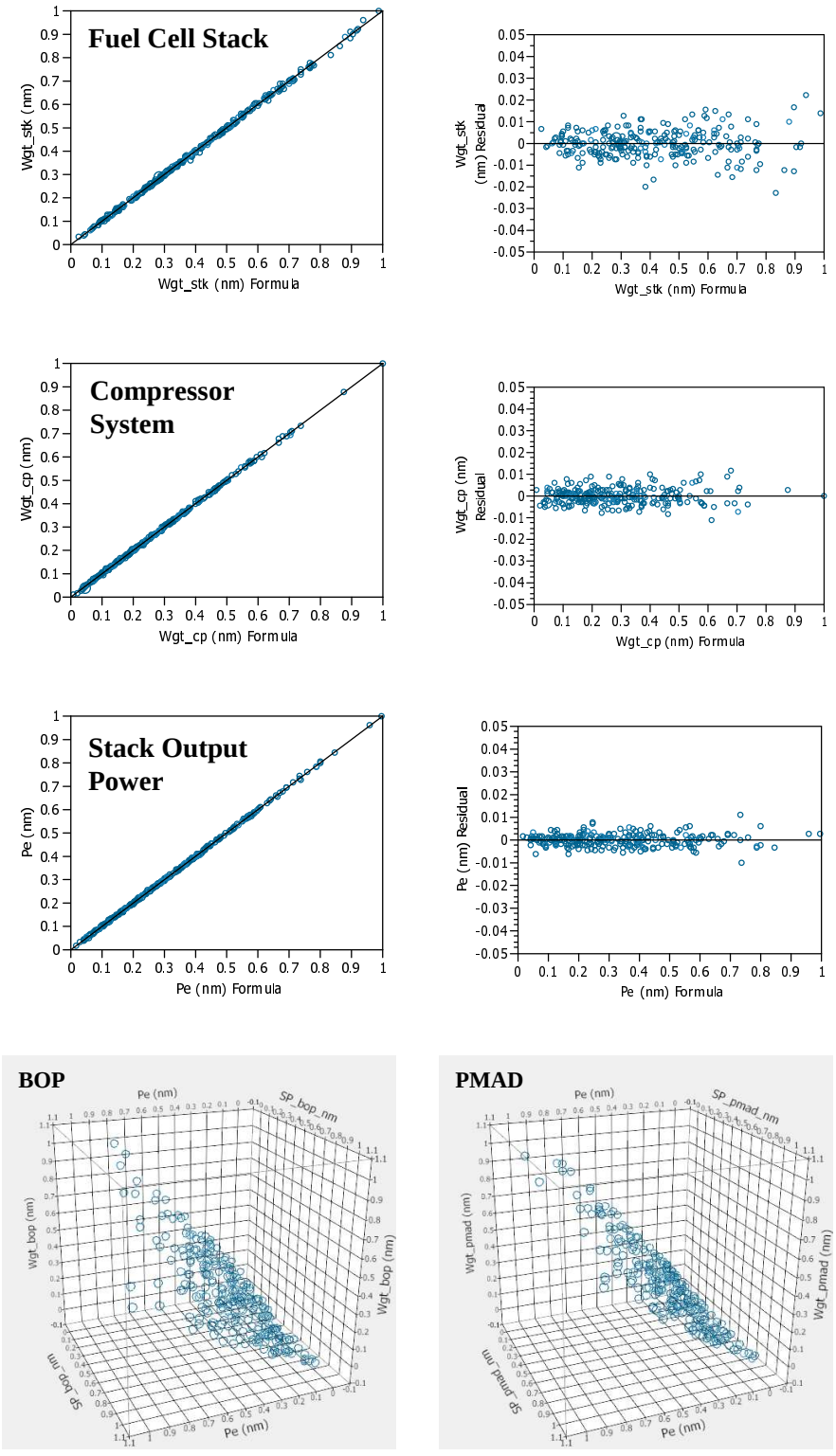

Figure 44: Actual by Predicted and Residual Plots & 3D Scatter Plots: **A3**

Table 16: First-Stage Value Function: Summary of Fit

Parameter	Symbol	Number of Neurons			R^2		
		A1	**A2**	**A3**	**A1**	**A2**	**A3**
Fuel Cell Stack Weight	M_3	7	9	7	0.99939	0.99967	0.99915
Compressor System Weight	M_4	7	6	7	0.99944	0.99907	0.99957
Stack Output Power	P_e	11	9	11	0.99988	0.99971	0.99981

Table 17: TPM Vectors: Summary of Fit

Parameter	Symbol	Number of Neurons			R^2		
		A1	**A2**	**A3**	**A1**	**A2**	**A3**
Fuel Cell Stack Efficiency at Loiter	$T_1(\mathbf{x}, \tilde{\xi}(\omega), \xi(\omega))$	16	15	16	0.99764	0.99438	0.99903
Available Shaft Power at Take-off	$T_2(\mathbf{x}, \tilde{\xi}(\omega), \xi(\omega))$	10	6	6	0.99784	0.99633	0.99906
Fuel Cell Stack Efficiency at Loiter	$T_1(\mathbf{y}, \xi(\omega), \xi(\omega))$	17	17	16	0.99867	0.99874	0.99865
Available Shaft Power at Take-off	$T_2(\mathbf{y}, \xi(\omega), \xi(\omega))$	6	10	9	0.99832	0.99770	0.99996

while holding all random parameters at their mean values (*i.e.*, $\tilde{\xi}(\omega)$). Next, off-design analyses at the "Warm up" and "Loiter" segments, as per Table 8, were performed with $\xi(\omega)$ according to each row of the DoE table. The same fitting procedure used in modeling the first-stage value function was applied here with success. Compared to the surrogates for $\mathbf{M}(\mathbf{x}, \xi(\omega))$, the data listed in Table 17 indicate that greater number of neurons were required to produce well-fit and generalizable surrogates for the two TPMs. Such a finding was not entirely surprising because the realization of uncertainty was expected to impart noticeable variations in system performance.

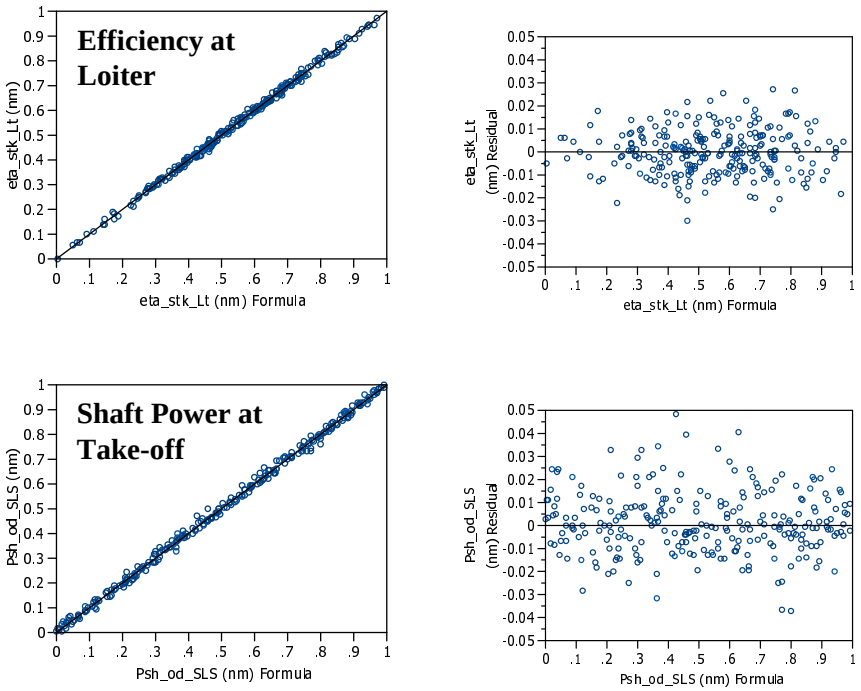

Figure 45: Actual by Predicted and Residual Plots of $\mathbf{T}(\mathbf{x}, \tilde{\xi}(\omega), \xi(\omega))$: **A1**

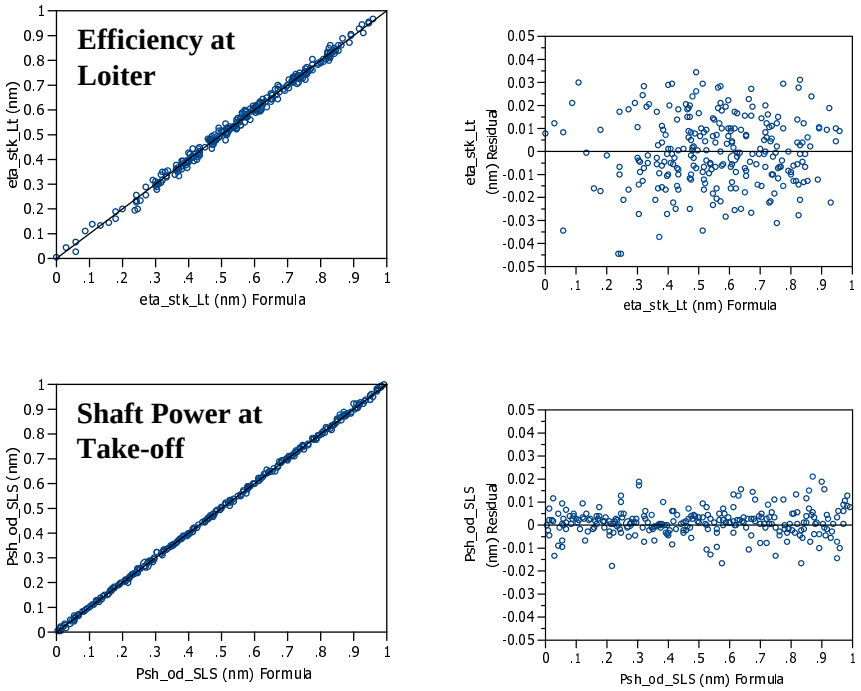

Figure 46: Actual by Predicted and Residual Plots of $\mathbf{T}(\mathbf{x}, \tilde{\xi}(\omega), \xi(\omega))$: **A2**

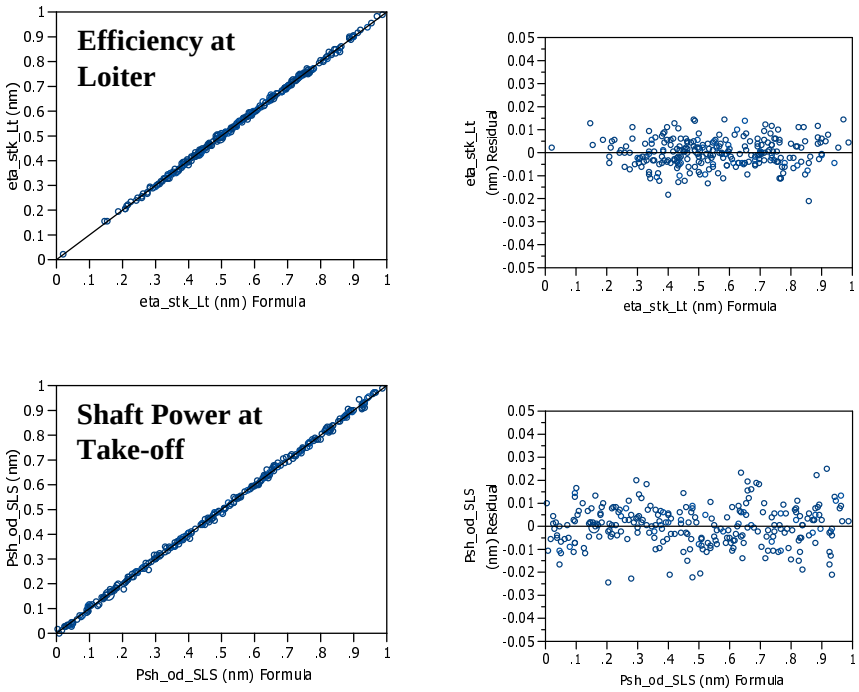

Figure 47: Actual by Predicted and Residual Plots of $\mathbf{T}(\mathbf{x}, \tilde{\xi}(\omega), \xi(\omega))$: **A3**

Essentially the above identical procedure was followed to create the NN-based surrogates for the second-stage TPM vector, $\mathbf{T}(\mathbf{y}, \xi(\omega), \xi(\omega))$. The only difference here was the fact that both on and off-design analyses were conducted at the same random parameter settings, as per the DoE cases. Although similar in name and mathematical form, the two TPM vectors represent two completely different design scenarios, and thus, should not be mistaken in their usage.

5.3.3 Modeling of Second-Stage Value Function

The final step of the surrogate modeling process is the generation of the second-stage value function NN as per Eqs.(10) and (11). For each DoE case, $\mathbf{g_1}(\mathbf{x}, \xi(\omega))$ serves as an indicator function that checks whether or not recourse is needed for the given first-stage design $\mathbf{x}$ and uncertainty realization $\xi(\omega)$. This evaluation is almost instantaneous thanks to the reusability of the surrogates created in the previous step. Likewise, the near-instantaneous evaluation of $\mathbf{g_2}(\mathbf{y}, \xi(\omega))$ and $\eta(\mathbf{x}, \mathbf{y}, \xi(\omega))$, which are

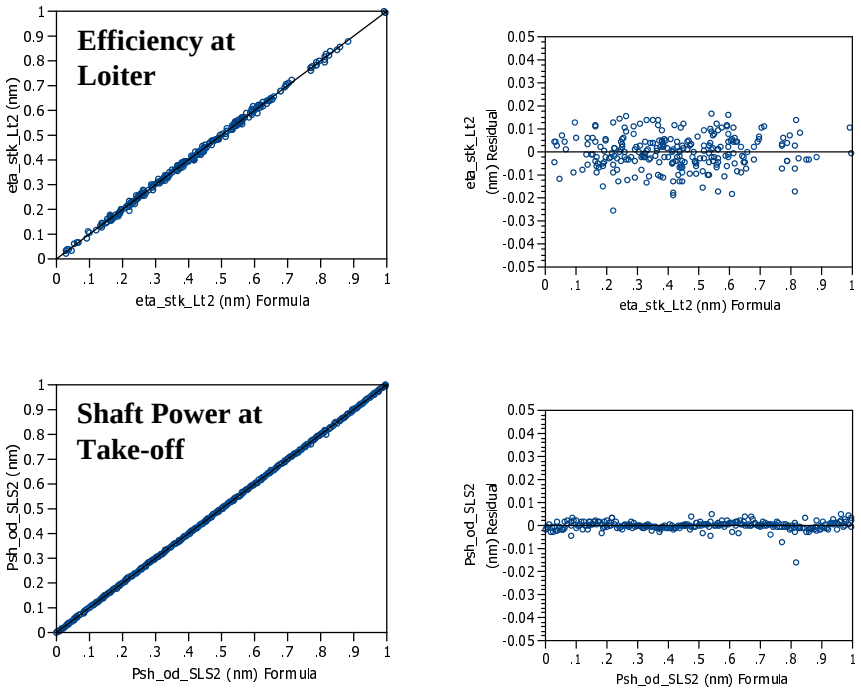

Figure 48: Actual by Predicted and Residual Plots of $\mathbf{T}(\mathbf{y}, \xi(\omega), \xi(\omega))$: **A1**

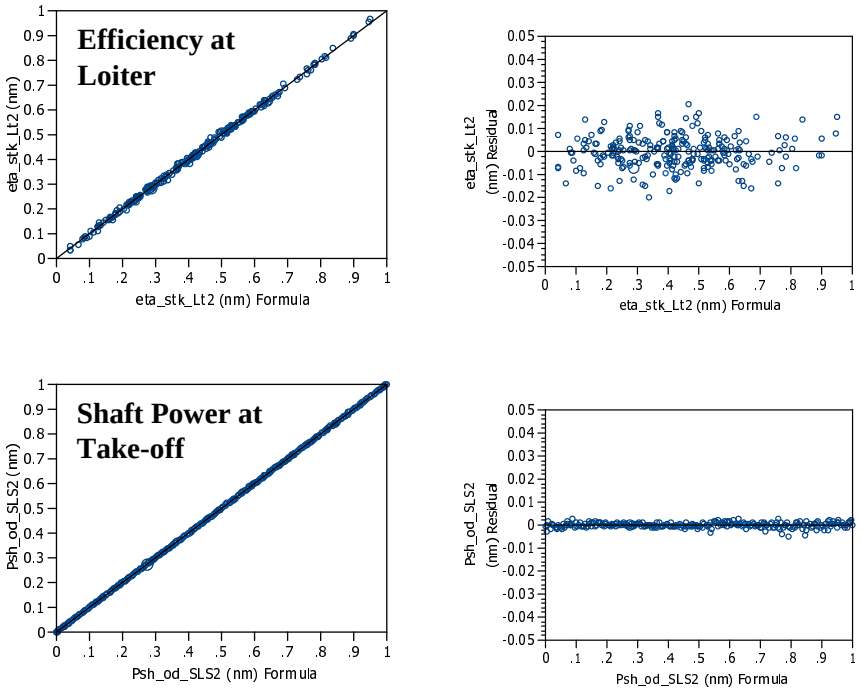

Figure 49: Actual by Predicted and Residual Plots of $\mathbf{T}(\mathbf{y}, \xi(\omega), \xi(\omega))$: **A2**

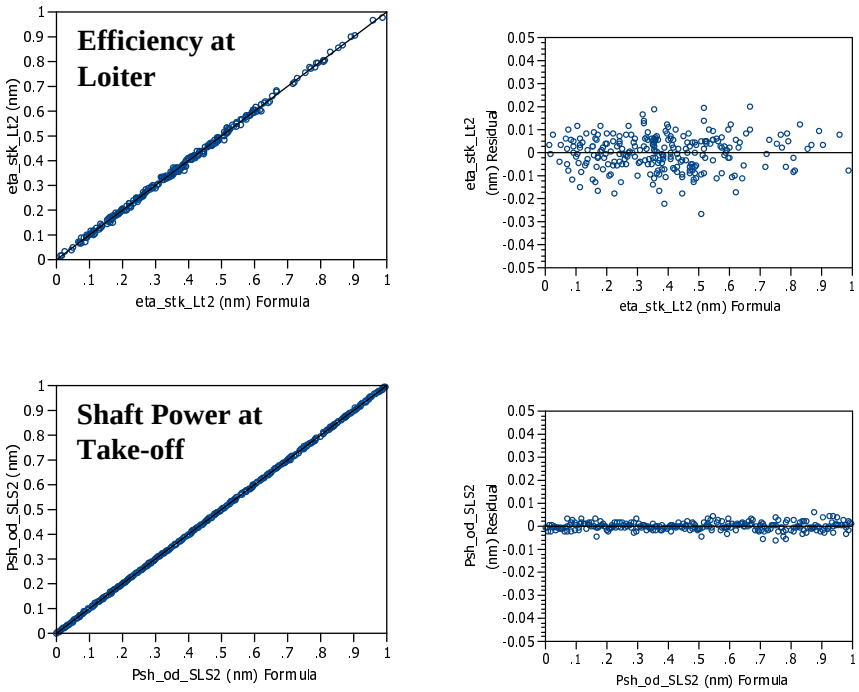

Figure 50: Actual by Predicted and Residual Plots of $\mathbf{T}(\mathbf{y}, \xi(\omega), \xi(\omega))$: **A3**

only possible due to the reusability of $\mathbf{M}(\mathbf{x}, \xi(\omega))$, $\mathbf{M}(\mathbf{y}, \xi(\omega))$ and $\mathbf{T}(\mathbf{y}, \xi(\omega), \xi(\omega))$, enables the application of a numerical optimizer to identify a specific instance of $Q(\mathbf{x}, \xi(\omega))$.

The above process, also illustrated in Figure 51, must be repeated for all rows of the DoE table so that sufficient sampling data become available to fit a surrogate model of $Q(\mathbf{x}, \xi(\omega))$. The ModelCenter implementation of this sampling process is illustrated in Figure 52. All surrogates are contained in the spreadsheet titled "nnets," whose outputs are passed down to "Recourse" in computing the second-stage value function by way of the "Optimizer." Amongst the user-provided values are the elements of $\mathbf{h}$ ("eta_th_target" and "Psh_od_target") as well as the optimization algorithm type ("Algorithm").

As it can be seen from Eq.(10), the value at the second stage is largely dependent on the vectors of constants - $\mathbf{q}$ and $\mathbf{h}$. The former acts as a multiplier controlling the

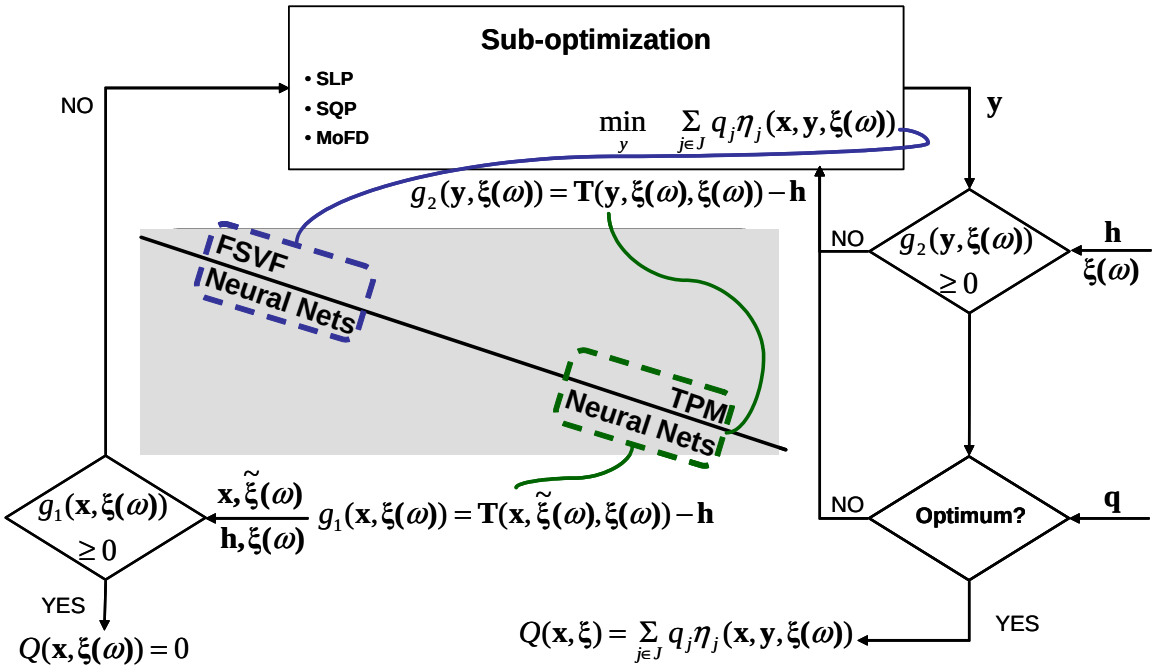

Figure 51: Substitution of Surrogates in Evaluating $Q(\mathbf{x}, \xi(\omega))$

penalty of design compensations, while the latter, together with $\mathbf{y_l}$ and $\mathbf{y_u}$, represents the degrees of freedom to perform the recourse. It is reasonable to expect the recourse cost to increase with more stringent target values, although an unrealistically high $\mathbf{h}$ would only serve to exceed the said design freedom. Unfortunately, it is more difficult to predict in advance whether or not a particular combination of $\mathbf{q}$ and $\mathbf{h}$ will contribute towards a unimodal space for z. This necessitates an iterative procedure that repeats the creation of the surrogates of $Q(\mathbf{x}, \xi(\omega))$ in conjunction with visualizing the design domain space.

5.4 Two-Stage Stochastic Optimization

It cannot be emphasized enough how important it is to geometrically verify the unimodalness of the solution space before delving into optimization. Not only does unimodalness safeguard against a gradient-based optimizer from being *trapped* - so to speak - in a locally optimal region, but it also supports the appropriateness of

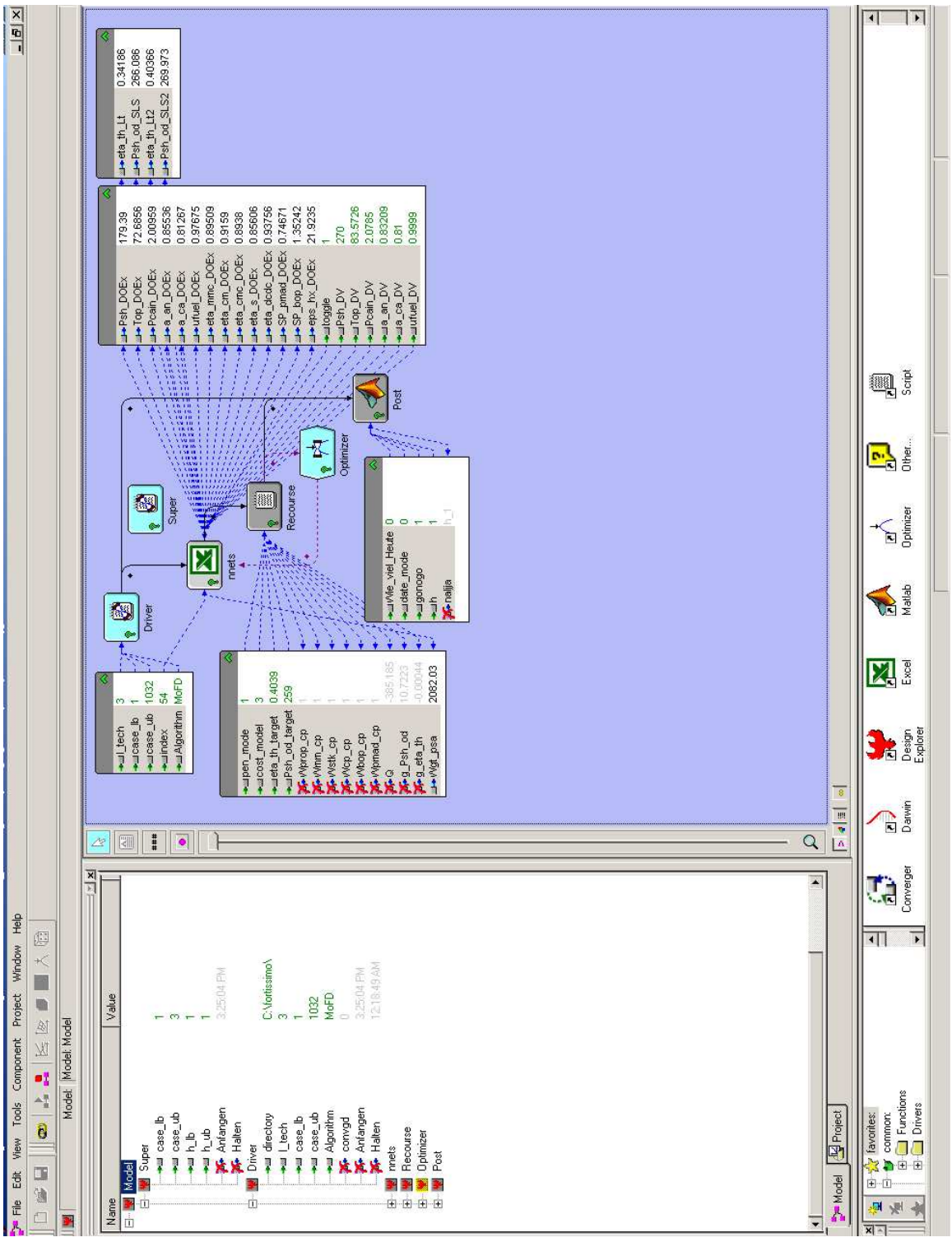

Figure 52: Automated Environment for Modeling $Q(\mathbf{x}, \xi(\omega))$

the applied recourse formulation. One interpretation of the two-stage stochastic optimization in an engineering design setting is that it is a trade between the optimality in the present and the average penalty of future corrections. Numerically, this translates to the sum of the functions $\mathbb{E}_\xi[f]$ and $Q(\mathbf{x})$ to contain at least one mode, a phenomenon which will only emerge for a pairing of the vectors $\mathbf{q}$ and $\mathbf{h}$, falling somewhere between unwarranted conservatism and unfounded optimism. It is when two such opposing spaces are combined that there is a possibility of unimodalness, and verifying it through geometric and parametric means is at the core of **Sub-task 3**.

5.4.1 Assignment of Input Probability Distributions

Because the random parameters listed in Table 13 are defined as those that are under the influence of epistemic uncertainty, they were assumed to be uniformly distributed as to remove any further sources of bias. The assignment was made within the uncertainty modeling and forecasting software Crystal Ball [160] in accordance with the real-value ranges of Table 15. Another useful feature of Crystal Ball is the calculation of sensitivities, which is based on the method of Pearson correlation coefficients [161]. The ensuing sensitivity index becomes helpful in screening out the dominant design variables for the purpose of visualization.

5.4.2 Visualization of Design Domain Space

Mapping out the N-dimensional spaces of $\mathbb{E}_\xi[f]$, $Q(\mathbf{x})$, and z is a computationally intensive process that marks the first time the random-variate generator is utilized in conjunction with the created surrogates. The primary objective here is to verify whether or not the prescribed TPM targets, which are the elements of the $\mathbf{h}$ vector, induce a uni-modal solution space when applied to the recourse model of Eq.(10). It is also a highly iterative process since the fitting of $Q(\mathbf{x}, \xi(\omega))$ must be revised as many times as necessary, depending on the outcome of the visualization.

Table 18: Matrix of TPM Target Values

Target Vector	TPMs	Units	**A1**	**A2**	**A3**
$\mathbf{h_1}$	$\eta_{stk\|\text{loiter}}$	N/A	0.3763	0.3841	0.4039
	$P_{sh\|\text{SLS}}$	hp	325	288	259
$\mathbf{h_2}$	$\eta_{stk\|\text{loiter}}$	N/A	0.3640	0.3737	0.3834
	$P_{sh\|\text{SLS}}$	hp	293	265	252
$\mathbf{h_3}$	$\eta_{stk\|\text{loiter}}$	N/A	0.3517	0.3633	0.3718
	$P_{sh\|\text{SLS}}$	hp	260	250	238
$\mathbf{h_4}$	$\eta_{stk\|\text{loiter}}$	N/A	0.4231	0.4214	0.4182
	$P_{sh\|\text{SLS}}$	hp	384	295	264

5.4.2.1 Impact of TPM Target Values

The first three rows of Table 18 correspond to the target sets that were initially used in studying how the **h** vector impacts the second-stage value function. For each alternative, three notional recourse scenarios were attempted, beginning with the most stringent efficiency and power targets. The rise in efficiency target values (which are referenced to the LHV of hydrogen) from **A1** to **A3** is intended to align with the technology growth assumptions built into the analysis models. Similarly, the decrease in available shaft power reflects the higher specific power of the more advanced alternatives. The environment shown in Figure 18 was utilized to sample 1,032 points for all 9 scenarios, and 9 NNs were subsequently fitted in JMP. In order to somewhat alleviate the burden of having to recreate the surrogates every time the penalty constants are altered, all elements of the **q** vector were set to 1 in creating these surrogate models. Such a scheme serves to enhance the reusability of the meta-models since the second-stage value function, with penalty, can be evaluated as follows:

$$Q(\mathbf{x},\xi(\omega)) \quad = \quad \begin{cases} (1-p_f)\cdot Q(\mathbf{x},\xi(\omega))_{NN} & \text{if} \quad Q(\mathbf{x},\xi(\omega))_{NN} < 0 \\ (1+p_f)\cdot Q(\mathbf{x},\xi(\omega))_{NN} & \text{if} \quad Q(\mathbf{x},\xi(\omega))_{NN} \geq 0 \end{cases} \tag{19}$$

where p_f is the penalty fraction taking a value between 0 and 1 and $Q(\mathbf{x},\xi(\omega))_{NN}$ can be any of the 9 surrogates.

Figures 53 through 55 show the fit and scatter of each $Q(\mathbf{x},\xi(\omega))_{NN}$, with the

Table 19: Second-Stage Value Functions: Summary of Fit

Target Vector	Number of Neurons			R^2		
	A1	**A2**	**A3**	**A1**	**A2**	**A3**
$\mathbf{h_1}$	29	33	35	0.99903	0.99936	0.99149
$\mathbf{h_2}$	22	33	35	0.99743	0.99971	0.98958
$\mathbf{h_3}$	20	31	33	0.99866	0.99986	0.99377
$\mathbf{h_4}$	30	34	34	0.99349	0.99924	0.99332

position of where zero recourse occurs on the normalized scale. The summary of fit for all shown $Q(\mathbf{x}, \xi(\omega))_{NN}$ models are listed in Table 19. It was discovered that the more stringent the target requirements were, the closer this position came to the center of the spread. Moreover, the so-called *shot-gun* pattern of the residuals are more prominently displayed for the higher targets than lower thresholds. Such a random spread of data points is another indicator that a surrogate model was fitted well enough to be accurate over the entirety of the sampled range. Because the shown plots - in and of themselves - do not point to the nature of the function spaces, an iterative procedure that leverages on surrogate-based visualization became necessary to settle on the final TPM targets ($\mathbf{h_4}$) listed on the last row of Table 18.

5.4.2.2 Sensitivity Analysis of Design Variables

An obvious obstacle to visualizing any N-dimensional space is that it quickly becomes tricky to illustrate solution spaces beyond three dimensions. It would, thus, be ideal if two out of the six design variables listed in Table 12 happen to dominate the others in influencing the expected outcomes of the first- and second-stage value functions when p_f is fixed at 0. Fortunately and as depicted in Figure 56, it turns out that P_{ref} and P_{stk} qualify as two such dominant variables here. When the six design variables were simultaneously perturbed 1,000,000 times within their respective real-value ranges (while fixing all random parameters at their mean values) in Crystal Ball, both variables collectively accounted for over 90% of the variability displayed by $\mathbb{E}_\xi[f]$ and $Q(\mathbf{x})$. It was also encouraging to learn that such a trend appeared

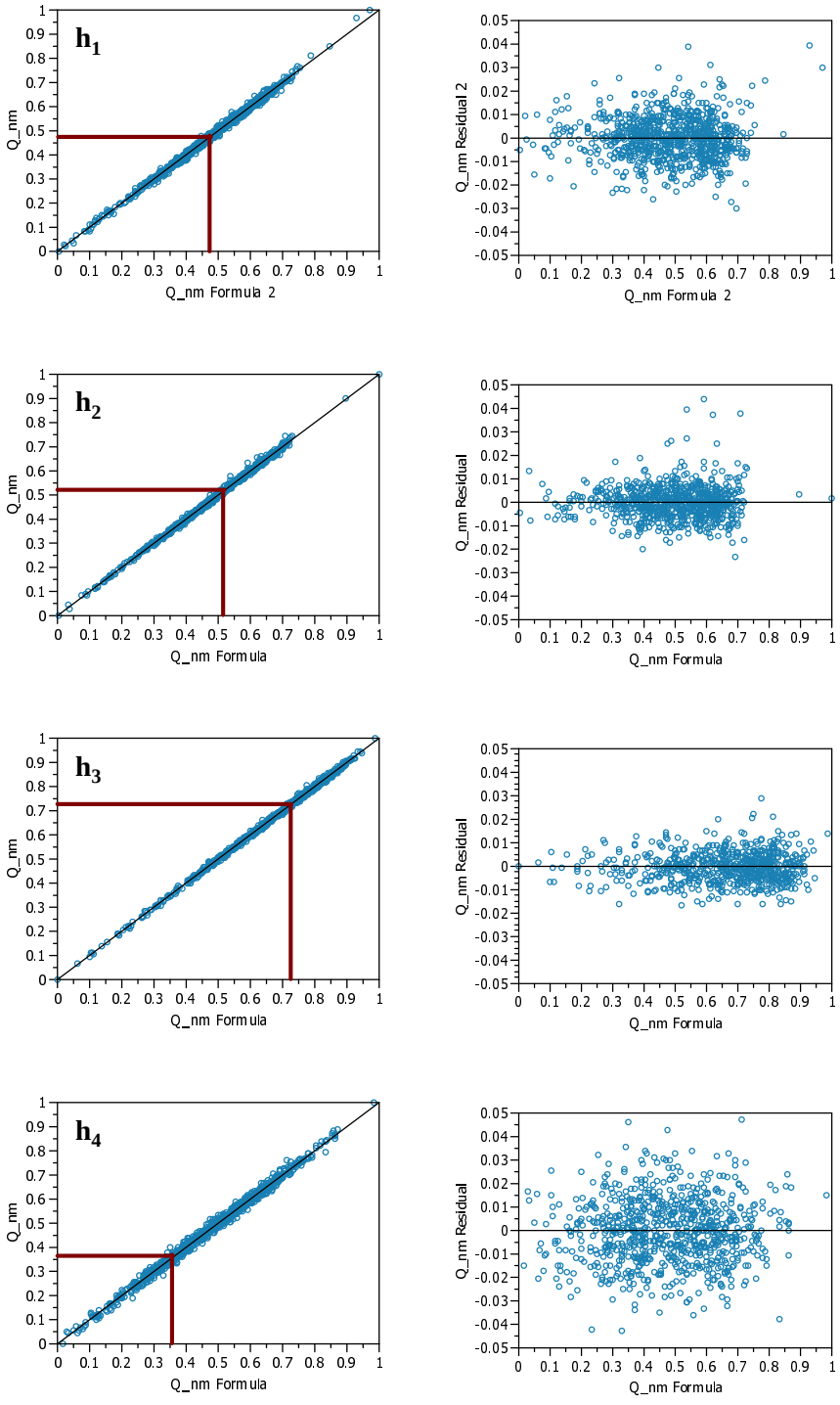

Figure 53: Actual by Predicted and Residual Plots of $Q(\mathbf{x}, \xi(\omega))_{NN}$: **A1**

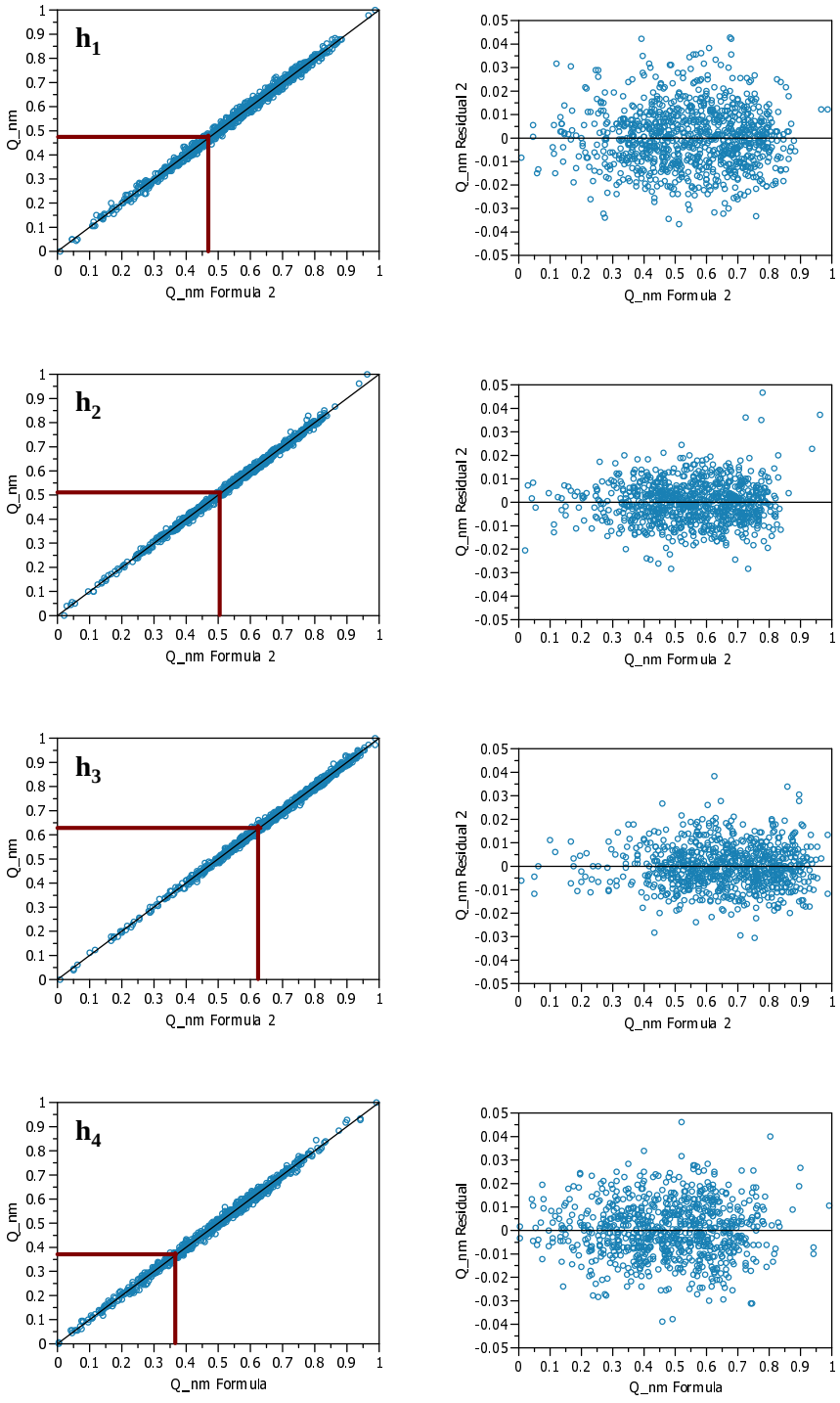

Figure 54: Actual by Predicted and Residual Plots of $Q(\mathbf{x}, \xi(\omega))_{NN}$: **A2**

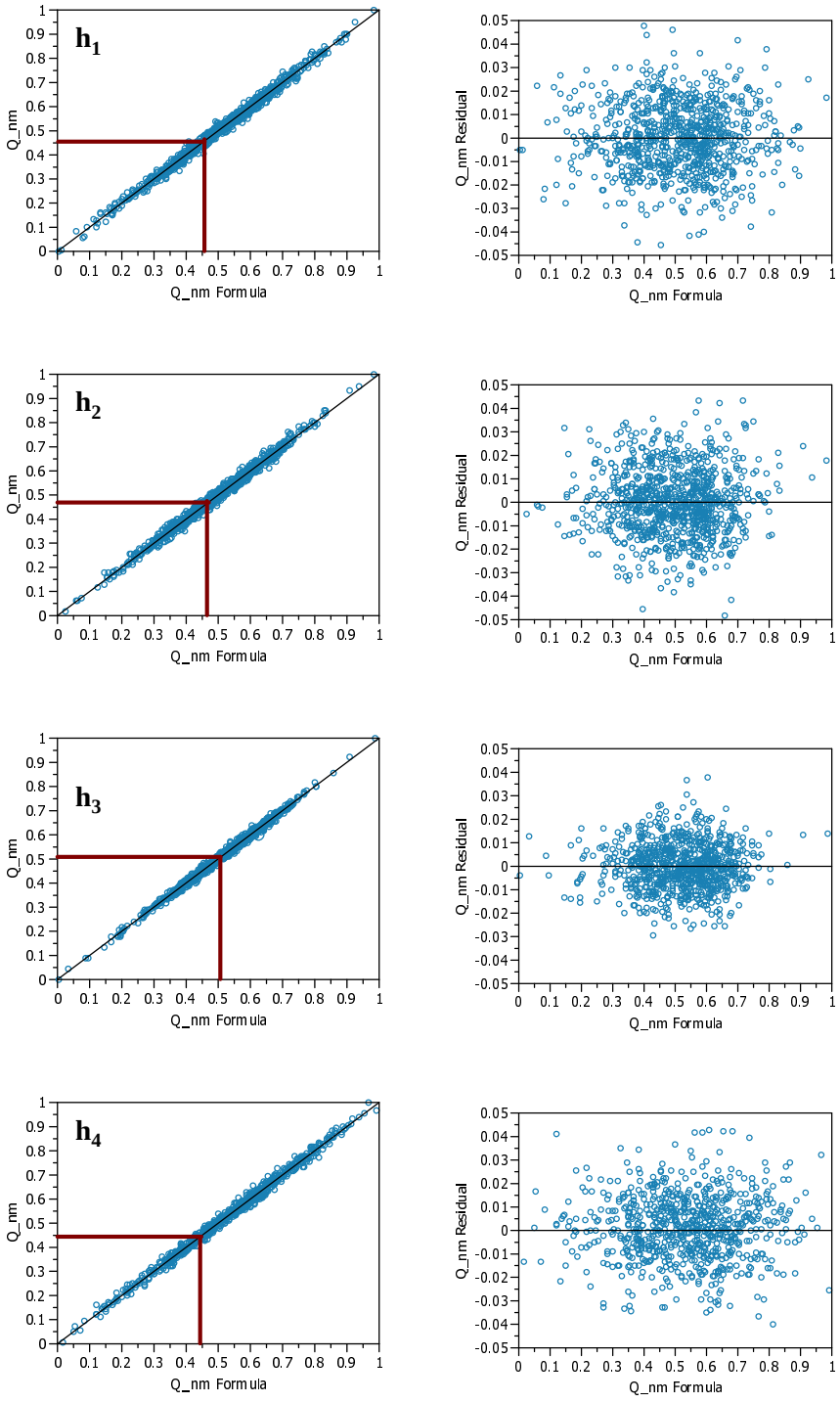

Figure 55: Actual by Predicted and Residual Plots of $Q(\mathbf{x}, \xi(\omega))_{NN}$: **A3**

consistently across all three alternatives, thus making the task of comparing inter-alternative solution spaces easier.

5.4.2.3 Finalization of TPM Targets via Visualization

In order to visually observe the dependencies of $\mathbb{E}_\xi[f]$ and $Q(\mathbf{x})$ to the two dominant design variables, another automated environment was created in ModelCenter. A 20 by 20 grid was subsequently prepared so that 400 combinations of P_{ref} and P_{stk} could be evaluated through the relevant surrogate models contained in "TSSPwR" of Figure 57. At each point on the grid, 100,000 random-variate cases were set up to be simulated via the Monte Carlo sampling engine within Crystal Ball to calculate all required mathematical expectations.

This computationally intensive procedure was repeated three times, with p_f fixed at 0 and the remaining four design variables fixed at their mean values, to create the contour and surface plots of $\mathbb{E}[f]$ depicted in Figure 58. The shown graphs are another confirmation of the validity of the NNs showcased in Figures 42, 43, and 44; a negative curvature is observed in the direction of decreasing power and pressure for all three alternatives.

On the contrary, an opposite trend should be noticeable in a $Q(\mathbf{x})$ space. A positive $Q(\mathbf{x}, \xi(\omega))$, according to Eqs.(10) and (11), represents an initially undersized system, whereas a negative value is indicative of an oversized first-stage design. Since a plot of $Q(\mathbf{x})$ represents a collection of *mathematical expectations* of $Q(\mathbf{x}, \xi(\omega))$, each point on the surface must be interpreted as the expected, or average, system weight the given first-stage design will likely gain or lose after recourse. This means that, regardless of which TPM target setting is driving the surface shape of the recourse function, the region where $\mathbb{E}_\xi[f]$ is high would likely display negative $Q(\mathbf{x})$, and vice versa.

Nevertheless, the initial visualization of the first nine recourse function spaces

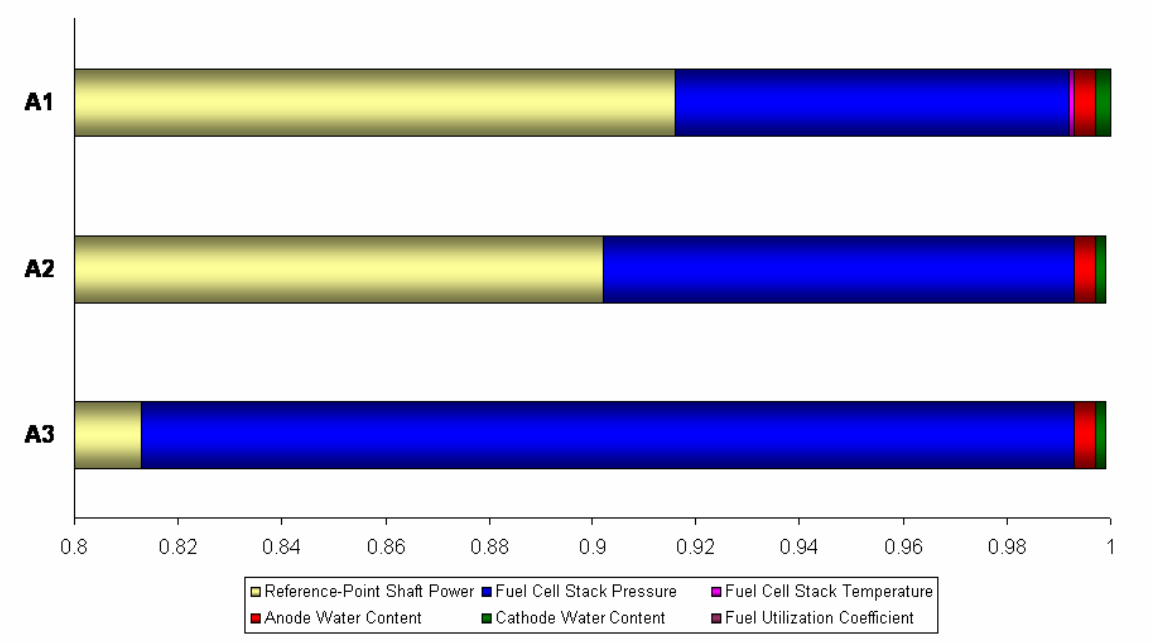

(a) Expectation of First-Stage Value Function

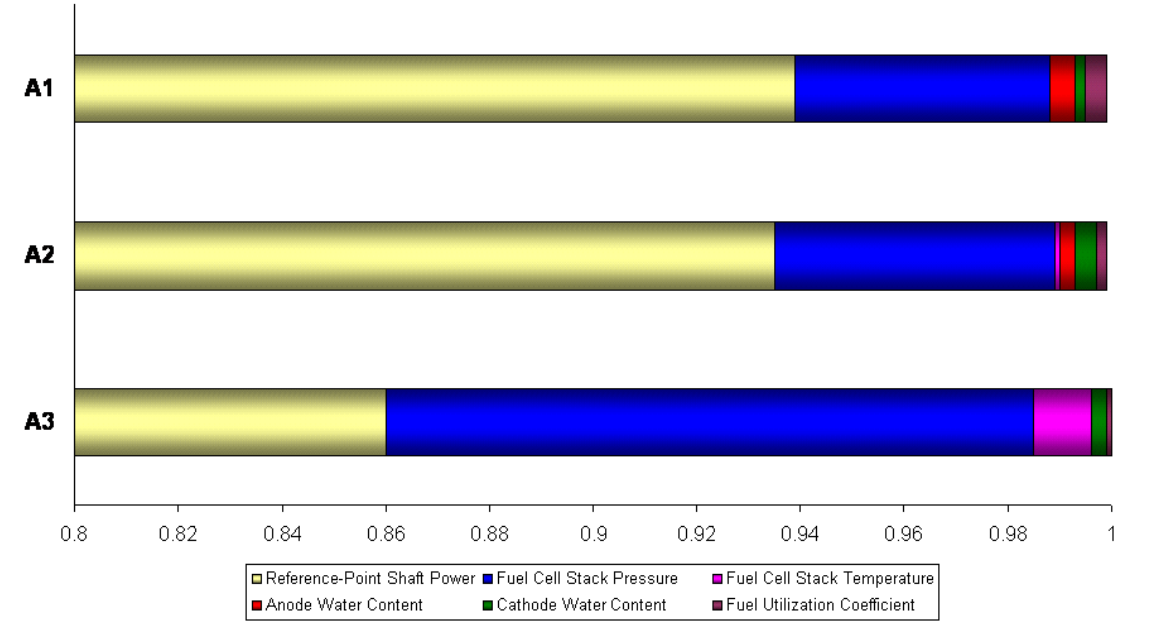

(b) Expectation of Second-Stage Value Function

Figure 56: Sensitivity Analysis Results of Value Functions: $\mathbf{h_4}$

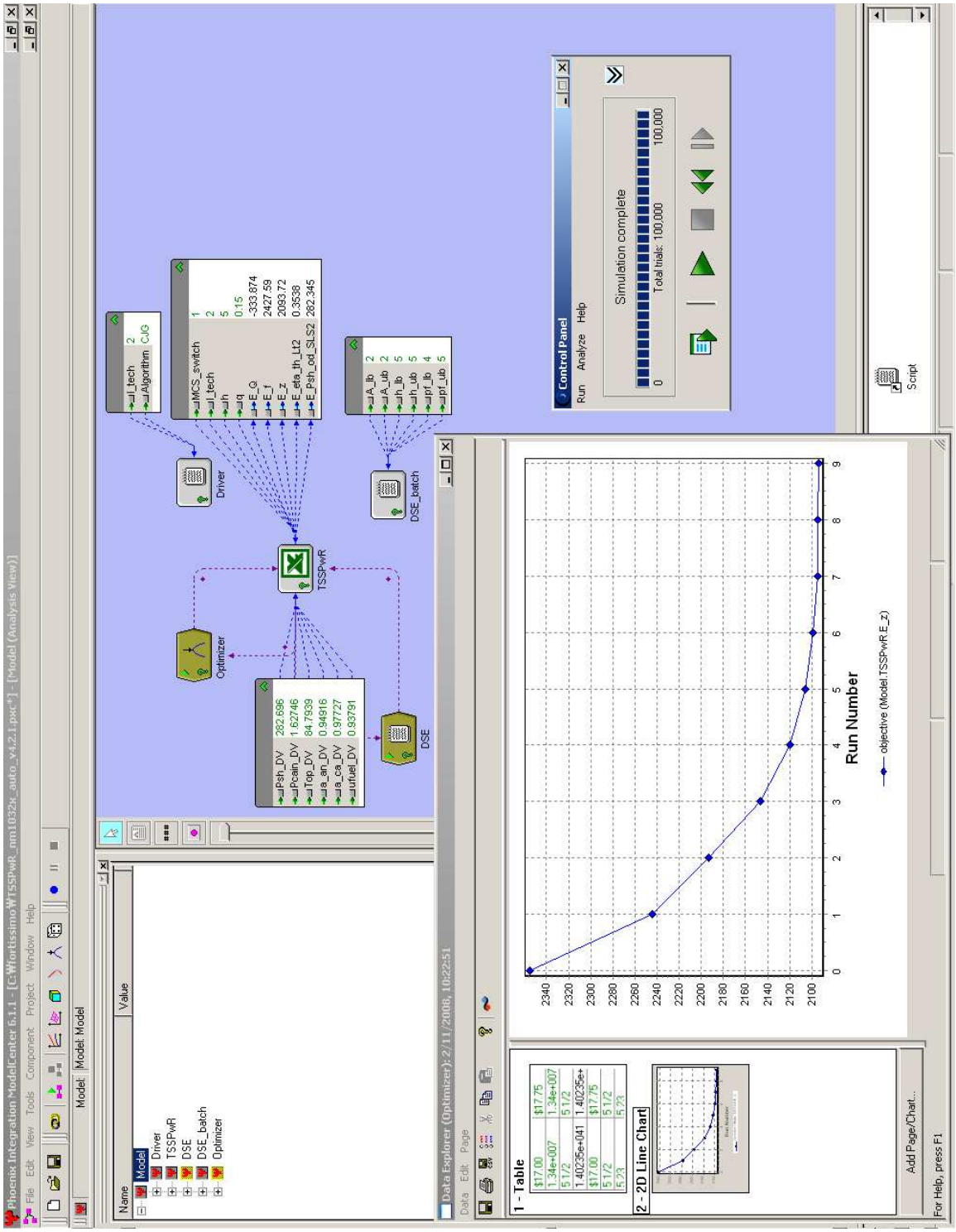

Figure 57: Automated Environment for Visualization and Optimization

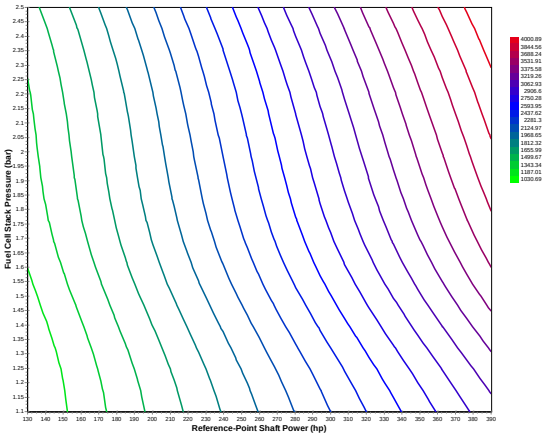

(a) Alternative 1

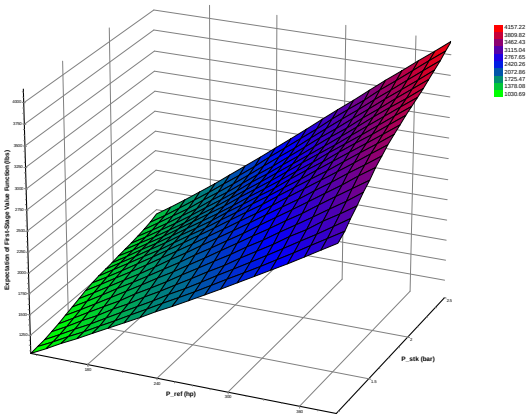

(b) Alternative 1

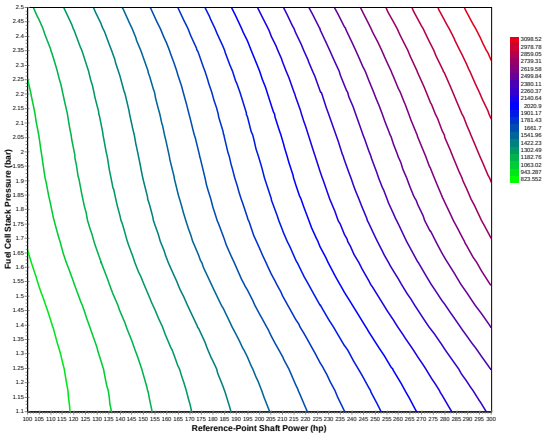

(c) Alternative 2

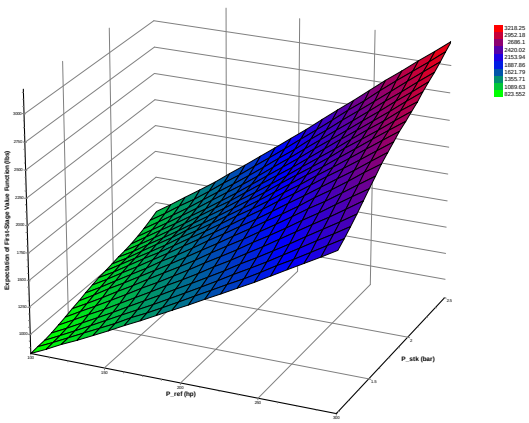

(d) Alternative 2

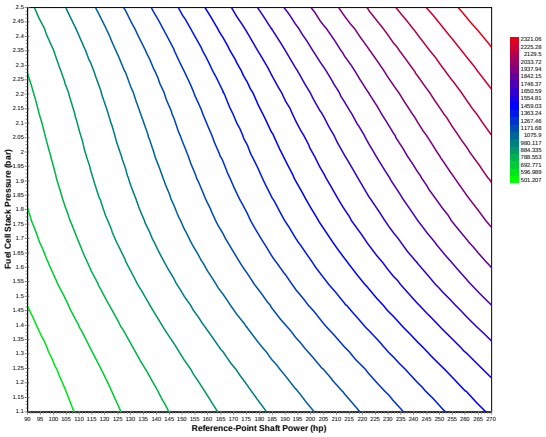

(e) Alternative 3

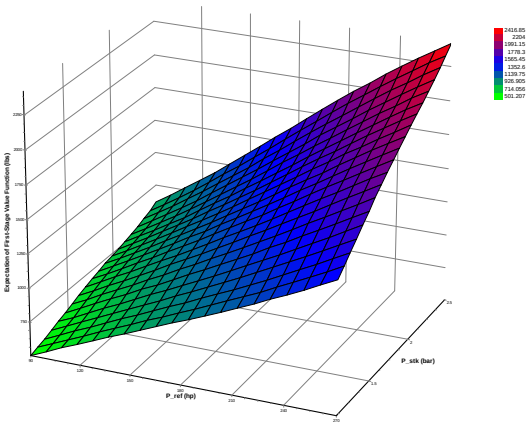

(f) Alternative 3

Figure 58: Contour and Surface Plots of First-Stage Space

yielded less than satisfactory findings. Although their contour and surface plots appeared to possess the correct overall trend of curving towards maximum P_{ref} and P_{stk}, all were marred by sharp discontinuities that rendered them non-smooth. Non-smooth function spaces are not only problematic for gradient-based optimizers, but also are - within the context of this method - indicative of poorly conditioned sub-optimization (second-stage) problems. Therefore, more detailed one-dimensional studies were conducted in the hope of isolating the cause behind such anomalies. One of those insights is the tendency of higher TPM targets to push the discontinuous regions beyond the design space boundaries. This characteristic was exploited to deduce the final TPM target values listed on the last row of Table 18 that enabled the attainment of smooth recourse function spaces shown in Figure 59.

5.4.2.4 Determination of Penalty Fractions

Investigating how different p_f values impact the curvature of the stochastic solution space constitutes the last step of the visualization process. This space is the sum of the $\mathbb{E}_\xi[f]$ and $Q(\mathbf{x})$ spaces, as per Eq.(12). By itself, $\mathbb{E}_\xi[f]$ has no numerical or functional ties to the penalty fractions. The recourse function, however, is indirectly affected through the second-stage value function, as defined by Eq.(19). It is thus imperative to parametrically ascertain whether an optimizable solution space exists over a reasonable band of penalty scenarios. Otherwise, another round of iterations retracing the procedures outlined in §5.4.2.1 through §5.4.2.3 becomes necessary.

The ModelCenter environment portrayed in Figure 57 was used in the same manner to map out the results on a 20 by 20 grid of P_{ref} and P_{stk}. Again, 100,000 Monte Carlo sampling cases took place for all random parameters, while the other four design variables were fixed at their mean values. Only this time, 5 settings of p_f (0.1 to 0.5) were attempted for each architecture, and it was the union of the two spaces that was recorded in both contour- and surface-plot forms.

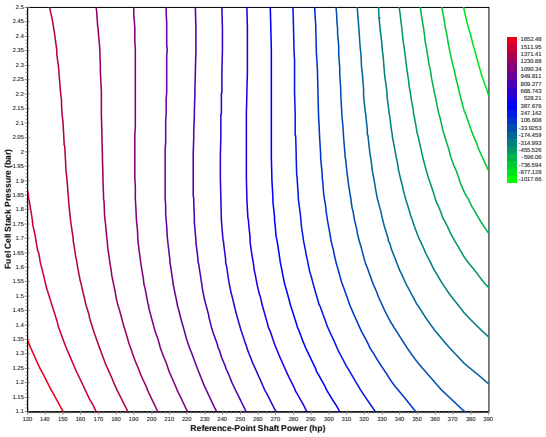

(a) Alternative 1

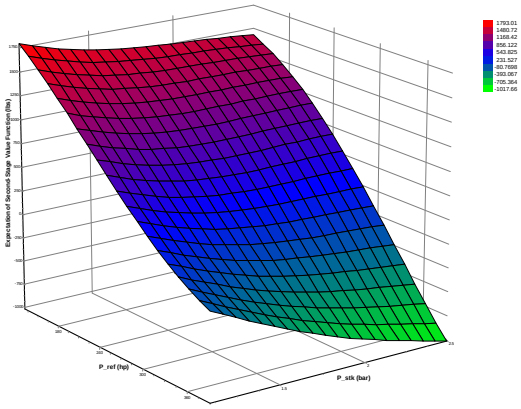

(b) Alternative 1

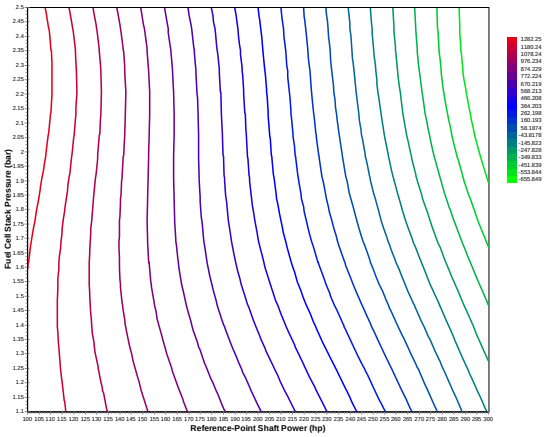

(c) Alternative 2

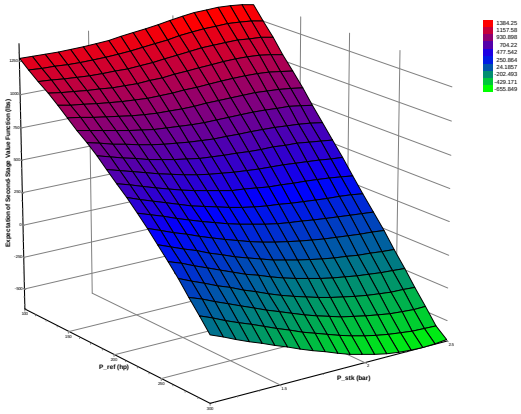

(d) Alternative 2

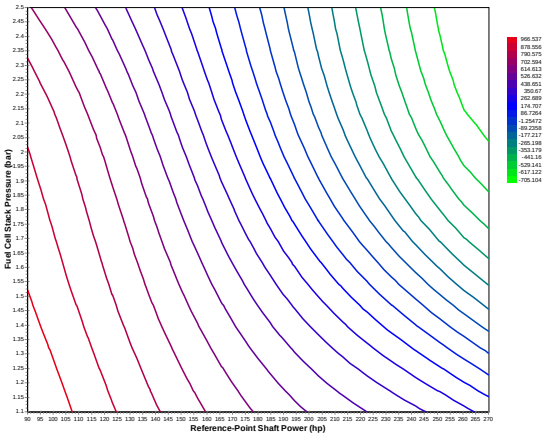

(e) Alternative 3

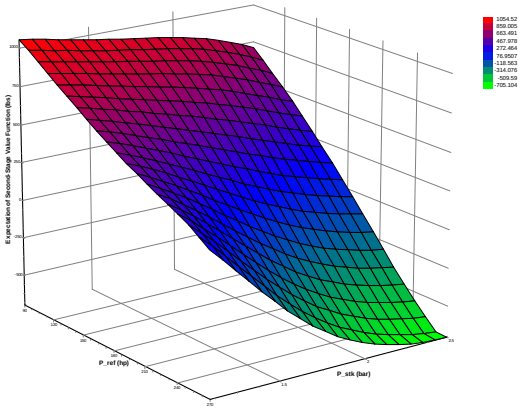

(f) Alternative 3

Figure 59: Contour and Surface Plots of Second-Stage Space: $\mathbf{h_4}$

Nowhere is it more evident than in the case of **A3** that penalty fractions exert significant influence on the topology of the design space. Figures 60 and 61 clearly show how bimodalness transforms to unimodalness with increasing p_f values. Although traces of a maximum still linger on the far left side of the grid, the protrusion becomes less obvious beyond an apparent threshold of 30 percent. Any fractional recourse penalty less than this threshold value would prove troublesome for path-building optimizers in reliably reaching the global optimum situated towards the far right of the solution space.

In the case of **A1**, multimodalness is not an issue, despite the fact that the space, as a whole, is hardly void of many peaks and troughs. The relatively flat surface dominating most of the low-pressure regions would prove especially problematic for a gradient-based optimizer, as there is the risk of its getting trapped near the undersized, first-stage designs. Fortunately, the curvature within these flat lands morphs into a less ambiguous surface that unequivocally displays a minimum when larger penalty fractions are prescribed. Beginning with recourse penalties that fall between 10 and 20 percent, it appears that any traditional optimizer would work satisfactorily, as shown in Figures 62 and 63.

Once the solution space of **A2** was examined in the same manner, it was revealed to be suffering from a more severe problem: the lack of an extremum within the boundaries of the design space. This observation is unmistakable in Figures 64 and 65. It can be seen that, with the exception of p_f equaling 0, all indicators for minimum z point toward the lower right-hand edge. With such a space, it is more likely to obtain trivial solutions; that is, designs with most, if not all, variables pushed to either their lower or upper limits. Nevertheless, the other four design variables do alter the curvature of the solution space, albeit at small magnitudes compared to P_{ref} and P_{stk}. It was, therefore, decided to implement more thorough optimization studies for this particular alternative to see whether or not meaningful optimal solutions exist.

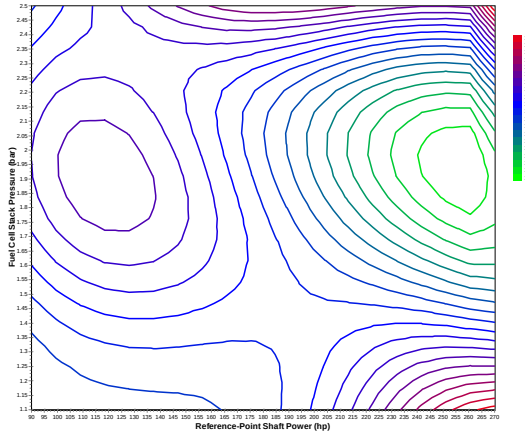

(a) 0 Percent Penalty

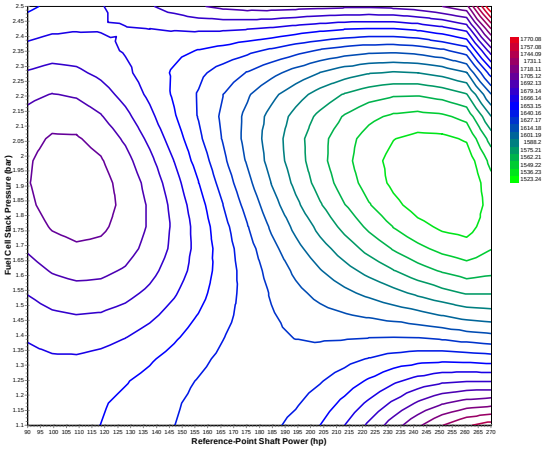

(b) 10 Percent Penalty

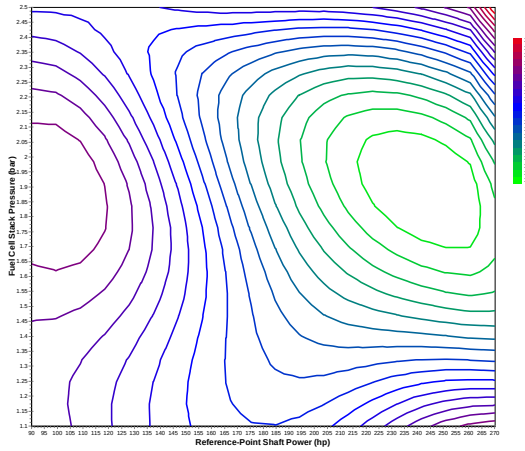

(c) 20 Percent Penalty

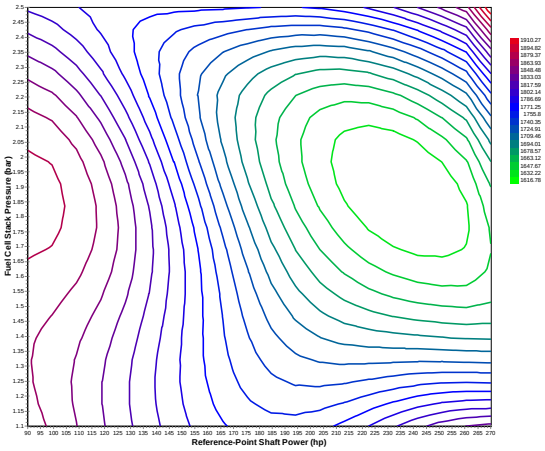

(d) 30 Percent Penalty

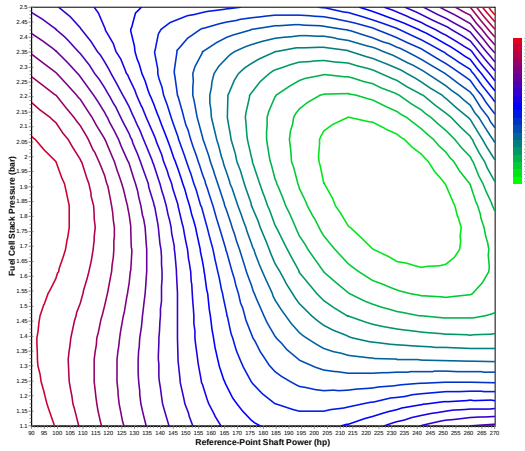

(e) 40 Percent Penalty

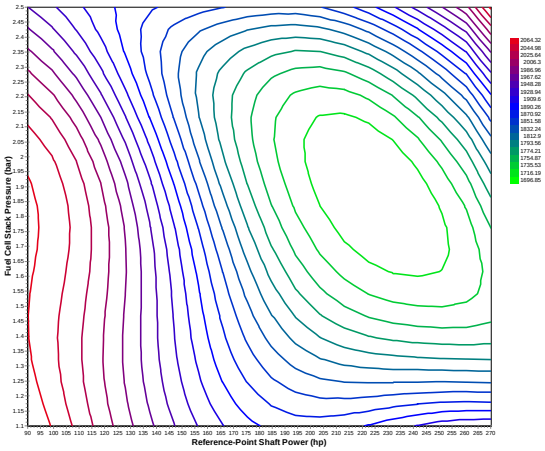

(f) 50 Percent Penalty

Figure 60: Contour Plots of Solution Space: **A3**

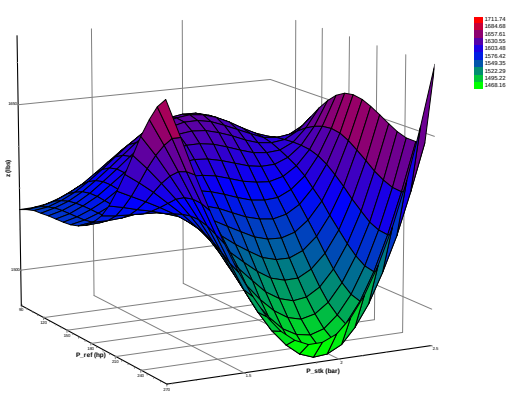

(a) 0 Percent Penalty

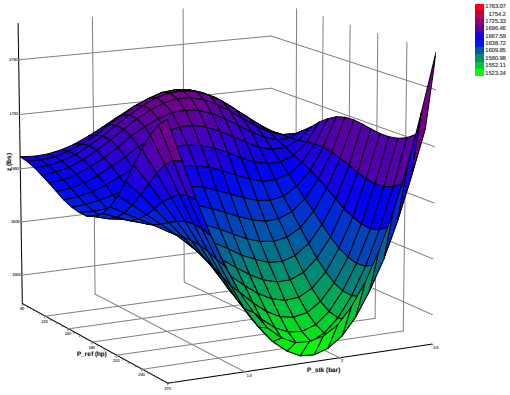

(b) 10 Percent Penalty

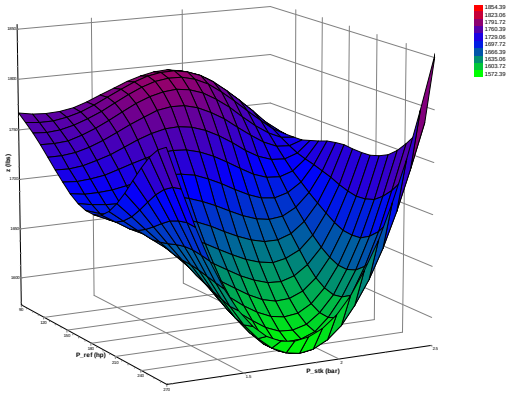

(c) 20 Percent Penalty

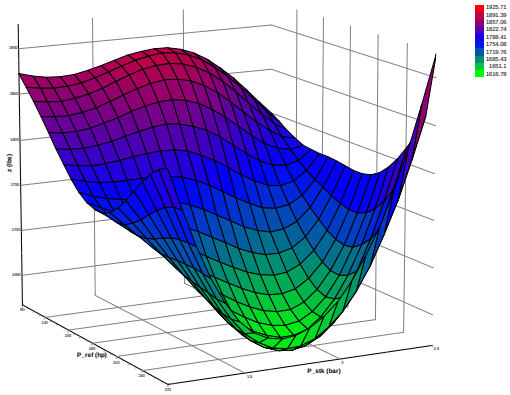

(d) 30 Percent Penalty

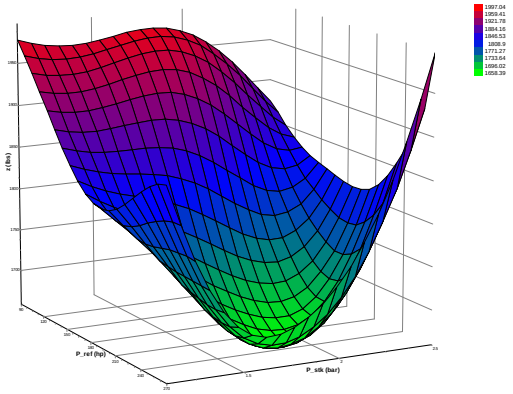

(e) 40 Percent Penalty

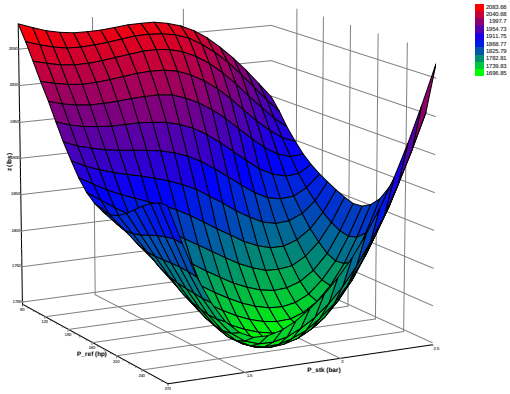

(f) 50 Percent Penalty

Figure 61: Surface Plots of Solution Space: **A3**

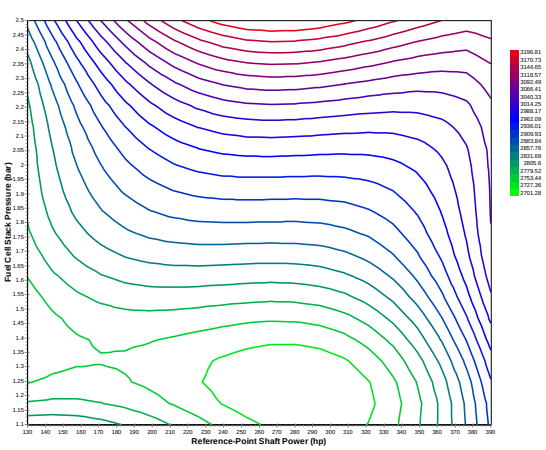

(a) 0 Percent Penalty

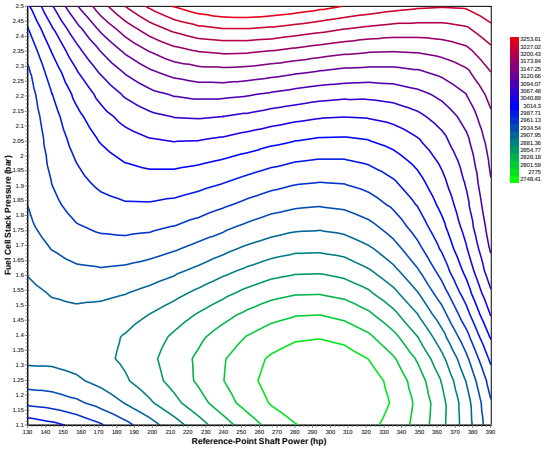

(b) 10 Percent Penalty

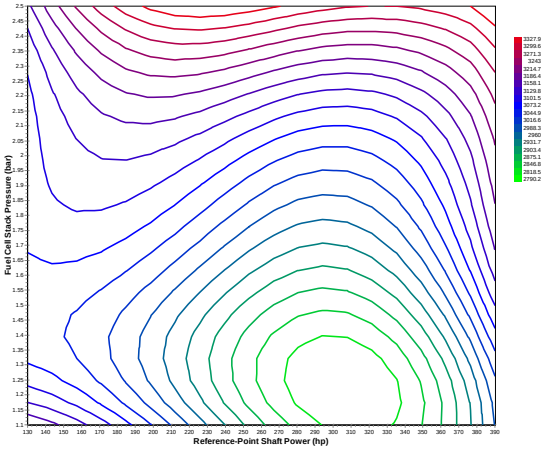

(c) 20 Percent Penalty

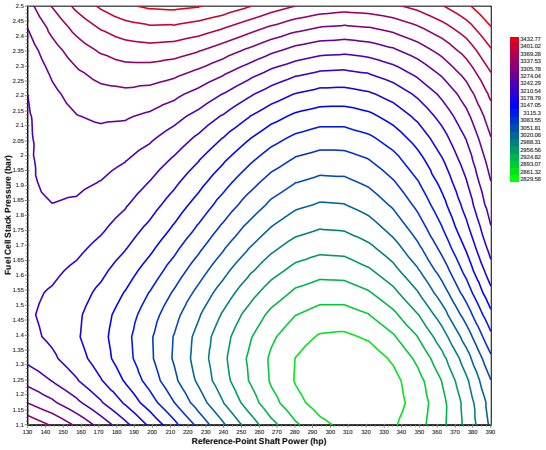

(d) 30 Percent Penalty

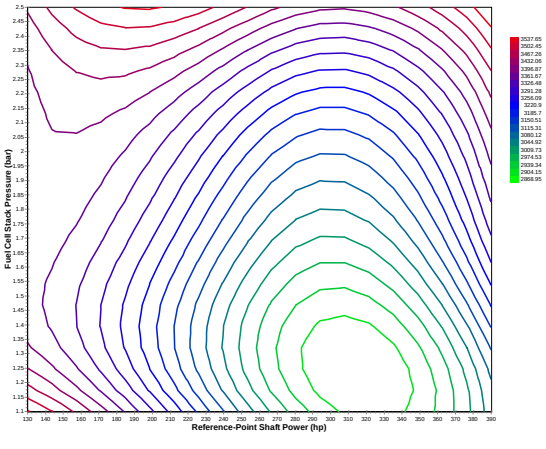

(e) 40 Percent Penalty

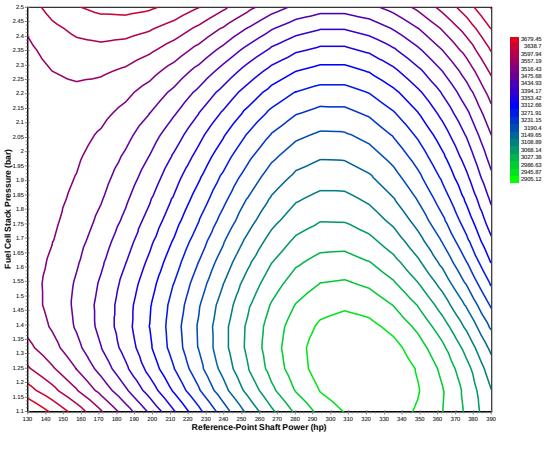

(f) 50 Percent Penalty

Figure 62: Contour Plots of Solution Space: **A1**

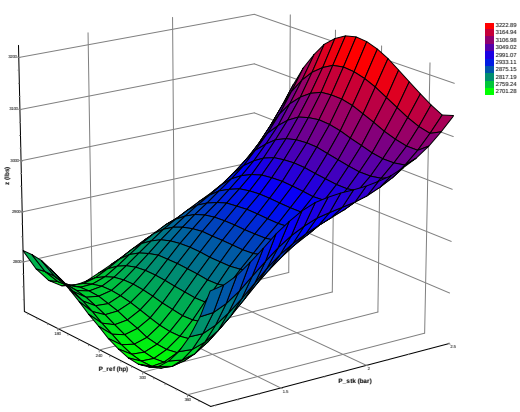

(a) 0 Percent Penalty

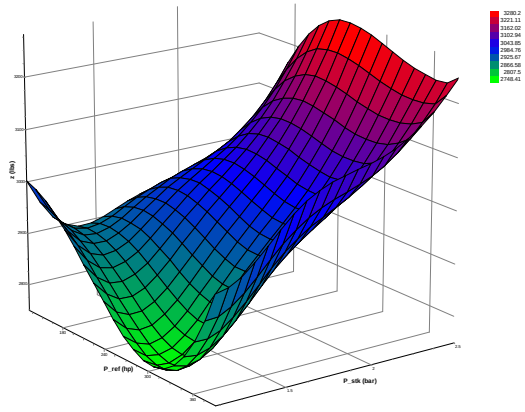

(b) 10 Percent Penalty

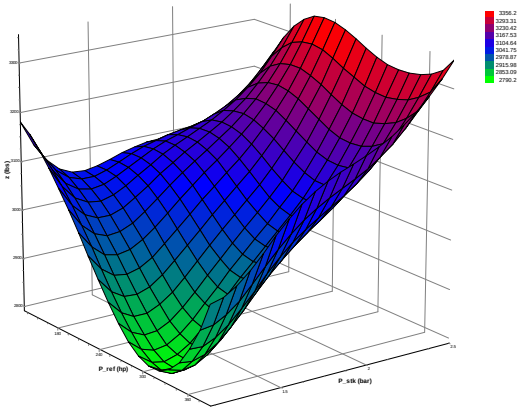

(c) 20 Percent Penalty

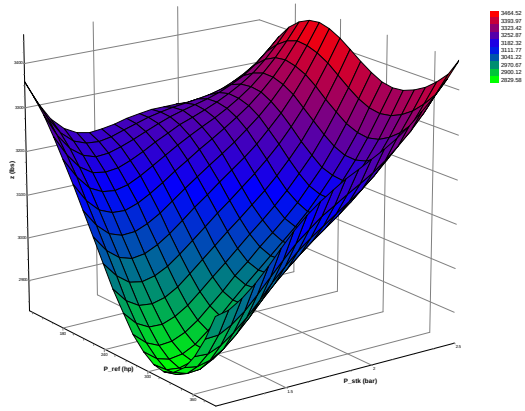

(d) 30 Percent Penalty

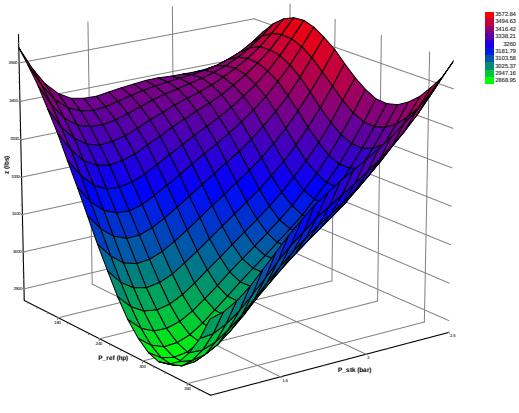

(e) 40 Percent Penalty

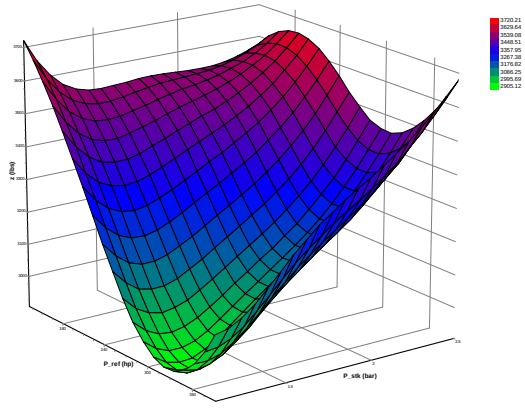

(f) 50 Percent Penalty

Figure 63: Surface Plots of Solution Space: **A1**

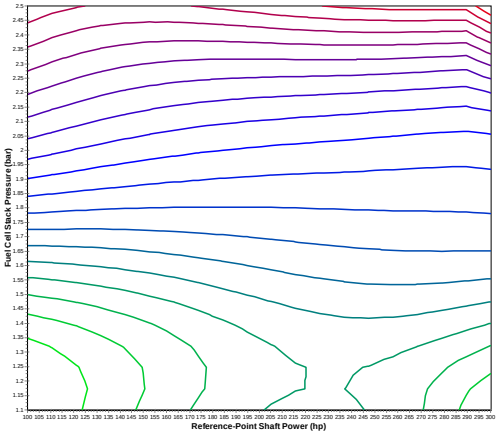

(a) 0 Percent Penalty

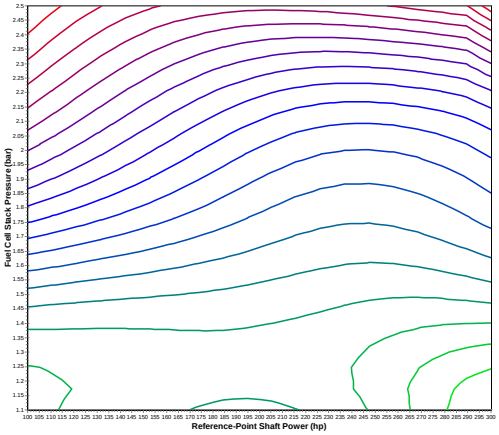

(b) 10 Percent Penalty

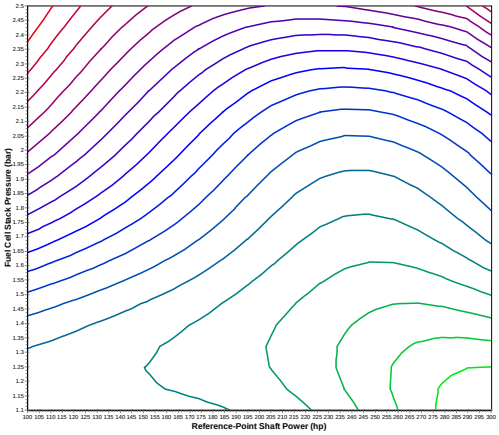

(c) 20 Percent Penalty

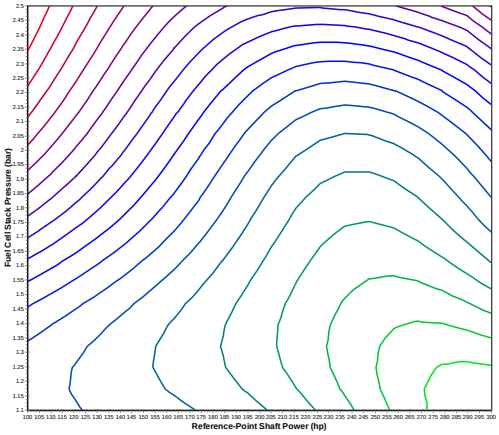

(d) 30 Percent Penalty

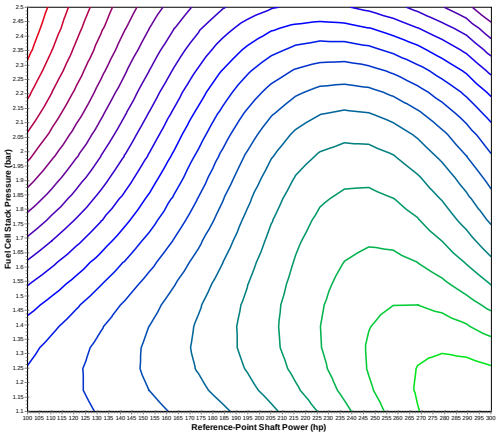

(e) 40 Percent Penalty

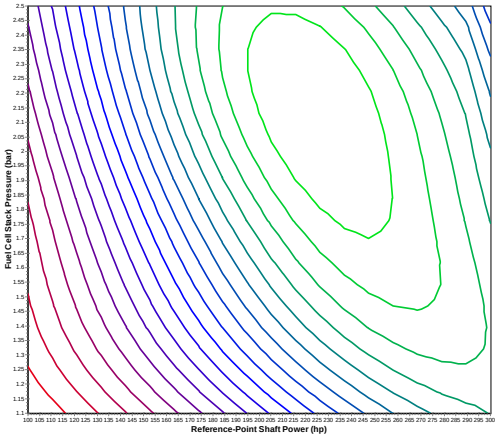

(f) 50 Percent Penalty

Figure 64: Contour Plots of Solution Space: **A2**

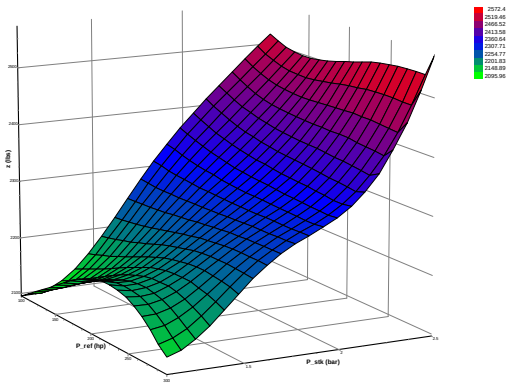

(a) 0 Percent Penalty

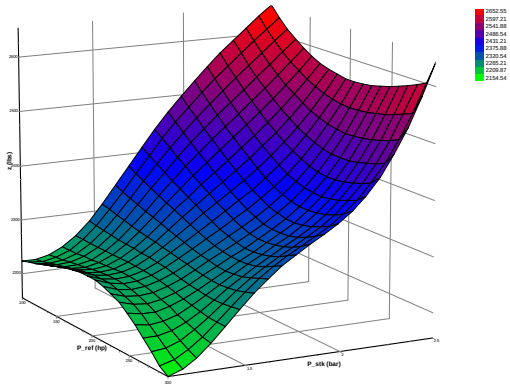

(b) 10 Percent Penalty

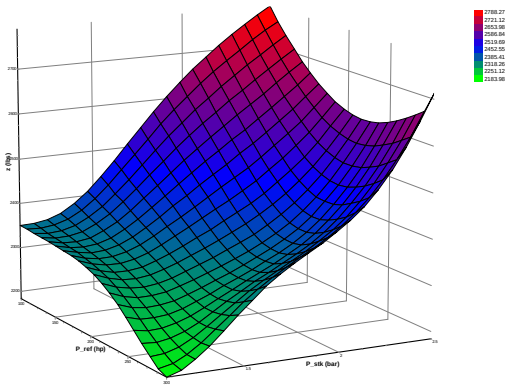

(c) 20 Percent Penalty

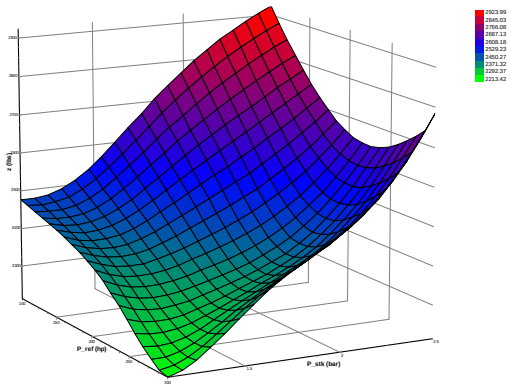

(d) 30 Percent Penalty

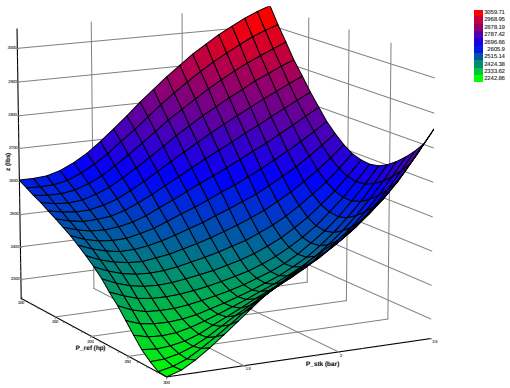

(e) 40 Percent Penalty

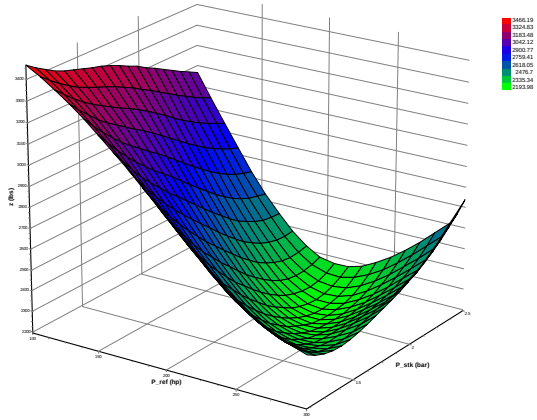

(f) 50 Percent Penalty

Figure 65: Surface Plots of Solution Space: **A2**

Table 20: Two-Stage Optimization Solutions of **A1**

Parameter	Symbol	$p_f = 0.25$	$p_f = 0.35$	$p_f = 0.40$	Units
Reference-Point Shaft Power	P_{ref}	292.4620	294.3053	289.4807	hp
Fuel Cell Stack Temperature	T_{stk}	71.2747	70.9527	73.1275	°C
Fuel Cell Stack Pressure	P_{stk}	1.2635	1.2699	1.3260	bar
Anode Water Content	a_{an}	0.8569	0.8568	0.8619	N/A
Cathode Water Content	a_{ca}	0.8831	0.8814	0.8793	N/A
Fuel Utilization Coefficient	u_f	0.9622	0.9620	0.9631	N/A
Recourse Function	$Q(\mathbf{x})$	265.1233	271.4361	315.5443	lbs
Stochastic Solution	z	2725.4419	2756.9265	2776.9910	lbs
EEV		2974.3336	3097.4295	3119.3600	lbs
VSS		248.8917	340.5029	342.3690	lbs

5.4.3 Value of Stochastic Solution

The iterative process outlined in §5.4.2 was painstakingly followed to produce three viable second-stage recourse models, each aligning with the technology-level assumptions behind the three system alternatives. Sufficient due diligence was also devoted to mapping out the design domain spaces in two and three dimensions, which subsequently led to the winnowing down of penalty fractions. Consequently, all prerequisites were finally met to carry out the last step of the proposed design method: two-stage stochastic optimization studies.

The same automated environment, first introduced in §5.4.2.3, was employed to solve Eq.(12) for a given p_f. In order not to compromise the validity of the surrogates during optimization, the upper and lower bounds listed in Table 15 were imposed as the side constraints of $\mathbf{x}$. Similarly, the same bounds were respected for all random parameters whenever 100,000 cases of Monte Carlo simulation had to be executed within the optimization loop. Unless otherwise specified, the reader can assume that the start value of each design variable was initialized at the average of its respective side constraints.

Tables 20 and 21 list the two-stage stochastic optimization outcomes, including the results for EEV and VSS. It is worth reiterating that the stochastic solution represents

Table 21: Two-Stage Optimization Solutions of **A3**

Parameter	Symbol	$p_f = 0.55$	$p_f = 0.65$	$p_f = 0.80$	Units
Reference-Point Shaft Power	P_{ref}	224.4308	217.2819	213.0056	hp
Fuel Cell Stack Temperature	T_{stk}	73.0427	67.5872	66.9299	°C
Fuel Cell Stack Pressure	P_{stk}	1.6042	1.5976	1.6464	bar
Anode Water Content	a_{an}	0.9775	0.9999	0.9999	N/A
Cathode Water Content	a_{ca}	0.9999	0.9999	0.9999	N/A
Fuel Utilization Coefficient	u_f	0.8595	0.8428	0.8276	N/A
Recourse Function	$Q(\mathbf{x})$	38.9860	104.6945	153.8706	lbs
Stochastic Solution	z	1506.9624	1525.0951	1566.6967	lbs
EEV		1547.5766	1580.9592	1688.0038	lbs
VSS		40.6142	55.8641	121.3071	lbs

a well-balanced compromise between unwarranted conservatism and blissful optimism, whereas a positive VSS is the direct measurement of the cost of neglecting recourse-causing uncertainties. The unconstrained optimization technique of choice here was the classical conjugate-gradient method developed by Fletcher and Reeves [162]. As seen from the confirmation results of Figures 66 and 67, which display the snapshots of the z space at different optimal designs, the Fletcher-Reeves method encountered little difficulty in correctly reaching the optimum in each case.

The same optimization technique, however, proved to be problematic in identifying the stochastic solutions for **A2**. When one compares what were ruled as converged solutions, listed in Table 22, against the visuals provided in Figures 68 and 69, it is apparent that the optimizer is prone to getting trapped in the flatter region before proceeding to the corner point (maximum power, minimum pressure) where the true minimum resides. Because experimenting with multiple start points yielded similar findings, another popular optimization technique as known as the Broydon-Fletcher-Goldfarb-Shanno (BFGS) algorithm [163, 164, 165, 166] was put to the test. The algorithm falls under a class of path-building optimization techniques referred to as variable metric methods. Compared to Fletcher and Reeves' conjugate-gradient method, variable metric methods should - in general - be able to identify the true

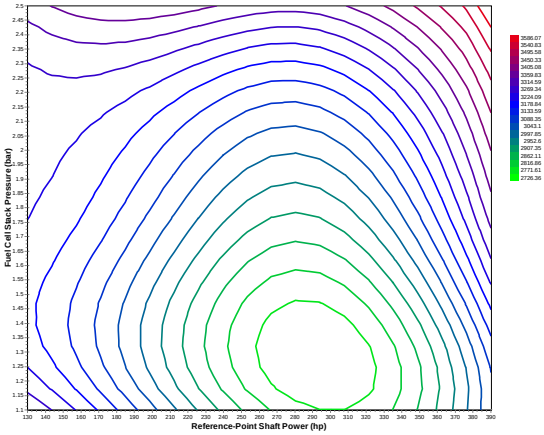

(a) Alternative 1 - 25 Percent

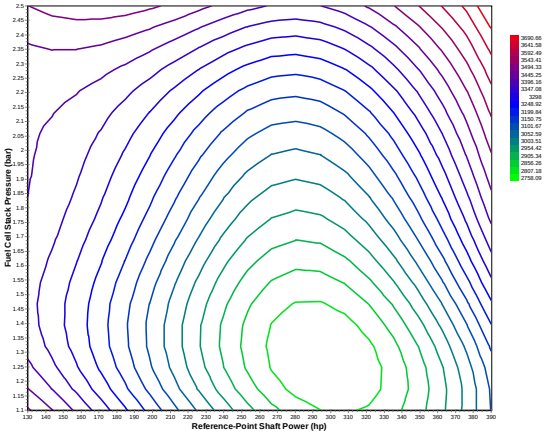

(b) Alternative 1 - 35 Percent

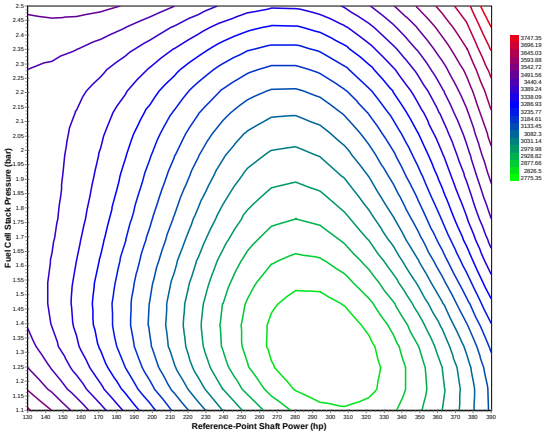

(c) Alternative 1 - 40 Percent

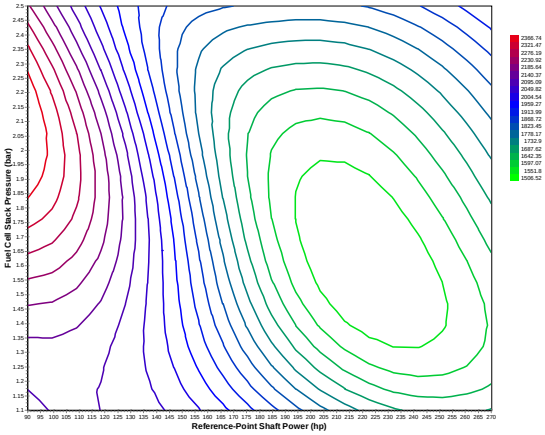

(d) Alternative 3 - 55 Percent

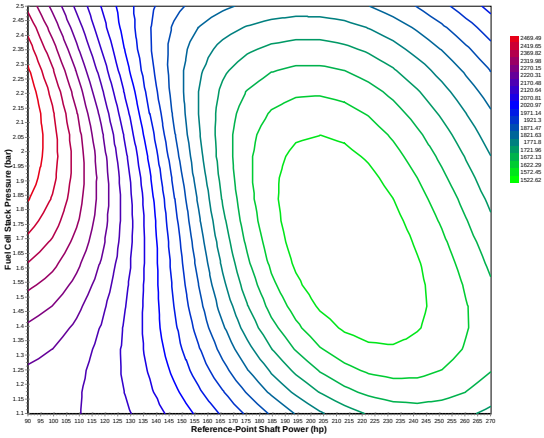

(e) Alternative 3 - 65 Percent

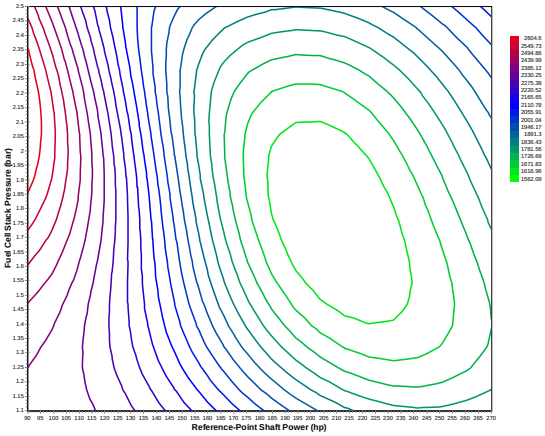

(f) Alternative 3 - 80 Percent

Figure 66: Contour Plots of Unimodal Solution Spaces: **A1** & **A3**

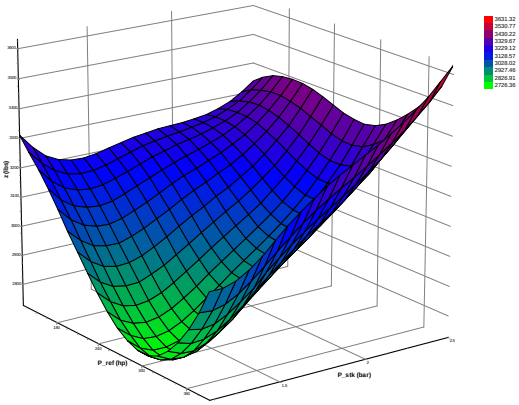

(a) Alternative 1 - 25 Percent

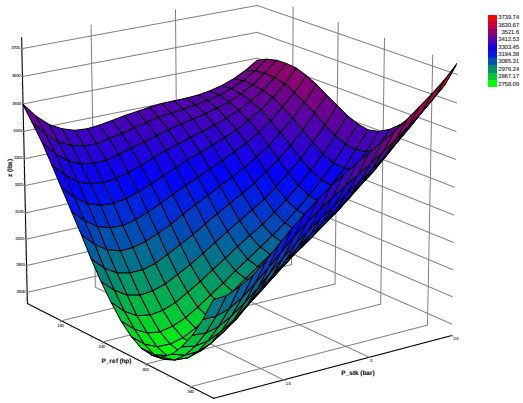

(b) Alternative 1 - 35 Percent

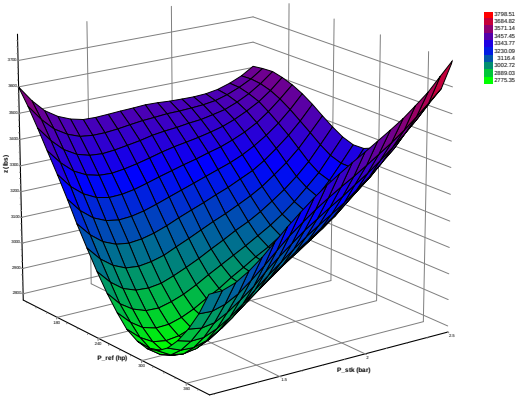

(c) Alternative 1 - 40 Percent

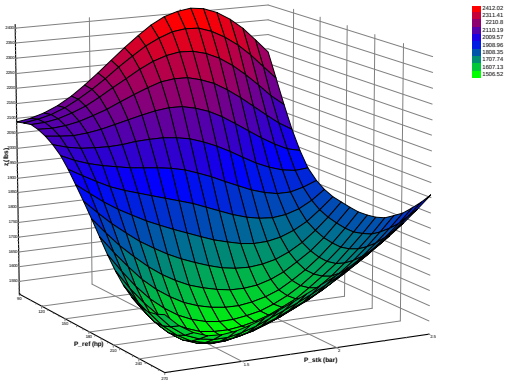

(d) Alternative 3 - 55 Percent

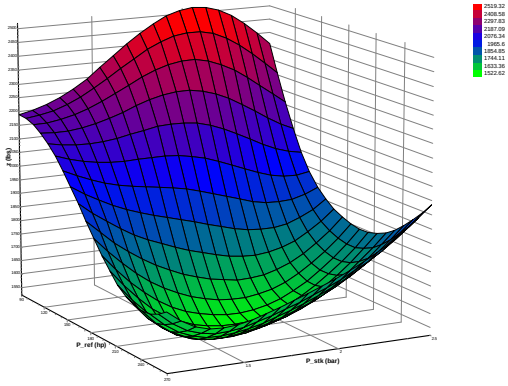

(e) Alternative 3 - 65 Percent

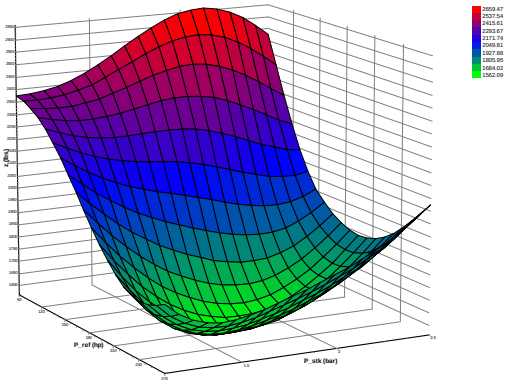

(f) Alternative 3 - 80 Percent

Figure 67: Surface Plots of Unimodal Solution Spaces: **A1** & **A3**

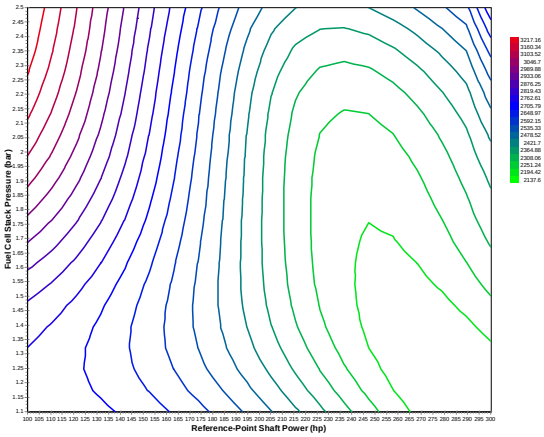

(a) 42.5 Percent

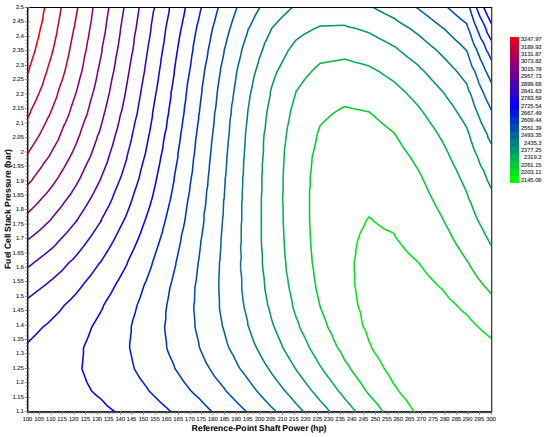

(b) 45 Percent

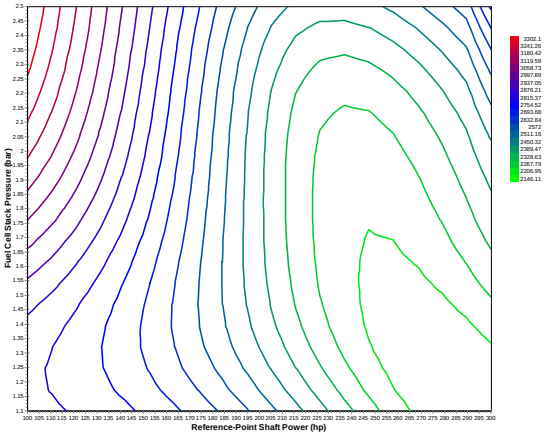

(c) 47.5 Percent

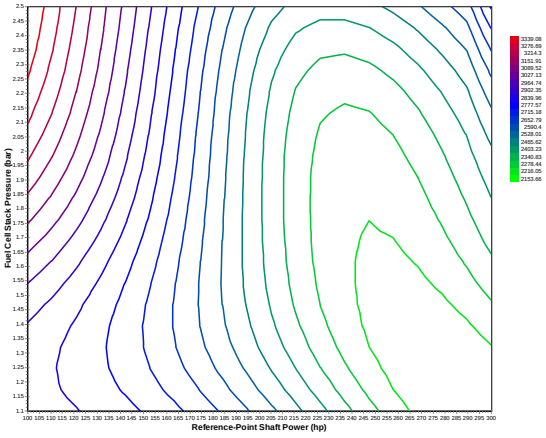

(d) 50 Percent

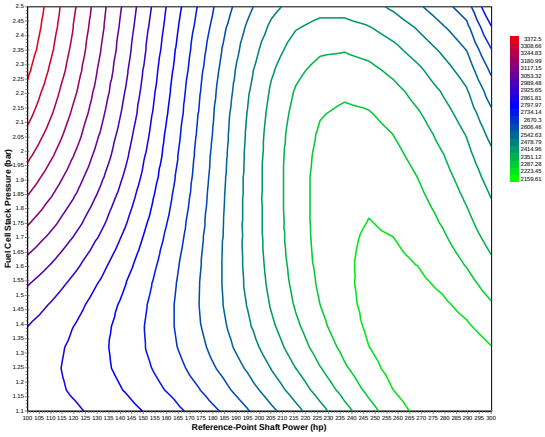

(e) 52.5 Percent

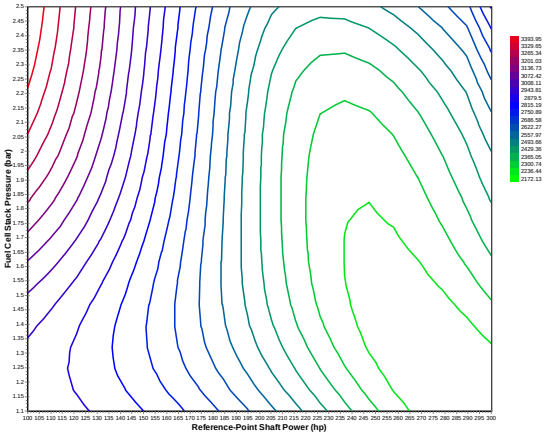

(f) 55 Percent

Figure 68: Contour Plots of Solution Space: **A2**

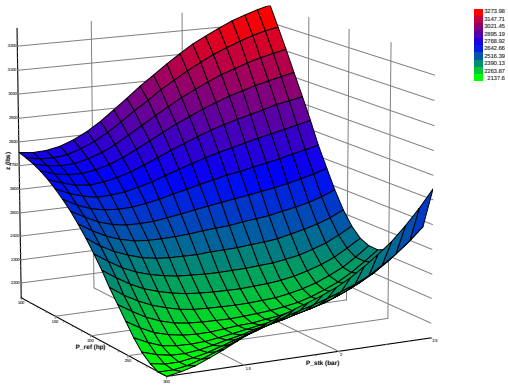

(a) 42.5 Percent

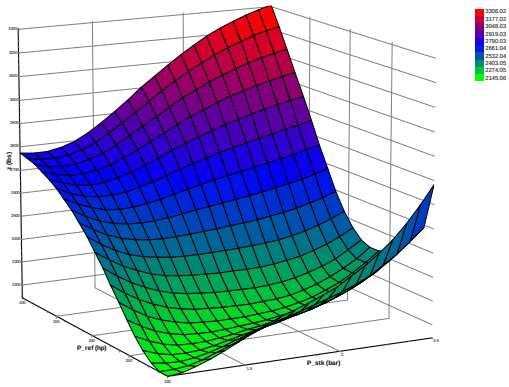

(b) 45 Percent

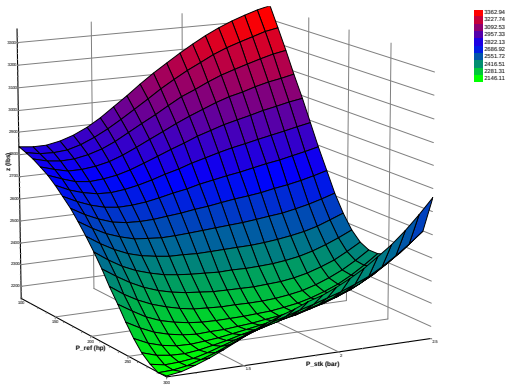

(c) 47.5 Percent

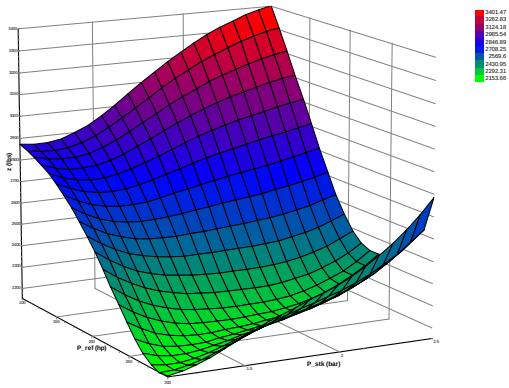

(d) 50 Percent

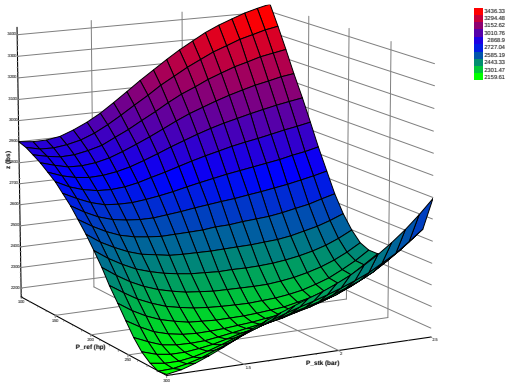

(e) 52.5 Percent

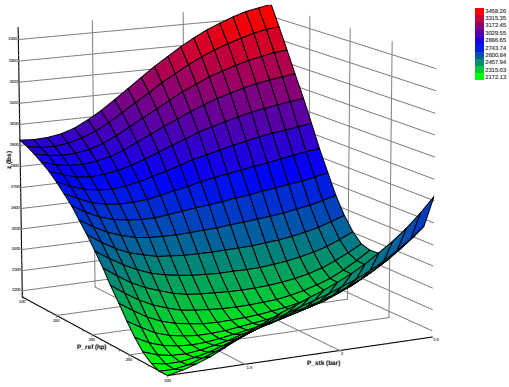

(f) 55 Percent

Figure 69: Surface Plots of Solution Space: **A2**

Table 22: Two-Stage Optimization Results of **A2**

Parameter	Symbol	$p_f = 0.475$	$p_f = 0.50$	$p_f = 0.525$	Units
Reference-Point Shaft Power	P_{ref}	250.3200	249.7562	248.7504	hp
Fuel Cell Stack Temperature	T_{stk}	82.1503	82.2231	82.2999	°C
Fuel Cell Stack Pressure	P_{stk}	1.6207	1.6174	1.6196	bar
Anode Water Content	a_{an}	0.9412	0.9404	0.9415	N/A
Cathode Water Content	a_{ca}	0.9630	0.9618	0.9627	N/A
Fuel Utilization Coefficient	u_f	0.9372	0.9366	0.9354	N/A
Recourse Function	$Q(\mathbf{x})$	52.4725	64.3637	80.4433	lbs
Stochastic Solution	z	2197.4386	2203.4612	2210.7328	lbs
EEV		2414.3921	2446.6129	2440.7364	lbs
VSS		216.9535	243.1517	230.0036	lbs

Table 23: Two-Stage Optimization Solutions of **A2**

Parameter	Symbol	$p_f = 0.45$	$p_f = 0.525$	$p_f = 0.55$	Units
Reference-Point Shaft Power	P_{ref}	225.0636	232.5555	231.9727	hp
Fuel Cell Stack Temperature	T_{stk}	72.6483	74.0998	74.1016	°C
Fuel Cell Stack Pressure	P_{stk}	2.1470	2.0117	2.0117	bar
Anode Water Content	a_{an}	0.9872	0.9814	0.9781	N/A
Cathode Water Content	a_{ca}	0.8985	0.9014	0.9030	N/A
Fuel Utilization Coefficient	u_f	0.9999	0.9999	0.9999	N/A
Recourse Function	$Q(\mathbf{x})$	19.8066	24.4777	35.1304	lbs
Stochastic Solution	z	2176.6760	2209.0469	2216.0394	lbs
EEV		2236.0785	2285.2764	2314.2563	lbs
VSS		59.4026	76.2296	98.2169	lbs

optimum more reliably due to their ability to store and then leverage upon greater information regarding previous iterations. It was thus found that the BFGS optimizer was able to satisfactorily identify the solutions listed in Table 23, whose optimality was confirmed through Figures 70 and 71.

It is evident from the optimization results for **A1** that higher penalty fractions appear to direct the design toward heavier solutions. Given how both the first- and second-stage value functions were chosen to be quantified in terms of system weight, a heavy stochastic solution represents a high-margin solution. Namely, this is a system to which some margins are allocated in a pre-emptive fashion as to minimize the cost of compensatory design that is expected to occur in the future. It can also be seen

that the expected change in system weight (*i.e.*, the value of "Recourse Function") is indeed larger at higher levels of allocated margins. The same trend is also noticeable in Tables 21 and 23.

More importantly, the stochastic solutions are those that possess not just any margins, but *optimal* amounts of built-in margins to counter the recourse penalties. Granted, the embedded margins in a stochastic solution will always make them heavier than the practically impossible *ideal* solution; that is, the designer has complete foresight with regards as to how each random parameter will become realized. But a stochastic solution, if obtained correctly, will not contain any excessive margins as to render the design overly conservative. This notion is substantiated by the fact that positive VSS outcomes can be found in all listed optimization cases. A positive VSS embodies the savings in system weight achievable by implementing the proposed approach. In other words, the EEV represents a poor method of hedging a design against recourse-causing uncertainties.

5.5 Lessons Learned

Implementing the preparatory steps outlined in §5.1.1 through §5.1.2 revealed the incompatibility of the SOFC-based alternatives with the conceived maritime border patrol mission. Additionally, the remaining three PEMFC-based alternatives were found to result in scalable aeropropulsion systems in §5.1.3, leading to the specific parameter-based synthesis algorithm described in §5.1.4. The ensuing aircraft sizing process was demonstrated to be sufficiently expedient to allow optimizing W_{TO} by perturbing the propulsion-level cycle parameters, as well as the design variables at the vehicle level: power-to-weight ratio and wing loading. It also led to the discovery of ultracapacitors as the most suitable auxiliary energy storage technology options on a PEMFC powered UAV. In this regard, the first half of the proposed method served as the quantitative means to screen out unsuitable propulsion system concepts, in

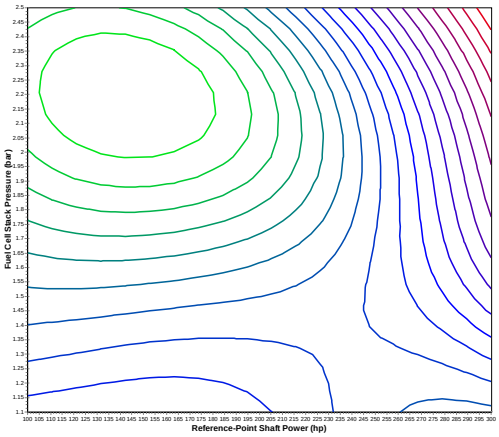

(a) 42.5 Percent

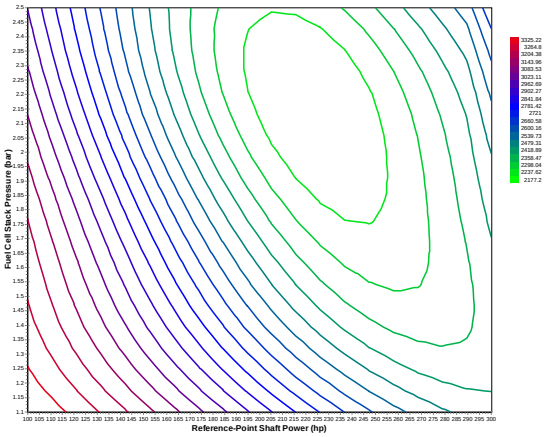

(b) 45 Percent

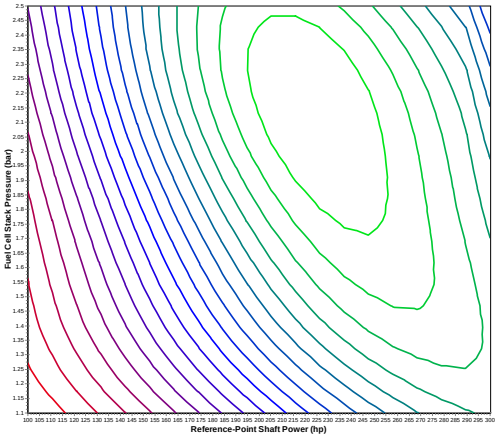

(c) 47.5 Percent

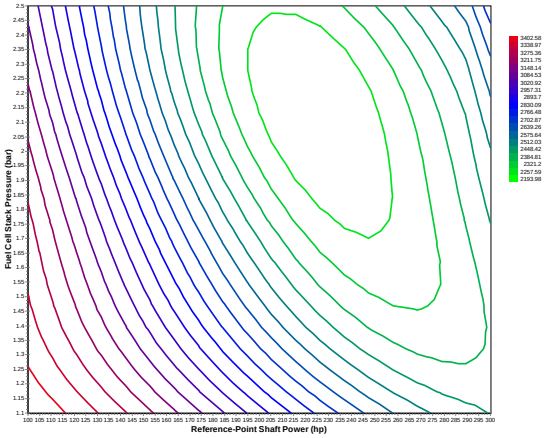

(d) 50 Percent

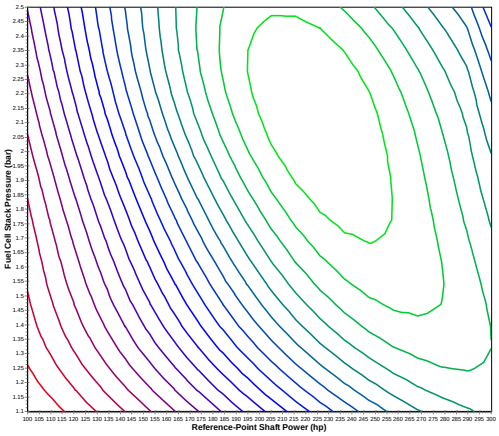

(e) 52.5 Percent

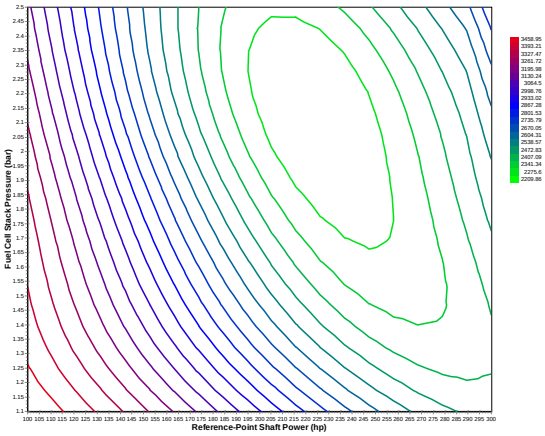

(f) 55 Percent

Figure 70: Contour Plots of Unimodal Solution Space: **A2**

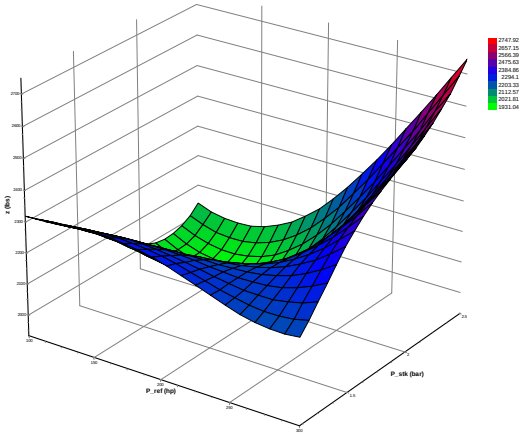

(a) 42.5 Percent

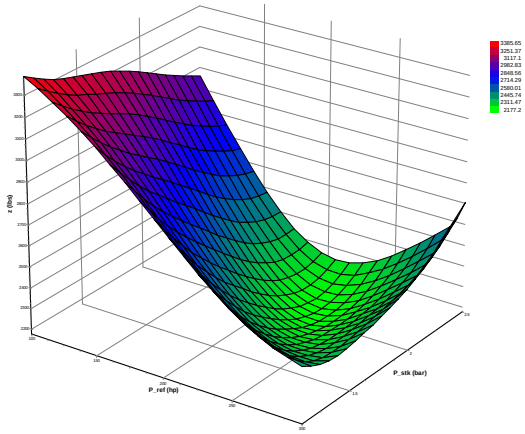

(b) 45 Percent

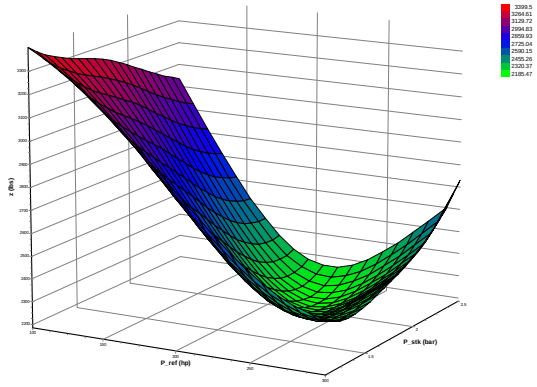

(c) 47.5 Percent

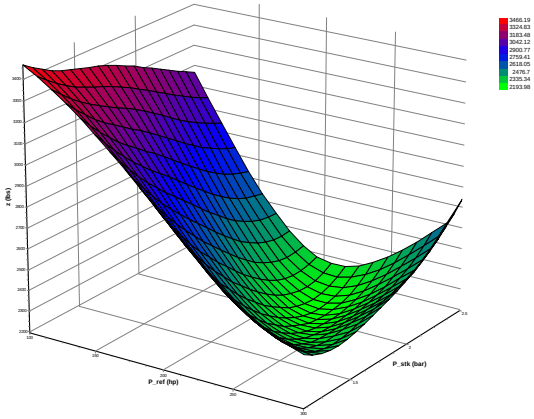

(d) 50 Percent

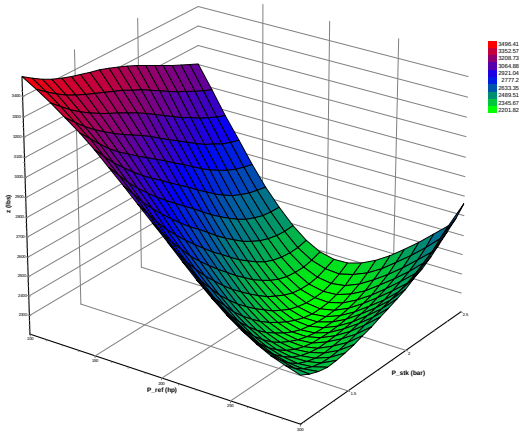

(e) 52.5 Percent

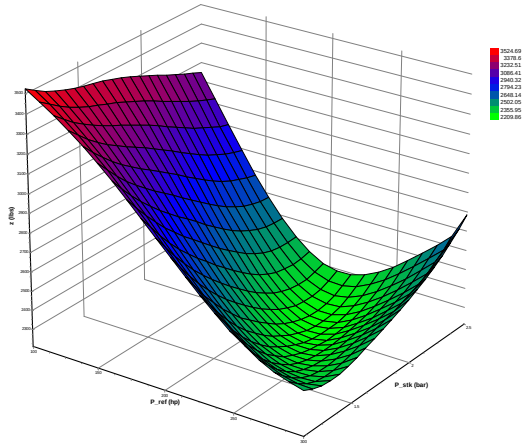

(f) 55 Percent

Figure 71: Surface Plots of Unimodal Solution Space: **A2**

addition to satisfying the action items of **Sub-task 1**.

In hindsight, much creative thinking was called for completing **Sub-task 2**. The sequence of stages defined in §4.4.2.1, for example, are intended to reflect how system design is first carried out by making the best educated guesses regarding the random parameters. In the aerospace domain, it is often the case that the quantities treated as assumptions in the previous design phase become better defined through further advancement of disciplinary knowledge in the current phase (*e.g.*, drag polar obtained from low-fidelity panel codes become successively refined through Computational Fluid Dynamics (CFD) analyses; structural design is iteratively updated in conjunction with Finite Element Analysis (FEA), etc.).

Linking the first- and second-stage value functions through system weight was another creative decision made in applying the solution approach to designing PEMFC aeropropulsion alternatives. This author believes that such is a very reasonable model for second-stage design corrections. A system that needs to be compensated for the flaws resulting from earlier assumptions, which had to have been made in the presence of uncertainty, will almost always be heavier than a system which, either through foresight or luck, turned out to be well-designed in the first stage.

Nevertheless, creativity should never be a replacement for reality in an actual product development environment. Questions with regards to where the boundaries must be drawn between stages, which activities constitute recourse, and how to quantify such costs (*e.g.*, it is entirely possible that the first- and second-stage value functions are more appropriate to be measured in a monetary currency) must be answered *only after* carefully evaluating all technical, scheduling, and budgetary constraints. In this sense, the value functions in the form of Eqs.(9), (10), and (11) could be helpful in assessing how much design freedom remains for recourse, and how much penalty should be imposed upon such fixes. For instance, the separation of $\mathbf{x}$ and $\mathbf{y}$ allows the cross-phasal nature of the remedial actions to be properly modeled even in

a variable-fidelity design environment more typical of post-conceptual design phases. Such is neither the case nor within the capability bounds of the simulation environment developed for this research because the notional design example was intended to showcase a solution process with which an engine manufacturer could explore optimal margin allocations to a yet-to-be-launched product line.

Some critics may argue that the visualization exercises of **Sub-task 3** are no substitutes for either mathematically proving the convexity of the functions or checking the necessary conditions for optimality. Although this author does not disagree with such criticisms on a purely theoretical basis, the following quote from Vanderplaats [167] is provided here as a counter-argument.

> In the application of optimization techniques to design problems of practical interest, it is seldom possible to ensure that the absolute optimum design will be found subject to the constraints. This may be because multiple solutions to the optimization problem exist or simply because numerical ill-conditioning in setting up the problem results in extremely slow convergence of the optimization algorithm. From a practical standpoint, the best approach is usually to start the optimization process from several different initial vectors, and if the optimization results in essentially the same final design, we can be reasonably assured that this is the true optimum.

If nothing else, visualizing the design domain space offers crucial geometrical insights into whether or not the underlying optimization problem is ill-conditioned. For example, it would not have been possible to derive the TPM targets that yield smooth recourse function spaces without the aid of surrogate-based visual tools[2]. The same

[2]Conversely, visualizing the solution space with the knowledge of clear TPM targets would have pointed towards the appropriate optimization techniques to apply.

environment was successfully used to identify the ranges of penalty fractions resulting in two-stage stochastic optimization problems that are solvable with path-building techniques. As far as the issue of optimality is concerned, visualizing what the solution space looks like at the optimal design variable conditions, served well in further confirming the numerical convergence of the **A2** solutions.

One last caveat with respect to designing a stochastic programming model around a real-world engineering problem is this: *know thy uncertainties*. Along with visualizing the domain space intended for optimization, this likely ranks as one of the most overlooked steps by those new to the more advanced topics in multidisciplinary analysis. Which theoretical probability distribution is applicable to what random parameter will depend on many factors, such as design phase, sources of imperfect information, availability and applicability of hard data, etc. As such, it is always safer to base the choice of an input probability distribution on statistical inference techniques. When the designer is left with no other options but to subjectively prescribe the distributions, he or she should remember that "failure to choose the *correct* distribution can also affect the accuracy of a model's results, sometimes drastically." [133]

Chapter VI

CONCLUSIONS

In the field of aerospace systems design, the past decade has seen a sustained interest in pushing the envelope of engineering design philosophies and practices. This dissertation extends the lineage of advanced design methods by introducing a system-level strategy that addresses a hitherto neglected aspect of engineering design. The outcome of the ideas, algorithms, and techniques documented herein is a new nondeterministic approach that allows an engineer to not only identify an optimal solution in the presence of uncertainty, but also to find the least costly solution in terms of future recourse.

6.1 Academic Contributions

Preliminary investigation into fuel cell technology as a revolutionary means of aeropropulsion inspired the two-part motivation for commencing this thesis. At the disciplinary level, there appeared to be an immediate need to research a computationally efficient algorithm for modeling and simulating fuel cell aeropropulsion systems. Furthermore, the aspiration to approach the issue from a method-oriented perspective identified an opportunity to address the remedial aspect of engineering, which has been hitherto left unexplored in the field of aerospace systems design. These motivating factors led to the declaration of three research questions, which are serially presented in Chapters 2 through 3. They were born not only out of necessity to attend to the challenges of formulating an innovative design strategy, but also served to jump-start the required literary and scientific erudition.

Question 1 is the derivative of **Observation 1** and thus asks: *Without sacrificing analysis accuracy, what algorithmic approach would result in a computationally*

efficient synthesis of a fuel cell aeropropulsion system design environment into an aircraft sizing framework? Inspired by how the same issue is successfully handled in the conceptual design of conventionally powered aircraft, it is proposed in **Hypothesis 1** that the thermodynamic scalability of the intended aeropropulsion system must be investigated prior to developing such an algorithm. The findings gathered from executing **Sub-task 1** supported the scalability of the PEMFC-based systems within the fidelity bounds of the created propulsion-level simulation environment, and justified developing the generalized specific value-based synthesis approach shown in Figure 37. Apart from this new algorithmic contribution to aerospace vehicle design, the computational implementation marked the first time the AIAS method was invoked in the specific parameter-based aircraft sizing mode.

Question 2 concerns the issues identified in **Observations 2** and **3** and thus asks: *Are there elements of existing advanced aerospace systems design methods that can serve as foundational formalisms for identifying an optimal recourse decision regarding fuel cell aeropropulsion system design?* The ensuing literature survey of relevant sub-fields within the aerospace engineering domain identified DoE, Surrogate Modeling, and random-variate sampling as potentially useful techniques. Nevertheless, it became clear that most hitherto developed probabilistic design methods are single-stage strategies, which embody and promote what can be characterized as an avoid-failure approach to developing aerospace systems under uncertainty. In contrast, recourse - as defined in §1.1 - is fundamentally a two-stage phenomenon which cannot be adequately modeled without some type of compensatory mechanism for constraint violations. This perceived gap in the state-of-the-art capability was the prime motivating factor for pursuing the method-oriented portion of this dissertation, as summarized in **Observation 4**.

As the derivative of the last observation, **Question 3** asks: *How can a recourse-based solution approach be formulated in such a way as to be relevant to the design*

of modern aerospace systems in general, and be applicable to the design of fuel cell aeropropulsion in particular? The desire to leverage upon the bi-phasal nature of research meant that some means of correcting an *a priori* design in an *a posteriori* manner had to constitute the core of the new formulation. The argument called for a noteworthy shift in perspective on how this generation of engineers should approach the design of modern aerospace systems, a task often complicated by the presence of revolutionary technology, uncertainty, or both.

Fortunately, a useful framework, known as two-stage stochastic programming was uncovered from the out-of-domain field of optimization under uncertainty during the extended literature-search phase. It is reiterated that the notion of *stages* is at the core of this particular optimization paradigm, which provides that the natural foundation represent not only the remedial, but also the temporal and nondeterministic aspects of aerospace systems design. Initially, a deterministic two-part strategy was proposed, whereby design activities are partitioned into stages following the sequence of *a priori* design (first stage), uncertainty realization, and *a posteriori* corrections (second stage). Penalizing costs were attached to the second-stage activities to reflect the reality that getting something done right from the beginning should be less costly than fixing it after the fact.

Unfortunately, one weakness of such a two-stage strategy is its limited application as a forecasting tool. What would be more valuable, given the time-phased nature of engineering design, is the capability to trade the design optimality in the present with the *expected* cost of recourse in the future. Therefore, it was further proposed that the original two-part strategy be embedded inside a larger optimization loop, so that the realization of numerous recourse paths can be simulated for a given first-stage design. It was also postulated, as summarized in **Hypothesis 2,** that this repetitive and numerically intensive procedure for computing the expected cost of recourse can be made more manageable via leveraging upon the tried-and-tested DoE, Surrogate

Modeling, and Monte Carlo sampling techniques. A feedback loop was designed to communicate this information to the aggregate-level optimizer, whose objective is to minimize the sum total of the first-stage metric, as well as the expected cost of recourse. If the resultant solution space is uni-modal, then relatively efficient path-building algorithms become applicable in identifying the solution that is well-hedged against the risk of failing to meet desired target performance measures, as postulated in **Hypothesis 3**.

Sub-tasks 2 and **3**, in conjunction with **Sub-task 1**, were designed specifically to culminate in the formulation of the recourse-based solution approach shown in Figure 21. The merit of implementing such a stochastic approach over the traditional deterministic regimen was demonstrated on the design of notional fuel cell aeropropulsion systems for naval applications. To the best of this author's knowledge, it marked the first time a stochastic recourse programming model was applied to a contemporary aerospace problem of interest. Showcasing the VSS to be an intuitive measure of accounting for recourse in an engineering environment is deemed to be the most significant contribution to the evolving field of aerospace systems design. Additional academic and intellectual contributions of this thesis are perhaps best quantified by the growing number of past Master's-level research (Refs. [168, 145, 169]), Ph.D. dissertations (Refs. [3, 66]), contract reports (Refs. [170, 138]), as well as an upcoming Ph.D. dissertation [171] that utilized, in part or whole, the simulation environment reported in §4.3.

6.2 Follow-up Research Paths

This thesis broaches a number of subject matters that are of contemporary interest to the aeronautics community. In doing so, the seemingly disparate topics of fuel cell systems design and optimization under uncertainty are shown to be intertwined. What results is a new nondeterministic systems design strategy, which has some of

the key concepts from each field woven into it. Because both are fields of academia that are still evolving, this author hopes that the following ideas will inspire and motivate others to pursue more innovative research paths.

6.2.1 Incorporation of Refined Simulation Models

Several opportunities for improving the propulsion-level simulation models were noticed over the course of the implementation phase. Although the developed simulation models are of adequate fidelity to support the objectives of this research, it was found that the sizing and performance analysis results were largely dependent on a couple of design variables. Both outcomes of the sensitivity analysis and two-stage stochastic optimization reflect the dominance of P_{ref} and P_{stk} in affecting system weight, as well as all TPMs of interest. Nevertheless, it would certainly be interesting to ascertain whether or not more refined simulation models, with a larger pool of influential cycle variables, yield further insights into the design aspects of fuel cell powered aerovehicles.

The availability of such higher fidelity models would also enable a more realistic demonstration of recourse-based design. In particular, an unequivocal demarcation between $\mathbf{x}$ and $\mathbf{y}$ will offer simulating recourse scenarios more resembling of actual second-stage corrective actions. Taking the PEMFC stack as an example, one can envisage a scenario in which the inadequacy of available shaft power is addressed by inserting additional cells into the existing system. This type of incremental engineering approach is arguably more likely to occur than tweaking the system's thermodynamic cycle, as formulated and implemented in the present study. Such direct measures of second-stage design modifications may also obviate the need to impose extra penalty fractions, whose parametric nature could be a source of contention in practice.

Any study that relies as heavily on simulation as this dissertation cannot evade the inevitable question regarding model validation. Considerable amounts of time

and effort were devoted to accumulate sufficient confidence in the accuracy of all integrated models. Unfortunately, the lack of usable experimental data has forced objective validation at the system level to become all but elusive. It is this author's sincere hope that the ultimate product of the Georgia Tech fuel cell powered flight project (§A.3.1) is a public repository of first-hand design knowledge and flight test data regarding fuel cell powered UAVs.

6.2.2 Exploration of Alternate Recourse Formulations

The method-oriented portion of this dissertation suggested a second-stage value function, which is a hybrid of the classical two-stage linear program (Eq.(5)) and simple recourse model (Eq.(6)). In short, it is intended to seek the least penalizing cost to compensate for a given instance of design infeasibility, arising as the result of uncertainty realization. Although this particular formulation was found to be useful in modeling the remedial aspect of engineering design, it is by no means the most singular nor general method of representing the activities at the second stage. Other capabilities for modeling recourse in the second stage are conceivable, as long as the following two basic philosophies are adhered to: (a) sufficient degrees of freedom for recourse must be available once all uncertainties are observed; and (b) there must always be a penalty for arriving at a design solution in an *a posteriori*, rather than an *a priori*, manner.

Such attempts at innovating the recourse function are readily found in literature outside the aerospace domain. For example, Haneveld and van der Vlerk propose integrated chance constraints (ICC) as alternatives to the traditional chance constraints

$$\mathbb{E}_\omega \left[\eta_i(\mathbf{x}, \omega)^- \right] \leq \beta_i, \qquad \beta_i \geq 0 \tag{20}$$

where β_i is a risk aversion parameter in $i \in I$ [82] and all other notations are the same as defined in the introduction of Eq.(6). The ICC are deliberately formulated to yield convex feasible sets even when ω follows a discrete probability distribution,

a property made even more desirable by the fact that such is usually not the case for the conventional chance constraints. The accompanying special purpose algorithm is claimed as the first of its kind, and offers a very efficient method of solving a simple recourse program when both the technology matrix, $\mathbf{T}(\omega)$, and second-stage vector, $\mathbf{h}(\omega)$, are discretely distributed.

Another example of modifying the accustomed recourse function of Eq.(4) is given by Riis and Schultz [172]. The authors contend that the formulation of the second stage, as the minimum risk problem, would be more appealing than the classical minimum expected value problem to the risk-averse decision maker. Because minimizing the expected value of recourse cost, as in Eq.(3), says nothing about the probability of its achievement, the proposal here is to let $Q(\mathbf{x})$ denote the probability of incurring a prohibitively large value above some pre-defined threshold value ϕ at the second stage. The global objective then becomes minimizing this probability, and thus risk, of exceeding ϕ by changing the first-stage decision variables $\mathbf{x}$.

Unfortunately, to the detriment of savvy aerospace systems designers who wish to apply the latest out-of-domain research to their engineering project, there appears to be a general tendency in the stochastic programming community to focus on large-scale linear programs under discrete probability distributions. Most engineering design tasks, on the contrary, are likely to be composed of non-linear functions requiring continuously distributed parameters. This preoccupation is also noted by Sahinidis [173], who comments on the relative lack of publications dealing with stochastic non-linear programming models with continuous parameter distributions. Although explicit reasons for the reluctance to aggressively pursue non-linear programs are difficult to uncover, it is this author's opinion that the existence of an exact deterministic equivalent solution and the convexity properties of the linearly programmed and discretely distributed $Q(\mathbf{x})$ attract those aspiring to advance the computational efficiency of general-purpose optimizers.

Due to the possibility of non-convexities in stochastic non-linear programs, Sahinidis expects "global" (exploratory) optimization algorithms to "play a major role toward the solution of optimization problems under uncertainty." [173] While this author does not disagree with this statement in principal, he remains skeptical of the approach's practicality in large-scale engineering tasks. It is reiterated that most single-objective optimization problems arising in engineering settings are likely to possess uni-modal properties over the design spaces of interest, making the application of a global optimizer an overkill. Exploratory optimization methods are, by nature, notoriously inefficient algorithms that require large numbers of function calls, even for purely deterministic cases, and thus the decision to utilize one such domain-spanning optimizer for a stochastic programming problem should be made with great care. Therefore, if multimodalness is suspected in the expectation of the first-stage value function, recourse function, or both, then the conscientious design engineer is urged to first map out the appropriate function spaces. The ranges of the pertinent variables and parameters can then be adjusted accordingly to bound each function space, enhancing the applicability of the more efficient path-building optimizers. Nevertheless, the case in which the design space of interest is not only noisy, with multiple local minima and maxima as shown in Figure 72(a), but also discontinuous at many locations, due to the presence of discrete variables as depicted in Figure 72(b), may not be possible to solve without resorting to exploratory optimization methods.

6.2.3 Extension to Multi-Stage Approaches

Extending the current two-stage formulation to a multi-stage approach would be the next logical step in demonstrating the benefits of accounting for the remedial aspect of engineering design in a product development process. A multi-stage approach would be a more comprehensive formulation than the developed two-stage approach for several reasons. For one, a multi-stage stochastic formulation could provide the engineer

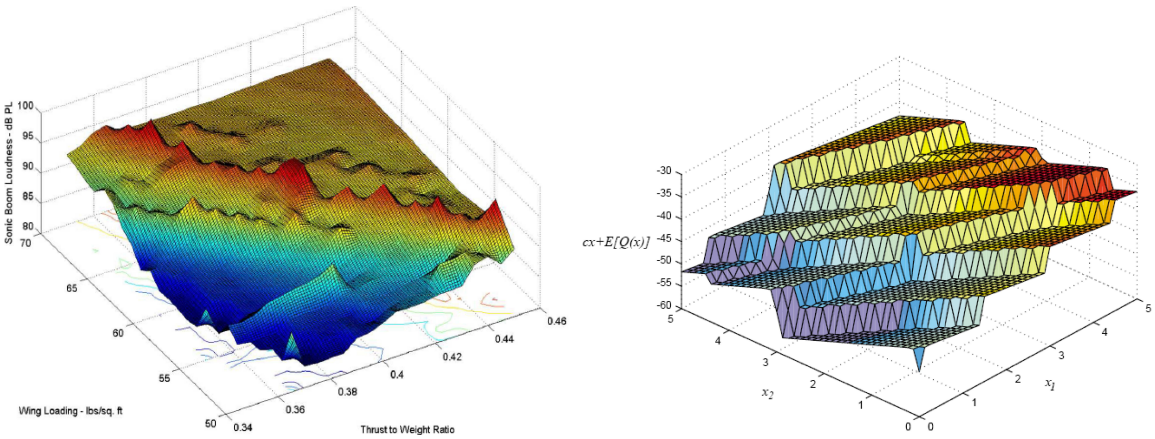

(a) Numerically Noisy Response (b) Discontinuous Response

Figure 72: Examples of Multi-modal Function Space [97, 174]

with insightful information on what would be an optimal solution at the beginning of each critical design phase, instead of a single optimum that spans two phases at most. This makes multi-stage approaches very attractive for long-term projects whose progress is measured in multiple months, if not years, but which nonetheless requires "nonanticipative [83]" planning. Here, the concept of nonanticipativity is similar to that invoked in Birge and Ho [175] - a nonanticipative solution at a specific point in time, t, can only be dependent on the information realized or observed up until t. The information also includes any knowledge that used to be unknown due to uncertainties in time less than t. Lastly, it is beyond the capability of a two-stage formulation to handle situations where either the vector of design variables at stage t, $\mathbf{x^t}$, or the random parameter vector at phase t, $\xi^{\mathbf{t}}$, is dependent on all the outcomes up to time $t-1$.

It is cautioned, however, that formulating a multi-stage strategy to handle the multi-period occurrence of recourse would be more difficult than making the philosophical transition from a two-stage to a multi-stage mindset. Above all, the most important message to be communicated here is that the multi-stage approach is *not*

equivalent to a sequential repetition of the two-stage formulation over t number of design phases. The structure of a multi-stage stochastic recourse program is necessarily more complex than that of its two-stage counterpart, with additional "aggregate-level [83]" constraints modeling the dependent relationships between the stages. With the increase in the number of modeled stages, also comes the unavoidable rise in the number of design variables, random parameters, constraints, and objective functions. Another conceivable challenge is that the dominant sources of uncertainty will likely vary from one stage to another, prompting $\xi^{\mathbf{t}}$ to differ in the number of parameters, as well as their underlying probability distributions to $\xi^{\mathbf{t-1}}$. This undoubtedly influences the shaping of the recourse function at each stage. Epistemic uncertainty, for example, may be the dominant uncertainty in the conceptual to preliminary design phases, for which the expected penalty-cost type model proposed in §4.4.2.2 was found to work well, as documented in §5.2.2. In contrast, aleatory uncertainty (*e.g.*, part tolerance) may be the largest concern, as the time draws closer to the manufacturing phase. Jagannathan proposes an interesting recourse model that utilizes the statistical information gained from finite sampling to better approximate the probability distribution of ξ using Bayesian theory [176]. Therefore, a similar model is likely to result in a more realistic embodiment of aleatory uncertainties, provided that the act of sampling is neither too cumbersome nor too expensive.

In summary, the formulation of a multi-stage approach to handle the multi-period nature of design recourse will require a deeper understanding of the given engineering project's workflow structure. If heavy iterations are foreseen to occur from one milestone to another, then the scope or structure of the multi-stage approach should be adjusted accordingly. Of equal importance is the knowledge regarding the availability of data and resources to the design engineering team that will be carrying out the stochastic study. It is conceivable that the lack of a suitable tool or set of tools to model the entire life-cycle of a particular engineering system may limit the boundaries

of the multi-stage optimization before manufacturing. Even within the confines of the three-stage conceptual, preliminary, and detail design, integration and fidelity issues between various CAD and CAE tools may force the team to further downscale the scope of implementation. On the whole, the desire to attempt multi-stage stochastic programming opens the door to a whole new world of design challenges. However, if the majority of the above-mentioned issues are not too dissimilar from those that get addressed at the systems engineering department of an industry company, then the value of the stochastic solution will be that much easier to appraise.

6.3 Recommendations for Future Work

One trend that can be observed from the first century of aviation is that new needs have often motivated the development of innovative technology, which, in time, would reveal further opportunities for newer technological solutions. For instance, the historical progress of jet fuel and aircraft engines precisely illustrates this kind of interdependent relationship. Schlaifer and Heron note that aircraft engine "development made it obvious that better fuels were needed, and when the improved fuel was used it immediately became evident that further engine development was necessary to make suitable use of the available fuel. As the engines caught up with the available fuel it became evident that still better engine performance would result from even better fuel." [177] Although its place in aviation has been brief thus far, all indications are that an analogous path lies ahead for the aeronautical applications of fuel cell technology.

The method of aeropropulsion and power generation via fuel cells has a higher thermal efficiency compared to that of a conventional aviation turbine engine. Such savings in fuel weight will primarily manifest as increased range and/or endurance, in terms of aircraft performance, allowing the same aerovehicle to complete longer-than-usual flights. From a vehicle-level standpoint, however, it must be remembered

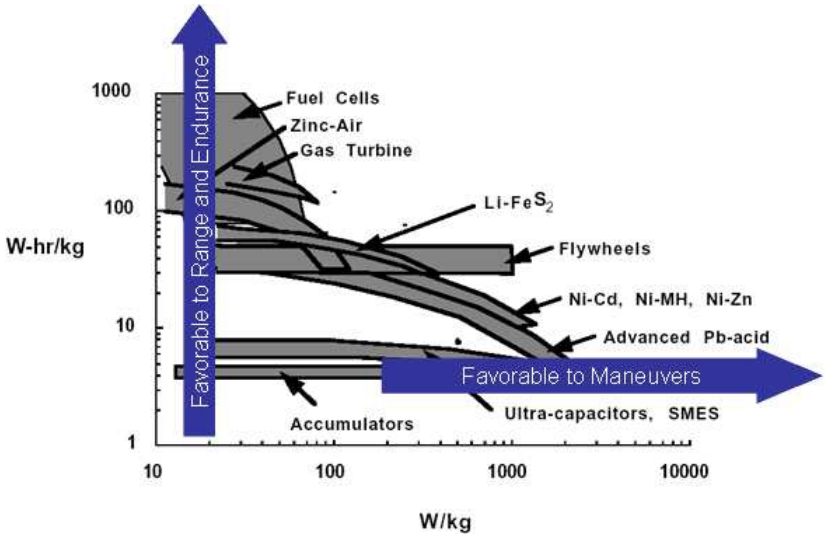

Figure 73: Ragone Plot of Various Power Plants [178]

that there will always be a trade between optimizing a power plant for power generation, which is favorable for maneuverability, and energy conversion, which benefits range and endurance. This point is apparent from Figure 73, which depicts the gravimetric characteristics of a wide variety of technologies suitable for vehicle power and propulsion: a power plant can possess either high specific power (W/kg) or specific energy (W-hr/kg) but not both. Fuel cells are shown to have the highest specific energy amongst all surveyed technologies, even surpassing GT engines by many orders of magnitude, but, as expected, the technology currently suffers from low specific power, which makes it yet unsuitable for high-speed or maneuver-intensive flights.

Therefore, the emergence of fuel cell based aeropropulsion and power generation technology presents a *new opportunity* for expanding the scope and capability of aeronautical missions, as well as vehicle systems. It motivates mission analysts to explore the portions of the mission space where a well-balanced compromise can be found between maximizing the intrinsically energy-efficient characteristics of a fuel cell system and minimizing the degradation in flight performance due to the technology's low power-to-weight ratio. During this process, aircraft designers have the opportunity to conceive, analyze, and downselect the most promising (in relation to the mission

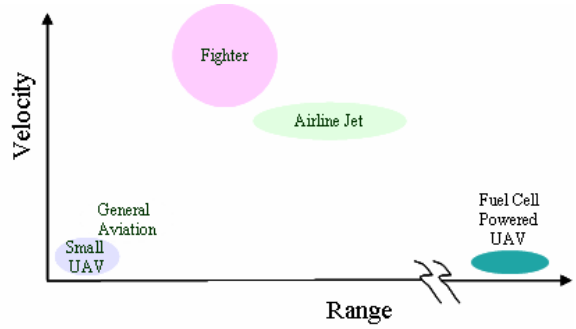

Figure 74: Notional Result of Mission Space Exploration [179]

objectives or goals) aerovehicle concept from an initial family of alternative vehicle systems. The conclusions derived from these vehicle-level trade studies may, in turn, be used to further refine the mission itself or its objectives.

One possible outcome of following the reasoning process outlined above is represented as Figure 74. It serves as an illustrative example of a previously unexplored mission space that is hypothetically discovered to be suitable for a fuel cell powered UAV. The shown mission space is envisaged to contain mission profiles with segments exploiting the aspects of high specific energy - such as greatly extended range, long endurance, or both - and mitigating the drawbacks of low specific power with relaxed performance expectations for takeoff field length, time to climb, cruise speed, and landing. Because the perceived endurance periods are on the order of weeks and beyond, it practically leaves no possibility for any manned vehicle systems. Although UAVs that are designed to remain on station for up to 24 hours have already seen extensive service in military aviation [180, 181], the movement to increase the civilian applications of this class of vehicle systems has only recently begun [182]. There currently exists a wide range of needs for long-endurance type aeronautical missions, with an operational window of 10 to 20 days. For example, the atmospheric and earth science community requires aerial sensing/imaging platforms for tracking hurricanes, monitoring weather patterns, measuring cloud formations, detecting wildfire, collecting data on forest fire plume constituents, etc. [183] Therefore, fuel cells represent

a new aeropropulsion technology that allows the civilian aviation sector to keep on capitalizing upon future opportunities, by providing the means to continually expand the aeronautical mission space and vehicle systems.

Once a capability to quantitatively substantiate this anticipated expansion of aviation mission space, due to fuel cell aeropropulsion technology becomes available, it would then be possible to further substantiate other envisioned benefits of fuel cell technology with increased confidence. For example, the most obvious beneficial outcome of applying fuel cells for aircraft power and propulsion is near zero emissions of criteria pollutants, hazardous air pollutants, and greenhouse gases. Due to the technology's electrochemical method of directly generating electricity from hydrogen or hydrogen-rich synthetic gas (syngas), fuel cell technology is expected to help mitigate aviation's impacts on the global atmosphere which, according to some, are "potentially significant and expected to grow." [184] Substantiating the potential role of fuel cells in allowing the reduction of environmentally harmful emissions from aviation systems is a worthy system-of-systems problem, which could directly leverage upon the outcome of this research.

6.4 Closing Remarks

Numerous technical challenges, as well as social, political, and economic obstacles, still lie ahead before a global hydrogen economy can successfully become established. Fortunately, all indications are that there appear to be at least a unified resolve and commitment amongst the world's most developed nations to realize a carbon-free energy infrastructure by the middle of the 21st century. As part of the larger transportation sector, aviation systems have historically aligned themselves with the energy infrastructure of their era. Aviation's gradual embracement of hydrogen as the primary energy carrier, similar to how it is envisioned to phase in for ground transportation in the pretext of an impending hydrogen economy, founds a solid

basis for the aeronautical applications of fuel cell technology.

Unfortunately, the early years of any technology development program are, more often than not, plagued with a slew of technical challenges, lower-than-expected performance results, scheduling delays, cost overruns, etc. Such problems, in many cases, lend support to the skeptics who paint a bleak future for the likelihood of the unprecedented system in holding up to its envisioned applicability. Even this author has encountered his share of skeptical remarks on fuel cell aeropropulsion over the course of this dissertation, including those from aviation experts, as well as specialists on electric power systems. Perhaps the most obvious source for criticism is the fact that as much as ten to twenty-fold increase in specific power (kW/kg) is forecast to be needed until fuel cell aeropropulsion systems become feasible for large commercial transports.

Or is it such an insurmountable impasse? Hans von Ohain, one of the inventors of the jet engine from that era, reports in the foreword to Mattingly [47] that over 60 years of intense development efforts were responsible for more than a ten-fold increase in engine specific power and an equally remarkable advancement in overall engine efficiency. At the 5th Aviation, Technology, Integration, and Operations Conference, Dr. William H. Wentz, professor Emeritus at Wichita State University, reminisced the time when the GT engine was considered a revolutionary aeropropulsion technology. He ended the presentation of his work (Ref.[185]) by showing the following uncredited quote:

> 1945: "The jet engine may be ok for military, but it will never be practical for civil aircraft."

in making the case for the future of fuel cell aeropropulsion. After all, who is to say that a similar evolutionary path does not lie ahead when governments around the world are pledging uninterrupted R&D funding, the proliferation of demonstration programs, and commercialization plans for fuel cell technology?

As if to prove this point, five cases of technology demonstrator aircraft have already been reported in the U.S. It is inspiring that two of those demonstrations were achieved by small student teams working under constrained budgets. The success stories are living proof that fuel cell powered flight on a limited scope is currently achievable with state-of-the-art technology and sound design approaches. The knowledge, experience, and heuristics that were accumulated from such pioneering efforts will undoubtedly contribute toward our ultimate goal of reaching a sustainable, hydrogen based economy.

Appendix A

AERONAUTICAL APPLICATIONS OF FUEL CELLS

Beyond the confines of academic research, there could be a number of commercial, scientific, political, and military needs for an aviation mission that leverages upon the high energy-conversion efficiency of fuel cell technology. Unfortunately, our still limited understanding of the technological boundaries of fuel cell aeropropulsion systems is the major obstacle impeding the establishment of realistic requirements for such missions of interest. The query - although not treated as a formal research question in this body of work - that naturally arises is, "What is the state-of-the-art maturity of fuel cell technology for aerovehicular power and propulsion applications?" A comprehensive literature review on the subject matter of fuel cell aeropropulsion was, thus, undertaken in order to ascertain further information on the maturity of this revolutionary technology as it currently stands in the aerospace domain.

A.1 Initiatives at National Institutions

NASA is the leading U.S. government office which oversees all major domestic aeronautical research activities. The agency sponsors and directs the development of new aerospace technology to a Technology Readiness Level (TRL) of 6, after which it is transitioned to the industry for further commercialization. To date, three NASA centers have been involved in a variety of R&D activities related to fuel cell aeropropulsion. Other national institutions which have been involved in the aeropropulsion aspect of fuel cell utilization include the National Fuel Cell Research Center (NFCRC) and the Naval Research Laboratory (NRL).

A.1.1 Test Flights at NASA Dryden Flight Research Center

Started in 1994 under the management of NASA's Dryden Flight Research Center, the Environmental Research Aircraft and Sensor Technology (ERAST) program provided an early outlet for the pioneering work on applying fuel cells to aircraft. The Helios prototype was envisioned to be the world's first HALE UAV to achieve perpetual flight, building upon the successful heritage of AeroVironment's past solar-powered experimental drones: Pathfinder, Pathfinder Plus, and Centurion. As early as 2000, AeroVironment revealed plans for further developing the Helios flying wing into a solar and PEMFC powered aircraft [186]. The company's engineers began experimenting with a regenerative power generation scheme that would stretch the endurance of Helios from hours to months, thereby allowing it to serve as an "atmospheric satellite [187]" for telecommunications, observation, or environmental science purposes. As illustrated in Figure 75(a), the idea was to interface an integrated electrolyzer-PEMFC system with photovoltaic (PV) cells for round-the-clock power generation [188]. In December of 2001, however, persistent reliability issues with the experimental RFC system forced the project to pursue a less risky non-regenerative PEMFC system for the final long-endurance demonstration [189]. Unfortunately, the Helios project came to an abrupt and untimely end when the aircraft crashed into the Pacific Ocean on June 26, 2003, before the non-regenerative PEMFC system on board the aircraft could be tested.

A.1.2 Conceptual Design Efforts by NASA Langley Research Center

Some of the earliest paper studies on the aeropropulsion applications of fuel cells were conducted in the first half of the 1980s. It was during this time that the analytical foundations for designing solar and fuel cell powered HALE UAVs were laid. Such seminal publications on this topic were either authored or commissioned by personnel at NASA LaRC. Since then, the center has continued its legacy of being at the

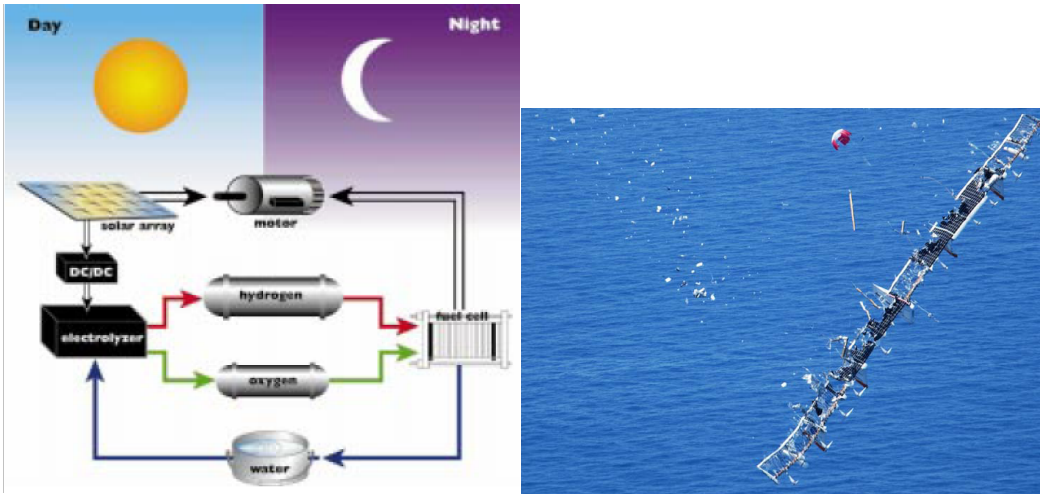

(a) Regenerative Fuel Cell System (b) Final Moments of the Helios Prototype

Figure 75: AeroVironment's Helios Prototype [190, 189]

forefront of aeronautics research by sponsoring conceptual design efforts related to fuel cell powered flight.

A.1.2.1 Regeneratively Powered Solar High Altitude Powered Platform Studies

The work of Youngblood and Talay [100] in 1982 and that of Hall et al [191] in 1983 appear to be among the first attempts at suggesting a design approach for what was then known as regeneratively powered solar High Altitude Powered Platforms (HAPPs). HAPPs were originally proposed as alternatives to orbital satellites for various civilian, coast guard, and military missions. Therefore, remotely piloted aircraft possessing multi-month endurance capabilities became the design objective of early fuel cell aircraft studies. The researchers at the time postulated that such uninterrupted propulsion power on a daily basis could be met by integrating PV cells, an electrolyzer, and fuel cells into a regenerative power system.

Perhaps the greatest achievement of the early studies on HAPPs was the development of an algorithm for computing the daily energy balance between the solar cells, electrolyzer, and fuel cells. Under such an architecture, which is very much like the one shown in Figure 75(a), all electrical loads on the aircraft are completely powered

by the PV cells, as long as solar insolation is available at the HAPP's location. In the hours when excess solar energy is available, it is provided to the electrolyzer, which creates hydrogen and oxygen gas from on-board liquid water. The accumulated gases enable the fuel cells to entirely sustain the night-time electrical load requirements. If this type of regenerative power system can be designed in such a way that the excess energy available during the day light hours is sufficient to generate enough reactants to fuel the fuel cells through the night, then it is theoretically possible for the aircraft to stay aloft indefinitely.

Although this concept never came to fruition, the above design approach was adopted in the early phases of the Helios project when the RFC system was still under development. As shown in Figure 76, there is a clear resemblance between the two energy balance diagrams. The same design approach was also used to design one

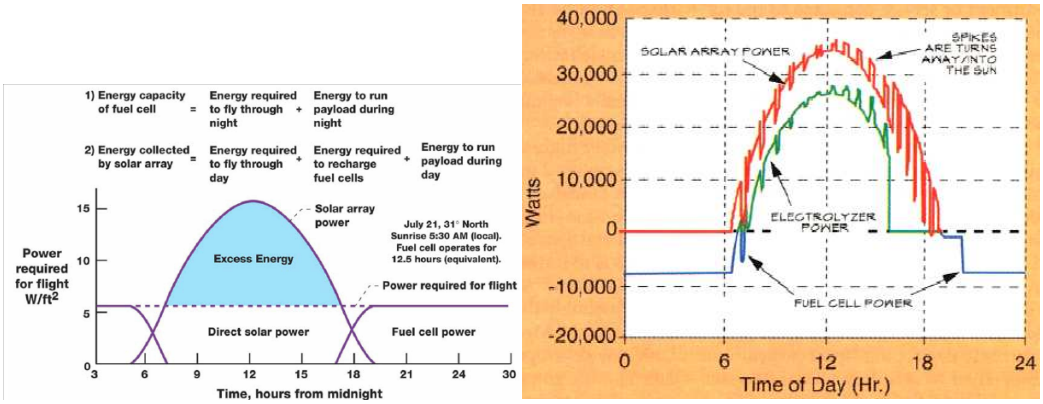

(a) Original Diagram as Conceived for HAPPs

(b) Helios Energy Balance Diagram

Figure 76: Daily Energy Balance Diagrams [192, 186]

of two concepts for a long endurance Mars flyer [193]. Another LaRC study, published in 1984, extended the same algorithm to analyze a non-regeneratively powered solar HAPP with an endurance capability of several days, rather than months [101].

A.1.2.2 Emissionless Transport Aircraft Study

Unlike the previous HAPP studies, a more recent LaRC-sponsored design study of a fuel cell powered aircraft was motivated by environmental concerns rather than a need for a new type of aviation mission. Concerned about water vapor emissions from transport aircraft at altitudes above 25,000 ft, LaRC commissioned MSE Technology Applications to investigate a wide array of advanced and breakthrough energy-related technologies - collectively termed "advanced energetics" by MSE - that could help NASA address the global warming issue [110].

Over the course of this work, a conceptual design study of an advanced transport aircraft powered by SOFCs was implemented [109]. As shown in Figure 77, the idea was to assess the feasibility of a totally "emissionless aircraft" that would retain all of the product water on-board during cruise, thereby emitting nothing to the atmosphere above 25,000 ft. The emissionless aircraft concept was further endowed

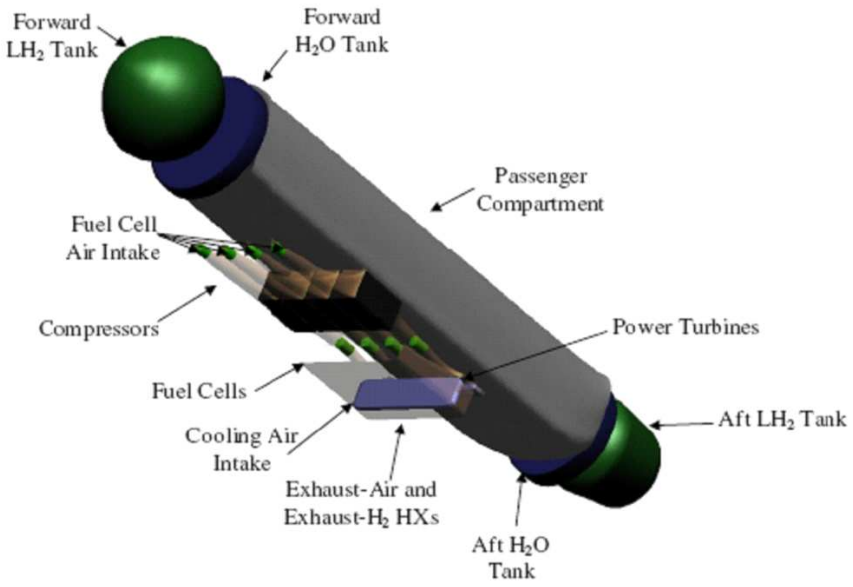

Figure 77: Internal Fuselage Arrangement of Emissionless Transport [110]

with the following advanced energetics elements: improved aerodynamics; insulated

storage tanks for liquid hydrogen fuel; cryogenically cooled, but not superconducting, electric motors for driving propulsion fans; and carbon nanotube composites or foamed metals that could offer a structural weight reduction up to a factor of 3. The design analysis was aided by a LaRC computer program named Flight Optimization System (FLOPS). FLOPS is one of LaRC's flagship legacy codes that allows the sizing of a conventional aerovehicle via a process similar to the specific parameter-based approach shown in Figure 10(b) [194]. The code is also capable of evaluating the performance of a fixed-size aircraft, such as range and endurance.

Because the envisioned aerovehicle was an unconventional concept, whose weight at take-off would be less than its weight at landing, LaRC engineers made the necessary modifications to FLOPS so that it could be used to evaluate the performance of the emissionless aircraft concept. All component weight figures, as well as efficiency values required for FLOPS, were drawn from MSE's benchmarking of advanced energetics. Based on the company's survey results, two technology growth scenarios were created and subsequently applied in designing an emissionless, 300 PAX transport aircraft. MSE concluded that such an emissionless transport vehicle would be feasible in the near term with advanced technologies, but would be made more practical with long-term, breakthrough energetics.

A.1.3 Experimental and Modeling Work from NASA Glenn Research Center

In recent years, researchers at NASA GRC have actively pursued and sponsored research related to both regenerative and non-regenerative fuel cell systems. The center's involvement with RFC systems began with its support of the ERAST project. Specifically, experimental work on the prototype RFC system intended for the Helios aircraft was carried out there. Moreover, a parallel effort was undertaken to develop energy storage systems based on the more advanced Unitized Regenerative Fuel Cells (URFCs).

Much of the impetus behind GRC's investigation into non-regenerative fuel cell technology was provided by the "NASA Aeropropulsion Vision," first reported by Campbell in 2003 [195]. This vision acknowledged the potential contributions of fuel cell based aeropropulsion to enabling the environmentally friendly expansion of aviation under the Alternative Energy and Power Revolution. Consequently, both PEMFC and SOFC system architectures were studied as candidate alternatives to the current family of aeronautical ICEs. Special emphasis was placed on creating new computational models that would allow the quantitative assessment of fuel cell based aeropropulsion systems.

A.1.3.1 Work Associated with Regenerative Fuel Cell Systems

Since January of 2000, a dedicated test stand capable of evaluating the performance of electrolyzer technology has been in operation at the Rocket Combustion Laboratory of GRC. Another stand-alone rig that allows the testing of a PEMFC stack has been operational since September of 2000. Both stands allow the open-loop characterizations of multi-cell stacks and were utilized in support of the ERAST program. For example, the hydrogen-oxygen fuel cell test stand was used multiple times to assess the reliability of the PEMFCs intended for the Helios UAV over the course of the stack's development [196].

Building upon these existing capabilities, a new test rig for measuring the performance of a RFC system was constructed between 2002 and 2003 [197]. Even though the RFC system was no longer part of the Helios program by the end of 2001, the funding for developing the rig was, nonetheless, provided by the ERAST program. Unlike its two predecessors, this particular test rig was designed to be a closed-loop system capable of simulating a diurnal charge/discharge cycle of the original Helios concept explained in §A.1.2. A DC power source was integrated to simulate the *charging* cycle done by the PV cells unto the electrolyzer during daylight hours, while a

DC sink-load designed to dissipate the power output from the PEMFCs was present to simulate the nocturnal, or *discharging*, portion of the cycle. Ancillary equipment, such as pumps, valves, pressure regulators, tubing, hydrogen and oxygen storage tanks, and instrumentation, required for the control, monitoring, and data acquisition of the RFC system were also part of the test rig. The completed version is able to house a single PEMFC stack of up to 5.25 kW (100 A at 52.5 V) and a 15 kW (150 A at 100 V) electrolyzer stack for a cyclic charging/discharging duration of 12 hours. The test rig was recently benchmarked as the state-of-the-art RFC energy storage system in the conceptual study of a newer, self-contained and pressure-following RFC architecture [198].

Another research thrust that is worthy of mentioning is the work related to URFCs. A URFC is a novel, dual-function fuel cell, whose membrane-electrode-assembly supports both electrolysis and redox reactions. Compared to a conventional RFC system, some of the more obvious, advantageous implications of an energy storage system based on URFCs are reduction in system weight and volume, as well as reduction in complexity, due to reduced-part-count. Therefore, URFCs have been investigated under the Energetics Research Program for various aerospace applications, including HALE vehicles. Burke first proposed a compact URFC system that utilizes its gas storage tanks as thermal control surfaces for drying and humidifying the reactants [199]. This concept synergistically exploits the cyclic temperature variations of the tank surfaces to either remove excessive moisture content from the product gases in electrolyzer mode or humidify the reactant streams in fuel cell mode. Subsequent analyses and tests in a thermal vacuum chamber confirmed the potential of the concept to achieve a specific energy greater than 400 W-hr/kg [200].

A.1.3.2 Tool Development for Non-Regenerative PEMFC Architecture

Initial efforts related to non-regenerative fuel cell technology were focused on developing in-house parametric models for an electric aeropropulsion system architecture based on PEMFCs. As shown in Figure 78, the architecture was envisioned to consist of an electric motor that drives a propeller; an electric compressor system for pressurizing the fuel cells; ancillary equipment, such as a humidifier and a heat exchanger, as well as other auxiliary components; a battery acting as the secondary power source; and a PMAD system. In addition, ten different methods of hydrogen storage were

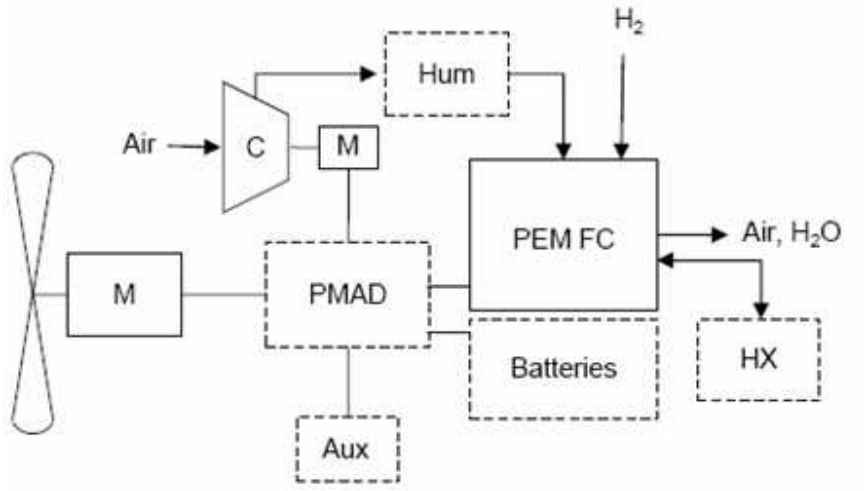

Figure 78: GRC's Baseline PEMFC Aeropropulsion System Architecture [201]

investigated in conjunction with the above architecture [118].

Overall, the modeling approach taken by researchers was to first create individual models for each sub-system component, and then to integrate them into a unified environment for future high-level simulations [201]. Weight models for all of the illustrated sub-system components were developed, while analysis models that allowed performance prediction were developed only for the propeller, electric motors, compressor, and PEMFCs. In-house expertise, such as guidance from the Electrochemistry Branch, as well as a variety of sources outside the aerospace sector, were reportedly consulted in obtaining the required data and assumptions for building each

model. Three levels of technology assumption - namely, off-the-shelf, intermediate, and advanced - were also incorporated into the weight models. Lastly, all developed models were encoded into the Numerical Propulsion Systems Simulation (NPSS) environment, which provided an integrated framework to evaluate the new aeropropulsion system architecture as a whole. Although NPSS was originally developed to be used primarily for steady-state, zero-dimensional GT and rocket engine analysis [202], it possesses many features which makes it an attractive platform for integrating new aeropropulsion models (*e.g.*, an object-oriented programming structure, built-in thermodynamic and chemical equilibrium analysis capability, map generating capability for turbo-machinery, and an input/output structure that is compatible with most aircraft sizing and synthesis codes such as FLOPS).

The resulting NPSS environment was subsequently utilized for several retrofit studies of existing airframes with the PEMFC aeropropulsion system shown in Figure 78. For example, Freeh et al sized an aeropropulsion system of this architecture to meet the peak shaft power of the Rotax 912 engine, which is a small ICE for general aviation (GA) aircraft [201]. A follow-up study by Berton et al assessed the impact of fuel cells at the aerovehicle level by simulating a retrofit of a MCR01 airframe, which is actually powered by a single Rotax 912 engine, with the same PEMFC aeropropulsion system [102]. A series of mission analyses were performed on the retrofitted electric GA aircraft using FLOPS to evaluate its new still-air range capability. As this was a retrofit study, the aircraft was never re-sized. Wickenheiser et al expanded upon these earlier studies to derive how much advancement would be required to make the same PEMFC aeropropulsion system feasible for larger, short-range transport aircraft, such as an Embraer ERJ145 and a Boeing 717-200 [103]. Again, no sizing was attempted for either aerovehicle in deriving the requirements. Ultimately, GRC's modeling activities outlined above, culminated in a collaborative study with LaRC [203]. The same analysis environment in NPSS was run in conjunction with

FLOPS to design a hydrogen fuel cell powered, blended-wing-body aircraft shown in Figure 79(a). Since this was a conceptual design study of an unconventional looking aircraft, the sizing capability of FLOPS did get utilized as per the mission segment shown in Figure 79(b). Unlike the earlier LaRC-sponsored study which opted for

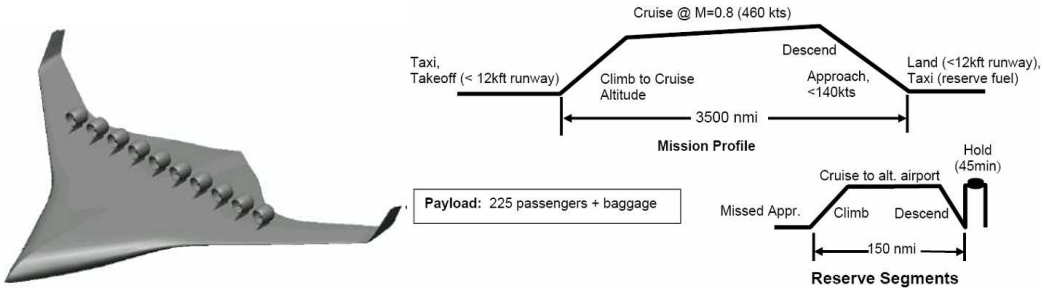

(a) Notional Quiet Green Transport

(b) Mission Profile for Vehicle Sizing

Figure 79: Quiet Green Transport Study [203]

an emissionless concept, the LaRC study limited the aircraft's maximum cruise altitude to 25,000 ft, in order to allow the emission of water vapor from the fuel cell aeropropulsion system.

As a result of the aforementioned retrofit and sizing studies, a number of insights into the propulsion-level characteristics of the PEMFC aeropropulsion system were gained. The architecture of the system resulted in a weight breakdown, in which the weight of the fuel cells themselves were not the heaviest. When the assumptions regarding the technology levels of sub-system components were extrapolated from GA to commercial transport applications, the gravimetric characteristics of the PMAD system and ancillary equipment were found to be the limiting factors. The low specific power of these components contributed towards the overall weight of the most advanced PEMFC aeropropulsion system to be still moderately heavier than that of a conventional ICE, when both systems were designed for the same output power. While carrying cryogenically cooled, liquid hydrogen in insulating tanks was determined to be the most gravimetrically and volumetrically efficient method of fuel

storage, the complexity and weight penalty associated with integrating such a tank into an airframe still remain a non-trivial challenge. Collectively, all of the above factors prevent all but the most aggressively forecast PEMFC aeropropulsion systems to be considered feasible for the range, speed, altitude, and payload requirements of commercial transport missions.

A.1.3.3 Tool Development for SOFC Architecture

The latest publications on fuel cell modeling work indicate that the center's focus has shifted from PEMFCs to SOFCs. More specifically, the architecture, which has been the subject of numerous studies, is that of an SOFC/GT hybrid system, briefly introduced in §1.2.1. A number of factors appear to have motivated researchers to examine the aeronautical potential of SOFCs. Above all, the higher operating temperature ranges of SOFCs enable them to have much higher electrochemical efficiencies than PEMFCs. High-temperature operations also allow a meaningful synergy with bottoming cycles, such as those of GT engines, in improving the overall system efficiency, in addition to increasing the likelihood of direct-reformation. Both aspects can have synergistic implications for aerovehicles, whose performance can be sensitive to the fuel fraction. Furthermore, SOFCs are inherently fuel-flexible, unlike the PEMFCs that require extremely pure hydrogen, as these solid-state cells are quite tolerant of CO and CO_2. Therefore, an SOFC-based aeropropulsion system could utilize ordinary hydrocarbon fuels that are commonly in use today, such as Jet A, without the logistical, infrastructural, or storage concerns that are associated with using hydrogen as a new aviation fuel. This is an additional advantage from a vehicle-level perspective, as hydrogen, even in its liquid state, is not as volumetrically energy dense as any liquid hydrocarbon fuel.

Figure 80 shows the notional SOFC/GT hybrid system envisioned for aeronautical applications. The hybrid nature of the system is shown by the bottoming cycle with

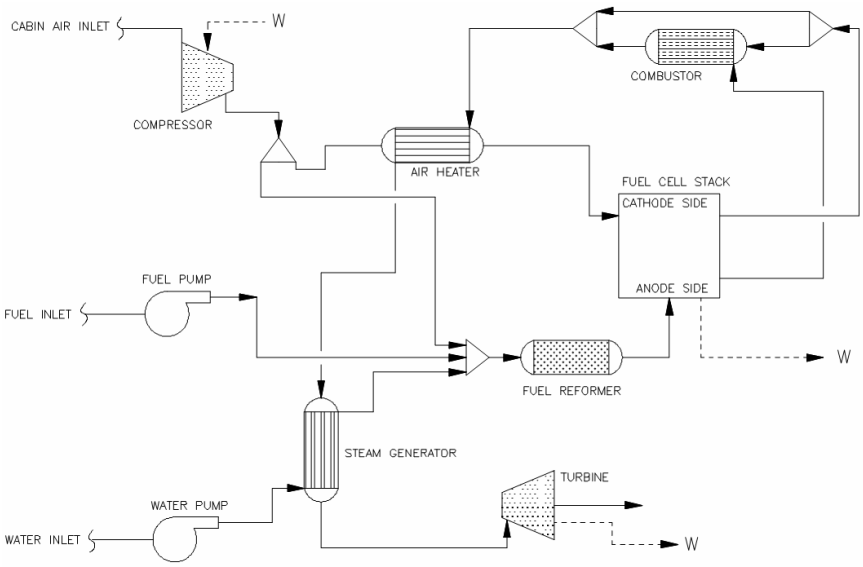

Figure 80: GRC's Baseline SOFC/GT Hybrid Power Plant Architecture [105]

the GT. As seen, the hot exit stream out of the SOFCs is further combusted to serve three purposes: to match the air temperature to that of the stack temperature, which can be in the range of 700 to 1100°C, prior to the oxidant stream's insertion into the cathode; to generate the steam required for the reformer from liquid water; and finally to drive the radial turbine, which in turn, drives the centrifugal compressor for air delivery and stack pressurization. Compared to the PEMFC architecture of Figure 78, the hybrid architecture is a more detailed topology of what constitutes the fuel cell system itself. It would, thus, be more appropriate to call the shown architecture a power plant than a propulsion system, as links to the components such as PMAD, electric motor, and propulsor are not included.

The NPSS was once again employed as the framework for integrating the subsystem analysis and sizing models. Unlike previous models for the PEMFC aeropropulsion system, a concerted effort was made to increase the fidelity of the assessment capability by minimizing the number of empirical models. For instance, Freeh et al [104] developed a parametric, bulk SOFC voltage model from first electrochemical principles, rather than curve-fitting existing data, an approach that was adopted

for modeling the PEMFC. The performance of all remaining components could be adequately modeled through the use of built-in heat exchanger, combustor, turbomachinery, and chemical equilibrium modules in NPSS. Tornabene et al [105] developed parametric weight and volume models for all of the sub-system components shown in Figure 80. The models were based on a minimum number of empirical relationships, as most of them contain physics-based, standard industrial practice (*i.e.*, textbook type equations). Models for estimating the weight and dimensions of other sub-system components that are invisible in Figure 80, such as interconnecting piping and tubing, hot box assemblies, and starter/generator, were also included.

Together, these models were subsequently applied to the design of a large, commercial transport class SOFC/GT hybrid APU. Both packaging [106] and off-design analysis [107] results have been reported. Most recently, a modified version of the simulation environment was used to assess the applicability of a cryogenic hydrogen-fueled hybrid SOFC/GT power plant for UAV applications [108]. This latest -sponsored study found that a mission duration of at least 10 days would be required for a meaningful trade between lowered fuel weight and increased power system weight fractions to occur.

A.1.4 Other National Laboratories

The NFCRC, located at the University of California at Irvine, is one of the few public laboratories in the U.S. dedicated to experimental fuel cell research. One area of the center's specialty lies with the beta testing of prototype fuel cell components and hardware. Such experimental work is crucial in providing new insights into the behavior of a previously untried fuel cell application, for which theoretical research alone may not be able to sufficiently predict the figures of merit (*e.g.*, performance, reliability, usability, etc.).

Consequently, recent interest in the aeropropulsion applications of fuel cells motivated Pratt et al at the NFCRC to measure the performance of an air-breathing PEMFC stack at lower-than-atmosphere pressures [204]. A test environment that could simulate the atmospheric conditions of up to 55,000 ft was created using a vacuum chamber, although data pertaining to altitudes of up to 35,000 ft were analyzed. The major contribution of the study was identifying the dominant loss mechanism responsible for degrading an air-breathing fuel cell's output voltage with decreasing ambient pressure.

In November of 2005, the NRL became the first national laboratory in the U.S. to successfully test-fly a fuel cell powered UAV [205]. A small group of NRL researchers integrated a fuel cell power plant consisting of a 100 W Protonex PEMFC, high-pressure hydrogen tank, radiator, humidifier, water and air pump, hydrogen purge valve, and timer circuit into a customized sail plane design named Spider-Lion [206]. Weighing at just 5.6 pounds and with a wingspan of 7.2 ft, small enough to be classified as a Micro Aerial Vehicle (MAV), the Spider-Lion MAV reportedly flew for 3 hours and 19 minutes on 15 grams of hydrogen. Future plans for the NRL project include replacing the compressed hydrogen gas tank with chemical hydrides. The resulting method of hydrogen storage would be the first step toward improving the Spider-Lion's endurance beyond the current MAV threshold of 8 hours. Figure 81 illustrates the Spider-Lion MAV, Protonex fuel cell, and custom-made ancillary equipment that were integrated into the airframe. The success of the Spider-Lion allowed Protonex to be awarded a contract with the U.S. Air Force to further perfect the company's technology for military UAV applications [207].

A.2 Activities in the Aviation Industry

To date, only a handful of companies in the aviation industry have expressed an interest in pursuing fuel cell technology as a revolutionary means of aeropropulsion. A

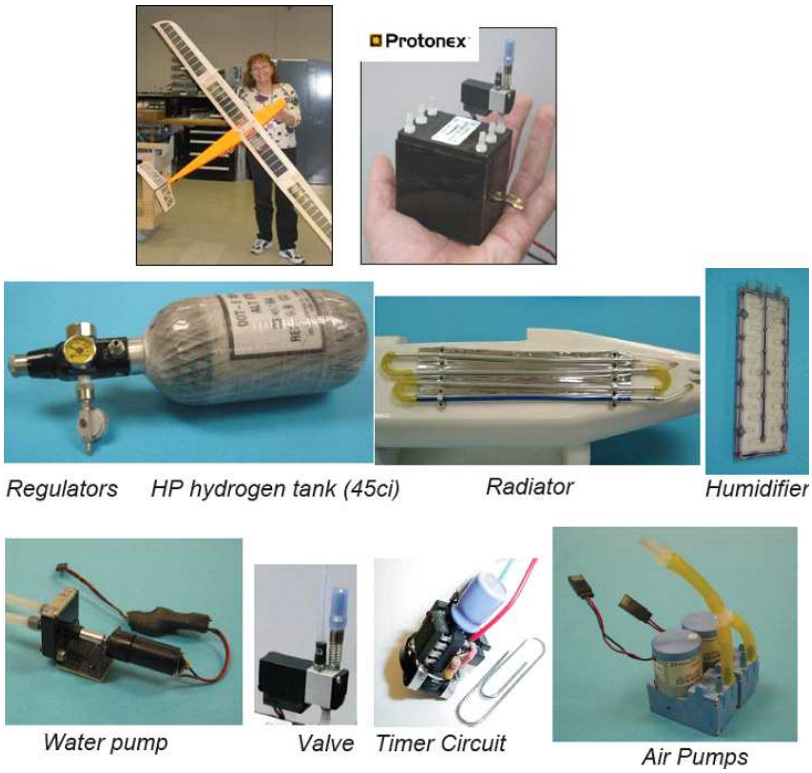

Figure 81: NRL's Fuel Cell Powered MAV [206]

couple of these companies have already begun to work on producing a scaled-down prototype or a full-scale technology demonstrator. Perhaps, due to the competitive and high-risk nature of such ventures, there are currently very few publications or publicly available data regarding the industry's achievement with fuel cell aeropropulsion technology.

A.2.1 AeroVironment, Inc.

Drawing on the company's past success with solar powered electric aircraft, AeroVironment has once again achieved a couple of industry-firsts with fuel cell aeropropulsion. At present, it is the sole member of the industry that has reported, not one, but two cases of successful flight of uninhabited drones with fuel cells as the main on-board power source.

The world's first fuel cell powered aircraft is the Hornet MAV which flew on

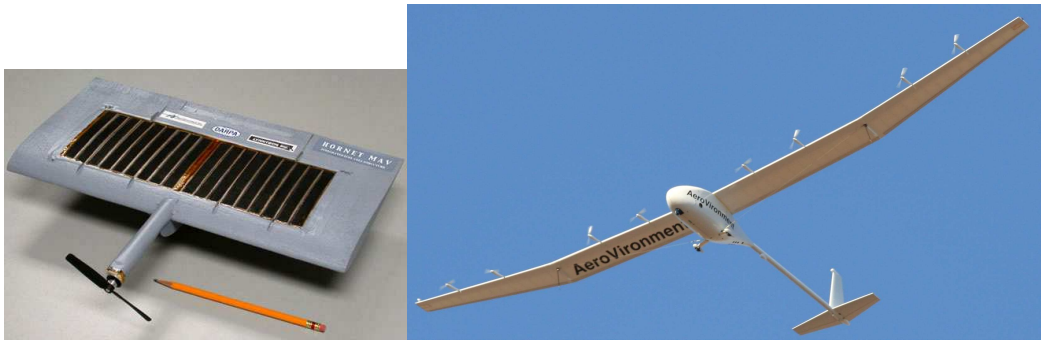

(a) Hornet MAV (b) Global Observer UAV

Figure 82: AeroVironment's Fuel Cell Powered Aircraft [208, 121]

March 21, 2003 [208]. The MAV, shown in Figure 82(a), with a wingspan of 15 inches and a gross weight (including the hydrogen fuel) of 6 ounces, was flown a total of three times with a combined endurance of 15 minutes. The program was sponsored by the U.S. Defense Advanced Research Projects Agency: specifically, the Synthetic Multifunctional Materials program. As such, the fuel cells also acted as load carrying members of the wing. The small fuel cell system built by Lynntech, which also developed the RFCs for Helios, was supported by a unique hydrogen delivery method that allowed an average output power of 10 W during flight. A dried, solid pellet reportedly released hydrogen gas when hydrated with liquid water, which was also carried on board.

Following the success of the Hornet, AeroVironment moved on to develop the Global Observer, the world's first UAV to be powered by liquid hydrogen fueled fuel cells [121]. A scaled-down prototype, shown in Figure 82(b), was successfully test-flown on May 26, 2005 and again on June 2, 2005. The 50-ft wingspan prototype also demonstrated that the aircraft could be both remotely piloted and autonomously flown. The company's experience with the Helios project aided the design of the Global Observer prototypes' structures, propulsion, and control systems. Eight electric motors are distributed along the wing span, similar to the distributed propulsion

scheme chosen for the Helios platform. Although AeroVironment designers are planning multiple variants of the planned UAV, the final production version's wingspan and gross weight will be limited to 250 ft and 10,000 lbs, respectively [209].

Anticipating the need for a HALE aircraft for various military (surveillance, reconnaissance, intelligence gathering), government (border patrol, weather monitoring, hurricane tracking), commercial (telecommunications), and scientific (aerial imaging, remote sensing, agricultural/environmental data acquisition) missions, the Global Observer project was pursued with internal company funding. The company's decision to abandon solar cells, due to their high cost and complexity, will nonetheless, restrict the endurance of the UAV to 7 to 10 days, at an operating altitude of 65,000 ft and a payload of up to 1000 lbs. To augment this shortcoming, AeroVironment has proposed operational concepts, in which at least two Global Observer UAVs operate one after another, to enable missions requiring longer endurance. AeroVironment is currently publicizing that a full-scale Global Observer can be produced within 2 years of a customer's order.

A.2.2 The Boeing Company

In 2003, the Boeing Company announced its intention to develop a manned fuel cell demonstrator airplane. A Diamond HK 36 Dimona glider was to be retro-fitted with a new aeropropulsion system, based on PEMFCs, as shown in Figure 83. The presence of a backup battery, intended for starting up the fuel cells and augmenting the primary power system in short-duration, high-power maneuvers, such as take-off and climb, is consistent with the architecture envisioned by researchers, shown in Figure 78. Boeing designers opted for the high-pressure gas storage method over liquid hydrogen because the demonstrator was not meant to have a range greater than of 100 nmi. Originally scheduled for flight in 2004, the launch date kept getting delayed to early 2005 [211] to the middle of 2006 [212]. At the time of this writing, however, no new information

Figure 83: Boeing's Planned Fuel Cell Demonstrator Airplane [210]

regarding this project has been reported since September of 2006, and Boeing is no longer publicizing a definite date for the demonstrator's maiden flight [213].

Working independently from the Boeing Research & Technology Europe center in Madrid, which is leading the fuel cell demonstrator airplane program, Phantom Works carried out a comparative study of aeropropulsion system architectures based on SOFC, PEMFC, and ICE technologies [111]. The hypothetical application was a notional HALE UAV, cruising at an altitude of 60,000 ft with an endurance of 14 days. For this study, Atreya et al set 2010 as the target year for all architectures to reach TRLs of 6, and assumed a common fuel storage and delivery method for all of the studied architectures. Liquid hydrogen, stored on board cryogenically in light-weight insulated tanks, was the sole option considered due to the low volumetric density of hydrogen in gaseous form. In compliance with MIL-STD-704, fuel cell systems were sized so that an output voltage of 270 V could be maintained within a tolerance band of 10% and withstand a "high wind" event, modeled as a flight scenario requiring 1.75 times the power level at cruise. The study concluded that although the SOFC technology has the lowest TRL amongst the reviewed candidate technologies, its higher thermal efficiency, when reviewed at the vehicle level, in terms of realizable

endurance and hydrogen fuel weight, allows an aeronautical power plant, based on SOFCs, to be the most attractive option for HALE applications.

A.2.3 Cessna Aircraft Company

Anecdotal accounts of Cessna's inquisitiveness into fuel cells have been reported as early as 2003; for example, see Ref.[204]. The first technical publication that can be traced to the Cessna Aircraft Company is the study by Chang and Gallman, who tested the applicability of a 1.2 kW Ballard Nexa fuel cell system as a replacement for GA aircraft batteries [214]. Additionally, other published sources, whose authors are affiliated with Cessna, are those of Wentz and Mohamed [215] and Wentz et al [185]. Wentz and Mohamed compared the feasibility of hydrogen-fueled ICEs with that of a fuel cell aeropropulsion system for a wide range of representative aerovehicles, including a wide body transport, medium transport, business jet, and single engine propeller airplane. The follow-up work by Wentz et al was the same type of comparative study between a single engine propeller, business jet, twin-turboprop, and regional jet GA aircraft.

For each class of aircraft, the distribution of weight fractions amongst the fuel, propulsion system, and fuel storage tanks were re-calculated within a prescribed boundary of maximum gross weight and range. The payload weight was maintained, and so was the basic (wing, structure, cabin) configuration of each aircraft. The gravimetric characteristic of the fuel cell power plant was allowed to be altered freely in order to maintain the same thrust-to-weight ratio and maximum gross weight. For all concepts, the fuel cell efficiency was estimated to be fixed at 60%.

It is important to comprehend how the Cessna studies are different from the retrofit studies done by NASA, as presented in §A.1.3. The former efforts aim to determine what levels of technical maturity fuel cells need to be attained in order for existing aircraft to not be penalized, in terms of mission capability and gross

weight, whereas the latter studies assess how much vehicle-level performance can be squeezed out of an aerodynamically efficient airframe with an immature power plant technology. Furthermore, the two Cessna studies suggest the most efficient (both aerodynamically and structurally) layout configurations for integrating fuel cells to conventional aircraft architectures.

A.2.4 Pratt & Whitney and United Technologies

A collaborative study done in 2003 between researchers at Pratt & Whitney and United Technologies Corporation discuss the potential, implications, and challenges of adapting hydrogen as a new aviation fuel [216]. Although fuel cells were not the specific focus of this particular study, Brand et al do conclude that a "breakthrough in fuel cell technology " would be needed before the electric fan propulsion concepts can be commercially viable. Because larger aerovehicles usually operate at flight regimes which exceed the performance limitations of most aircraft propellers, in terms of required forward flight speed, as well as thrust, ducted fans, driven by electric motors, are envisaged to be applicable to future aircraft of the regional/commuter types, and also for even larger commercial passenger aircraft [103]. Figures 84(a) and (b) illustrate the synergistic application potentials of fuel cell technology, as envisioned by NASA, with such motor-driven thrust fans. The first sub-figure shows how multiple PEMFC systems, embedded along an aircraft's wingspan, can serve the dual purpose of energy conversion and structural load sharing. Each fuel cell system may be designed to power one or more of the laterally distributed ducted fans, whose unconventional configuration offers further aerodynamic and acoustic benefits at the vehicle level. Another airframe-embedded propulsion concept is shown in Figure 84(b). In this common-core, multi-propulsor configuration, the fuel cell system, which is shown to be completely integrated with the wing-shaped airframe and the on-board sources of hydrogen, serves as a highly efficient common-core that supplies

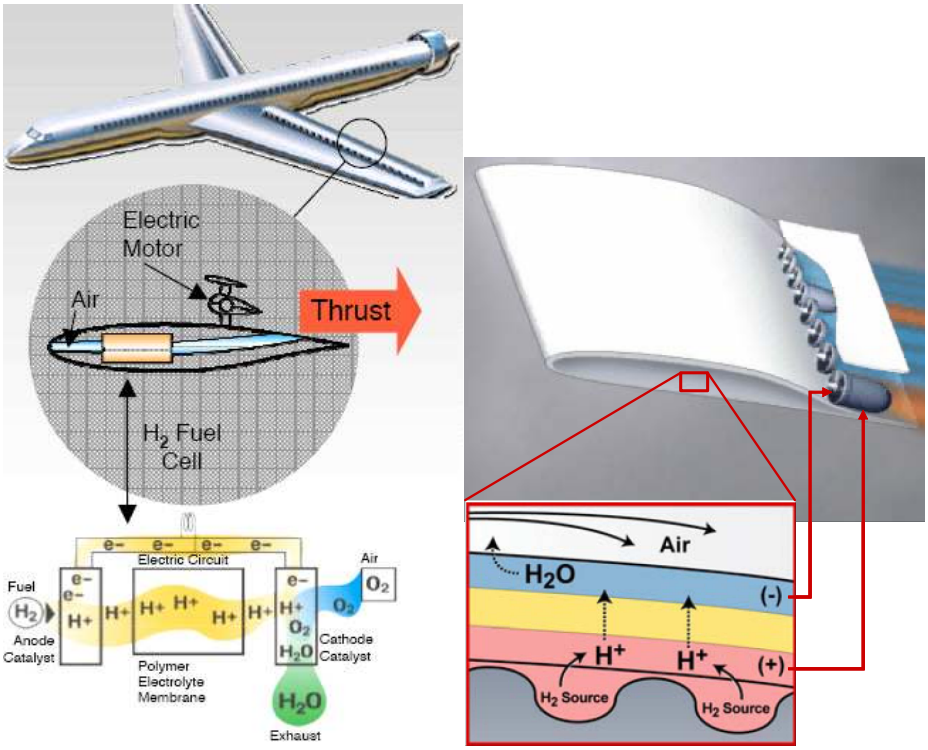

(a) Distributed Vectored Propulsion (b) Common-Core, Multi-Propulsor Fuel Cell Wing

Figure 84: Fuel Cell Powered Aerovehicles in New Era of Aviation [37, 4]

energy to multiple electric thrust fans. Such a holistic integration of the airframe, fuel cell power plant, electric motors, and ducted fans is believed to be more efficient and lighter compared to the vehicle configuration of Figure 84(a). Additionally, the mitigation of safety concerns and increased reliability are anticipated since only the flow of electric energy, and not the fuel (hydrogen), needs to be managed around the various sub-systems. The study assigned a TRL of 2 to this method of fuel cell based aeropropulsion.

A.3 Contributions from Academia

Academia often serves as a neutral ground where scholars from different professional backgrounds can share information in order to advance the state of human knowledge. It is also the responsibility of academic organizations to facilitate the dissemination

of such knowledge through higher education. Therefore, the academic community is currently in a unique position to make significant contributions to the emerging field of fuel cell aeropropulsion by encouraging peer-reviewed research and fostering the next generation of fuel cell experts. This section reviews the achievements of two academic programs in the U.S., in which small groups of students have succeeded in designing, building, and test-flying fuel cell powered aircraft.

A.3.1 Georgia Tech Fuel Cell Powered Flight Project

Since the summer of 2004, an effort has been underway at the Georgia Institute of Technology, in collaboration with the Georgia Tech Research Institute, to design, build, and fly a medium-scale, remotely piloted fuel cell demonstrator aircraft. The Georgia Tech fuel cell powered flight project was led by a small team of graduate students from both the aerospace and mechanical engineering departments.

By late September of 2005, the first version of the Georgia Tech fuel cell demonstrator prototype was ready to be test-flown on battery power [217]. This initial twin-boom, pusher propeller configuration with an inverted V-tail, shown in Figure 85(a); had a wingspan of 18.04 ft and weighed 43.61 lbs, of which more than half (26.57 lbs) was the weight of the fuel cell power plant. In constructing the fuel cell aeropropulsion system, commercially available hardware was used as much as possible to minimize cost and time. The completed system, thus, consisted of a Bolly 22x20 propeller, a Hacker C50-13XL DC electric motor, and a 500W BCS fuel cell stack consisting of 32 PEMFCs. Furthermore, an air management system, a thermal management system, a hydrogen storage and management system, and a controller for the fuel cells were custom made from a variety of off-the-shelf components. Although a series of battery powered test flights were successfully done at a reduced weight of 35.9 lbs, the prototype was heavily damaged in its eleventh battery powered flight test, forcing the design team to re-construct the aircraft. During this time, members

of the design team authored two follow-on studies based on their experience with the first demonstrator prototype [218, 219].

The second version of the demonstrator was not a duplicate of the original and contained several key design modifications [220]. First, both the wing and the empennage were enlarged. Wing area was increased from 17 ft^2 to 20.24 ft^2, aspect ratio changed from 19.2 to 23, and wingspan elongated from 18.04 ft to 21.59 ft. The tail area was also increased from 3.61 ft^2 to 4.9 ft^2. Secondly, the fuselage weight was reduced by 1.67 lbs. The weight-saving was possible due to a new construction technique that utilized carbon fiber materials, as opposed to the previous fiberglass fuselage built from a custom mold. Thirdly, the weight of the fuel cell power plant was reduced by making the following modifications. The design team decided to abandon the earlier method of hydrogen storage and delivery from a system made out of $MmNi_{4.1}Fe_{0.9}$ metal hydride tanks and to, instead, adopt a system with a single compressed hydrogen tank. This allowed the hydrogen storage and management system's weight to decrease from 7.05 lbs to 2.62 lbs. Additionally, the endplates of the original BCS fuel cell stack was eliminated to reduce the stack weight from 14.06 lbs to 10.93 lbs. Both endeavors resulted in a significantly lighter aircraft, with a take-off gross weight of 36.14 lbs, without sacrificing the aerodynamic efficiencies. The two prototypes are compared in Figures 85(a) through (d).

With the plane shown in Figure 85(d), the first steady-level, fuel cell powered flight was achieved on June 15, 2006. The achievement was a first for an academic institute and the fifth overall in the world. The duration of the inaugural test flight was 50 seconds and the UAV cleared a maximum altitude of 11.48 ft. Five more test flights were completed until September 18, 2006, during which the UAV successfully completed a series of short, single circuit flight tests. Based on the data that was gathered wirelessly during these flight tests, the projected performance of this prototype, should it use the entire capacity of the hydrogen tank (192 Standard L at 30

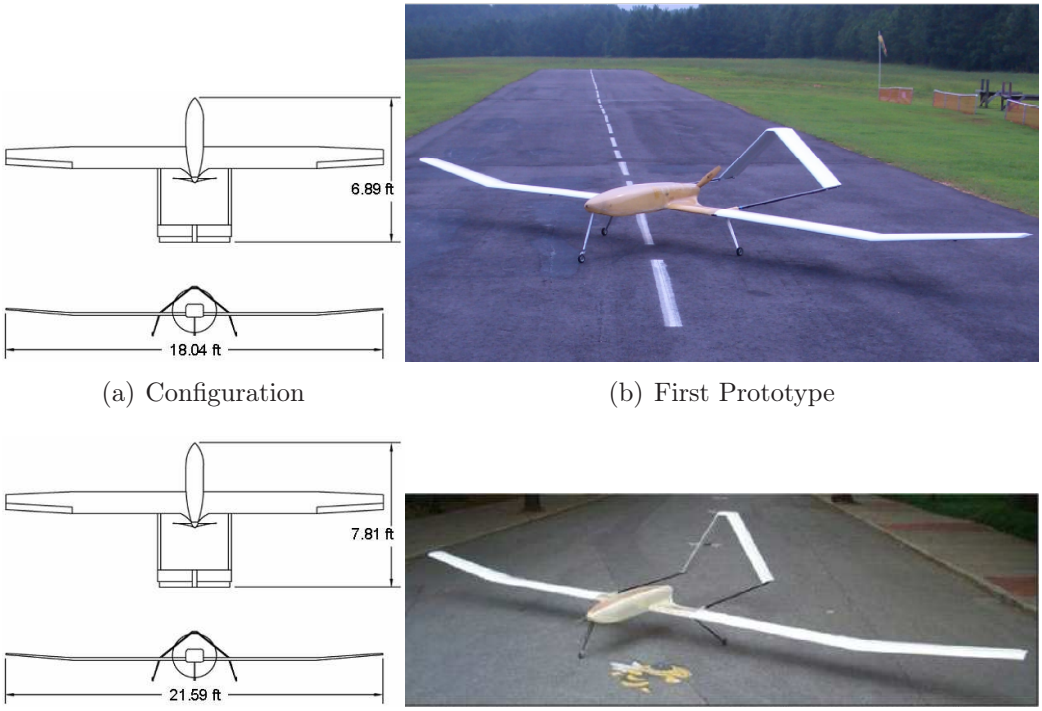

(a) Configuration (b) First Prototype

(c) Configuration (d) Second Prototype

Figure 85: Georgia Tech Fuel Cell Demonstrator Aircraft [217, 218, 220]

MPa), is 43 minutes of cruising flight at an altitude of 984 ft [221].

A.3.2 Fuel Cell Powered UAV for Environmental Research Missions

A team of undergraduate and graduate students allowed California State University, Los Angeles to become the second academic organization to remotely pilot a fuel cell powered aircraft in August of 2006. This was a culmination of an effort that has been led by the Multidisciplinary Flight Dynamics and Control Laboratory (MFDCLab) since January of 2004 [222]. Through a partnership with the Center for Environmental Analysis-Center for Research Excellence in Science and Technology (CEA-CREST), the MFDCLab has been working toward designing an autonomous UAV suitable for environmental research. Such aerial missions would require remote sampling of carbon dioxide levels in the atmosphere, for which an aerial platform that does minimal polluting is desirable for obtaining uncontaminated data. Therefore, a UAV powered

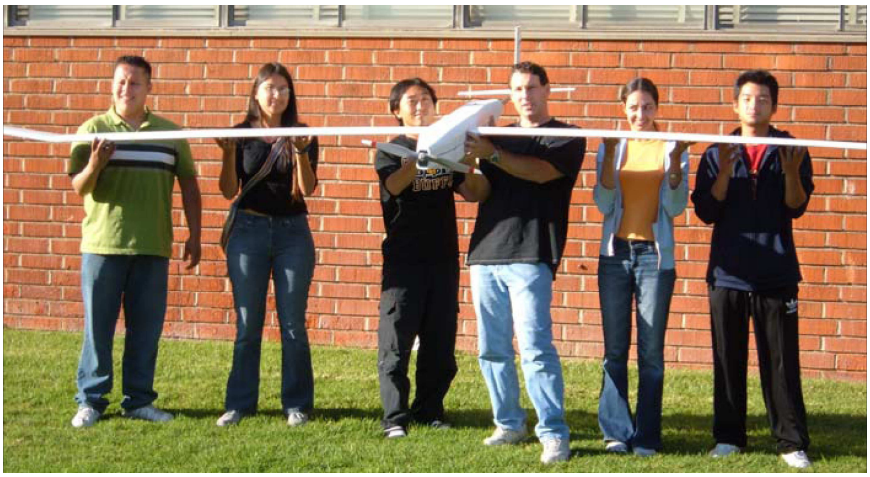

Figure 86: Fuel Cell Powered UAV at California State University, Los Angeles [223]

by a hydrogen oxygen fuel cell emitting nothing but innocuous water vapor in flight was deemed desirable by CEA-CREST.

By early 2006, the MFDCL completed the design work, as well as the fabrication of all major parts of the airframe [223]. The structure was mostly made out of composite materials, such as fiberglass, carbon fiber and aramid, to reduce weight. An FEA of the wing's structure was carried out to predict its bending and torsional frequencies. Additionally, a CFD analysis was done on the airframe to evaluate the aerodynamic characteristics. Laboratory tests of a Horizon PEMFC rated at a maximum power of 670 W and a 700 W AstroFlight motor were also carried out in parallel.

After a series of three battery powered flights, which began on June 2, 2006, the team succeeded in remotely piloting the fuel cell powered configuration, shown in Figure 86, to an altitude of 100 ft on August 25, 2006 [224]. The UAV had a wingspan of 18 ft and weighed 28.5 pounds, inclusive of a pound of payload that would be carried on an environmental science mission. It has been reported, however, that the aircraft will be tested for no additional flights and will be preserved for posterity.

Appendix B

PROPULSION-LEVEL SIMULATION ENVIRONMENT

The final version of the fuel cell aeropropulsion analysis and sizing environment, which was used to gather all of the simulation results reported in Chapter 5, is a rather complex product. Containing well over 8,300 lines of source code, the environment represents the assembly of more than 15 different legacy, commercial, and home-grown tools. More than 50 technical references were consulted in coding not only the individual models, but also perfecting the algorithmic structure displayed in Figure 87. What follows are brief explanations about the interdependencies between the shown on-design, sizing, and off-design steps, including the sources for the major thermodynamic, electrochemical, electromechanical, and scaling laws. More detailed documentation on both the theoretical and user-oriented aspects of the environment will be made available as a separate publication [225].

B.1 On-Design Analysis

The sequence of on-design activities begins with the specification of a reference point. Since all six downselected aeropropulsion system alternatives are propeller-driven concepts as illustrated in Figure 31, the design point can be uniquely defined in terms of flight altitude (h), free-stream Mach number (M_∞), and P_{ref}. Unless noted otherwise, this point is usually set at SLS condition for aircraft engine design, serving as the sizing point for most of the major sub-systems.

Given the reference-point altitude, a statistical moist atmosphere model outputs the molecular breakdown of the atmosphere constituents that includes water vapor. The model is based on the regression analyses reported in Ref.[226], which are valid

Figure 87: On- and Off-Design Analysis Structure

up to 160 km: well beyond the range of most air-breathing propulsion applications. In estimating the relative humidity (ϕ_{amb}) of moist air at the given h, the model takes into account both the mixing ratio and saturation mixing ratio. The former, which is the ratio of the mass of water vapor to that of dry air, is interpolated from several water vapor profiles that vary with ambient pressure and latitude [227]. The latter is estimated via polynomials found in Ref.[228] which allows the evaluation of various psychrometric charts found in the Smithsonian Meteorological Tables [229] as functions of ambient temperature and pressure values. Dividing the mixing ratio by the saturation mixing ratio finally yields ϕ_{amb}, which is especially an important quantity to know for predicting cell humidification and water management issues for PEMFC-based systems.

Next, an in-house propeller code named the Georgia Tech PROPeller program, whose heritage can be traced back to Ref [230], is capable of computing the available thrust (T_r), rotational speed (Ω), and propeller efficiency (η_p). These figures of merit are evaluated based on the number of blades (BLADT) and blade diameter (BDIA), which gets internally optimized for maximum η_p [231].

The knowledge of both P_{ref} and Ω allows the assessment of electric torque (Γ_{mm}) that must supplied by the main propulsion motor. Figure 88 shows how motor efficiency (η_{mm}) can be evaluated from a torque-speed map. Following the precedent set in Ref.[232] and reinforced in ADVISOR 2002, such efficiency maps are linearly scaled with Γ_{mm} for system alternatives with conventional motor technologies. For the advanced technology-level alternatives, the physics-based analysis method coded by Masson et al [233] is utilized to estimate the losses occurring through two types (cylindrical or discoid design) of HTS machine. Various electrical (maximum voltage or current), thermal (hot-spot temperature), or mechanical (maximum rotational speed) constraints are also taken into account during the electromechanical analyses.

In the case of the PEMFC system model, the input of five major parameters,

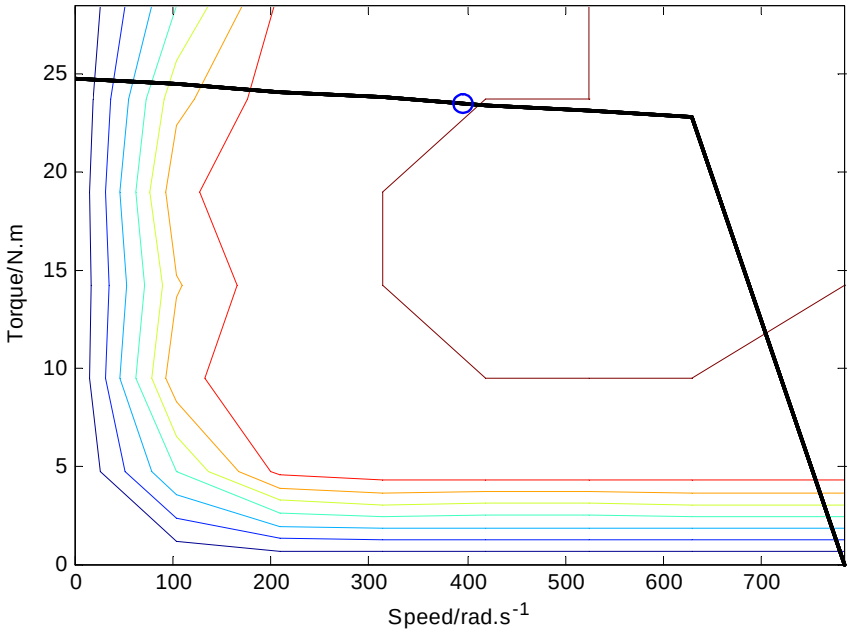

Figure 88: Example Performance Map of a Conventional Electric Motor

which are also treated as counterparts to engine cycle parameters (§5.1.3), is required to evaluate the electrochemical performance of the cells in the form of stack voltage (V_{fc}), current density (i), and η_{stk}. The determination of i at the MPP is aided by the fitting of a fourth-order polynomial to the area specific power trend, followed by its solving as a quartic equation. All stack related models - namely the voltage model, anode and cathode flow models, and membrane hydration model - are replicates of Ref.[125] with multipliers that emulate technology growth as per Ref.[117]. Unlike the PEMFC voltage model, which simulates all three technology levels off of one baseline, the voltage model for the SOFC-based systems contains a variety formulations at each technology level. For instance, OTS technology level is baselined as per Ref.[29], intermediate in accordance with Ref.[104], and advanced contains data from Ref.[129] to simulate DIR. Parameters dictating membrane hydration (a_{an} and a_{ca}) are obviously not part of the SOFC voltage model, but molar steam to carbon ratio becomes an important cycle parameter-like design variable for system alternatives with CPOX reformers.

The remainder of the on-design analysis is an iterative procedure of power balance, which seeks convergence on stack output power, while also aiming to satisfy any mass flow and psychrometric constraints. For the PEMFC-based systems, the main BOP issue is water management necessary to keep the cells well hydrated. It is assumed that an ideal cooler first matches the hot exit-air temperature out of the compressor to that of T_{stk} at the cathode, and then the relative humidity of the cooled air (ϕ_{cl}) is estimated to be compared with the desired humidity at the cathode (ϕ_{ca}). Should ϕ_{cl} be found to be less than ϕ_{ca}, then the flow rate of vapor injection can be estimated via assuming perfect humidifier control, and also checked against the steady-state water production rate on the cathode side. What is not shown in Figure 87 is an internal iterative routine that determines the correct mass flow rate of air, π_c, and the number of stoichs (NOS) through the centrifugal compressor based on the design point altitude, cycle parameter setting, and humidification concern.

A similar power-balancing iteration is necessary for the SOFC-based systems, but the BOP analysis becomes much more complicated, due to the presence of more components. Where it lacks the internal iterations regarding water management, the complexity is more than made up for by the need to calculate the mass flows, pressure drops, and temperature changes across several highly interconnected components, such as compressor, turbine, fuel pump, heat exchanger, combustor, reformer, SOFC stack, etc. Wherever appropriate, the Chemical Equilibrium with Applications program is used to aid the assessment of various thermodynamic state variables [234].

B.2 Component Sizing

The ground rule regarding the development of component sizing models was to keep everything physics-based as much as possible, with simpler regression models filling in the gaps. As indicated by both the DSM shown in Figure 19 and the process flow map of Figure 87, most components at the sub-system level are sized in terms

Table 24: Database of Conventional Electric Machines

Description of Motor	Source
Siemens AC 30 kW induction motor/controller at 216 V	ADVISOR 2002 [56]
59 kW AC induction motor/controller	Menne et al [235]
62 kW AC induction motor/controller	Menne et al [235]
Westinghouse 75 kW AC induction motor/inverter at 320 V	Lester et al [236]
AC Propulsion AC-150 motor/controller	AC Propulsion Inc. [237]
Unique Mobility 15.8 kW BLDC motor/controller at 100V	ADVISOR 2002 [56]
Lynx Motion 15 kW BLDC at 275 V	ADVISOR 2002 [56]
Unique Mobility DR156s/CR20-150 BLDC motor/controller at 180 V	ADVISOR 2002 [56]
Leroy-Somer/SAGEM 16 kW BLDC motor/controller	Ortiz et al [238]
Mannesmann Sachs 25 kW BLDC motor/controller at 130 V	Bauch-Banetzky et al [239]
Unique Mobility SR180p/CR20-300 BLDC motor/controller at 195 V	ADVISOR 2002 [56]
Unique Mobility SR218N/CA40-300L BLDC motor/controller at 300 V	ADVISOR 2002 [56]
Auxilec Thomson 32 kW BLDC motor/controller	Biais et al [240]
Honda 49 kW BLDC motor/controller	ADVISOR 2002 [56]
Aachen University 58 kW BLDC motor/controller	Menne et al [235]
Prius Japan 30kW BLDC motor/controller	ADVISOR 2002 [56]

of electrical power. But as it is delineated below, other figures of merit also play a role in estimating the overall fuel cell aeropropulsion system weight and volume. For brevity, however, only those scaling laws that were directly researched by this author are outlined herein since such relationships for the propeller code and the HTS motor concepts are documented in Refs.[230] and [233].

All conventional electric motors are sized in terms of reference-point torque. The following two scaling relationships were obtained by regressing the weight values of 5

Table 25: List of Select References for PEMFC Stack Sizing Model

Stack Constituent	Source
Membrane	Refs.[241, 242]
Electrode	ETEK [243]
Catalyst	Lee et al [244]
Bipolar Plate	Refs.[190, 245]
End Plate	Density of aluminum foam

AC induction and 11 BLDC motors (lbs) against their maximum rated torque (Nm):

$$W_{mm} = \begin{cases} 0.5217 \cdot \Gamma_{mm} + 59.381 & \text{if} \quad \text{AC} \\ 0.2090 \cdot \Gamma_{mm} + 69.362 & \text{if} \quad \text{BLDC} \end{cases} \tag{21}$$

Moreover, a correlation between motor weight and equivalent surface area given in Ref.[56] is used to estimate the diameter and length of the motor (minus the shaft), as per the shape factor, whose default value is 1.3. The data for these motors were initially found to be contained in ADVISOR 2002, and, whenever possible, those numbers were also verified against their original sources, which are listed in Table 24.

A more thorough approach was embedded in the PEMFC stack sizing model, which leverages on the characterization of system mass and dimensions in terms of basic material and geometric properties, such as number of cells, active area, thickness, density, and loading (mass per unit area). Factors are built in to modify the appropriate elements, as well as the cell active area in accordance with the technology growth plans of Ref.[117] for PEMFC stacks and assumptions outlined in Ref.[106] for SOFC-based systems. Assuming that each cell is serially connected to one another, the required number of each element can then be estimated for a given P_e. Table 25 lists some of the primary sources of information that were used in constructing the PEMFC stack sizing model. The values used in the sizing model of SOFC alternatives were extracted from the spreadsheet implementation of Ref.[105], which was made available to this author under the UAPT agreement.

Due to the lack of reliable mass and volume data regarding the BOP components

Table 26: Methods Applicable to Design of BOP Sub-systems

BOP Component	Source
Fuel / Water Pumps and Motors	Gorman Rupp Industries [251]
Compressor	Wilson et al [246]
Turbine	Wilson et al [246]
Starter/Generator	WATE [252]
Heat Exchanger	Kays et al [253]
Reformer	Refs.[128, 145]
Combustor	Lefebvre [254]
Hot Boxes	Tornabene et al. [105]
Interconnect Piping/Tubing	Tornabene et al. [105]

in the public domain, especially for PEMFC systems, there were no other viable options than to linearly estimate W_{bop} with respect to P_e. Consequently, the upper and lower ranges of BOP specific power listed in Table 15, from Ref.[201], were used in all reported simulation cases. The only exceptions to this were the compressor, compressor motor, and its controller, which were sized according to the method of Ref.[246], as well as specifications found in Refs.[127, 247, 248, 249, 250].

In the case of SOFC-based systems, this author's access to the spreadsheet tool developed by Tornabene et al [105] led to the discovery of several textbook type relationships that are also applicable to the design of fuel cell BOP components. Table 26 lists the original sources referenced in the spreadsheet, in addition to a few more that were added by this author.

Perhaps the most difficult component for which to create a sizing model was the PMAD system. The analysis of the findings from both a literature survey as comprehensive as Ref.[255] and a more top-level survey carried out in-house at ASDL led to the conclusion that such load converters do not scale well with either throughput power or current. Therefore, it was decided to adopt the distribution of PMAD specific power values listed in Table 15, as suggested in Ref.[201], until more useful sizing relationships could be developed or discovered.

The sheer diversity of available options for auxiliary energy storage compelled

a broader approach to sizing batteries and ultracapacitors. Fortunately, a Ragone plot offers not only a visually intuitive format to compare different energy storage technologies, but also a simple, yet an effective means to size them. As illustrated in Figure 39, a designer can make the judgment as to which option is the most energy-dense, power-dense, or both given the total discharge time, as per some load profile.

B.3 Off-Design Analysis

In creating the sequence of off-design analysis depicted in Figure 87, every effort was made to embrace the principles of the forward-looking modeling approach outlined in §2.2.3. All geometric and gravimetric quantities of the system are fixed as per the results of on-design analysis and sizing steps, while the system's TPMs are evaluated at an off-design point. The goal here is to evaluate the steady-state operation of the fuel cells that results in an equilibrium between the supply and demand of electrical power at a given flight condition, rather than designing the system to be capable of generating a certain amount of power.

If it is desired to evaluate the system's maximum available shaft power at an altitude of h and a forward flight speed of M_∞, then the balance of power must be found by perturbing Γ_{mm} as well as the flow rate of air supplied to the cathode ($\dot{m}_a$). The former represents the demand of power, whereas the latter controls the supply side of the equation by affecting key state variables such as π_c (and thus P_{stk}), ϕ_{ca}, and compressor efficiency (η_{cp}), which, in turn, determine stack performance (V_{fc}, i, η_{stk}, *NOS*, and ultimately P_e). If, on the other hand, the power demand is fixed at a specific partial power-lapse ratio (α_{pt}), then only the supply side needs to be iteratively controlled until convergence on P_e is achieved.

The data for constructing a normalized compressor map and its operating line came from several technical sources. Ref.[256] was helpful in generating the performance charts, and Ref.[124] was consulted in determining a corresponding operating

line. Both formulations are used in the off-design analysis of all three PEMFC-based systems. Because all three SOFC-based alternatives utilize CHP cycles, it was more appropriate to use the normalized versions of the compressor and turbine maps found in Ref.[107]. As with on-design analysis, all electrical, mass flow, and psychrometric constraints are checked during the convergence process.

Appendix C

NEURAL NETWORK MODELING

Without any exceptions, the statistical software package JMP was used to create the NNs utilized over the course of this research. The resulting surrogate models are all single-layer designs, and each neuron, or hidden node, contains the same transcendental function to fit the sampled data. For the i^{th} hidden node with n number of input variables, this structure is as follows:

$$H_i = \frac{b_0}{(1 + \exp(-1 \cdot (b_1 + \sum_{j=1}^{n} h_j x_j)))} \tag{22}$$

where x_j represents the j^{th} input variable, and the rest are constants, whose values get determined through a series of iterative, pattern-matching procedures. Subsequently, an NN model of an output, or a response, variable is constructed as a function of all fitted neurons:

$$Y = B_0 \sum_{i=0}^{m} H_i + B_1 \tag{23}$$

where m, B_0, and B_1 respectively represent the total number of neurons, as well as two additional network-level coefficients.

Appendix D

OPTIMIZER SETTINGS

Figure 89 shows the advanced optimization settings for the "Global Optimization" loop displayed in Figure 90. Its implementation resulted in the solutions listed in Tables 20, 21, and 23. Those solutions are also graphically illustrated in Figures 91 and 92. The ranges used in normalizing the first-stage design variables are the same as those listed in Table 15.

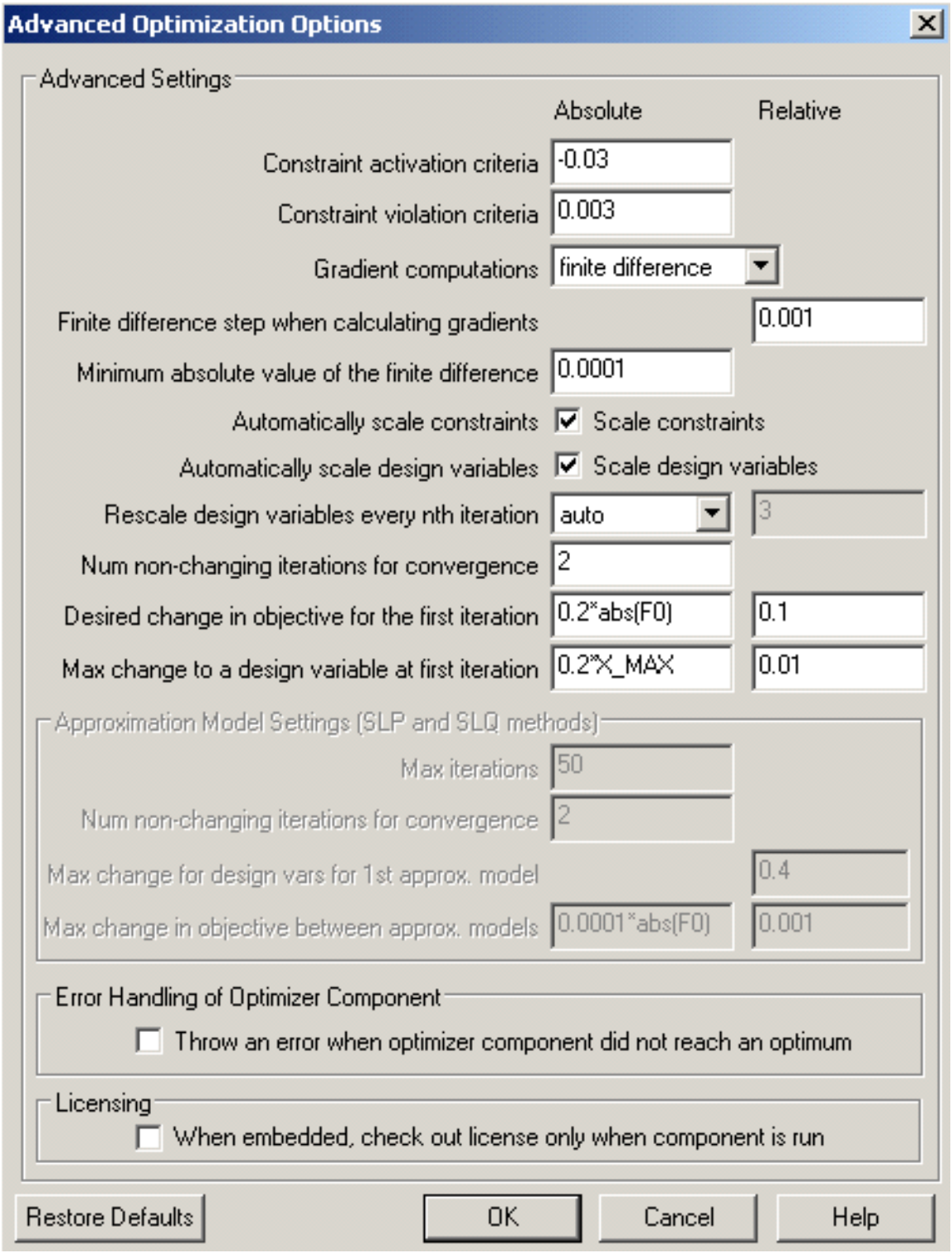

Figure 89: Advanced Optimizer Settings

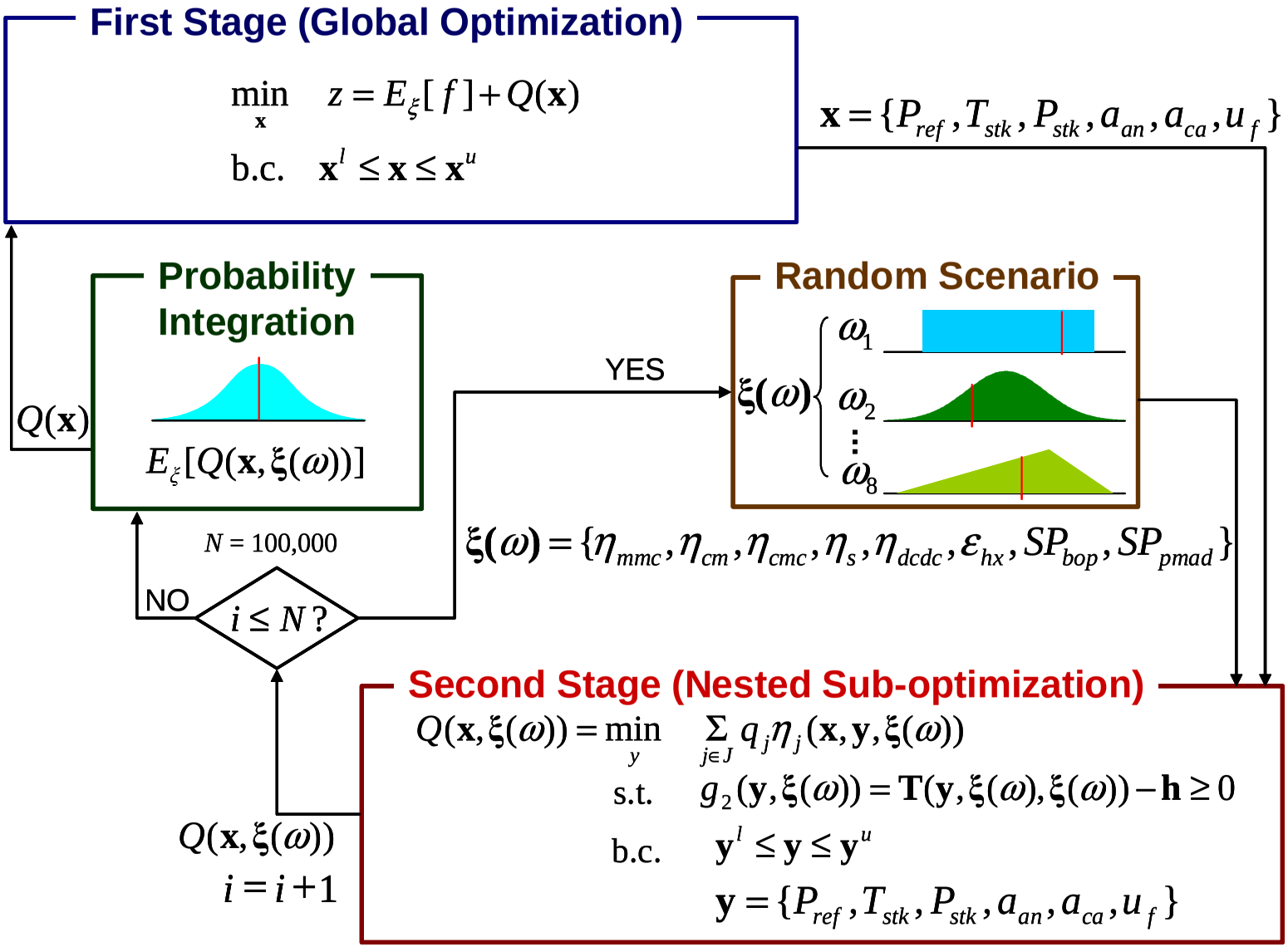

Figure 90: Optimization Flow Map of Two-Stage Formulation

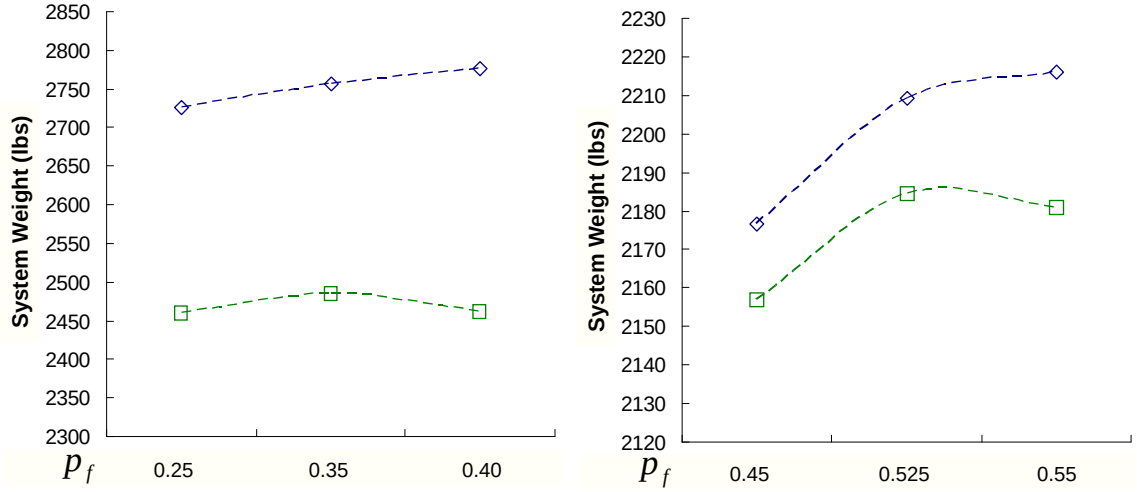

(a) Alternative 1

(b) Alternative 2

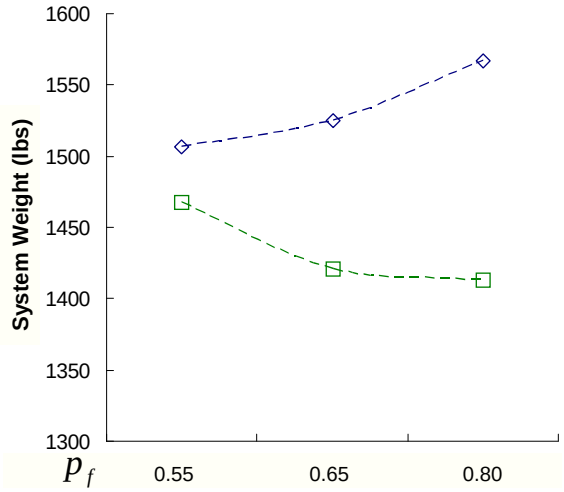

(c) Alternative 3

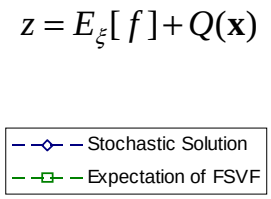

(d) Legend

Figure 91: Two-Stage Optimization Results

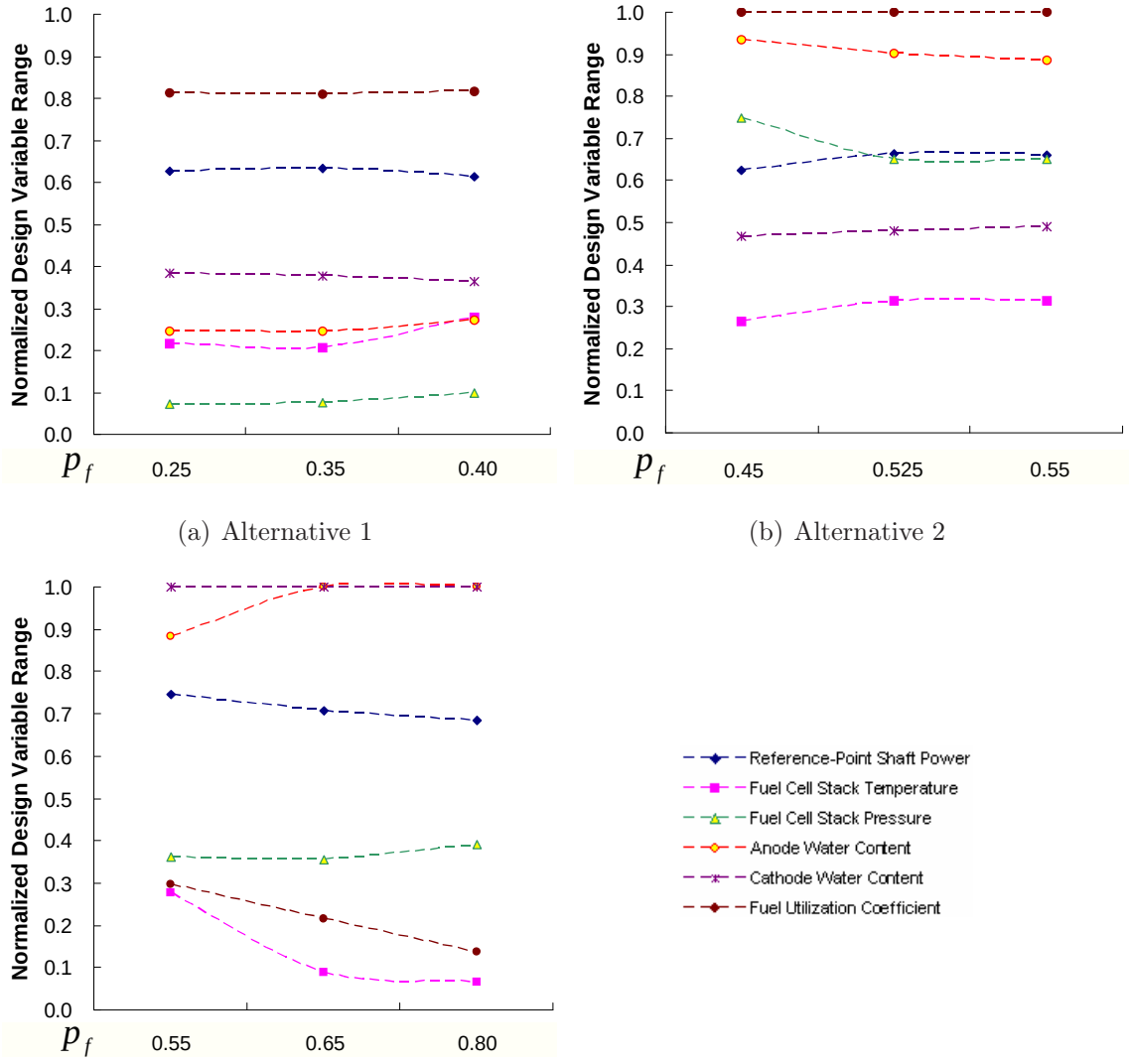

(a) Alternative 1

(b) Alternative 2

(c) Alternative 3

(d) Legend

Figure 92: Optimal First-Stage Design Decisions

REFERENCES

[1] Borer, N. K., *Decision Making Strategies for Probabilistic Aerospace Systems Design*. PhD thesis, Georgia Institute of Technology, May 2006.

[2] Soban, D. and Upton, E., "Towards Electric Aircraft: Progress Under the NASA URETI for Aeropropulsion and Power Technology," in *SAE Power Systems Conference*, (New Orleans, LA), Society of Automotive Engineers, November 7-9 2006.

[3] McClure, E., *An Evolving-Requirements Technology Assessment Process for Advanced Propulsion Concepts*. PhD thesis, Georgia Institute of Technology, August 2006.

[4] Maclin, H. and Haubert, C., "Fifty Years Down-Fifty Years to Go," in *AIAA/ICAS International Air and Space Symposium and Exposition: The Next 100 Years*, no. AIAA 2003-2788, (Dayton, OH), American Institute of Aeronautics and Astronautics, July 14-17 2003.

[5] Larminie, J. and Dicks, A., *Fuel Cell Systems Explained*. Chichester, England: John Wiley & Sons, 2nd ed., 2003.

[6] Fuel Cell Test and Evaluation Center, "Fuel Cell Basics." `http://www.fctec.com/fctec_basics.asp`. [Online; accessed 08-November-2006].

[7] U.S. Department of Energy's Office of Energy Efficiency and Renewable Energy, "Hydrogen, Fuel Cells and Infrastructure Technologies Program: Multi-Year Research, Development and Demonstration Plan - Planned

program activities for 2003-2010," tech. rep., U.S. Department of Energy, February 2005.

[8] EG&G Technical Services, Inc., *Fuel Cell Handbook*. Morgantown, WV: U.S. Department of Energy, 7th ed., November 2004.

[9] U.S. Department of Energy's Office of Energy Efficiency and Renewable Energy, "Comparison of Fuel Cell Technologies." `http://www.eere.energy.gov/hydrogenandfuelcells/fuelcells/pdfs/fc_comparison_chart.pdf`, August 2006. [Online; accessed 08-November-2006].

[10] Appleby, A., "From Sir William Grove to today, fuel cells and the future," *Journal of Power Sources*, vol. 29, pp. 3–11, January 1990.

[11] Warshay, M. and Prokopius, P., "The fuel cell in space: yesterday, today and tomorrow," *Journal of Power Sources*, vol. 29, pp. 193–200, January 1990.

[12] International Energy Agency, *Hydrogen and Fuel Cells: Review of National R&D Programs*. Paris: IEA PUBLICATIONS, December 2004.

[13] Meyer, A., Gorman, M., Flanagan, D., and Boudreau, D., "Progress in the Development of PEM Fuel Cell Engines for Transportation," in *SAE 2001 World Congress*, no. SAE 2001-01-0540, (Detroit, MI), Society of Automotive Engineers, March 5-8 2001.

[14] Fuel Cells 2000, "Fuel Cell Vehicles (From Auto Manufacturers)." `http://www.fuelcells.org/info/charts/carchart.pdf`, October 2006. [Online; accessed 10-November-2006].

[15] Fuel Cells 2000, "Fuel Cell Buses." `http://www.fuelcells.org/info/charts/buses.pdf`, May 2006. [Online; accessed 10-November-2006].

[16] Prater, K., "The renaissance of the solid polymer fuel cell," *Journal of Power Sources*, vol. 29, pp. 239–250, January 1990.

[17] Hamnett, A., "Mechanism and electrocatalysis in the direct methanol fuel cell," *Catalysis Today*, vol. 38, pp. 445–457, November 1997.

[18] Dohle, H., Schmitz, H., Bewer, T., Mergel, J., and Stolten, D., "Development of a compact 500 W class direct methanol fuel cell stack," *Journal of Power Sources*, vol. 106, pp. 313–322, April 2002.

[19] Dyer, C., "Fuel cells for portable applications," *Journal of Power Sources*, vol. 106, pp. 31–34, April 2002.

[20] Brenscheidt, T., Janowitz, K., Salge, H., Wendt, H., and Brammer, F., "Performance of ONSI PC25 PAFC cogeneration plant," *International Journal of Hydrogen Energy*, vol. 23, pp. 111–122, January 1998.

[21] Wimmer, R., "Fuel cell transit bus testing and development at Georgetown University," in *Proceedings of the 32nd Intersociety Energy Conversion Engineering Conference*, vol. 2, pp. 825–30, 27 July-1 Aug. 1997.

[22] Romano, S. and Larkins, J., "Georgetown University Fuel Cell Transit Bus Program," *Fuel Cells*, vol. 3, pp. 128–132, November 2003.

[23] Dicks, A., "Advances in catalysts for internal reforming in high temperature fuel cells," *Journal of Power Sources*, vol. 71, pp. 111–122, March 1998.

[24] Bischoff, M. and Huppmann, G., "Operating experience with a 250 kW molten carbonate fuel cell (MCFC) power plant," *Journal of Power Sources*, vol. 105, pp. 216–221, March 2002.

[25] Dicks, A. and Siddle, A., "Assessment of commercial prospects of molten carbonate fuel cells," *Journal of Power Sources*, vol. 86, pp. 316–323, March 2000.

[26] Steele, B. and Heinzel, A., "Materials for fuel-cell technologies," *Nature*, vol. 414, pp. 345–352, November 2001.

[27] Clarke, S., Dicks, A., Pointon, K., Smith, T., and Swann, A., "Catalytic aspects of the steam reforming of hydrocarbons in internal reforming fuel cells," *Catalysis Today*, vol. 38, pp. 411–423, November 1997.

[28] Hassmann, K., "SOFC Power Plants, the Siemens-Westinghouse Approach," *Fuel Cells*, vol. 1, pp. 78–84, june 2001.

[29] Liese, E., Gemmen, R., Smith, T., and Haynes, C., "A Dynamic Bulk SOFC Model Used In A Hybrid Turbine Controls Test Facility," in *Proceedings of GT2006 ASME Turbo Expo 2006: Power for Land Sea and Air*, no. GT2006-90383, (Barcelona, Spain), American Society Of Mechanical Engineers, May 8-11 2006.

[30] Xia, C., Lang, Y., and Meng, G., "Recent Advances to the Development of Low-Temperature Solid Oxide Fuel Cells," *Fuel Cells*, vol. 4, pp. 41–47, April 2004.

[31] Tachtler, J., Dietsch, T., and Goetz, G., "Fuel Cell Auxiliary Power Unit - Innovation for the Electric Supply of Passenger Cars?," in *SAE 2000 World Congress*, no. SAE 2000-01-0374, (Detroit, MI), Society of Automotive Engineers, March 6-9 2000.

[32] Read, C., Thijssen, J., and Carlson, E., "Fuel Cell Auxiliary Power Systems: Design and Cost Implications," in *SAE 2001 World Congress*, no. SAE 2001-01-0536, (Detroit, MI), Society of Automotive Engineers, March 5-8 2001.

[33] Lamp, P., Tachtler, J., Finkenwirth, O., Mukerjee, S., and Shaffer, S., "Development of an Auxiliary Power Unit with Solid Oxide Fuel Cells for Automotive Applications," *Fuel Cells*, vol. 3, pp. 146–152, November 2003.

[34] Holtappels, P., Mehling, H., Roehlich, S., Liebermann, S., and Stimming, U., "SOFC System Operating Strategies for Mobile Applications," *Fuel Cells*, vol. 5, pp. 499–508, December 2005.

[35] Burke, A. F., "Hybrid-Electric Vehicle Technology (1990-2000)," Tech. Rep. UCD-ITS-RR-99-13, Institute of Transportation Studies, University of California, Davis, August 1999.

[36] Whitlow, Woodrow, J., "NASA's Vision for 21st Century Aircraft," Tech. Rep. 20020091965, National Aeronautics and Space Administration, Cleveland, OH, October 2002.

[37] Sehra, A. and Shin, J., "Revolutionary Propulsion Systems for 21st Century Aviation," Tech. Rep. NASA/TM-2003-212615, National Aeronautics and Space Administration, October 2003.

[38] Nikolaidis, E., "Types of Uncertainty in Design Decision Making," in *Engineering Design Reliability Handbook* (Nikolaidis, E. and Ghiocel, D.M.and Singhal, S., eds.), ch. 8, Boca Rotan, FL: CRC Press, 2005.

[39] AIAA, "Current state of the art on multidisciplinary design optimization (MDO)," white paper, American Institute of Aeronautics and Astronautics, Washington, D.C., September 1991.

[40] Raymer, D., *Aircraft Design: A Conceptual Approach.* AIAA Education Series, Reston, VA: American Institute of Aeronautics and Astronautics, 3rd ed., 1999.

[41] Dieter, G., *Engineering design: a materials and processing approach.* McGraw-Hill, 3rd ed., 2000.

[42] Asimow, M., *Introduction to Design.* Englewood Cliffs, NJ: Prentice-Hall, 1962.

[43] National Aeronautics and Space Administration, "NASA Systems Engineering Handbook." SP-610S, June 1995.

[44] Kandebo, S. W., "PUTTING F135 TO THE TEST," *Aviation week and space technology*, vol. 160, pp. 52–54, March 22 2004.

[45] Kirby, M., *A Methodology for Technology Identification, Evaluation, and Selection in Conceptual and Preliminary Aircraft Design.* PhD thesis, Georgia Institute of Technology, 2001.

[46] Maier, M. W. and Rechtin, E., *The Art of Systems Architecting.* Boca Raton, FL: CRC Press, 2nd ed., 2000.

[47] Mattingly, J., *Elements of Gas Turbine Propulsion.* Singapore: McGraw-Hill International Editions, 1996.

[48] Mattingly, J., Heiser, W., and Pratt, D., *Aircraft Engine Design.* Reston, VA: American Institute of Aeronautics and Astronautics, 2nd ed., 2002.

[49] Oates, G. C., *Aerothermodynamics of Gas Turbine and Rocket Propulsion.* Reston, VA: American Institute of Aeronautics and Astronautics, 3rd ed., 1997.

[50] Kerrebrock, J., *Aircraft Engines and Gas Turbines.* Cambridge, MA: MIT Press, 1972.

[51] Walsh, P. P. and Fletcher, P., *Gas Turbine Performance.* Fairfield, NJ: Blackwell Science, 2004.

[52] Hollingsworth, D., "Workflow Management Coalition: The Workflow Reference Model," Tech. Rep. TC00-1003, The Workflow Management Coalition, Hampshire, UK, January 1995.

[53] Turner, L., Larsen, R., Duoba, M., McBroom, S., Nedungadi, A., and Wipke, K., "Modeling future automobiles: the role of industry and government," *COMPEL: The International Journal for Computation and Mathematics in Electrical and Electronic Engineering*, vol. 19, pp. 1036–1044, December 2000.

[54] Jacobson, B., "On Vehicle Driving Cycle Simulation," Tech. Rep. SAE 950031, Society of Automotive Engineers, 1995.

[55] Heath, R. and Mo, C., "A Modular Approach to Powertrain Modeling for the Prediction of Vehicle Performance, Economy and Emissions," Tech. Rep. SAE 960427, Society of Automotive Engineers, 1996.

[56] Brooker, A., Haraldsson, K., Hendricks, T., Johnson, V., Kelly, K., Kramer, B., Markel, T., O'Keefe, M., Sprik, S., Wipke, K., Zolot, M., Bharathan, D., Burch, S., Cuddy, M., and Rausen, D., *ADVISOR Documentation*. National Renewable Energy Laboratory, 2002 ed., April 30 2002.

[57] Hauer, K.-H., *Analysis Tool for Fuel Cell Vehicle Hardware and Software (Controls) with an Application to Fuel Economy Comparisons of Alternative System Designs*. PhD thesis, Unversity of California Davis, Institute of Transport Studies, 2001.

[58] Endres, T. E., "Advantages of Rapid Prototyping," in *Automated Fastening Conference & Exposition*, no. SAE 1999-01-3433, (Nashville, TN), Society of Automotive Engineers, 1999.

[59] Mattingly, J., *AEDsys Program User Guide*, September 2002.

[60] Oates, G. C., ed., *Aerothermodynamics of Aircraft Engine Components*. New York: American Institute of Aeronautics and Astronautics, 1985.

[61] Oates, G. C., ed., *Aircraft Propulsion Systems Technology and Design*. Washington, DC: American Institute of Aeronautics and Astronautics, 1989.

[62] Kowalski, E. J. and Atkins, R. A. J., "Computer Code For Estimating Installed Performance of Aircraft Gas Turbine Engines. Volume II User's Manual," Tech. Rep. NASA CR-159692, National Aeronautics and Space Administration, 1979.

[63] Klann, J. L. and Snyder, C. A., *NEPP Users Manual (NASA Engine. Performance Program)*. Aeropropulsion Analysis Office, NASA Glenn Research Center, Cleveland, OH, March 1997.

[64] GEREND, R. and ROUNDHILL, J., "CORRELATION OF GAS TURBINE ENGINE WEIGHTS AND DIMENSIONS," in *6th Propulsion Joint Specialist Conference*, no. AIAA 1970-669, (San Diego, CA), American Institute of Aeronautics and Astronautics, 15-19 June 1970.

[65] Onat, E. and Klees, G., "A Method To Estimate Weight and Dimensions of Large and Small Gas Turbine Engines," Tech. Rep. NASA CR-159481, National Aeronautics and Space Administration, 1979.

[66] Nam, T., *A Generalized Sizing Method for Revolutionary Concepts under Probabilistic Design Constraints*. PhD thesis, Georgia Institute of Technology, May 2007.

[67] SAE, "Gas Turbine Engine Steady-State Performance Presentation for Digital Computer Programs." Society of Automotive Engineers, 1989. Aerospace Standard, AS681 Rev. E.

[68] Gallie, W., *Uncertainty as a philosophical problem*, ch. 1. Liverpool University Press, 1957.

[69] Koch, P. N., "Probabilistic Design: Optimizing for Six Sigma Quality ," in *43rd AIAA/ASME/ASCE/AHS/ASC Structures, Structural Dynamics, and Materials Conference*, no. AIAA-2002-1471, (Denver, CO), American Institute of Aeronautics and Astronautics, April 22-25 2002.

[70] Smithson, M., *Ignorance and Uncertainty: Emerging Paradigms*. New York: Springer-Verlag, 1989.

[71] ASDL, "Aerospace Systems Design Laboratory." `http://www.asdl.gatech.edu/`, May 2007. [Online; accessed 01-May-2007].

[72] Chae, H. G., *A Possibilistic Approach to Rotorcraft Design through a Multi-Objective Evolutionary Algorithm*. PhD thesis, Georgia Institute of Technology, December 2006.

[73] Noor, A., "Perspectives on Nondeterministic Approaches," in *Engineering Design Reliability Handbook*, CRC Press, 2005.

[74] Zadeh, L., "Fuzzy sets as a basis for a theory of possibility," *Fuzzy Sets and Systems*, vol. 1, pp. 1–28, 1978.

[75] Mavris, D. N., Bandte, O., and DeLaurentis, D. A., "Robust Design Simulation: A Probabilistic Approach to Multidisciplinary Design," *Journal of Aircraft*, vol. 36, no. 1, pp. 298–307, 1999.

[76] Parks, J. M., "On stochastic optimization: Taguchi Methods(TM) demystified; its limitations and fallacy clarified," *Probabilistic Engineering Mechanics*, vol. 16, pp. 87–101, 2001.

[77] Bandte, O., *A Probabilistic Multi-Criteria Decision Making Technique for Conceptual and Preliminary Aerospace Systems Design.* PhD thesis, Georgia Institute of Technology, September 2000.

[78] Roth, B. and Mavris, D., "Commercial Engine Architecture Selection in the Presence of Uncertainty and Evolving Requirements," in *XVth International Symposium on Air Breathing Engines*, no. ISABE 2001-1169, (Bangalore, India), International Symposium on Air Breathing Engines, September 2-7 2001.

[79] Nam, T., Shih, K.-C., and Mavris, D., "Assessment of Environmental and Regulatory Uncertainty Impacts on Propulsion System Design," in *3rd Aircraft, Technology Integration, and Operations (ATIO) Forum*, no. AIAA 2003-6805, (Denver, CO), American Institute of Aeronautics and Astronautics, November 17-19 2003.

[80] Nam, T., Soban, D., and Mavris, D., "A Non-Deterministic Aircraft Sizing Method under Probabilistic Design Constraints," in *47th AIAA/ASME/ASCE/AHS/ASC Structures, Structural Dynamics, and Materials Conference*, no. AIAA-2006-2062, (Newport, RI), American Institute of Aeronautics and Astronautics, May 1-4 2006.

[81] Charnes, A., Cooper, W., and Symonds, G., "Cost horizons and certainty equivalents: an approach to stochastic programming of heating oil," *Management Science*, vol. 4, pp. 235–263, 1958.

[82] Haneveld, K. and van der Vlerk, M. H., "Integrated chance constraints: reduced forms and an algorithm," Tech. Rep. 02A33, University of Groningen, Groningen, The Netherlands, May 27 2002.

[83] Birge, J. and Louveaux, F., *Introduction to Stochastic Programming*. Springer Series in Operations Research, New York: Springer-Verlag, 1997.

[84] Kirkpatrick, S., Gelatt, C., and Vecchi, M., "Optimization by Simulated Annealing," *Science*, vol. 220, pp. 671–680, May 1983.

[85] Hajela, P., "Genetic Search - An Approach to the Nonconvex Optimization Problem," *AIAA Journal*, vol. 26, pp. 1205–1210, July 1990.

[86] Dantzig, G., "Linear programming under uncertainty," *Management Science*, vol. 1, pp. 197–206, 1955.

[87] Beale, E., "On minimizing a convex function subject to linear inequalities," *J. Royal Statistical Society*, vol. Series B 17, pp. 173–184, 1955.

[88] Saliby, E., "Descriptive Sampling: A Better Approach to Monte Carlo Simulation," *J. Opl. Res. Soc.*, vol. 41, pp. 1133–1142, December 1990.

[89] Vanderplaats, G. N., "An efficient Feasible Directions Algorithm for Design Synthesis," *AIAA Journal*, vol. 22, pp. 1633–l640, October 1984.

[90] Madansky, A., "Inequalities for stochastic linear programming problems," *Management Science*, vol. 6, pp. 197–204, 1960.

[91] Shannon, R., *Systems simulation the art and science*. Englewood Cliffs, NJ: Prentice-Hall,, 1975.

[92] Sargent, R., "Verification and validation of simulation models," in *Proceedings of the 2005 Winter Simulation Conference*, pp. 130–143, 2005.

[93] Zwicky, F., "Morphology of aerial propulsion," *Helvetica Physica Acta*, vol. XXI, no. 5, pp. 299–340, 1948.

[94] Zwicky, F., *Discovery, Invention, Research - Through the Morphological Approach*. Toronto, Canada: The Macmillian Company, 1969.

[95] Engler, W. O., Biltgen, P. T., and Mavris, D. N., "Concept Selection Using an Interactive Reconfigurable Matrix of Alternatives (IRMA)," in *45th AIAA Aerospace Sciences Meeting and Exhibit*, no. AIAA 2007-1194, (Reno, NV), American Institute of Aeronautics and Astronautics, January 8-11 2007.

[96] Soban, D. and Upton, E., "Design of a UAV to Optimize Use of Fuel Cell Propulsion Technology," in *Infotech@Aerospace*, no. AIAA 2005-7135, (Arlington, VA), American Institute of Aeronautics and Astronautics, September 26-29 2005.

[97] Buonanno, M. A., *A Method for Aircraft Concept Exploration Using Multicriteria Interactive Genetic Algorithms*. PhD thesis, Georgia Institute of Technology, December 2005.

[98] Villeneuve, F., *A Method for Concept and Technology Exploration of Aerospace Architectures*. PhD thesis, Georgia Institute of Technology, August 2007.

[99] Larminie, J. and Lowry, J., *Electric vehicle technology explained*. Chichester, England: John Wiley & Sons, 2003.

[100] Youngblood, J. and Talay, T., "Solar-Powered Airplane Design for Long-Endurance, High-Altitude Flight," in *2nd International Very Large Vehicles Conference*, no. AIAA 1982-0811, (Washington, DC), American Institute of Aeronautics and Astronautics, May 17-18 1982.

[101] Youngblood, J., Talay, T., and Pegg, R., "Design of Long-Endurance Unmanned Airplanes Incorporating Solar and Fuel Cell Propulsion," in *AIAA/SAE/ASME 20th Joint Propulsion Conference*, no. AIAA 1984-1430, (Cincinnati, OH), American Institute of Aeronautics and Astronautics, June 11-13 1984.

[102] Berton, J., Freeh, J., and Wickenheiser, T., "An Analytical Performance Assessment of a Fuel Cell-Powered, Small Electric Aircraft," in *Symposium on Novel and Emerging Vehicle and Vehicle Technology Concepts*, (Brussels, Belgium), Applied Vehicle Technology Panel of the NATO Research and Technology Agency, April 2003.

[103] Wickenheiser, T., Sehra, A., Seng, G., Freeh, J., and Berton, J., "Emissionless aircraft: requirements and challenges," in *AIAA/ICAS International Air and Space Symposium and Exposition: The Next 100 Years*, no. AIAA 2003-2810, (Dayton, OH), American Institute of Aeronautics and Astronautics, July 14-17 2003.

[104] Freeh, J., Pratt, J., and Brouwer, J., "Development of a solid-oxide fuel cell/gas turbine hybrid system model for aerospace applications," Tech. Rep. NASA/TM-2004-213054, National Aeronautics and Space Administration, May 2004.

[105] Tornabene, R., Wang, X., Steffen, C., and Freeh, J., "Development of Parametric Mass and Volume Models for an Aerospace SOFC/GAS Turbine Hybrid System," Tech. Rep. NASA/TM 2005-213819, National Aeronautics and Space Administration, July 2005.

[106] Steffen, C. J., Freeh, J., and Larosiliere, L., "Solid Oxide Fuel Cell/Gas Turbine Hybrid Cycle Technology For Auxiliary Aerospace Power," Tech.

Rep. NASA/TM-2005-213586, National Aeronautics and Space Administration, April 2005.

[107] Freeh, J., Steffen, C., and Larosiliere, L., "Off-Design Performance Analysis of a Solid-Oxide Fuel Cell/Gas Turbine Hybrid for Auxiliary Aerospace Power," Tech. Rep. NASA/TM-2005-213805, National Aeronautics and Space Administration, December 2005.

[108] Himansu, A., Freeh, J. E., Steffen, C. J. J., Tornabene, R. T., and Wang, X.-Y. J., "Hybrid Solid Oxide Fuel Cell/Gas Turbine System Design for High Altitude Long Endurance Aerospace Missions," Tech. Rep. NASA/TM-2006-214328, National Aeronautics and Space Administration, May 2006.

[109] Alexander, D., Lee, Y., Guynn, M., and Bushnell, D., "Emissionless Aircraft Study," in *38th AIAA/ASME/SAE/ASEE Joint Propulsion Conference & Exhibit*, no. AIAA-2002-4056, (Indianapolis, IN), American Institute of Aeronautics and Astronautics, July 7-10 2002.

[110] Alexander, D., "Advanced Energetics for Aeronautical Applications," Tech. Rep. NASA CR-2003-212169, MSE Technology Applications, Inc., Butte, MT, February 2003.

[111] Atreya, S., Mata, M., Jones, R., and Kohout, L., "Power System Comparisons for a High Altitude Lond Endurance (HALE) Remotely Operated Aircraft (ROA)," in *AIAA 5th Aviation, Technology, Integration, and Operations Conference*, no. AIAA 2005-7324, (Arlington, VA), American Institute of Aeronautics and Astronautics, September 26-28 2005.

[112] Wikipedia, "William Sturgeon." `http://en.wikipedia.org/wiki/William_Sturgeon`, June 2007. Online; accessed 07-June-2007.

[113] Purcell, E., *Electricity and Megnetism*, vol. 2 of *Berkeley Physics Course*. New York: McGraw-Hill, 2nd ed., 1985.

[114] Wikipedia, "Nikola Tesla." `http://en.wikipedia.org/wiki/Nikola_Tesla`, June 2007. Online; accessed 07-June-2007.

[115] Masson, P., Soban, D., Upton, E., Pienkos, J., and Luongo, C., "HTS motors in aircraft propulsion: design considerations," *IEEE Transactions on Applied Superconductivity*, vol. 15, pp. 2218–2221, June 2005.

[116] Masson, P. J., Soban, D. S., Brown, G. V., and Luongo, C. A., "HTS Machines as Enabling Technology for All-Electric Airborne Vehicles," *Superconductor Science and Technology*, vol. 20, pp. 748–756, August 2007.

[117] U.S. Department of Energy, "Hydrogen, Fuel Cells, & Infrastructure Technologies Program; Multi-Year Research, Development and Demonstration Plan: Planned program activities for 2003-2010." `www.nrel.gov/docs/fy05osti/34289.pdf`, March 2005. [Online; accessed 16-March-2006].

[118] Colozza, A., "Hydrogen Storage for Aircraft Applications Overview," Tech. Rep. NASA/CR-2002-211867, Analex Corporation, September 2002.

[119] Chambers, A., Park, C., Baker, R. T. K., and Rodriguez, N. M., "Hydrogen Storage in Graphite Nanofibers," *Journal of Physical Chemistry B*, vol. 102, pp. 4253–4256, May 28 1998.

[120] Atkinson, K., Roth, S., Hirscher, M., and Grunwald, W., "Carbon nanostructures: An efficient hydrogen storage medium for fuel cells?," *Fuel Cells Bulletin*, vol. 4, pp. 9–12, November 2001.

[121] AeroVironment Press Release, "AeroVironment Flies World's First Liquid Hydrogen Powered UAV." `https://www.aerovironment.com/news_`

detail.php?id=114&PHPSESSID=2ec9f49e867af8044a6c5c04b8dca83b, June 28 2005. [Online; accessed 8-December-2006].

[122] Williams, K., Keith, W., Marcel, M., Haskew, T., Shepard, W., and Todd, B., "Experimental investigation of fuel cell dynamic response and control," *Journal of Power Sources*, vol. 163, pp. 971–985, January 2007.

[123] Kulp, G. W., "A Comparison of Two Air Compressors for PEM Fuel Cell Systems," Master's thesis, Virginia Polytechnic Institute and State University, Blacksburg, Virginia, December 2001.

[124] Cunningham, J. M., "Air System Management for Fuel Cell Vehicle Applications," Master's thesis, University of California Davis, 2001.

[125] Pukrushpan, J. T., *Modeling and control of fuel cell systems and fuel processors*. PhD thesis, The University of Michigan, Ann Arbor, Michigan, 2003.

[126] Fletcher, J., Sharma, R., and Lear, W., "Effect of Non-Ideal Component and Subsystem Performance on Water Balance of PEM Fuel Cell Systems," in *3rd International Energy Conversion Engineering Conference*, no. AIAA 2005-5605, (San Francisco, CA), American Institute of Aeronautics and Astronautics, August 15-18 2005.

[127] Gee, M. K., "VII.H.1 Cost and Performance Enhancements for a PEM Fuel Cell System Turbocompressor," in *DOE Hydrogen Program 2005 Annual Progress Report*, ch. VII.H, pp. 985–988, Washington, DC: U.S. Department of Energy, November 2005.

[128] Budge, J. R., Kantak, M. V., Perna, M. A., Scotto, M. V., and Birmingham, D. P., "Distillate Fuel Reformer Development for Fuel Cell Applications," in *5th Annual Dept. of Defense Logistic Fuel Processing Conference*, (Panama City Beach, FL), January 25-26 2005.

[129] Paz, E., "Performance Improvements in Copper Based Direct Oxidation SOFC." http://www.franklinfuelcells.com/FCS-Paz.pdf, November 2005. [Online; accessed 28-March-2006].

[130] Phoenix Integration, *ModelCenter 6.1.* Phoenix Integration, Inc., Wayne, PA, 2005.

[131] Parsons, S., *Qualitative Methods for Reasoning under Uncertainty.* Cambridge, MA: The MIT Press, 2001.

[132] Shapiro, A. and Philpott, A., *A Tutorial on Stochastic Programming.* The Committee on Stochastic Programming, January 20 2007.

[133] Law, A. and Kelton, W., *Simulation Modeling and Analysis.* New York: McGraw-Hill, 3rd ed., 2000.

[134] Kirby, M. R., *An Overview of Response Surface Methodology.* Aerospace Systems Design Laboratory, Atlanta, GA, March 2007. Tutorial.

[135] Matheron, G., "Krigeage d'un panneau rectangulaire par sa périphérie," CG 28, Ecole des Mines de Paris, Paris, 1960.

[136] Hajela, P. and Berke, L., "Nerual Networks in Structural Analysis and Design: An Overview," *International Journal for Computing Systems in Engineering*, vol. 3, no. 1-4, pp. 525–539, 1992.

[137] Li, W. and Padula, S., *Approximation Theory XI: Gatlinburg 2004*, ch. Approximation methods for conceptual design of complex systems, pp. 241–278. Brentwood, TN: Nashboro Press, 2005.

[138] Mavris, D., Soban, D., Upton, E., Harcrow, A., and DeKock, B., "System Level Assessment of an Uninhabited Aerial Vehicle (UAV) Utilizing Fuel Cell Technology." Final Report, submitted to NAVAIR, November 2005.

[139] Naval Air Systems Command, "Naval Air Systems Command Solicitation: RFP Number N00019-00-R-0292." http://www.fas.org/irp/program/collect/docs/solicitation_view_action.htm, February 16 2000. [Online; accessed 18-March-2006].

[140] Jones, C. A., "UNMANNED AERIAL VEHICLES (UAVS): AN ASSESSMENT OF HISTORICAL OPERATIONS AND FUTURE POSSIBILITIES," Tech. Rep. AU/ACSC/0230D/97-03, Air Command and Staff College, March 1997.

[141] National Aeronautics and Space Administration, "(VSP) Vehicle Sketch Pad." http://nspires.nasaprs.com/external/viewrepositorydocument/81236/SACD_Analysis_Tool_Archive(04-28-06).htm. [Online; accessed 11-October-2007].

[142] Baker, W. M., Elliott, R. D., and Miranda, L. R., "A generalized vortex lattice method," Tech. Rep. LAR-12636, National Aeronautics and Space Administration, September 1 1980.

[143] Middleton, W. D. and Lundry, J. L., "A System for Aerodynamic Design and Analysis of Supersonic Aircraft. Part 1 - General Description and Theoretical Development," Tech. Rep. NASA CR-3351, National Aeronautics and Space Administration, December 1980.

[144] Chambliss, K., Kelly, S., and Kimble, J., "CRYOGENIC FLUID STORAGE FOR THE MISSION TO MARS," tech. rep., Texas Tech University, April 27 1999.

[145] Agrawal, B., "Feasibility of Solid Oxide Fuel Cells as the Primary Method for Aircraft Power and Propulsion." AE8900 Special Problem Report, May 2006.

[146] Beliakov, G., *Matlab toolbox LibLip for multivariate scattered data interpolation. Version 2.1. User Manual*, 2006.

[147] Rajashekara, K., "Propulsion System Strategies for Fuel Cell Vehicles," in *SAE 2000 World Congress*, no. SAE 2000-01-0369, (Detroit, MI), Society of Automotive Engineers, March 6-9 2000.

[148] Office of the Federal Register, *Code of Federal Regulations, Title 14, Aeronautics and Space, Pt. 1-59, Revised as of January 1, 2007.* the United States of America: National Archives and Records Administration, April 19 2007.

[149] Srinivasan, V. and Newman, J., "A Model-based Comparison of Various Li-ion Chemistries," *ECS Meeting Abstracts*, vol. 502, no. 4, pp. 234–234, 2006.

[150] Ahluwalia, R. K. and Wang, X., "Direct hydrogen fuel cell systems for hybrid vehicles," *Journal of Power Sources*, vol. 139, pp. 152–164, January 4 2005.

[151] Miller, J., *Propulsion Systems for Hybrid Vehicles.* No. 45 in IEE Power and Energy Series, London: The Institution of Electrical Engineers, 2004.

[152] Objerkampf, W., DeLand, S., Rutherford, B., Diegert, K., and Alvin, K., "Error and Uncertainty in Modeling and Simulation," *Reliability Engineering and System Safety*, vol. 75, pp. 333–357, 2002.

[153] Parsons, S. and Hunter, A., "A Review of Uncertainty Handling Formalisms," in *Applications of Uncertainty Formalisms* (Hunter, A. and Parsons, S., eds.), pp. 8–37, Berlin Heidelberg: Springer-Verlag, 1998.

[154] SAS Institute Inc., *JMP User Guide, Release 6.* No. JMP 6.0.2, Cary, NC: SAS Institute Inc., November 2005.

[155] Samarasinghe, Sandhya, *Neural Networks for Applied Sciences and Engineering: From Fundamentals to Complex Pattern Recognition*. Boca Raton, FL: Auerbach Publications, September 2006.

[156] The MathWorks, Inc., "lhsdesign." `http://www.mathworks.com/access/helpdesk/help/toolbox/stats/index.html?/access/helpdesk/help/toolbox/stats/lhsdesign.html`, 2007. [Online; accessed 13-June-2007].

[157] Hair, J., Anderson, R., Tatham, R., and Black, W., *Multivariate data analysis*. Saddle River, NJ: Prentice Hall, 4th ed., 1995.

[158] Halinski, R. and Feldt, L., "The selection of variables in multiple regression analyses," *Journal of Educational Measurement*, vol. 7, no. 3, pp. 151–158, 1970.

[159] Miller, D. and Kunch, J., "Prediction and statistical overkill revisited," *Measurement and Evaluation in Guidance*, vol. 6, no. 3, pp. 157–163, 1973.

[160] Decisioneering, Inc., *Crystall Ball 7.1: User Manual*. MAN-CBUM 070100-1 2/9/05, February 2005.

[161] Decisioneering, Inc., "How does crystal ball calculate sensitivity?." `http://www.crystalball.com/support/simulation/cbl_gen_004A.html`, April 1998. [Online; accessed 20-November-2006].

[162] Fletcher, R. and Reeves, C., "Function Minimization by Conjugate Gradients," *Br. Computer J.*, vol. 7, no. 2, pp. 149–154, 1964.

[163] Broydon, C., "The Convergence of a Class of Double Rank Minimization Algorithms, parts I and II," *J. Inst. Math. Appl.*, vol. 6, pp. 76–90, 222–231, 1970.

[164] Fletcher, R., "A New Approach to Variable Metric Algorithms," *Computer J.*, vol. 13, pp. 317–322, 1970.

[165] Goldfarb, D., "A Family of Variable Metric Methods Derived by Variational Means," *Math. Comput.*, vol. 24, pp. 23–36, 1970.

[166] Shanno, D., "Conditioning of Quasi-Newton Methods for Function Minimization," *Math. Comput.*, vol. 24, pp. 647–656, 1970.

[167] Vanderplaats, G., *Numerical Optimization Techniques for Engineering Design*. Vanderplaats Research & Development, Inc., third ed., 2001.

[168] White, T., "Design Space Exploration of a Fuel Cell Powered General Aviation Aircraft." AE8900 Special Problem Report, November 2004.

[169] Oruoch, G., "Performance and Sizing Simulation of Power Management and Distribution Systems for Aerospace Applications." AE8900 Special Problem Report, May 2006.

[170] Mavris, D., Soban, D., Upton, E., White, T., and Mattson, J., "Technology Assessment of a Fuel Cell Auxiliary Power System for Naval Aviation." Final Report, submitted to NAVAIR, October 31 2004.

[171] Balaba, D., "A Methodology for Rapid Vehicle Scaling and Configuration Space Exploration." PhD thesis proposal, Georgia Institute of Technology, January 2008.

[172] Riis, M. and Schultz, R., "Applying the Minimum Risk Criterion in Stochastic Recourse Programs," *Computational Optimization and Applications*, vol. 24, pp. 267–287, Feb/Mar 2003.

[173] Sahinidis, N., "Optimization under uncertainty: state-of-the-art and opportunities," *Computers & Chemical Engineering*, vol. 28, pp. 971–983, 2004.

[174] Ahmed, S., *Strategic planning under uncertainty: Stochastic integer programming approaches*. PhD thesis, University of Illinois, 2002.

[175] Birge, J. R. and Ho, J. K., "Optimal flows in stochastic dynamic networks with congestion," *Operations Research*, vol. 41, pp. 203–216, Jan/Feb 1993.

[176] Jagannathan, R., "Use of sample information in stochastic recourse and chance-constrained programming models," *Management Science*, vol. 31, p. 96, January 1985.

[177] Schlaifer, R. and Heron, S., *Development of Aircraft Engines and Fuels*. Boston, MA: Harvard University Graduate School of Business Administration, 1950.

[178] Bayles, G., "New power source technologies for electric wheelchairs," Tech. Rep. Technical Report 2, Rehabilitation Engineering Research Center, University of Pittsburgh, PA, July 1994.

[179] Choi, T. P., Nam, T., and Soban, D. S., "Novel Synthesis and Analysis Methods Development towards the Design of Revolutionary Electric Propulsion and Aircraft Architectures," in *Infotech@Aerospace*, no. AIAA 2005-7188, (Arlington, VA), American Institute of Aeronautics and Astronautics, September 26 -29 2005.

[180] Anselmo, J., "Build it and they will come," *Aviation week and space technology*, vol. 162, pp. 50–56, May 2005.

[181] Wall, R., "Maritime Focus," *Aviation week and space technology*, vol. 162, p. 56, June 2005.

[182] Dornheim, M., "Civilians Try Drones," *Aviation week and space technology*, vol. 162, pp. 54–56, June 2005.

[183] Sullivan, R., Palko, J., Tornabene, R., Bednarcyk, B., Powers, L., Mital, S., Smith, L., Wang, X.-Y. J., and Hunter, J., "Engineering Analysis Studies for Preliminary Design of Lightweight Cryogenic Hydrogen Tanks in UAV Applications," Tech. Rep. NASA TP-2006-214094, National Aeronautics and Space Administration, 2006.

[184] U.S. General Accounting Office, "Aviation and the Environment: Aviation's Effects on the Global Atmosphere Are Potentially Significant and Expected to Grow." Washington, DC, February 2000.

[185] Wentz, W., Myose, R., and Mohamed, A., "Hydrogen-Fueled General Aviation Airplanes," in *AIAA 5th Aviation, Technology, Integration, and Operations Conference*, no. AIAA 2005-7324, (Arlington, VA), American Institute of Aeronautics and Astronautics, September 26-28 2005.

[186] Dornheim, M., "Special Fuel Cells Key to Months-Long Flight," *Aviation week and space technology*, vol. 153, pp. 58–61, February 28 2000.

[187] NASA Dryden Flight Research Center, "Past Projects - Helios Prototype Solar-Powered Aircraft." `http://www.nasa.gov/centers/dryden/history/pastprojects/Helios/index.html`, February 17 2005. [Online; accessed 22-March-2005].

[188] Velev, O., "Regenerative fuel cell system for an unmanned solar powered aircraft," in *35th Intersociety Energy Conversion Engineering Conference*, no. AIAA 2000-2873, (Las Vegas, NV), American Institute of Aeronautics and Astronautics, July 24-28 2000.

[189] Noll, T. E., Brown, J. M., Perez-Davis, M. E., Ishmael, S. D., Tiffany, G. C., and Gaier, M., "Investigation of the Helios Prototype Aircraft Mishap," tech. rep., National Aeronautics and Space Administration, January 2004.

[190] Thomas, S., Zalbowitz, M., and Cruz, J., *Fuel Cells - Green Power*. No. LA-UR-99-3231, Los Alamos, NM: Los Alamos National Laboratory, 1999.

[191] Hall, D., Fortecnbach, C., Dimiceli, E., and Parks, R., "A Preliminary Study of Solar Powered Aircraft and Associated Power Trains," Tech. Rep. NASA CR-3699, National Aeronautics and Space Administration, December 1983.

[192] Bents, D. J., Scullin, V. J., Chang, B.-J., Johnson, D. W., and Garcia, C. P., "Hydrogen-Oxygen PEM Regenerative Fuel Cell Energy Storage System," Tech. Rep. NASA/TM-2005-213381, National Aeronautics and Space Administration, January 2005.

[193] Colozza, A., "Preliminary Design of a Long-Endurance Mars Aircraft," Tech. Rep. NASA CR-185243, National Aeronautics and Space Administration, April 1990.

[194] McCullers, L. A., "Aircraft configuration optimization including optimized flight profiles," Tech. Rep. N87-11743, National Aeronautics and Space Administration, Jaunary 1984.

[195] Campbell, D. J., "Revolutionary Propulsion and Power for 21st Century Aviation," in *AIAA/ICAS International Air and Space Symposium and Exposition: The Next 100 Years*, no. AIAA 2003-2561, (Dayton, OH), American Institute of Aeronautics and Astronautics, July 14-17 2003.

[196] Bents, D., Scullin, V., Chang, B., Johnson, D., Garcia, C., and Jakupca, I., "Test of hydrogen-oxygen PEM fuel cell stack at NASA Glenn research center," in *1st International Energy Conversion Engineering Conference*, no. AIAA 2003-6123, (Portsmouth, VA), American Institute of Aeronautics and Astronautics, August 17-21 2003.

[197] Chang, B., Johnson, D., Garcia, C., Jakupca, I., Scullin, V., and Bents, D., "Regenerative Fuel Cell Test Rig at Glenn Research Center," in *1st International Energy Conversion Engineering Conference August*, no. AIAA 2003-5942, (Portsmouth, VA), American Institute of Aeronautics and Astronautics, August 17-21 2003.

[198] Jakupca, I. and Wendell, J., "Self-Contained Aerospace Pressure Following Regenerative Fuel Cell Energy Storage System," in *3rd International Energy Conversion Engineering Conference*, no. AIAA 2005-5679, (San Francisco, CA), American Institute of Aeronautics and Astronautics, August 15-18 2005.

[199] Burke, K., "Unitized regenerative fuel cell system development," in *1st International Energy Conversion Engineering Conference*, no. AIAA 2003-5939, (Portsmouth, VA), American Institute of Aeronautics and Astronautics, August 17-21 2003.

[200] Burke, K. and Jakupca, I., "Unitized Regenerative Fuel Cell System Gas Dryer/Humidifier Analytical Model Development," in *2nd International Energy Conversion Engineering Conference*, no. AIAA 2004-5700, (Providence, RI), American Institute of Aeronautics and Astronautics, August 16-19 2004.

[201] Freeh, J., Liang, A., Berton, J., and Wickenheiser, T., "Electrical Systems Analysis at NASA Glenn Research Center: Status and Prospects," Tech.

Rep. NASA/TM-2003-212520, National Aeronautics and Space Administration, August 2003.

[202] Follen, G. J. and Naiman, C. G., "Common Analysis Tool Being Developed for Aeropropulsion: The National Cycle Program Within the Numerical Propulsion System Simulation Environment," Tech. Rep. NASA/TM-1999-208815, National Aeronautics and Space Administration, April 1999.

[203] Guynn, M., Freeh, J., and Olson, E., "Evaluation of a Hydrogen Fuel Cell Powered Blended-Wing-Body Aircraft Concept for Reduced Noise and Emissions," Tech. Rep. NASA/TM-2004-212989, National Aeronautics and Space Administration, February 2004.

[204] Pratt, J., Brouwer, J., and Samuelsen, G., "Experimental Performance of an Air-Breathing PEM Fuel Cell at High Altitude Conditions," in *43rd AIAA Aerospace Sciences Meeting and Exhibit*, no. AIAA 2005-0953, (Reno, NV), American Institute of Aeronautics and Astronautics, January 10-13 2005.

[205] Boland, R., "Experimental Power System Expands Flight Capabilities." `http://www.afcea.org/signal/articles/anmviewer.asp?a=1101&print=yes`, March 2006. [Online; accessed 1-February-2007].

[206] Kellogg, J. C., Monforton, L., White, D., and Vick, M., "Fuel Cells for Micro Air Vehicles." Joint Service Power Expo, Tampa, FL, May 5 2005. Presentation.

[207] Protonex, "Protonex Awarded U.S. Air Force Contract for Unmanned Aerial Vehicle Power Systems." `http://www.protonex.com/UAV%20Award%20FINAL.pdf`, January 2006. [Online; accessed 1-February-2007].

[208] AeroVironment Press Release, "AeroVironment's "Hornet" Micro Air Vehicle Completes First Fuel Cell Powered Flight." `http://www.`

aerovironment.cn/news/news-archive/hornet62.html, March 21 2003. [Online; accessed 10-February-2007].

[209] Dornheim, M., "Fuel Cell Flier," *Aviation week and space technology*, vol. 162, p. 52, June 2005.

[210] Daggett, D., "Hydrogen Fueled Airplanes." Hydrogen Production and NW Transportation, Seattle, WA, June 16 2003.

[211] Jenkins, M., "Cool Fuel." http://www.boeing.com/news/frontiers/archive/2003/august/i_atw.html, August 2003. [Online; accessed 13-February-2005].

[212] Spenser, J., "International fuel cell efforts include Boeing." http://www.boeing.com/news/frontiers/archive/2004/july/ts_sf7b.html, July 2004. [Online; accessed 30-January-2007].

[213] EV World, "Boeing Explores Fuel Cell Flight." http://www.evworld.com/view.cfm?page=article&storyid=1100, September 2006. [Online; accessed 14-February-2007].

[214] Chang, V. and Gallman, J., "Altitude Testing of Fuel Cell Systems for Aircraft Applications," in *Power Systems Conference*, no. SAE 2004-01-3200, (Reno, NV), Society of Automotive Engineers, November 2004.

[215] Wentz, W. H. J. and Mohamed, A., "Preliminary Design Considerations for Zero Greenhouse Gas Emission Airplanes," in *General Aviation Technology Conference & Exhibition*, no. SAE 2004-01-1803, (Wichita, KS), Society of Automotive Engineers, April 2004.

[216] Brand, J., Sampath, S., Shum, F., Bayt, R. L., and Cohen, J., "Potential use of hydrogen in air propulsion," in *AIAA/ICAS International Air and Space*

Symposium and Exposition: The Next 100 Years, no. AIAA 2003-2879, (Dayton, OH), American Institute of Aeronautics and Astronautics, July 14-17 2003.

[217] Moffitt, B., Bradley, T., Parekh, D., and Mavris, D., "Design and Performance Validation of a Fuel Cell Unmanned Aerial Vehicle," in *44th AIAA Aerospace Sciences Meeting and Exhibit*, no. AIAA-2006-0823, (Reno, NV), American Institute of Aeronautics and Astronautics, January 9-12 2006.

[218] Bradley, T. H., Moffitt, B. A., Mavris, D., and Parekh, D. E., "Validated modeling and synthesis of medium-scale polymer electrolyte membrane fuel cell aircraft," in *4th International ASME Conference on Fuel Cell Science, Engineering and Technology*, no. FUELCELL2006-97233, (Irvine, CA), American Society of Mechanical Engineers, June 18-21 2006.

[219] Moffitt, B. A., Bradley, T. H., Mavris, D., and Parekh, D. E., "Design Space Exploration of Small-Scale PEM Fuel Cell Long Endurance Aircraft," in *6th AIAA Aviation Technology, Integration and Operations Conference*, no. AIAA 2006-7701, (Wichita, KS), American Institute of Aeronautics and Astronautics, September 25-27 2006.

[220] Bradley, T. H., Moffitt, B. A., Thomas, R. W., Mavris, D., and Parekh, D. E., "Test Results for a Fuel Cell-Powered Demonstration Aircraft," in *SAE Power Systems Conference*, (New Orleans, LA), Society of Automotive Engineers, November 7-9 2006.

[221] Bradley, T. H., Moffitt, B. A., Mavris, D. N., and Parekh, D. E., "Flight Test Results for a Fuel Cell Unmanned Aerial Vehicle," in *45th AIAA Aerospace Sciences Meeting and Exhibit*, no. AIAA 2007-32, (Reno, NV), American Institute of Aeronautics and Astronautics, January 8-11 2007.

[222] Ofoma, U. and Wu, C., "Design of a Fuel Cell Powered UAV for Environmental Research," in *AIAA 3rd "Unmanned Unlimited" Technical Conference, Workshop and Exhibit*, no. AIAA 2004-6384, (Chicago, IL), American Institute of Aeronautics and Astronautics, September 20-23 2004.

[223] Herweth, C., Ofoma, U., Wu, C., Matsuyama, S., and Clark, S., "Development of a Fuel Cell Powered UAV for Environmental Research," in *44th AIAA Aerospace Sciences Meeting and Exhibit*, no. AIAA 2006-0237, (Reno, NV), American Institute of Aeronautics and Astronautics, January 9-12 2006.

[224] California State University Press Release, "Cal State L.A.'s fuel-cell plane passes key flight test." `http://www.calstatela.edu/univ/ppa/newsrel/fuelcellplaneflight.htm`, August 2006. [Online; accessed 07-February-2007].

[225] Choi, T. P., *Simulation Evironment for Design of Revolutionary Fuel Cell Aerorpropulsion Systems: Theory and User's Manual.* Aerospace Systems Design Laboratory, Georgia Institute of Technology, under revision ed., to be published 2008.

[226] Sutherland, L. and Bass, H., "Atmospheric absorption in the atmosphere up to 160 km," *J. Acoust. Soc. Am.*, vol. 115, pp. 1012–1032, March 2004.

[227] English, S., "Estimation of Temperature and Humidity Profile Information from Microwave Radiances over Different Surface Types," *Journal of Applied Meteorology*, vol. 38, pp. 1526 – 1541, October 1999.

[228] Schlatter, T. and Baker, D., "Algorithms, Comparisons and Source References by Schlatter and Baker." `http://wahiduddin.net/calc/density_algorithms.htm`, June 1991. [Online; accessed 18-July-2006].

[229] List, R. J., *Smithsonian meteorological tables*, vol. 114 of *Smithsonian Miscellaneous Collections*. Washington, D.C.: The Smithsonian Institution, 6th ed., 1951.

[230] Worobel, R. and Mayo, M., "Advanced General Aviation Propeller Study," Tech. Rep. NASA CR 114289, Hamilton Standard, Windsor Locks, CT, April 1971.

[231] Levine, S., "HSQFAN Q-Fan Analysis Program User's Manual." Aerospace Systems Design Laboratory, Georgia Institute of Technology, Version 1.0, June 2004.

[232] Wipke, K. and Cuddy, M., "Using an Advanced Vehicle Simulator (ADVISOR) to Guide Hybrid Vehicle Propulsion System Development," Tech. Rep. NREL/TP-425-21615, National Renewable Energy Laboratory, August 1996.

[233] Masson, P., Morega, A., and Tixador, P., "Preliminary Motor Design 200 kW - 2700 rpm," tech. rep., Center for Advanced Power Systems, Florida State University, Tallahassee, FL, September 2004.

[234] McBride, B. J. and Gordon, S., "Computer Program for Calculation of Complex Chemical Equilibrium Compositions and Applications," Tech. Rep. NASA RP-1311, National Aeronautics and Space Administration, June 1996.

[235] Menne, M., Reinert, J., and De Doncker, R. W., "Energy-Efficiency Evaluation of Traction Drives for Electric Vehicles," in *Proceedings of the 15th International Electric Vehicle Symposium*, (Brussels, Belgium), October 1998.

[236] Lester, L., Someone, S., Someone, S., and Someone, S., "An Induction Motor Power Train for EVs–The Right Power at the Right Price," in *Advanced Components for Electric and Hybrid Electric Vehicles: Workshop Proceedings*, (Gaithersburg, MD), October 27-28 1993.

[237] AC Propulsion, Inc., "AC-150 Gen-2 EV Power System: Integrated Drive and Charging for Electric Vehicles." http://www.acpropulsion.com/technology/ac150_gen2_specs.pdf, December 2001. [Online; accessed 14-August-2006].

[238] Ortiz, F., Buisset, R., and C., A., "VEDELIC: New Technologies for Electric Vehicles, Results of Tests and Demonstration," in *Proceedings of the 15th International Electric Vehicle Symposium*, (Brussels, Belgium), October 1998.

[239] Bauch-Banetzky, D., Berwind, B., Someone, S., and Someone, S., "Permanent magneterregte Synchronmaschine mit Nd-Fe-B Dauermagneten fuer den Einsatz in Personenkraftfahrzeugen," in *VDI (Verein Deutscher Ingenieure) Berichte 1459: Entwicklung Konstruktion Vertrieb HYBRIDANTRIEBE*, (Duesseldorf, Germany), VDI Verlag GmbH, 1999.

[240] Biais, F. and Langry, P., "Optimization of a permanent magnet traction motor for electric vehicle," in *Proceedings of the 15th International Electric Vehicle Symposium*, (Brussels, Belgium), October 1998.

[241] DuPont, "DuPont Nafion PFSA Membranes N-112, NE-1135, N-115, N-117, NE-1110." Product Information, February 2004.

[242] Son, D.-H., Sharma, R. K., Shul, Y.-G., and Kim, H., "Preparation of Pt/zeolite-Nafion composite membranes for self-humidifying polymer electrolyte fuel cells," *Journal of Power Sources*, vol. 165, pp. 733–738, March 2007.

[243] E-TEK, "A-1 Carbon Cloth Electrode (ECC)." SPECIALTY PRODUCTS-SECTION A: Gas Diffusion Electrodes & Services, February 2004.

[244] Lee, J. and Lalk, T., "Modeling fuel cell stack systems," *Journal of Power Sources*, vol. 73, no. 1, pp. 229–241, 1998.

[245] Pylkkaenen, T. and Scherer, G., "FUEL CELLS WITH FLEXIBLE GRAPHITE BIPOLAR PLATES," in *Scientific Report 2000* (Daum, C. and Leuenberger, J., eds.), vol. V of *General Energy*, Switzerland: Paul Scherrer Institut, March 2001.

[246] Wilson, D. G. and Korakianitis, T., *The Design of High Efficiency Turbomachinery and Gas Turbines*. Prentice Hall, 2nd ed., January 1998.

[247] Gee, M. K., "A. Turbocompressor for PEM Fuel Cells," in *FY 1999: Progress Report for Fuel Cells for Transportation*, ch. VI, pp. 121–123, Washington, DC: U.S. Department of Energy, October 1999.

[248] Gee, M. K., "A. Turbocompressor for PEM Fuel Cells," in *FY 2000: Progress Report for Fuel Cell Power Systems*, ch. VI, pp. 127–130, Washington, DC: U.S. Department of Energy, October 2000.

[249] Gee, M. K., "A. Turbocompressor for PEM Fuel Cells," in *FY 2001: Progress Report for Fuel Cells for Transportation*, ch. VI, pp. 175–177, Washington, DC: U.S. Department of Energy, December 2001.

[250] Gee, M. K., "IV.E.1 Turbocompressor for PEM Fuel Cells," in *FY 2002: Progress Report for Hydrogen, Fuel Cells, and Infrastructure Technologies Program*, ch. VI.E, pp. 490–493, Washington, DC: U.S. Department of Energy, November 2002.

[251] Gorman-Rupp Industries, "Gear Pumps 2000 Series." `http://www.gripumps.com/pdfs/GEAR_5.pdf`, February 2001. [Online; accessed 30-June-2006].

[252] Boeing Military Airplane Development, *Weight Analysis of Turbine Engine*. NASA Glenn Research Center, Cleveland, OH, 1979.

[253] Kays, W.M. and London, A.L., *Compact Heat Exchangers.* New York: McGraw-Hill, 3rd ed., 1998.

[254] Lefebvre, A. H., *Gas Turbine Combustion.* Philadelphia: Taylor & Francis, 2nd ed., 1999.

[255] Baldwin, T., Brooks, N., Williams, L., Fredrickson, P., Ordonez, J., and Brinson, T., "Integrated Power Management (IPM)," tech. rep., Center for Advanced Power Systems, FAMU-FSU College of Engineering, July 2004.

[256] Pukrushpan, J. T., Stefanopoulou, A. G., and Peng, H., *Control of Fuel Cell Power Systems: Principles, Modeling, Analysis and Feedback Design.* Springer, 2004.

VITA

Taeyun Paul Choi was born on June 2, 1980 in Seoul, South Korea. Prior to graduating from the International School of Duesseldorf in 1998, he had lived in Daejun, South Korea; Lexington, Kentucky; and Pohang, South Korea. In 2002, he received his Bachelor's degree in Mechanical Engineering with High Distinction from Worcester Polytechnic Institute, where he also minored in International Relations. He then joined the Aerospace Systems Design Laboratory to pursue his graduate studies in Aerospace Engineering at the Georgia Institute of Technology. Besides his experience as a graduate research assistant, Mr. Choi worked as an undergraduate cooperative engineer at General Electric Power Systems in Schenectady, New York and completed an internship with the Korea Aerospace Research Institute after receiving his Master's degree in 2003. He is a brother of Sigma Alpha Epsilon fraternity, and also a member of several distinguished academic honor societies including Tau Beta Pi, Pi Tau Sigma, Sigma Mu Epsilon, and the International Honor Society.